UNIVERSITY OF CALIFORNIA
SANTA CRUZ

APPLYING MOLECULAR CHIRALITY TOOLS TO AMYLOID β AND ALZHEIMER'S DISEASE

A dissertation submitted in partial satisfaction
of the requirements for the degree of

DOCTOR OF PHILOSOPHY

in

CHEMISTRY

by

Luis Alejandro Rodríguez Foley

December 2020

The dissertation of Luis Alejandro Rodriguez Foley is approved:

_____
Professor Jevgenij Raskatov, Chair

_____
Professor R. Scott Lokey

_____
Professor Glenn L. Millhauser

_____
Quentin Williams
Acting Vice Provost and Dean of Graduate Studies

TABLE OF CONTENTS

Page

LIST OF FIGURES

Page

ABSTRACT

APPLYING MOLECULAR CHIRALITY TOOLS TO AMYLOID β AND ALZHEIMER'S DISEASE

Luis Alejandro Rodríguez Foley

Protein misfolding and amyloid formation is associated with several disorders, including type II diabetes (T2D), Alzheimer's disease (AD) and Parkinson's disease (PD). While these diseases are some of the most common and costly pathologies in the modern world, effective treatments to prevent and reverse them are still lacking. There is an urgent unmet need for novel approaches to understand the molecular mechanisms driving these diseases and to develop therapeutic strategies to prevent and stop these pathological processes.

A common mechanistic feature of protein misfolding disorders is a complex aggregation pathway that leads to the fibrillar state, where multiple, rapid-interconverting aggregation intermediates, i.e. oligomeric species, are generated upon the self-association of unfolded or partially folded conformations. These transient oligomeric entities are thought to be the most toxic species during the aggregation cascade. Nonetheless, oligomers are exceedingly difficult to target therapeutically due to their heterogeneous and dynamic nature, and thus classical structure-activity relationships are exceedingly hard to determine and to implement in drug design.

One of the most prominent characteristics of AD pathology is the deposition of amyloid fibrils of the amyloid β (Aβ) peptide in brain tissue. Aβ is an intrinsically disordered peptide, majorly consisting of 40-42 amino acids, and its assembly into oligomers and amyloid fibrils is thought to lead to the development of AD. The molecular mechanisms by which Aβ oligomerizes and interacts with the cellular environment are still not fully understood. The work performed in this thesis aims to provide

new insights into these mechanisms using molecular chirality as the main mechanistic tool, and combined techniques ranging from chemical synthesis to biophysics and cellular assays.

In Chapter 2, we designed a focused chiral mutant library (FCML) of Aβ, and identified several point D-substitutions that allowed us to modulate Aβ aggregation propensity and biological activity. Surprisingly, the reduced propensity towards aggregation and the stabilization of oligomeric intermediates did not always correlate with an increase in toxicity. This directly challenges the current working hypothesis of AD research, where these soluble aggregation intermediates are thought to represent the most neurotoxic species of Aβ. Additionally, we found that the subtle L-Ser26 to D-Ser26 mutation (S26s) led to reduced fibril formation propensity and inhibited toxicity, which appears to be related to the resultant peptide's lack of ability to adopt a fibril-seeding conformations based on NMR and DFT results.

In Chapter 3, we employed mirror-image Aβ as a strategy to enhance fibril formation and prevent oligomer formation of the Aβ peptide. This was accompanied by an almost complete abolishment of toxicity, setting one of the few examples of enhancing aggregation as an alternative approach to inhibit Aβ toxicity. Furthermore, we determined that the non-aggregating segment comprising amino acids 1-30 of Aβ, i.e., Aβ(1-30), is taken up by cells in a stereoselective fashion (about 3-fold difference), and found Aβ(1-30) cellular internalization to depend on cellular prion protein PrP^C in the cellular membrane. To the best of our knowledge, this is the first time that Aβ aggregation and its cellular, receptor-mediated neuronal uptake have been disentangled.

The work performed in this thesis highlight how chirality can be a powerful tool for studying Aβ structure-activity relationships. Additionally, the concepts presented here should be broadly applicable to study many other amyloidogenic proteins and peptides

ACKNOWLEDGEMENTS

Completing this thesis would have not been possible without the support of many people at University of California Santa Cruz (UCSC), including friends, departmental staff, and mentors, who have accompanied me over the past 5 years and supported me with everything that I needed to complete my degree. I am also grateful and fortunate that my research and training as a graduate student was funded by several institutions, such as UCSC the National Institutes of Health (NIH), and the Society for Advancement of Chicanos/Hispanics & Native Americans in Science (SACNAS).

I wish to start by thanking my advisor, Prof. Jevgenij Raskatov. His passion and dedication to science has been a major driving force in my progression as a scientist, and has led me to academic and scientific-publishing achievements that I could hardly had foreseen when I was starting my PhD. He has been an excellent research mentor and also an excellent educator, who taught me how to become an independent researcher at every possible level; from writing manuscripts and fellowships and designing experiments, to how to become a Doctor of Philosophy *per se* and train brain and thoughts to thrive in the times that we live in. I would also like to thank all my colleagues in the Raskatov laboratory. Dr. Christopher Warner and Dr. Subrata Dutta were incredible mentors who were always supportive and willing to help me, and who introduced me to almost all the techniques that I later applied in my research projects. I was also very lucky for having shared my stay in the Raskatov laboratory with lab mates that contributed to a friendly and supportive environment: Graduate students Tommy Finn, Ariel Kuhn, and Ka Chan, and undergraduate and post-graduate students Diana Lucas-Baca, Timothy Kung, and Amanda Smart, who were very dedicated mentees and whose work had a significant positive impact in my research.

I am also very grateful for an outstanding thesis committee. I thank Prof. Scott Lokey and Prof. Glenn Millhauser for their continuous critical feedback on my progress as a PhD student, for their support and active involvement in my research projects, and for the letters of recommendation for my post-graduate applications. Also, I want to thank outside committee member Prof. Annelise Barron

(Stanford University) for always being very supportive and passionate about my work. Additional thanks to Prof. David Kliger, who served as replacement committee member for my second-year seminar.

Additionally, I wish to extend my gratitude to my past mentors, who had a pivotal role on my being able to attend UCSC to conduct my PhD studies. As an undergraduate student, I was awarded an Erasmus Scholarship and I had the opportunity to study a year abroad in France. There, I joined Prof. Alain Burger's lab at the University of Nice Sophia-Antipolis, where I conducted research on the chemical synthesis of bioactive molecules. This was my first experience in an organic research laboratory and what I learnt there ignited my interest and started my path in organic synthesis. The following year, I joined Prof. Enrique Oltra's laboratory at the University of Granada (Spain). Prof. Oltra gave me the opportunity to work on the total synthesis of natural products, which resulted in a co-authorship publication, and in a laboratory experience that had a major influence on my future achievements. Once I finished my Degree in Chemistry in Spain, I moved to the USA. Wishing to perform disease-oriented research and to learn new biomedical techniques, I volunteered as a research assistant for four months in Dr. Marshall Summar's laboratory at Children's National Medical Center in Washington, D.C, where I worked with Dr. Juan Cabrera Luque. His support was crucial in the launching of my career as a scientist in the USA. Shortly after, I obtained a NIH Cancer Research Training Award to work in Dr. Kirk Gustafson's natural products chemistry group at the National Cancer Institute, and although not for the originally intended reasons, it is mostly thanks to him that I ended at UCSC.

Although not "official" mentors, I have been very fortunate to cross paths with outstanding individuals who have had a very important role on my progression as a scientist. I want to thank Dr. Rafael Lucena (soon to be Prof. Rafael Lucena) and Dr. Maria Alcaide for their friendship and mentorship. Your guidance, support, and advise over these years have been incredibly valuable. I miss visiting you in your lab to talk about anything. I am also very grateful for having had Yulianna Ortega and Prof. Melissa Jurica as additional mentors from the UCSC STEM Diversity programs. Thank you very much for all your community building activities, and for your much-needed support during my last years of graduate school. Also, thanks to program staff Xingci Situ and Daniela Bolanos for all your help

and behind-the-scenes work. Special thanks to Yulianna Ortega for hosting my thesis defense celebration in her house with amazing food, cake, and drinks! I also consider as mentors and friends Dr. Matthew Naylor, Dr. Angel Resendez, Dr. Jorge Jimenez, and Dr. Miguel Pinto, who not only shared fun times with me but also served as role models on how to succeed in graduate school. It would have definitely been much harder without your help. I am also thankful to many friends who accompanied me during this time: Dr. Evan Vickers, Dr. Graham Roseman, Dr. Longbo Li, Dr. Tianyi Kou, Dr. Michael Roders, and soon to be doctors: Rene Mercado, Amanda Brambila, Tannia Lau, Francisco Mendez, Oscar Fernandez, David Delgadillo, Gustavo Chata, A'Lester Allen, Gabriella Amberchan, and Kevin Schilling.

The amazing and dedicated support of UCSC staff and personnel have been instrumental for my projects. Dr. Eefei Chen and Prof. Dave Kliger were always available to help me with the photo-crosslinking and spectroscopy experiments, and Dr. Jack Lee's expertise was crucial to help me obtain insightful NMR data for my projects. Dr. Ben Abrams spent many hours teaching me how to use the EM and confocal microscopes, and he always provided thoughtful insights for experimental design and data analysis. At the same time, I am very grateful to Bari Holm for taking care of the cell culture facilities and for running all the flow cytometry experiments with me. In addition, I wish to thank the collaborators that I have had over the years and who have helped me to improve my research projects: Prof. Marco Rolandi and graduate student Manping Jia for their help with the atomic force microscope, and Dr. Asa Hatami for his help with the antibodies work. Besides experiments, I also want to thank Prof. Carrie Partch and David States for revising my grant applications, and Prof. Michele Vendruscolo (University of Cambridge) and Prof. David Teplow (University of California Los Angeles) for their critical feedback during my manuscripts' preparation stage.

The work performed here was carried forward thanks to several funding institutions. I thank the University of California for the Regents Fellowship and for the President's Dissertation Year Fellowship, UCSC Graduate Association for the travel scholarships, and the UCSC Women's Club for the STARS Scholarship. I also thank SACNAS for the two travel scholarships to attend and present my work at its

national conferences, and the NIH for the IMSD fellowship. My gratitude as well to the NIH and UCSC for funding my advisor Prof. Jevgenij Raskatov, which allowed me to carry my research projects.

And lastly, but most importantly, I am really grateful for the unconditional support that I have received from my family. I have been blessed by having them support every decision that I made, even when every one of them took me millions of steps further away from home. But I was never alone in this journey. I was fortunate enough to have my amazing wife, Irene, with me every step of the way., Her company provided me with the energy and motivation that I needed. Thanks to my parents, Pedro and Marisa, and grandparents, Luis, Maria, Donald, and Carmen, for always letting me make my own decisions and for believing that I can achieve anything that I set my mind to. Thanks to my siblings, cousins, and parents-in-law for their continuous support, and to my uncles and aunts who welcomed me in their homes when I moved to the USA. This would not have been possible without you all.

The text of this dissertation includes reprints of the following previously published material:[Warner, Christopher JA, Subrata Dutta, Alejandro R. Foley, and Jevgenij A. Raskatov. "Introduction of d-Glutamate at a Critical Residue of Aβ42 Stabilizes a Prefibrillary Aggregate with Enhanced Toxicity." Chemistry (Weinheim an der Bergstrasse, Germany) 22, no. 34 (2016): 11967; Warner, Christopher JA, Subrata Dutta, Alejandro R. Foley, Eefei Chen, David S. Kliger, and Jevgenij A. Raskatov. "Using chiral peptide substitutions to probe the structure function relationship of a key residue of Aβ42." Chirality 29, no. 1 (2017): 5-9; Dutta, Subrata, Alejandro R. Foley, Christopher JA Warner, Xiaolin Zhang, Marco Rolandi, Benjamin Abrams, and Jevgenij A. Raskatov. "Suppression of Oligomer Formation and Formation of Non-Toxic Fibrils upon Addition of Mirror-Image Aβ42 to the Natural l-Enantiomer." Angewandte Chemie 129, no. 38 (2017): 11664-11668; Foley, Alejandro R., and Jevgenij A. Raskatov. "A DFT-assisted topological analysis of four polymorphic, S-shaped Aβ42 fibril structures." Chembiochem: a European journal of chemical biology 20, no. 13 (2019): 1722; Foley, Alejandro R., Thomas S. Finn, Timothy Kung, Asa Hatami, Hsiau-Wei Lee, Manping Jia, Marco Rolandi, and Jevgenij A. Raskatov. "Trapping and Characterization of Nontoxic Aβ42 Aggregation Intermediates." ACS chemical neuroscience 10, no. 8 (2019): 3880-3887; Dutta, Subrata, Alejandro R. Foley, Ariel J. Kuhn,

Benjamin Abrams, Hsiau-Wei Lee, and Jevgenij A. Raskatov. "New insights into differential aggregation of enantiomerically pure and racemic Aβ40 systems." Peptide Science 111, no. 6 (2019): e24139; Foley, Alejandro R., Hsiau-Wei Lee, and Jevgenij A. Raskatov. "A Focused Chiral Mutant Library of the Amyloid β 42 Central Electrostatic Cluster as a Tool To Stabilize Aggregation Intermediates." The Journal of Organic Chemistry 85, no. 3 (2019): 1385-1391; Foley, Alejandro R., and Jevgenij A. Raskatov. "Assessing Reproducibility in Amyloid β Research: Impact of Aβ Sources on Experimental Outcomes." ChemBioChem (2020);Foley, Alejandro R., Graham P. Roseman, Ka Chan, Amanda Smart, Thomas S. Finn, Kevin Yang, R. Scott Lokey, Glenn L. Millhauser, and Jevgenij A. Raskatov. "Evidence for aggregation-independent, PrPC-mediated Aβ cellular internalization." Proceedings of the National Academy of Sciences (2020);].The co-authors listed in these publications [Jevgenij A. Raskatov, R. Scott Lokey, Glenn L. Millhauser] directed and supervised the research which forms the basis for the dissertation. I acknowledge the permission from the co-authors and copyright holders giving their approval for the material to be used in this dissertation, and I also acknowledge the contributions of all co-authors to the publications.

DEDICATION

To my family.

CHAPTER 1:

Introduction

The phenomenon of protein misfolding and amyloid formation is associated with over fifty different disorders, including Alzheimer's disease (AD), Parkinson's disease (PD), and type II diabetes (T2D.(1, 2) In this pathologies, abnormal aggregates of specific proteins are found in the affected organs, such as amyloid β (Aβ) protein aggregates in brain tissue of AD patients,(3) α-synuclein (α-syn) protein aggregates in brain tissue of PD patients,(4) and human islet amyloid polypeptide aggregates (hIAPP) in patients suffering from T2D.(5) Due to their unstructured nature, these proteins/peptides are classified as intrinsically disordered proteins (IDPs). Unlike proteins with a defined three-dimensional structure, IDPs do not have a well-defined native state.(6). Rather, IDPs have a relatively flat energy landscape, with low energy barriers that facilitate the coexistence of a vast array of aggregation intermediates, ranging from monomers to oligomeric and protofibrillar structures.(7, 8) Ultimately, these intermediates aggregate into insoluble fibrillar assemblies with β-sheet structure,(9, 10) which are thought to be the most thermodynamically stable state.(11–13)

A common mechanistic feature of protein misfolding and amyloidogenic diseases is the conception that the aggregation process causes a detrimental effect on surrounding cellular tissue, ultimately leading cell dysfunction and death.(2, 14) While amyloid fibrils have been shown to be cytotoxic and were originally thought to be the most toxic species in amyloidogenic diseases,(15, 16) current models suggest that oligomeric intermediates are the most toxic entities in the aggregation cascade.(14, 17–20) From a structural point, high-resolution fibril structures of amyloidogenic proteins are progressively becoming more available,(21–26) however, although important advances on the structural nature of oligomeric intermediates have been made,(27–33) obtaining structure-activity relationships of these oligomers still represents a challenge due to their heterogeneous and dynamic nature.

AD is the most prevalent amyloid disease, and also the most common neurodegenerative disorder, with nearly 50 million people currently suffering from AD or related dementia, and with an estimated world population count of 131 million affected by 2050.(34) AD was first reported in 1906 by Dr. Alois Alzheimer, who had identified abundant neuritic plaques and a neurofibrillary tangles in

the *post-mortem* brain of Auguste Deter, a patient suffering dementia and cognitive disfunction.(35) As observed in the brain, this pathology was also accompanied by a remarkable brain tissue loss in diseased patients compared to healthy individuals (Figure 1).

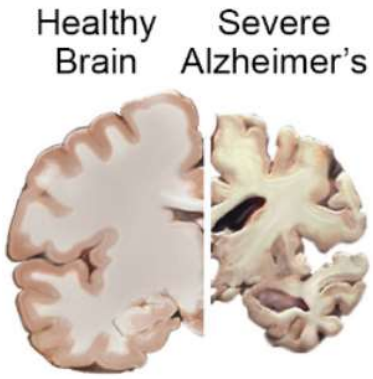

Figure 1. Brain deterioration in AD.. Healthy individual (left) vs AD brain (right). Source: National Institute on Aging.

However, it was not until 1984 when researchers G. Glenner and C. Wong identified "a novel cerebrovascular amyloid protein" in diseased AD patients brains, which was termed amyloid β (Aβ).(36) More than a hundred years later from their initial discovery, and with over four hundred failed clinical trials,(37) a cure for AD remains elusive, and over 100 agents are currently active in clinical trials for Alzheimer's disease (AD) (source: clinicaltrials.gov). From these, 96 target disease modification, from which 40% are focused on Aβ.(34) Nowadays, it is known that Aβ is an intrinsically disordered, majorly 39-43 amino acid long peptide produced upon the proteolytic cleavage of the amyloid precursor protein (APP) and the majority component of amyloid plaques.(38) Initial hypotheses, such as the amyloid cascade hypothesis, pointed to amyloid fibrils as the seminal etiological agent of the disease,(39, 40) however, it is now believed that Aβ soluble intermediates, i.e. oligomers, represent the most toxic entities during the amyloid aggregation cascade.(18, 41, 42) Unfortunately, the lack of mechanistic and structural information on Aβ oligomers limits the development of therapies to treat AD. Thus, a better understanding of the structure and molecular mechanisms underlying Aβ oligomer and fibril formation in *in vitro* and *in vivo* settings are needed to deepen our knowledge of AD progression. To this end,

developing new tools to modulate Aβ aggregation, stabilize aggregation intermediates, and determine how the latter interact with cellular environments, are of great relevance for improving our understanding of the molecular mechanisms underlying AD.

Thesis outline and objectives

This thesis focuses on determining the molecular mechanisms driving Aβ aggregation and neurotoxicity. The objective of the work presented in this thesis is to obtain novel molecular-level information of Aβ neurotoxic intermediates and to understand how these species interact with the cellular environment. Creating new knowledge of the structure-function relationships of these species will allow the rational design of new therapeutic approaches to prevent AD.

As an overall theme in this thesis, the use of strategies based on fundamental concepts of molecular chirality offers important advantages to study amyloidogenic systems. The rationale for this approach is further extended in Chapter 2 introduction. Adopting this strategy was possible due to the approach followed in this thesis. The work performed here combines three areas of research: chemical synthesis, biophysics, and cellular biology. This cross-disciplinary approach has provided me the necessary means to stablish a solid and systematic understanding of the structure-function properties of Aβ.

Chemical synthesis: Each of the research projects associated with my dissertation begin with the solid-phase peptide synthesis of Aβ, offering the opportunity to introduce point D-amino acid mutations (or full-length D-Aβ) into the Aβ sequence. Additionally, it also allows for introducing fluorescent tags at the N-terminus of the rein-peptides. The peptides are then purified by reverse-phase high performance liquid chromatography (HPLC) to afford peptides with purities exceeding 95% purity. This is of seminal importance for the Aβ research given the issues with cross-laboratory reproducibility usually observed in this field. This important point is further addressed in the reprinted manuscript included in this chapter (Foley et al. *ChemBioChem* 2020).

Biophysics: Next, a biophysical characterization of these peptides is performed, including studying the kinetics of aggregation and fibril formation by fluorescence assays and CD spectroscopy, the size and morphology of the newly generated structures by electron microscopy, and atomic force

microscopy, and the atomic-level interactions that arise in these new structures by nuclear magnetic resonance, and density functional theory computational analysis (performed by Prof. Raskatov).

Cellular biology: Finally, to obtain structure-activity relationships of the Aβ system, we investigate how the Aβ peptides induce cellular toxicity in model cell lines, as well as measuring differences in the cellular uptake by flow cytometry and confocal microscopy. Combining results from biophysical and biological studies allowed to identify key regions and amino acids that modulate Aβ structure-function properties, offering novel information that can be exploited by novel therapies to attenuate Aβ aggregation and toxicity.

Applying this approach in different ways has allowed to stabilize and characterize Aβ aggregation intermediates though the use of chiral mutant libraries of the Aβ peptide (Chapter 2), and provided with key mechanistic structural insights into Aβ aggregation and toxicity and its interaction with cellular environments and cellular receptors (Chapter 3).

ChemBioChem

Viewpoint
doi.org/10.1002/cbic.202000125

Assessing Reproducibility in Amyloid β Research: Impact of Aβ Sources on Experimental Outcomes

Alejandro R. Foley[a] and Jevgenij A. Raskatov*[a]

The difficulty of synthesizing and purifying the amyloid β (Aβ) peptide, combined with its high aggregation propensity and low solubility under physiological conditions, leads to a wide variety of experimental results from kinetic assays to biological activity. Thus, it becomes challenging to reproduce outcomes, and this limits our ability to rely on reported results as the foundation for new research. This article examines variability of the Aβ peptide from different sources, comparing purity, and oligomer and fibril formation propensity side by side. The results highlight the importance of performing rigorous controls so that meaningful biophysical, biochemical, and neurobiological results can be obtained to improve our understanding on Aβ.

Introduction

One of the main characteristic features in Alzheimer's disease (AD) is the presence of amyloid plaques in the brain, as discovered by Dr. Alois Alzheimer in 1906 when examining the postmortem brain of Auguste Deter, a patient who suffered from dementia and memory loss.[1] However, it was not until 78 years later when the amyloid β (Aβ) peptide, the predominant component of the amyloid plaques, was first identified and characterized by Glenner and Wong.[2] Advances in the field have been made since then. In 1991, Cotman et al.[3] linked *in vitro* Aβ aggregation to neurotoxicity, and the amyloid cascade hypothesis was postulated as the driving force for AD model (Hardy and Higgins, Selkoe),[4,5] stating that the aggregation process of Aβ into fibrils was the seminal etiological agent of the disease. At the same time, it was observed that Aβ was produced by normal metabolic activity on cells,[6] showing that the production of Aβ is not only associated to AD patients exclusively. In fact, reports have shown that picomolar concentrations of Aβ have positive long-term potentiation (LTP) modulation effects.[7]

Since the amyloid cascade hypothesis was first postulated, the quantity of manuscripts published on Aβ has been exponentially increasing (Figure 1A). While initial research focused on amyloid fibrils and plaques as the main disease culprit, the field has evolved during the past two decades towards the consensus that soluble aggregation intermediates, commonly referred to as *oligomers*, represent the most neurotoxic agents.[8–10] This represented a shift towards a more complex mechanism, where a vast number of oligomers may aggregate in several pathways, generating an equilibrium of multiple transient conformations and different molecular sizes,[11] with each oligomerization state potentially contributing to neurodegeneration to a different degree.[12,13] Aβ oligomers have been reported to adopt ring,[14,15] annular,[16] spherical,[17] or β-barrel[18] structures, and the number of Aβ subunits in these metastable intermediates is also important. For example, Aβ dimers from AD brains are thought to be the minimal synaptotoxic oligomeric species,[19,20] and dodecameric units termed as Aβ*56 are associated to memory impairment in 3xTg-AD transgenic mice.[21] Aβ protofibrils, defined as short, curved fibrils with molecular weight $>$100,000 (one hundred thousand) kDa and $<$200 nm length,[22] also seem to have an important role in patients carrying the "Arctic" familial mutation.[23] These oligomeric intermediates are thought to assemble in different pathways, and are often termed as "on pathway" and "off pathway" depending whether or not they lead to fibril formation.[24,25] The mechanism by which they aggregate into fibrils also depends on the nucleation type, with elongation, primary nucleation, and secondary nucleation as principal mechanisms of fibril formation,[26] being the latter considered to be the most relevant for the proliferation of neurotoxic species.[27] It is therefore not surprising to observe structural variability in published high-resolution Aβ40[28] and Aβ42 fibrils.[29–34] Recent findings even suggest that Aβ fibrils could even act as protective reservoirs against toxic Aβ oligomers[35,36] and enhancing Aβ aggregation was established as a strategy to reduce Aβ toxic effects.[37–39]

In February 2020, a search in *Web of Science* using the words "amyloid beta" found 69010 documents, "amyloid beta aggregation" resulted in 12715 documents, and "amyloid beta toxicity" found 6684 documents. With such a vast amount of literature on a very diverse spectrum of research areas (Figure 1B), one should expect that the biophysical, biochemical, and biological properties of the Aβ peptide should be well-defined, and therefore adopted by new researchers to build new hypotheses and improve the understanding of Aβ aggregation and toxic actions. However, an insufficient level of rigor often impairs the possibilities of using this new knowledge to produce significant contributions and generate reproducible results that could be compared across different laboratories.[40,41] Although efforts have been made to classify the multiple

[a] *A. R. Foley, Prof. Dr. J. A. Raskatov*
Department of Chemistry and Biochemistry
University of California Santa Cruz
1156 High Street, Santa Cruz, CA 95064 (USA)
E-mail: jraskato@ucsc.edu

aggregation intermediates and structures that Aβ can generate, that is, by Glabe,[13] strikingly, as summarized by Teplow,[40] the Aβ field even suffers from not having a precise and systematic nomenclature, where usual terms such as *oligomers*, *protofibrils*, *on-pathway species*, or *off-pathway species*, among others, can have a different meaning depending on who writes about it.

Sources of Aβ

Although Aβ is known for its problems with batch-to-batch reproducibility,[42,43] very little of this aspect is shown in published manuscripts, where sometimes, the employed Aβ material is ambiguously defined or insufficiently characterized. Obtaining Aβ from commercial sources might lead to the assumption that the peptide should have the expected physicochemical and biological properties, such as propensity to form oligomers and fibrils, and the ability to elicit toxic actions in cellular cultures and neuronal networks. However, because not all laboratories can check the ability of the peptide to form oligomers and fibrils before starting the experiments, assumptions are made about its properties based on reported literature. This fact is exemplified in Figure 2, where HPLC and mass spectrometry traces from two different commercial sources of Aβ42 are shown, and compared with peptide from our laboratory. The traces obtained for commercial Aβ – sold as >95% purity – analyzed under the exact same conditions of our laboratory synthesized and characterized Aβ[38] is evidentially different, with Aβ from commercial source 1 displaying substantially lower purity by HPLC and mass spectrometry. Additionally, thioflavin T (ThT) kinetic assays and photo-induced crosslinking experiments were performed on these samples to show how peptide purity and quality can also influence aggregation kinetics and oligomerization propensity (Figure 3). While Aβ42 from commercial source 2 is comparable with our laboratory Aβ42 preparation, the Aβ42 sample obtained from commercial source 1 shows minimal aggregation propensity when monitored by ThT (Figure 3A–C). This difference is also reflected in the ability of the peptides to form low-order oligomers when subjected to photo-induced crosslinking, where laboratory and commercial Aβ42 sources show oligomerization profiles similar to previously described by other laboratories,[10] but with commercial source 1 displaying almost no oligomer formation. It is therefore not surprising that different commercial sources of Aβ might lead to morphologically different Aβ structures,[14] and ultimately to distinct peptide properties and experiment conclusions that might be limited to a single Aβ preparation. Thus, it is advisable to check that Aβ samples pass baseline quality standards before starting to use it for experiments, such as ensuring peptide purity and its ability to aggregate into oligomers and fibrils. An additional factor to consider is the use of synthetic or recombinant sources of Aβ, where studies have shown that recombinant sources are more neurotoxic and aggregate faster,[44,45] a difference that could be arising from the distinct structures that the peptides might adopt or due to the nature of the contaminants and impurities obtained from each source.

Variability on aggregation and toxicity profiles

Even at trace levels, impurities can have a profound effect on the aggregation and toxicity properties of Aβ.[45] These impurities might not only originate from synthesis or expression, but also from widely adopted Aβ pre-treatments. For example, acidic pretreatment with 1,1,1,3,3,3-hexafluoropropan-2-ol (HFIP) or trifluoroacetic acid (TFA), commonly employed to de-aggregate Aβ samples, can lead to increased toxicity of Aβ,[46] and it also can modify the aggregation propensity, stability, and morphology of the peptide.[47] In a similar way, high-pH pre-treatment like NaOH can lead to amino acid epimerization,[48] which can also drastically change the aggregation and biological activity of Aβ.[49–51] With such many variables, it is not surprising to find reports with fibril formation kinetic assays varying from minutes to days, and cytotoxicity values ranging from low-nanomolar to micromolar ranges in model cell lines. *In vivo* studies in rats show that Aβ oligomers can have negative hippocampal LTP modulation effects at nanomolar concentrations.[52] However, Aβ concentrations used in *in vitro* cytotoxicity experiments are typically within the micro-

Alejandro Rodriguez Foley obtained his B.S. in Chemistry at University of Sevilla (Spain). He is currently a PhD candidate in organic chemistry in J.A.R.'s laboratory. His research lies at the interface of chemistry and biology, specifically studying amyloid β aggregation and neurotoxicity through biochemical, biophysical, and biological approaches. His scientific interests include peptide and protein chemistry and the application of fundamental chemistry concepts to biomedical research.

Jevgenij Raskatov received his Diplom from Heidelberg University before moving to Oxford to study with Prof. John Brown, FRS (2006–2009). He subsequently received a Feodor von Lynen postdoctoral fellowship from the Alexander von Humboldt foundation to study DNA-binding Py–Im polyamides with Prof. Peter Dervan (2009–2014). The Raskatov lab uses a chemical neuroscience approach that combines peptide synthesis with biological techniques, using chirality as a unique probe of structure and function of Alzheimer's Aβ and recently developed Aβ chiral inactivation as a molecular approach to converting toxic natural "all-L" Aβ oligomers to nontoxic "all-D" fibrils using mirror-image Aβ as the structural converter.

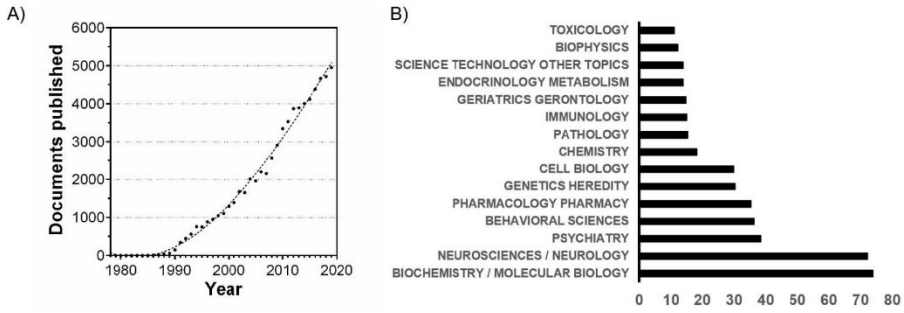

Figure 1. Document search using "amyloid beta" as keywords. The search did not exclude results related to amyloid precursor protein (APP). A) Documents published per year using "amyloid beta" as keywords. Datapoints are fit with a cubic polynomial curve ($R^2 = 0.994$). B) Percentage of 69 010 documents organized by research areas. Note that some areas may overlap. Source: Web of Science.

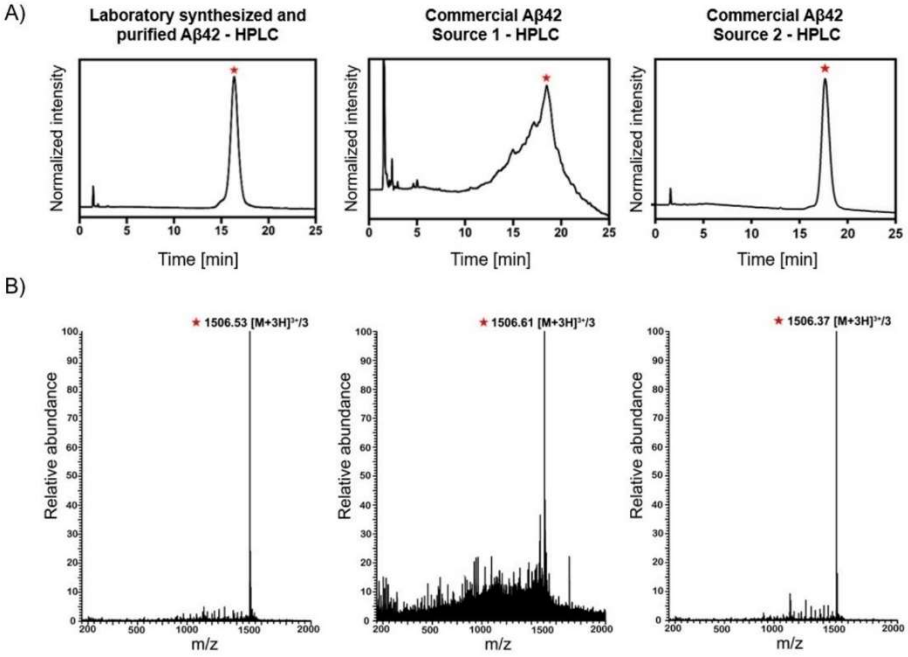

Figure 2. A) HPLC traces of different sources of Aβ42. Commercial Aβ42 source 1: AAPPTec. Commercial Aβ42 source 2: AnaSpec. B) Linear trap quadrupole (LTQ) mass spectra of different sources of Aβ42, analyzed at the same sample concentration (1 mg/mL). Asterisks: target Aβ42 peak.

molar range.[37,53,54] Furthermore, Aβ has different cytotoxic activity depending on the cell type,[55] cell confluence,[56] and cell differentiation.[57] Because Aβ binding to cellular membranes is thought to play a critical role in Aβ aggregation and toxicity,[58,59] these disparities could be a consequence of the distinct interaction of Aβ with cells having different membrane

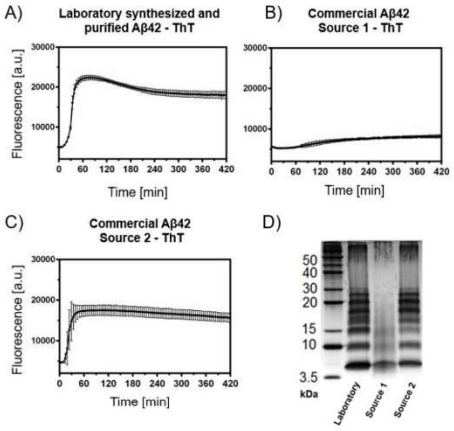

Figure 3. Aggregation and oligomerization propensity of distinct Aβ42 sources. Commercial Aβ42 source 1: AAPPTec. Commercial Aβ42 source 2: AnaSpec. (A–C) ThT-monitored aggregation kinetics at 37 °C and continuous shaking of different Aβ42 sources. Peptide concentration and ThT concentration was 20 μM in all cases. D) Oligomerization propensity analyzed by PICUP at 20 μM concentration of each Aβ42 source. After crosslinking, samples were subjected to SDS–PAGE and developed by silver staining.

lipid composition. For example, while specific interactions between Aβ and phosphatidylethanolamine monolayers are limited,[60] incorporation of polar and negatively charged phospholipids leads to increased electrostatic interactions that can template Aβ aggregation by inducing β-sheet conformation.[61,62] The nature of Aβ oligomers is also important, since non-fibrillary oligomers have been observed to cause macroscale membrane deformations in model lipid monolayers, while fibrillary oligomers induce membrane thinning and instability.[63] These are significant factors to consider as membrane poration and formation of calcium channels are thought to play a relevant role in Aβ toxicity.[64,65] Thus, Aβ reproducibility and variability issues do not only have a direct impact on the results itself, but it can also be one of the reasons why drugs against Aβ are not as efficient when tested in clinical trials.[66] As of July 2019, there were 38 amyloid-related ongoing trials,[67] with previous 23 amyloid-related drugs discontinued (source: Alzforum), and recent news of 2 new failures: Phase II/III study of solanezumab (Lilly) and gantenerumab (Roche/Genentech).

Improving consistency and reproducibility

Aβ research is frequently conducted in *phenomenological* fashion, describing observations of Aβ behavior without assessing robustness or reproducibility of the work; do the observed trends endure through different Aβ batches and show the same results by orthogonal techniques? In many cases of published work, the Aβ source either remains constant for the whole study (e.g., Aβ is always used from the same seller), or it is unspecified (e.g., if synthetic Aβ was used, did it all come from the same synthetic batch or from different batches?). While using a unique source could provide meaningful and valid results if the system is well-characterized, it might not ensure that other laboratories would be able to reproduce them. How does one then make sure that the obtained results are reproducible? From the commercial and the synthetic perspective, reproducing key results with Aβ from more than one seller, or with more than one synthetic batch, might ensure that results are reliable and reproducible by other laboratories. While there will always be some batch-to-batch variations, key and distinct findings must be consistent between batches.[43,51] This is not uncommon in other fields, for example, in medicinal chemistry, where "hits" obtained from screening assays are typically validated in a multifunctional process.[68]

Conclusions

To date, almost 70000 documents have been published on Aβ research, with this number increasing year by year. However, the intricate properties of Aβ and the varied methodologies and sources commonly used to work with this peptide make it challenging to obtain reliable and reproducible results. Here, our goal was to emphasize the influence that different Aβ sources can have over experiments' outcomes, which can ultimately lead to unreproducible or unrepresentative results. Thus, it becomes very important to ensure that experiments are performed with material that passes certain minimal quality controls. We propose that this baseline should include HPLC, mass spectrometry, and aggregation and oligomerization propensity assays, as well as validating the results by using multiple Aβ batches. Batch-to-batch variations should be regarded as an intrinsic property of Aβ rather than an inconsistency, and reporting these results as part of the manuscript should also become a common practice so researchers know what to expect when attempting to reproduce experiments. This increased diligence will provide with knowledge and results that other laboratories might find easier to adopt, and would help to increase the productivity and efficiency on Aβ research. We believe that more discussion is needed on this topic and hope this manuscript will stimulate such.

Experimental Section

Materials. Laboratory Aβ42 was synthesized by solid-phase Fmoc chemistry on a Liberty Blue CEM peptide synthesizer assisted by a CEM discovery microwave, and purified by reverse-phase HPLC as previously described.[50] Commercial sources of Aβ42 were dissolved in 20 mM NH_4OH aqueous solution, aliquoted, and lyophilized prior to the experiments.

Thioflavin T (ThT) assay. Aβ42 samples were dissolved in 20 mM NaOH (not exceeding 3% volume of NaOH in final dilution amount) and diluted to 20 μM concentration with pH 7.4 1x PBS with 20 μM

ThT. Aβ42 solutions were placed on a black, clear bottom 96-well plate and placed in a Molecular Device Gemini EM fluorescence plate reader to measure fluorescence (λ_{em} = 444 nm, λ_{ex} = 485 nm). Aβ42–ThT solutions were 37°C with continuous shaking and datapoints obtained every 5 minutes.

Photo-induced crosslinking (PICUP) and SDS–PAGE. PICUP experiments were performed as previously described.[50] Briefly, lyophilized Aβ42 samples were dissolved in 20 mM NaOH and diluted in pH 7.4 1x PBS. For the crosslinking reaction, 4 μL of 1 mM $[Ru(bipy)_3]^{2+}$ and 4 μL of 20 mM ammonium persulfate were added to 32 μL of the Aβ42 solutions, and irradiated with light for 1.2 s. The solutions were then quenched with 40 μL of loading buffer with 5% 2-mercaptoethanol. Finally, crosslinked samples were run on 12% tris-tricine polyacrylamide gels and developed by silver staining.

Author Contributions

A.R.F. acquired the data. A.R.F and J.A.R interpreted the data and wrote the manuscript.

Acknowledgements

Authors thank David B. Teplow, Ariel Kuhn and Ka Chan for helpful discussions during manuscript preparation stage. Authors acknowledge AnaSpec Inc. for providing Aβ samples (commercial Aβ42 source 2). J.A.R. and A.R.F. thank the NIH for funding (R21AG058074 and 2R25GM058903-20 IMSD, respectively).

Conflict of Interest

The authors declare no conflict of interest.

[1] A. Alzheimer, *Neurol. Zentralblatt* **1906**, *25*, 1134.
[2] G. G. Glenner, C. W. Wong, *Biochem. Biophys. Res. Commun.* **1984**, *120*, 885–890.
[3] C. J. Pike, A. J. Walencewicz, C. G. Glabe, C. W. Cotman, *Brain Res.* **1991**, *563*, 311–314.
[4] J. A. Hardy, G. A. Higgins, *Science* **1992**, *256*, 184–185.
[5] D. J. Selkoe, *Neuron* **1991**, *6*, 487–498.
[6] C. Haass, M. G. Schlossmacher, A. Y. Hung, C. Vigo-Pelfrey, A. Mellon, B. L. Ostaszewski, I. Lieberburg, E. H. Koo, D. Schenk, D. B. Teplow, D. J. Selkoe, *Nature* **1992**, *359*, 322–325.
[7] D. Puzzo, L. Privitera, E. Leznik, M. Fà, A. Staniszewski, A. Palmeri, O. Arancio, *J. Neurosci.* **2008**, *28*, 14537–14545.
[8] R. Kayed, E. Head, J. L. Thompson, T. M. McIntire, S. C. Milton, C. W. Cotman, C. G. Glabe, *Science* **2003**, *300*, 486–489.
[9] C. Haass, D. J. Selkoe, *Nat. Rev. Mol. Cell Biol.* **2007**, *8*, 101–112.
[10] G. Bitan, M. D. Kirkitadze, A. Lomakin, S. S. Vollers, G. B. Benedek, D. B. Teplow, *Proc. Natl. Acad. Sci. USA* **2003**, *100*, 330–335.
[11] J. A. Raskatov, D. B. Teplow, *Sci. Rep.* **2017**, *7*, 12433.
[12] M. Bucciantini, E. Giannoni, F. Chiti, F. Baroni, N. Taddei, G. Ramponi, C. M. Dobson, M. Stefani, *Nature* **2002**, *416*, 507–511.
[13] C. G. Glabe, *J. Biol. Chem.* **2008**, *283*, 29639–29643.
[14] M. Y. Suvorina, O. M. Selivanova, E. I. Grigorashvili, A. D. Nikulin, V. V. Marchenkov, A. K. Surin, O. V. Galzitskaya, *J. Alzheimer's Dis.* **2015**, *47*, 583–593.
[15] O. V. Galzitskaya, A. K. Surin, A. V. Glyakina, V. V. Rogachevsky, O. M. Selivanova, *J. Alzheimer's Dis. Reports* **2018**, *2*, 181–199.
[16] H. A. Lashuel, D. Hartley, B. M. Petre, T. Walz, P. T. Lansbury, *Nature* **2002**, *418*, 291.
[17] M. Hoshi, M. Sato, S. Matsumoto, A. Noguchi, K. Yasutake, N. Yoshida, K. Sato, *Proc. Natl. Acad. Sci. USA* **2003**, *100*, 6370–6375.
[18] A. Laganowsky, C. Liu, M. R. Sawaya, J. P. Whitelegge, J. Park, M. Zhao, A. Pensalfini, A. B. Soriaga, M. Landau, P. K. Teng, D. Cascio, C. G. Glabe, *Science* **2012**, *335*, 1228–1231.
[19] G. M. Shankar, S. Li, T. H. Mehta, A. Garcia-Munoz, N. E. Shepardson, I. Smith, F. M. Brett, M. A. Farrell, M. J. Rowan, C. A. Lemere, C. M. Regan, D. M. Walsh, B. L. Sabatini, D. J. Selkoe, *Nat. Med.* **2008**, *14*, 837–842.
[20] M. Jin, N. Shepardson, T. Yang, G. Chen, D. Walsh, D. J. Selkoe, *Proc. Natl. Acad. Sci. USA* **2011**, *108*, 5819–5824.
[21] S. Lesné, T. K. Ming, L. Kotilinek, R. Kayed, C. G. Glabe, A. Yang, M. Gallagher, K. H. Ashe, *Nature* **2006**, *440*, 352–357.
[22] D. M. Walsh, D. M. Hartley, Y. Kusumoto, Y. Fezoui, M. M. Condron, A. Lomakin, G. B. Benedek, D. J. Selkoe, D. B. Teplow, *J. Biol. Chem.* **1999**, *274*, 25945–25952.
[23] C. Nilsberth, A. Westlind-Danielsson, C. B. Eckman, M. M. Condron, K. Axelman, C. Forsell, C. Stenh, J. Luthman, D. B. Teplow, S. G. Younkin, J. Naslund, L. Lanfelt, *Nat. Neurosci.* **2001**, *4*, 887–893.
[24] C. Soto, S. Pritzkow, *Nat. Neurosci.* **2018**, *21*, 1332–1340.
[25] J. Schnabel, *Nature* **2011**, *475*, S12–S14.
[26] G. Meisl, X. Yang, E. Hellstrand, B. Frohm, J. B. Kirkegaard, S. I. A. Cohen, C. M. Dobson, S. Linse, T. P. J. Knowles, *Proc. Natl. Acad. Sci. USA* **2014**, *111*, 9384–9389.
[27] D. A. White, E. Hellstrand, S. I. A. Cohen, S. Linse, L. M. Luheshi, L. Rajah, T. P. J. Knowles, M. Vendruscolo, D. E. Otzen, C. M. Dobson, *Proc. Natl. Acad. Sci. USA* **2013**, *110*, 9768–9763.
[28] R. Tycko, *Neuron* **2015**, *86*, 632–645.
[29] T. Lührs, C. Ritter, M. Adrian, D. Riek-Loher, B. Bohrmann, H. Döbeli, D. Schubert, R. Riek, *Proc. Natl. Acad. Sci. USA* **2005**, *102*, 17342–7.
[30] Y. Xiao, B. Ma, D. McElheny, S. Parthasarathy, F. Long, M. Hoshi, R. Nussinov, Y. Ishii, *Nat. Struct. Mol. Biol.* **2015**, *22*, 499–505.
[31] M. T. Colvin, R. Silvers, Q. Z. Ni, T. V. Can, I. Sergeyev, M. Rosay, K. J. Donovan, B. Michael, J. Wall, S. Linse, R. G. Griffin, *J. Am. Chem. Soc.* **2016**, *138*, 9663–9674.
[32] M. A. Wälti, A. Böckmann, B. H. Meier, H. Arai, F. Ravotti, C. G. Glabe, P. Güntert, J. S. Wall, R. Riek, *Proc. Natl. Acad. Sci. USA* **2016**, *113*, E4976–E4984.
[33] L. Gremer, D. Schölzel, C. Schenk, E. Reinartz, J. Labahn, R. B. G. Ravelli, M. Tusche, C. Lopez-Iglesias, W. Hoyer, H. Heise, D. Willbold, G. F. Schroder, *Science* **2017**, *358*, 116–119.
[34] M. Kollmer, W. Close, L. Funk, J. Rasmussen, A. Bsoul, A. Schierhorn, M. Schmidt, C. J. Sigurdson, M. Jucker, M. Fändrich, *Nat. Commun.* **2019**, *10*, 4760.
[35] S. Treusch, D. M. Cyr, S. Lindquist, *Cell Cycle* **2009**, *8*, 1668–1674.
[36] D. J. Selkoe, J. Hardy, *EMBO Mol. Med.* **2016**, *8*, 595–608.
[37] J. Bieschke, M. Herbst, T. Wiglenda, R. P. Friedrich, A. Boeddrich, F. Schiele, D. Kleckers, J. M. Lopez Del Amo, B. A. Grüning, Q. Wang, M. R. Schmidt, R. Lurz, R. Anwyl, S. Schnoegl, M. Fändrich, R. F. Frank, B. Reif, S. Gunther, D. M. Walsh, E. E. Wanker *Nat. Chem. Biol.* **2012**, *8*, 93–101.
[38] S. Dutta, A. R. Foley, C. J. A. Warner, X. Zhang, M. Rolandi, B. Abrams, J. A. Raskatov, *Angew. Chem. Int. Ed.* **2017**, *56*, 11506–11510; *Angew. Chem.* **2017**, *129*, 11664–11668.
[39] R. Limbocker, S. Chia, F. S. Ruggeri, M. Perni, R. Cascella, G. T. Heller, G. Meisl, B. Mannini, J. Habchi, T. C. T. Michaels, P. K. Challa, M. Ahn, S. T. Casford, N. Fernando, C. K. Xu, N. D. Kloss, S. I. A. Cohen, J. R. Kumita, C. Cecchi, M. Zasloff, S. Linse, T. P. J. Knowles, F. Chiti, M. Vendruscolo, C. M. Dobson, *Nat. Commun.* **2019**, *10*, 225.
[40] D. B. Teplow, *Alzheimer's Res. Ther.* **2013**, *5*, 39.
[41] *Nat. Neurosci.* **2011**, *14*, 399.
[42] C. Soto, E. M. Castaño, R. Asok Kumar, R. C. Beavis, B. Frangione, *Neurosci. Lett.* **1995**, *200*, 105–108.
[43] D. B. Teplow, *Methods Enzymol.* **2006**, *413*, 20–33.
[44] V. H. Finder, I. Vodopivec, R. M. Nitsch, R. Glockshuber, *J. Mol. Biol.* **2010**, *396*, 9–18.
[45] D. J. Adams, T. G. Nemkov, J. P. Mayer, W. M. Old, M. H. B. Stowell, *PLoS One* **2017**, *12*, e0182804.
[46] M. I. Lioudyno, M. Broccio, Y. Sokolov, S. Rasool, J. Wu, M. T. Alkire, V. Liu, J. A. Kozak, P. R. Dennison, C. G. Glabe, M. Losche, J. E. Hall, *PLoS One* **2012**, *7*, e35090.
[47] M. R. Nichols, M. A. Moss, D. K. Reed, S. Cratic-McDaniel, J. H. Hoh, T. L. Rosenberry, *J. Biol. Chem.* **2005**, *280*, 2471–2480.
[48] R. Liardon, R. F. Hurrell, *J. Agric. Food Chem.* **1983**, *31*, 432–437.
[49] T. Tomiyama, S. Asano, Y. Furiya, T. Shirasawa, N. Endo, H. Mori, *J. Biol. Chem.* **1994**, *269*, 10205–10208.

[50] C. J. A. Warner, S. Dutta, A. R. Foley, J. A. Raskatov, *Chem. Eur. J.* **2016**, *22*, 11967–11970.
[51] A. R. Foley, T. S. Finn, T. Kung, A. Hatami, H.-W. Lee, M. Jia, M. Rolandi, J. A. Raskatov, *ACS Chem. Neurosci.* **2019**, *10*, 3880–3887.
[52] D. M. Walsh, I. Klyubin, J. V. Fadeeva, W. K. Cullen, R. Anwyl, M. S. Wolfe, M. J. Rowan, D. J. Selkoe, *Nature* **2002**, *416*, 535–539.
[53] K. Ono, M. M. Condron, D. B. Teplow, *Proc. Natl. Acad. Sci. USA* **2009**, *106*, 14745–14750.
[54] I. Kuperstein, K. Broersen, I. Benilova, J. Rozenski, W. Jonckheere, M. Debulpaep, A. Vandersteen, I. Segers-Nolten, K. Van Der Werf, V. Subramaniam, D. Breaken, G. Callewaert, C. Bartic, R. D'Hooge, I. C. Martins, F. Rousseau, J. Schymkowitz, B. De Strooper, *EMBO J.* **2010**, *29*, 3408–3420.
[55] Y. Zhang, R. McLaughlin, C. Goodyer, A. LeBlanc, *J. Cell Biol.* **2002**, *156*, 519–529.
[56] M. Balcells, J. S. Wallins, E. R. Edelman, *Neurosci. Lett.* **2008**, *441*, 319–322.
[57] J. Krishtal, O. Bragina, K. Metsla, P. Palumaa, V. Tõugu, *PLoS One* **2017**, *12*, e0186636.
[58] H. Yamaguchi, M. L. C. Maat-Schieman, S. G. Van Duinen, F. A. Prins, P. Neeskens, R. Natté, R. A. C. Roos, *J. Neuropathol. Exp. Neurol.* **2000**, *59*, 723–732.
[59] S. Jin, N. Kedia, E. Illes-Toth, I. Haralampiev, S. Prisner, A. Herrmann, E. E. Wanker, J. Bieschke, *J. Biol. Chem.* **2016**, *291*, 19590–19606.
[60] E. Maltseva, G. Brezesinski, *ChemPhysChem* **2004**, *5*, 1185–1190.
[61] E. Maltseva, A. Kerth, A. Blume, H. Möhwald, G. Brezesinski, *ChemBioChem* **2005**, *6*, 1817–1824.
[62] E. Y. Chi, C. Ege, A. Winans, J. Majewski, G. Wu, K. Kjaer, K. Y. C. Lee, *Proteins Struct. Funct. Genet.* **2008**, *72*, 1–24.
[63] C. M. Vander Zanden, L. Wampler, I. Bowers, E. B. Watkins, J. Majewski, E. Y. Chi, *Langmuir* **2019**, *35*, 16024–16036.
[64] N. Arispe, E. Rojas, H. B. Pollard, *Proc. Natl. Acad. Sci. USA* **1993**, *90*, 567–571.
[65] R. Kayed, Y. Sokolov, B. Edmonds, T. M. McIntire, S. C. Milton, J. E. Hall, C. G. Glabe, *J. Biol. Chem.* **2004**, *279*, 46363–46366.
[66] A. J. Doig, M. P. Del Castillo-Frias, O. Berthoumieu, B. Tarus, J. Nasica-Labouze, F. Sterpone, P. H. Nguyen, N. M. Hooper, P. Faller, P. Derreumaux, *ACS Chem. Neurosci.* **2017**, *8*, 1435–1437.
[67] J. Cummings, G. Lee, A. Ritter, M. Sabbagh, K. Zhong, *Alzheimer's Dement. Transl. Res. Clin. Interv.* **2019**, *5*, 272–293.
[68] J. P. Hughes, S. S. Rees, S. B. Kalindjian, K. L. Philpott, *Br. J. Pharmacol.* **2011**, *162*, 1239–1249.

Manuscript received: February 29, 2020
Revised manuscript received: April 4, 2020
Accepted manuscript online: April 5, 2020
Version of record online: May 5, 2020

ChemPubSoc Europe

DOI: 10.1002/cbic.201900036

CHEMBIOCHEM Full Papers

A DFT-Assisted Topological Analysis of Four Polymorphic, S-Shaped Aβ42 Fibril Structures

Alejandro R. Foley and Jevgenij A. Raskatov*[a]

Amyloid β 42 (Aβ42) is an inherently disordered peptide, whose toxic actions are believed to play important roles in the etiology of Alzheimer's disease. Four fibril structures of the peptide that display broadly similar characteristics were recently published, but a systematic comparison of these structures is lacking. In this paper, a topological framework was created to enable such understanding and produced new insights into subtle structural elements that underlie the overall structural diversity. A DFT-based analysis illuminated some of the energetic differences that arise as a consequence.

Aβ42 is an aggregation-prone peptide, and its toxic actions are believed to play an important role in the etiology of Alzheimer's disease (AD).[1] The Aβ framework is inherently disordered and, as such, capable of sampling a vast conformational space; this allows it to yield diverse structures in response to minute modifications of the aggregation conditions.[2]

Four Aβ42 fibrillary structures were recently published that share a common S-shaped feature that extends from the central hydrophobic cluster (CHC) ^{17}LVFF^{20} through to the C terminus, thus spanning amino acids 17 through 42.[3] The N-terminal domain of Aβ42 (amino acids 1–16) is flexible, prone to disorder and was only resolved in two of four structures, in contrast the S-shaped fibril core element was observed in all four structures. Although clearly displaying strong structural similarities at the qualitative level, the S-shaped folding elements are different in subtle but significant ways between the four structures (Figure 1 A). The purpose of this paper is to provide a topological framework to enable a more systematic comparison between the four structures and to use density functional theory (DFT)-based approaches to better understand the stabilities of the hydrophobic C-terminal region of the peptide, which is believed to be responsible for the initial steps of Aβ42 folding that leads to its aggregation into fibrils.

The significance of the C-terminal hydrophobic loop formation (loop 2) and its subsequent folding onto the CHC leading to the formation of loop 1 (Figure 1 B, C) has previously been recognized as a key structural event that is needed for the formation of these folded scaffolds.[4] However, an adequate framework within which these assemblies can be compared in a quantitative fashion is lacking.

A straightforward topological framework has been created to enable a systematic comparison of the four S-shaped motifs (extending from L17 to A42) associated with the Aβ42 fibril structures (Figure 2). The hydrophobic side chains of residues 17–20 of CHC form hydrophobic segment LVFF (A) and can be projected into or away from loop 1. This can be represented through a simple 4×2 "chessboard" motif, in which the direction of residue projection is represented by a filled square and the absence of the residue is represented by an open square. Analogously, the I31–I32 segment (B in Figure 2) can project its side chains into loop 1 or loop 2 (a 2×2 chessboard motif), and the segments L34–M35–V36 and V39–V40–I41 (C and D in Figure 2) can project their side chains either into or away from loop 2 (2×3 chessboard motifs).

The four structures were subjected to this topological analysis. The analysis of the chessboard patterns reveals that the most recently obtained structure, PDB ID: 5OQV, is the most distinct one of the four. It shows topological equivalence with 2MXU in segment 3, whereas segments 1, 2, and 4 are different in orientation at at least one of the four residues. There is no topological equivalence, defined in this paper as qualitative identity at the level of the simplified chessboard patterns shown in Figure 2, in any of the four segments when compared with 2NAO and 5KK3, and segment 4 of 5OQV (out-in-out) is fully inverted as compared with the other three structures (in-out-in). The structure 2MXU is topologically equivalent with structures 2NAO and 5KK3 in segments 1, 2, and 4, but different in segment 3 (out-in-out vs. out-out-in); structures 2NAO and 5KK3 are topologically identical. Topological identity is not to be mistaken for the more subtle local conformational differences, which clearly still exist between 5KK3 and 2NAO. None of the four segments shows topological equivalence across all four structures. This is noteworthy, as there is evidence that fibrillar deposits can differ structurally between different AD patients.[5] We believe that our topological framework could provide a helpful tool to facilitate systematic comparison and a deeper molecular-level analysis of such structures.

The formation of loop 2 is believed to be one of the early Aβ42 folding events; this is readily rationalized through its highly hydrophobic nature.[4a,6] The experimentally well-documented, increased Aβ42-fibril-forming propensity at elevated temperatures is likely to arise, at least in part, as a consequence of the loss of hydrophobic hydration of loop 2 upon

[a] A. R. Foley, Prof. J. A. Raskatov
Department of Chemistry and Biochemistry
University of California Santa Cruz
Physical Science Building 356, 1156 High Street, Santa Cruz, CA 95064 (USA)
E-mail: jraskato@ucsc.edu

Supporting information and the ORCID identification numbers for the authors of this article can be found under https://doi.org/10.1002/cbic.201900036.

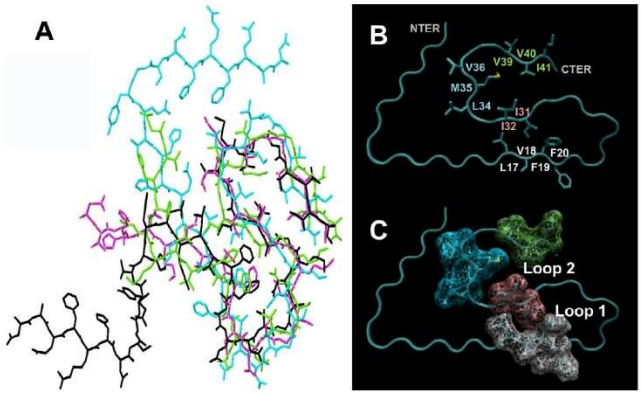

Figure 1. A) Superposition of the four Aβ42 structural motifs found in the structures 5OQV (——), 5KK3 (——), 2MXU (——) and 2NAO (——). B), C) Location of the hydrophobic regions of Aβ42 (5OQV): central hydrophobic cluster (CHC) LVFF; C-terminal loop 2 IIGLMVGGVVIA, with the three hydrophobic segments shown.

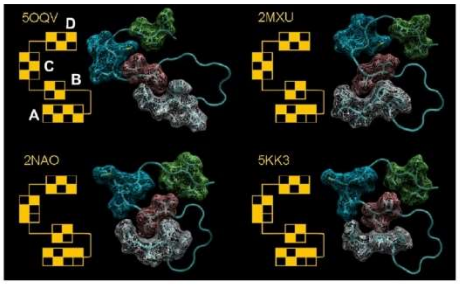

Figure 2. A topological analysis of the four S-shaped fibril core regions of Aβ42 to classify the structures with regard to their similarity. Residues 17–42 are shown with the four hydrophobic segments highlighted by space filling.

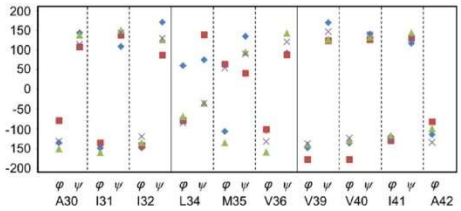

Figure 3. Ramachandran angles for the segments AII, LMV and VVIA from 5OQV (◆), 5KK3 (▲), 2MXU (×) and 2NAO (■).

heating,[2a] although other factors, such as enhanced sampling of fibril-seeding conformers is also likely to contribute.[4c,7]

In an effort to better understand the local conformational differences of loop 2, the Ramachandran angles associated with the three segments were systematically analyzed (Figure 3 and Table 1). A high degree of variance was noted, particularly for the LMV fragment, in which some of the angles covered a range significantly larger than 90° (e.g., $\Delta\psi_{L34}=173.3°$ and $\Delta\phi_{M35}=161.0°$). The values associated with I41, on the other hand, were amongst the most tightly circumscribed ones (Figure 3, see also Figure S1 in the Supporting Information), ranging from $\phi_{I41}=-117.6°$ (5KK3) to $-128.9°$ (2NAO) and $\psi_{I41}=+116.0°$ (5OQV) to $+143.1°$ (5KK3), which is noteworthy because I41 is the key residue that is responsible for structural and functional differences between Aβ42 and its more soluble and less toxic Aβ40 counterpart.[8]

To better understand the energetics of loop 2 of Aβ42 in those four structures, DFT calculations were conducted. For

Table 1. Ramachandran angles for the hydrophobic fragments AII, LMV, and GVVIA of the loop 2 region of Aβ42.

Residue	Angle	5OQV	2NAO	5KK3	2MXU
A30	ϕ	−135.7	−79.1	−150.9	−131.05
	ψ	+143.3	+107.3	+137.3	+114.9
I31	ϕ	−149.2	−135.6	−160.0	−140.85
	ψ	+108.0	+137.7	+149.4	+143.6
I32	ϕ	−148.1	−142.4	−135.3	−119.6
	ψ	+170.2	+86.7	+125.4	+129.3
L34	ϕ	+59.8	−78.8	−68.5	−85.6
	ψ	+74.5	+137.8	−35.5	−35.0
M35	ϕ	−106.4	+63.7	−135.3	+53.6
	ψ	+134.2	+41.4	+93.3	+90.1
V36	ϕ	−103.2	−101.2	−159.0	-132.0
	ψ	+91.2	+88.1	+141.75	+120.1
V39	ϕ	−148.3	−177.5	−139.3	−137.5
	ψ	+168.7	+123.7	+126.1	+146.4
V40	ϕ	−136.3	−127.5	−128.85	−123.2
	ψ	+139.9	+126.4	+132.1	+137.8
I41	ϕ	−119.65	−128.9	−117.6	−128.8
	ψ	+116.0	+130.2	+143.1	+128.7
A42	ϕ	−114.0	−81.3	−100.0	−134.5
	ψ	n.a.	n.a.	n.a.	n.a.

n.a.: not applicable.

this purpose, Aβ42 was truncated after residue 28, and G9 was replaced by an acetyl cap to yield the four singly negatively charged, folded hydrophobic peptides Ac-AIIGLMVGGVVIA, referred to as 5OQV-L2, 2MXU-L2, 2NAO-L2 and 5KK3-L2 (Figure S2). The lack of charge separation in the loop 2 region makes it a system that is particularly well suited for a DFT computational study, in which solvent contribution is modeled through a dielectric continuum, which can lead to issues with multiply charged frameworks, especially if opposite charges are present.[9] The backbone dihedral angles of the four peptides were frozen to remain in the conformations found in fibrils and the rest were optimized. 2MXU-L2 was found to be the most stable of the four conformers ($E_{rel;2MXU\text{-}L2} = 0.0$ kcal mol^{-1}), followed by 2NAO-L2 ($E_{rel;2NAO\text{-}L2} = +3.1$ kcal mol^{-1}), 5KK3-L2 ($E_{rel;5KK3\text{-}L2} = +4.9$ kcal mol^{-1}) and, finally, 5OQV-L2 ($E_{rel;5OQV\text{-}L2} = +9.5$ kcal mol^{-1}), thus establishing that the structural flexibility of the loop 2 region of Aβ42 endows it with the ability to adopt shapes that are structurally sufficiently distinct to cover a rather wide energetic window of ≈10 kcal mol^{-1}. The lower stability of 5OQV-L2 in our DFT calculations might reflective of the fact that organic co-solvent was employed in the protocol that was used to grow Aβ42 fibrils for structural determination in that study.[3d]

The conformational flexibility of the hydrophobic loop 2 region is likely to be one of the key aspects of Aβ42 that underlie the remarkable structural diversity of this peptide. Although the 2MXU-L2 motif has emerged as the most stable one of the four from this computational study, it has to be kept in mind that other, more thermodynamically stable conformational states of loop 2 might exist but not have been reached in any of those structures for kinetic reasons.

Computational Details

All DFT computations were performed with the Gaussian 09 program package[10] by using the M062X functional, which has been recommended for computations of compounds composed of main group elements (such as peptides).[11] All input structures were modified from the deposited PDB datafiles by using the programs Molden and Chemcraft. Solvent (water) was modeled by using the polarizable continuum model (PCM), as implemented in Gaussian 09 ($\varepsilon_r = 78.3553$). Backbone torsion angles were frozen at values found in fibrils, and the rest were optimized at the M062X/6-31G* level of theory. The optimized structures were subsequently subjected to single point calculations at the M062X/6-311++G** level of theory to then rank their relative energies.[12] Coordinate superpositions to generate Figure 1A were performed with the Schrödinger Maestro 2009 program package by simultaneously minimizing the distances of the C_α atoms of amino acids 17–42 in all structures. All geometry-optimized coordinate sets have been deposited as part of the Supporting Information.

Acknowledgements

J.A.R. thanks the UC Santa Cruz for unrestricted access to computational facilities and flexible start-up funds, as well as the NIH for funding (R21AG058074).

Conflict of Interest

The authors declare no conflict of interest.

Keywords: amyloid beta-peptides · foldamers · hydrophobic interactions · topology

[1] a) D. J. Selkoe, J. Hardy, *EMBO Mol. Med.* **2016**, *8*, 595–608; b) F. Chiti, C. M. Dobson, *Annu. Rev. Biochem.* **2006**, *75*, 333–366; c) H. W. Querfurth, F. M. LaFerla, *N. Engl. J. Med.* **2010**, *362*, 329–344.

[2] a) J. A. Raskatov, D. B. Teplow, *Sci. Rep.* **2017**, *7*, 12433; b) D. B. Teplow, *Alzheimers Res. Ther.* **2013**, *5*, 39; c) W. Close, M. Neumann, A. Schmidt, M. Hora, K. Annamalai, M. Schmidt, B. Reif, V. Schmidt, N. Grigorieff, M. Fändrich, *Nat. Commun.* **2018**, *9*, 699.

[3] a) M. A. Wälti, F. Ravotti, H. Arai, C. G. Glabe, J. S. Wall, A. Boeckmann, P. Guentert, B. H. Meier, R. Riek, *Proc. Natl. Acad. Sci. USA* **2016**, *113*, E4976–E4984; b) M. T. Colvin, R. Silvers, Q. Z. Ni, T. V. Can, I. Sergeyev, M. Rosay, K. J. Donovan, B. Michael, J. Wall, S. Linse, R. G. Griffin, *J. Am. Chem. Soc.* **2016**, *138*, 9663–9674; c) Y. Xiao, B. Ma, D. McElheny, S. Parthasarathy, F. Long, M. Hoshi, R. Nussinov, Y. Ishii, *Nat. Struct. Mol. Biol.* **2015**, *22*, 499–505; d) L. Gremer, D. Schölzel, C. Schenk, E. Reinartz, J. Labahn, R. B. G. Ravelli, M. Tusche, C. Lopez-Iglesias, W. Hoyer, H. Heise, D. Willbold, G. F. Schröder, *Science* **2017**, *358*, 116–119.

[4] a) B. Urbanc, L. Cruz, S. Yun, S. V. Buldyrev, G. Bitan, D. B. Teplow, H. E. Stanley, *Proc. Natl. Acad. Sci. USA* **2004**, *101*, 17345–17350; b) N. G. Sgourakis, Y. L. Yan, S. A. McCallum, C. Y. Wang, A. E. Garcia, *J. Mol. Biol.* **2007**, *368*, 1448–1457; c) J. T. Jarrett, E. P. Berger, P. T. Lansbury, *Biochemistry* **1993**, *32*, 4693–4697.

[5] R. Tycko, *Neuron* **2015**, *86*, 632–645.

[6] R. Roychaudhuri, M. Yang, A. Deshpande, G. M. Cole, S. Frautschy, A. Lomakin, G. B. Benedek, D. B. Teplow, *J. Mol. Biol.* **2013**, *425*, 292–308.

[7] D. Granata, F. Baftizadeh, J. Habchi, C. Galvagnion, A. De Simone, C. Camilloni, A. Laio, M. Vendruscolo, *Sci. Rep.* **2015**, *5*, 15449.

[8] a) G. Bitan, M. D. Kirkitadze, A. Lomakin, S. S. Vollers, G. B. Benedek, D. B. Teplow, *Proc. Natl. Acad. Sci. USA* **2003**, *100*, 330–335; b) W. Kim, M. H. Hecht, *J. Biol. Chem.* **2005**, *280*, 35069–35076.

[9] J. A. Raskatov, M. Jakel, B. F. Straub, F. Rominger, G. Helmchen, *Chem. Eur. J.* **2012**, *18*, 14314–14328.

[10] M. J. Frisch, G. W. Trucks, H. B. Schlegel, G. E. Scuseria, M. A. Robb, J. R. Cheeseman, G. Scalmani, V. Barone, B. Mennucci, G. A. Petersson, H. Nakatsuji, M. Caricato, X. Li, H. P. Hratchian, A. F. Izmaylov, J. Bloino, G. Zheng, J. L. Sonnenberg, M. Hada, M. Ehara, K. Toyota, R. Fukuda, J. Hasegawa, M. Ishida, T. Nakajima, Y. Honda, O. Kitao, H. Nakai, T. Vreven, Jr, J. E. Peralta, F. Ogliaro, M. Bearpark, J. J. Heyd, E. Brothers, K. N. Kudin, V. N. Staroverov, R. Kobayashi, J. Normand, K. Raghavachari, A. Rendell, J. C. Burant, S. S. Iyengar, J. Tomasi, M. Cossi, N. Rega, J. M. Millam, M. Klene, J. E. Knox, J. B. Cross, V. Bakken, C. Adamo, J. Jaramillo, R. Gomperts, R. E. Stratmann, O. Yazyev, A. J. Austin, R. Cammi, C. Pomelli, J. W. Ochterski, R. L. Martin, K. Morokuma, V. G. Zakrzewski, G. A. Voth, P. Salvador, J. J. Dannenberg, S. Dapprich, A. D. Daniels, Farkas, J. B. Foresman, J. V. Ortiz, J. Cioslowski, D. J. Fox, *Gaussian 09 Revision A.02*, Gaussian Inc. Wallingford CT, **2009**.

[11] Y. Zhao, D. G. Truhlar, *Theor. Chem. Acc.* **2008**, *120*, 215–241.

[12] a) P. C. Hariharan, J. A. Pople, *Theo. Chim. Acta* **1973**, *28*, 213–222; b) W. J. Hehre, R. Ditchfield, J. A. Pople, *J. Chem. Phys.* **1972**, *56*, 2257–2261; c) R. Ditchfield, W. J. Hehre, J. A. Pople, *J. Chem. Phys.* **1971**, *54*, 724–728.

Manuscript received: January 20, 2019
Accepted manuscript online: February 28, 2019
Version of record online: May 21, 2019

CHAPTER 2:

D-amino acid substituted frameworks to study structure-activity relationships of Aβ and to stabilize Aβ conformations

Introduction to Chapter 2

One of the key milestones that still remains elusive in AD and Aβ research is the structural elucidation of Aβ neurotoxic oligomeric intermediates at atomic level and high resolution. This is because these metastable species do not tend to adopt well-defined three dimensional and stable structures, but rather generate dynamic and heterogeneous populations of conformers including multiple shapes and aggregation states. This includes monomers, oligomers, and protofibrils, with Aβ oligomers reported to adopt spherical,(43) annular,(44) cylindrical barrels,(45) and protofibrillar (46) shapes, among others. In addition, each of these species can potentially contribute to Aβ toxicity in different ways.(17) For example, oligomeric Aβ*56 (a 56-kDa dodecameric, soluble Aβ assembly) has been directly linked with memory impairment in triple AD transgenic (3×Tg-AD) mice,(47) and one of the genetic familial AD mutations (FAD) leading to early onset AD, the "Arctic" (E22G) FAD, is characterized by its tendency to stabilize Aβ protofibrils.(48) Therefore, stabilizing Aβ oligomeric intermediates and establishing defined structure-activity relationships for these species becomes critical to advance our understanding of Aβ toxicity.

To this end, the work performed in this thesis, and as outlined in this chapter, describes the use of chiral point mutations (which we refer to as chiral editing) within the Aβ sequence as strategy to stabilize Aβ aggregation intermediates. This approach offers the advantage of keeping the physicochemical properties of Aβ unaltered, such as such as side-chain size, flexibility, hydropathy, charge, or polarizability, and it allowed us to solely focus on how the side chain orientation of the mutated residues influenced the overall conformation of the generated species. Through this strategy, we were able to stabilize Aβ aggregation intermediates and to elucidate interactions that dramatically change the aggregation and toxicity properties of Aβ.

JOC The Journal of Organic Chemistry

pubs.acs.org/joc Article

A Focused Chiral Mutant Library of the Amyloid β 42 Central Electrostatic Cluster as a Tool To Stabilize Aggregation Intermediates

Alejandro R. Foley, Hsiau-Wei Lee, and Jevgenij A. Raskatov*

Cite This: *J. Org. Chem.* 2020, 85, 1385–1391 Read Online

ACCESS | Metrics & More | Article Recommendations | Supporting Information

ABSTRACT: Amyloidogenic peptides and proteins aggregate into fibrillary structures that are usually deposited in tissues and organs and are often involved in the development of diseases. In contrast to native structured proteins, amyloids do not follow a defined energy landscape toward the fibrillary state and often generate a vast population of aggregation intermediates that are transient and exceedingly difficult to study. Here, we employ *chiral editing* as a tool to study the aggregation mechanism of the Amyloid β (Aβ) 42 peptide, whose aggregation intermediates are thought to be one of the main driving forces in Alzheimer's disease (AD). Through the design of a focused chiral mutant library (FCML) of 16 chiral Aβ42 variants, we identified several point D-substitutions that allowed us to modulate the aggregation propensity and the biological activity of the peptide. Surprisingly, the reduced propensity toward aggregation and the stabilization of oligomeric intermediates did not always correlate with an increase in toxicity. In the present study, we show how chiral editing can be a powerful tool to trap and stabilize Aβ42 conformers that might otherwise be too transient and dynamic to study, and we identify sites within the Aβ42 sequence that could be potential targets for therapeutic intervention.

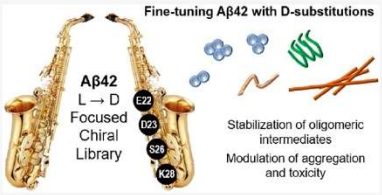

■ INTRODUCTION

Many proteins and peptides can self-assemble into highly ordered, β-sheet-rich fibrillary structures.[1] The accumulation of these fibrils, referred to as *amyloid plaques*, is associated with various pathologies. Some of the examples include Alzheimer's disease (AD) and the amyloid β (Aβ) peptide, Parkinson's disease and the α-synuclein protein, or type II diabetes and the islet amyloid polypeptide (IAPP), among others.[2] A common mechanistic feature of these disorders is the complex aggregation pathway leading to the fibrillary state, where multiple rapid-interconverting aggregation intermediates, i.e., *oligomeric species*, are generated upon the self-association of unfolded or partially folded conformations.[3] While fibrils are the most thermodynamically stable state, these fleeting oligomeric entities are thought to be the most toxic species during the amyloid aggregation cascade.[4−6]

Aβ is an intrinsically disordered peptide involved in the pathology of AD.[7] Aβ can range between 37 and 43 amino acids in length, with Aβ 1−40 (Aβ40) and Aβ 1−42 (Aβ42) being the most abundant isoforms, and Aβ42 oligomers considered as the most neurotoxic agents.[8−10] These oligomeric intermediates can exist in a wide variety of morphologies and structures including spherical,[11] annular,[12] β-barrel,[13] and protofibrillar[14] shapes, each of them potentially contributing to Aβ toxicity in different ways.[15] For example, oligomeric Aβ*56 (a 56-kDa dodecameric, soluble Aβ assembly) has been directly linked with memory impairment in 3 × Tg-AD transgenic mice,[16] and the "Arctic" (E22G) familial mutation is characterized by the abundant presence of protofibrils.[17] While high-resolution structures of Aβ42 fibrils have been elucidated,[18−22] obtaining structural information on Aβ42 oligomeric species remains exceptionally challenging, and it is limited to a large degree to in silico[23] or to model scaffold studies.[24]

Amino acid chemical mutagenesis has previously been employed as a tool to determine the structure−function properties the Aβ peptide, such as alanine[25] and proline[26] scanning, or incorporation of multiple cysteine residues, which are not present in the wild-type Aβ42 peptide.[27] Although providing significant information, these mutations modify the amino acid sequence of the peptide, altering the side chain functional groups and therefore the size, charge, polarity, hydropathy, and flexibility of the resultant Aβ mutant peptide. To keep these properties unaltered, D-amino acid substitution provides a suitable strategy to obtain structural information on intrinsically disordered peptides,[28] enabling researchers to

Special Issue: Modern Peptide and Protein Chemistry

Received: August 26, 2019
Published: December 25, 2019

https://dx.doi.org/10.1021/acs.joc.9b02312
J. Org. Chem. 2020, 85, 1385−1391

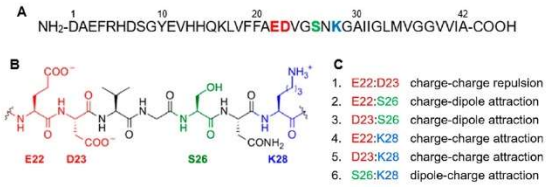

Figure 1. Select amino acid interactions in loop I region of Aβ42. (A) Aβ42 amino acid sequence, with mutated amino acids highlighted. Red: Negatively charged. Blue: Positively charged. Green: Polar −OH. (B) Central electrostatic region of Aβ42, showing side chains from amino acids 22 to 28. (C) Possible electrostatic interactions between side chains.

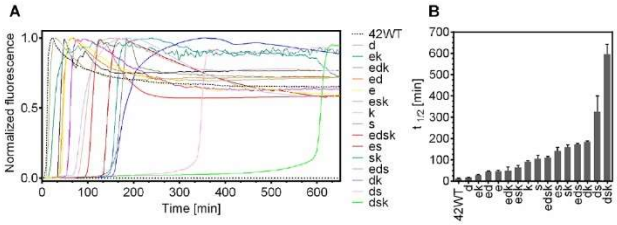

Figure 2. ThT-monitored aggregation kinetics of the Aβ42 chiral library. (A) Tht-monitored fibril formation with shaking at 37 °C in 20 mM phosphate buffer at 20 μM peptide concentration and 20 μM ThT. Peptides were spin-filtered at 15000*g* with a 100 kDa filter before the experiment to remove aggregates. Median value from three technical replicates shown. (B) Mean half-time ($t_{1/2}$) value with SD for each peptide, calculated from three technical replicates for each peptide. $t_{1/2}$ is defined as the time required for each curve to reach 1/2 of maximum intensity values. Each single small letter represents a chiral inversion at that amino acid (i.e., E22e (e), D23d (d), S26s (s), K28k (k), E22e-D23d-S26s-K28k (edsk)). Peptides are displayed from slower to faster $t_{1/2}$.

focus on how side-chain orientations change the structure−function relationships of the system. This strategy has previously been applied in the Aβ framework, which has provided valuable insights on the role of specific amino acids toward the aggregation and toxic properties of Aβ42.[29−32] The incorporation of D-amino acids modifies the backbone conformational landscape, and understanding its effect on the secondary structure can provide important information on structure−activity relationships.[28,33] For example, D-amino acid replacement in insulin has provided mechanistic insights into its active conformation and receptor binding ability,[34] and D-analogues of mammalian α-defensin 2 were employed to elucidate conformational motifs required for its antimicrobial activity.[35] Indeed, age-dependent amino acid racemization (specially aspartate (Asp), serine (Ser), and threonine (Thr) residues) is a physiological process that occurs in long-lived proteins, and it is associated with the development of diseases such as cataract formation,[36] where solubility changes due to epimerization lead to protein precipitation and loss of function. In the context of Aβ, Asp (D) and Ser (S) amino acids have been found to be epimerized in brain-derived amyloid plaques,[37] with these modifications being responsible for changes in the aggregation and toxicity of Aβ.[38,39]

Because the aggregation state of protein oligomers is thought to be directly linked with its toxic activity,[40] obtaining advanced information on these intermediate species becomes of seminal importance. Here, we employ molecular chirality as a tool to obtain mechanistic information on the assembly of Aβ42. Such subtle, structural perturbations allow us to solely focus on conformational changes, which allowed us to stabilize aggregation intermediates of Aβ42 in the past.[28] While only a subset of amino acids can epimerize under physiological conditions, Asp and Ser residues suffer from age-related epimerization and are part of the electrostatic cluster that comprises Glu22, Asp23, Ser26, and Lys28.

RESULTS AND DISCUSSION

Electrostatic Interactions in Aβ42. Loop I region of Aβ42 comprises amino acids 21−30. This electrostatic-rich region is found to adopt a β-hairpin structural motif in soluble Aβ oligomers[41] and in all published Aβ42 fibril structures,[18−22,42] being critical for the folding and aggregation propensity and toxicity of Aβ42.[43,44] This loop can be regarded as a structural hairpin mainly composed of charged and polar amino acids, flanked by phenylalanine (Phe) (Phe 19 and Phe 20) and isoleucine (Ile) (Ile31 and Ile32) residues that create a hydrophobic patch on the verges of the hairpin (Figure 1A). Furthermore, loop I region harbors a total of six identified disease-causing familial mutations (A21G, E22G, E22Q, E22K, E22Δ, D23N), which accelerate the aggregation of the peptide and dramatically increase the severity of the disease.[45]

Due to the functionality of its side chains, residues glutamate 22 (E22), aspartate 23 (D23), serine 26 (S26), and lysine 28 (K28) can interact in different ways: (I) E22−D23, charge−charge repulsion, (II) D23−S26, charge-dipole attraction, (III) E22−K28, charge−charge attraction, (IV) E22−K28, charge−charge attraction, (V) D23−K28, charge−charge attraction, (VI) S26−K28, charge−charge attraction (Figure 1B,C). The electrostatic interactions happening in this region have been reported to play a key role on the nucleation of Aβ42 in in

https://dx.doi.org/10.1021/acs.joc.9b02312
J. Org. Chem. 2020, 85, 1385−1391

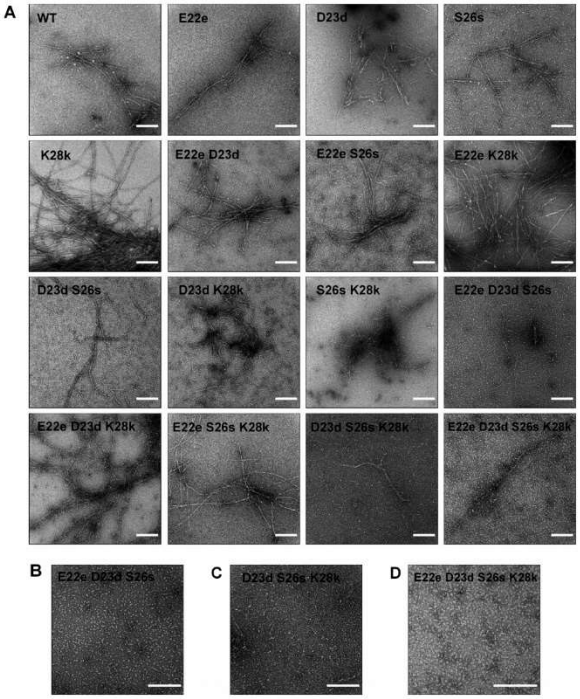

Figure 3. Fibril morphology of the Aβ42 chiral library after quiescent 7-day incubation. Scalebar: 200 nm in all cases. (A) Representative negative-stain TEM images of Aβ42-WT and Aβ42 diastereomers at 20 μM peptide concentration. After incubation, 3 μL of peptide-containing solution in pH 7.4, 20 mM phosphate buffer were aliquoted into carbon type-B, 200 mesh copper grids and stained with 1% uranyl acetate solution (B–D) Selected Aβ42 chiral variants show stabilization of smaller aggregation intermediates.

silico studies, pointing toward several H-bonding patterns involving these amino acids as being responsible for the formation of aggregates.[46,47] For example, Meredith et al. showed that, by stabilizing the interaction of D23 and K28 though a lactam bond formation, Aβ40 formed fibrils approximately 1000-fold faster than Aβ40-wild type (WT).[48] The fact that almost all familial AD-causing mutations within the Aβ42 sequence alter the charge of the mutated amino acids further highlights the relevance of this electrostatic-rich region,[49] making *chiral editing* a subtle and uniquely suitable probe to systematically probe electrostatic interactions in Aβ42.

Side-Chain Orientation Influences Aβ42 Aggregation. To obtain insights into the interactions happening in this region, we designed a FMCL of all possible Aβ42 diastereomers for the amino acids E22, D23, S26, and K28, leading to a total of $2^4 = 16$ possible diastereomers. These 16 peptides were synthesized by solid-phase peptide synthesis, and the peptides were purified by reversed-phase HPLC to a minimum of 97% purity (Figure S1), as described.[50]

We first examined how these chiral edits influenced fibril formation using the thioflavin T (ThT) assay (Figure 2), a small molecule which experiences fluorescence enhancement upon binding to amyloid fibrillary structures.[51] Results from the ThT assay showed a significant difference in the lag time within the 16 peptides, with the fastest half-time ($t_{1/2}$) being Aβ42-WT (11.8 $\pm$ 0.3 min) and the slowest being the triple chirally edited mutant Aβ42-D23d-S26s-K28k (Aβ42-dsk) (596.5 $\pm$ 45.6 min), showing a ~50-fold delay difference. A table with mean $t_{1/2}$ values for the 16 peptides is available in Figure S2. These results clearly highlight that the relative disposition of the side chains in the loop I region of Aβ42 determine the propensity of the peptides to aggregate and to form fibrils and that the possible electrostatic interactions happening in this domain influence Aβ42 aggregation kinetics.

Changes Induced by Chiral Editing Alter Fibril Structure. We then examined how these differences in aggregation kinetics influence the morphology of the peptides. Thus, we incubated Aβ42-WT and Aβ42 chiral variants for 7 days in 20 mM pH 7.4 phosphate buffer at 37 °C without shaking at a peptide concentration of 20 μM. After the incubation period, the morphology of the peptides was analyzed by transmission electron microscopy (TEM, Figure 3). Additional TEM images are available in the Supporting

https://dx.doi.org/10.1021/acs.joc.9b02312
J. Org. Chem. 2020, 85, 1385−1391

Information (TEM annex). The TEM images revealed that the observed difference in aggregation kinetics was also consistent with the tendency of the different chirally edited Aβ42 variants to form fibrillary structures. While no major differences were observed in the morphology of elongated fibrils, the propensity of the peptides to adopt such structures varied in a consistent fashion with the ThT results. Aβ42-WT and Aβ42 chiral variants with the faster aggregation kinetics tended to form elongated fibrils, while peptides with slower aggregation kinetics displayed stabilized smaller structures that did not completely develop into fibrils (Figure 3A). In fact, these chiral variants stabilized smaller spherical and protofibrillar structures (Figure 3B). This effect was previously identified and characterized by us for the Aβ42-S26s chiral variant, where introduction of D-Serine at position 26 led to the stabilization of nontoxic oligomers comparable in size and distribution to Aβ42-WT through the stabilization of an intracellular H-bond between Ser26 and Asn27.[31] The central loop region of Aβ (amino acids 21−30) is typically used as a model to study Aβ folding events by in silico simulations and solution-state NMR.[52,53] We had previously extended this model by incorporating neighboring Phe (19 and 20) and Ile (31 and 32) residues, resulting in the peptide Aβ(19−32), which we observed to also recapitulate the aggregation properties of full-length Aβ, as opposed to the 21−30 segment, which does not aggregate.[31]

Solution NMR analysis of the loop region model peptides Aβ(19−32)-WT, Aβ(19−32)-ds, and Aβ(19−32)-dsk showed changes on the α-hydrogen and N-hydrogen chemical shift of the D-substituted and neighboring amino acids (Figure S3 and Tables S1 and S2), indicating that conformational rearrangements derived from the these chiral substitutions might be responsible for the difference in aggregation kinetics. This observation remarks the importance of the interactions happening in this region, either through point substitutions of the charged residues (i.e., familial mutations) or due to the conformational reorganization of the amino acids within this loop, potentially allowing for the stabilization, or destabilization, of critical interactions. For example, Madhu et al. reported that curcumin, a disruptor of Aβ42 fibril formation that also reduces Aβ42 toxicity in mouse models, binds to this loop region and disrupts the Asp23-Lys28 salt bridge,[54] which is thought to play an important stabilizing role for the β-hairpin loop formation in Aβ oligomers and fibrils.[55]

Chiral Mutations Change the Biological Activity of Aβ42. We had previously reported that conformational changes through point D-mutations within this electrostatic-rich region changed the aggregation and cytotoxicity of the resultant Aβ42 mutant peptide, either to produce an increase (E22e)[29] or a decrease (S26s)[31] in toxicity. Because the chirally edited mutants displayed slower aggregation kinetics when compared to Aβ42-WT and stabilized aggregation intermediates, we investigated how this difference influenced the biological activity of the peptides. We therefore dosed human neuroblastoma SH-SY5Y cells with 50 μM peptide concentrations, incubated them for 3 days, and then assessed cell viability by the WST-1 assay (Figure 4). The Aβ42 chiral mutant peptides showed a varied range of cellular activity, ranging from similar levels to Aβ42-WT (*d, ek, edk, esk*) to almost no toxicity (*s, k, dk*).

This was surprising, given that these mutant peptides were able to form oligomers with comparable distribution to Aβ42-WT as observed by photoinduced cross-linking (PICUP)

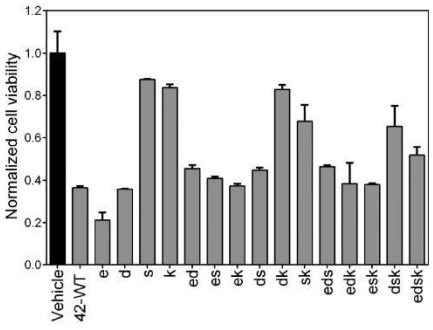

Figure 4. Cellular viability results in human neuroblastoma SH-SY5Y cell line. SH-SY5Y cells were treated with 50 μM of each peptide and cells were incubated for 3 days at 37 °C. After the incubation time, cells were dosed with the water-soluble tetrazolium salt WST-1 (10% final volume in well) and incubated for 2 h and 30 min. After incubation, absorbance was measured at λ = 490 nm to determine cellular viability. Bars show mean with error bars as SD of three technical replicates. Data were normalized against vehicle (media with no peptide).

(Figure S4, S5), a technique that allows stabilization and visualization of low molecular weight oligomers of Aβ42 by SDS-PAGE.[56] These oligomeric species, supposed to represent the most neurotoxic entities in the amyloid cascade hypothesis,[8−10] were no longer present after 3- and 7-day incubation for Aβ42-WT, but could be visualized for the chiral peptides with slower aggregation kinetics and reduced fibril formation propensity (Figure S5), indicating that the presence of oligomeric species is not the only factor required to elicit cytotoxicity.

From these results, it was not possible to establish a direct correlation between aggregation kinetics and biological activity observed. For example, the triple chirally edited mutant *dsk*, which had a ∼ 50-fold delay toward fibril formation compared to Aβ42-WT and stabilized oligomeric and protofibrillar structures, showed a 2-fold decrease on cellular toxicity vs Aβ42-WT. The single D-substitution at position E22 (which holds four familial mutations) was the only one observed to have an increased level of toxicity. Additionally, reports have shown that a turn at positions Glu22 and Asp23 generates highly neurotoxic species of Aβ42,[57] while covalently binding Gly25 and Ser26 leads to reduced toxicity.[58] These observations have led to the development of antibodies that target this toxic turn motif, and have recently been proposed as a new method for AD diagnosis.[58] This is consistent with our findings, which show that E22e substitution enhances toxicity while S26s attenuates it. These results suggest that specific conformations might have more influence than others toward the toxic activity of Aβ42, and that the aggregation state, i.e., presence of oligomeric structures, might not always be a pathogenic element. The fact that these subtle chiral perturbations only modify the conformational landscape and keep the rest of the physicochemical properties unaltered, might be indicative of the existence of stereospecific or conformational-dependent interactions required for Aβ42 to elicit its toxic actions.[40,59,60] In this regard, presynaptic

https://dx.doi.org/10.1021/acs.joc.9b02312
J. Org. Chem. 2020, 85, 1385−1391

receptors[61] and physiological prion protein (PrP^C)[62] have been postulated as possible receptors of toxic Aβ42 oligomers, and membrane-binding inhibition of Aβ42 oligomers using the aminoesterol small molecule trodusquemine resulted in the suppression of toxicity of Aβ42 in neuroblastoma cells.[63] Therefore, the ability to stabilize and acquire structural information on oligomeric intermediates with distinct biological activity could help understand why certain oligomeric structures are more toxic than others, and would facilitate the design of therapeutics specific to toxic conformations.

■ CONCLUSION

In summary, here we employ *chiral editing* as a tool to stabilize and to obtain information on amyloid aggregation intermediates that might otherwise be too transient and challenging to study. Through the design of a focused chiral mutant library (FCML) within the Aβ42 sequence, we were able to stabilize aggregation intermediates that had either higher, similar, or lower biological activity compared to Aβ42-WT. Our results suggest that the relative side chain orientation of the amino acids E22, D23, S26, and K28 have a profound influence on the ability of Aβ42 to aggregate and elicit toxic actions, therefore pointing to this electrostatic-rich region as a therapeutic target to inhibit Aβ42 assembly and toxicity. Furthermore, trapping these oligomeric species might allow the obtention of new structural information on the yet not sufficiently understood Aβ42 oligomeric intermediates. The *chiral editing* approach could also represent a useful tool to stabilize and obtain novel mechanistic information for other challenging amyloidogenic systems.

■ EXPERIMENTAL SECTION

Synthesis, Purification, And Characterization of Aβ42 and Chiral Variants. Aβ peptides were synthesized using a Liberty One CEM peptide synthesizer and assisted by a CEM discovery microwave. H-Ala-HMPB-ChemMatrix resin (Millipore Sigma, product no. 727822) was used in all cases as starting resin, and couplings were performed by Fmoc/hydroxybenzotriazole (HOBt)/*N*,*N*′-diisopropylcarbodiimide (DIC)/piperidine chemistry on a 0.1 mmol scale using previously described coupling methods.[29] After synthesis, resins were cleaved using a cocktail solution of trifluoroacetic acid (10 mL), 1, 2-diethanethiol (0.5 mL), triisopropylsilane (1 mL), and liquefied phenol (0.5 mL). After 2 h of continuous agitation, the cocktail solution containing the peptides was filtered and then evaporated to approximately 2 mL under nitrogen gas. The resultant viscous solution was transferred to a vial containing cold diethyl ether, allowing the peptide to precipitate. After centrifugation, the peptide pellet was washed with diethyl ether and then dissolved in a 1:1 mixture of water/acetonitrile with 20 mM NH_4OH. After lyophilization, the crude peptides were purified to ≥96% purity by reported reversed-phase HPLC protocols.[50]

Thioflavin T (ThT) Assay. Powdered lyophilized Aβ42 peptides were dissolved in minimal amount of 20 mM NaOH (maximum of 3% final dilution volume) and sonicated for 30 s. The dissolved peptides were then filtered through 100 kDa MWCO spin filters at 14000*g* for 10 min. The concentration of the filtrate was then measured by nanodrop (ε = 1490 M^{-1} cm^{-1} at 280 nm), and the peptides were then diluted to a final concentration of 20 μM using 20 mM phosphate buffer with 20 μM ThT. A 200 μL portion of peptide-ThT mixture was placed in black, clear bottom 96-well plates in a Molecular Device Gemini EM fluorescence plate reader set up for ThT fluorescence measurements (λ_{em} = 444 nm, λ_{ex} = 485 nm). The wells were sealed with optically clear adhesive film, and three replicates were prepared for each peptide. The peptides were monitored for 24 h at 37 °C, with readings collected every 5 min with continuous shaking.

Transmission Electron Microscopy (TEM). Aβ42 peptides were dissolved in a minimal amount of 20 mM NaOH as previously described and diluted to 20 μM using 20 mM pH 7.4 phosphate buffer. The peptides were then incubated for 7 days at 37 °C without shaking. After incubation, 5 μL of each peptide was spotted onto carbon-coated electron microscopy grid (Ted Pella, Cat. No. 01701-F). Peptides were allowed to adhere to the grid for 1 min, and then the solution was carefully removed. For staining, three consecutive additions of 10 μL 1% uranyl acetate solution (Electron Microscopy Sciences, Cat. No. 22400-1) were added and removed from the grids. All Aβ42 peptides were imaged using a JEOL 1230 microscope at an accelerating voltage of 120 kV.

Human Neuroblastoma SH-SY5Y Cellular Viability. SH-SY5Y cells were cultured in DMEM:F12K media (ATCC, Cat. No. 30-2006) supplemented with 10% fetal bovine serum (ATCC, cat. no. 30-2020). Cells were plated on 96-well plate at a density of 50k cells/well in 100 μL total volume and allowed to adhere for 24 h. Then the media was removed from the wells, and cells were dosed with 50 μM of each Aβ42 peptide dissolved in DMEM:F12K media. Cells were incubated for 3 days at 37 °C with three technical replicates per peptide. After the incubation time, 10 μL of WST-1 cell proliferation reagent (Millipore Sigma, cat. no. 5015944001) was added to each well, and cells were incubated for 2 h and 30 min. After incubation, absorbance was measured at λ = 490 nm to determine cellular viability.

■ ASSOCIATED CONTENT

Supporting Information

The Supporting Information is available free of charge at https://pubs.acs.org/doi/10.1021/acs.joc.9b02312.

Sample characterization and additional supplemental figures (PDF)

■ AUTHOR INFORMATION

Corresponding Author

Jevgenij A. Raskatov − *University of California Santa Cruz, Santa Cruz, California;* orcid.org/0000-0002-0082-9113; Email: jraskato@ucsc.edu

Other Authors

Alejandro R. Foley − *University of California Santa Cruz, Santa Cruz, California;* orcid.org/0000-0002-8644-0546

Hsiau-Wei Lee − *University of California Santa Cruz, Santa Cruz, California*

Complete contact information is available at: https://pubs.acs.org/10.1021/acs.joc.9b02312

Author Contributions

A.R.F. and J.A.R. designed the study. A.R.F. and H.L. collected the data and made the figures. A.R.F., H.L., and J.A.R. interpreted the data. A.R.F. and J.A.R. wrote the manuscript.

Notes

The authors declare no competing financial interest.

■ ACKNOWLEDGMENTS

We thank Dr. Benjamin Abrams for technical support with TEM images acquisition and the UCSC microscopy facility and Prof. Melissa Jurica for granting access to the JEOL 1230 TEM microscope. J.A.R. thanks UC Santa Cruz for flexible start-up funds,and the NIH for funding (R21AG058074). A.R.F. thanks NIH for funding (2R25GM058903-20 IMSD). Ms. Ariel Kuhn is gratefully acknowledged for helpful discussions during manuscript preparation stage.

REFERENCES

(1) Stefani, M.; Dobson, C. M. Protein Aggregation and Aggregate Toxicity: New Insights into Protein Folding, Misfolding Diseases and Biological Evolution. *J. Mol. Med.* **2003**, *81* (11), 678−699.

(2) Chiti, F.; Dobson, C. M. Protein Misfolding, Functional Amyloid, and Human Disease. *Annu. Rev. Biochem.* **2006**, *75* (1), 333−366.

(3) Knowles, T. P. J.; Vendruscolo, M.; Dobson, C. M. The Amyloid State and Its Association with Protein Misfolding Diseases. *Nat. Rev. Mol. Cell Biol.* **2014**, *15* (6), 384−396.

(4) Kayed, R.; Head, E.; Thompson, J. L.; McIntire, T. M.; Milton, S. C.; Cotman, C. W.; Glabe, C. G. Common Structure of Soluble Amyloid Oligomers Implies Common Mechanism of Pathogenesis. *Science* **2003**, *300* (5618), 486−489.

(5) Selkoe, D. J. Folding Proteins in Fatal Ways. *Nature* **2003**, *426* (1), 900−904.

(6) Ahmed, M.; Davis, J.; Aucoin, D.; Sato, T.; Ahuja, S.; Aimoto, S.; Elliott, J. I.; Van Nostrand, W. E.; Smith, S. O. Structural Conversion of Neurotoxic Amyloid-B 1−42 Oligomers to Fibrils. *Nat. Struct. Mol. Biol.* **2010**, *17* (5), 561−567.

(7) Haass, C.; Selkoe, D. J. Soluble Protein Oligomers in Neurodegeneration: Lessons from the Alzheimer's Amyloid β-Peptide. *Nat. Rev. Mol. Cell Biol.* **2007**, *8* (2), 101−112.

(8) Walsh, D. M.; Klyubin, I.; Fadeeva, J. V.; Cullen, W. K.; Anwyl, R.; Wolfe, M. S.; Rowan, M. J.; Selkoe, D. J. Naturally Secreted Oligomers of Amyloid β Protein Potently Inhibit Hippocampal Long-Term Potentiation in Vivo. *Nature* **2002**, *416* (6880), 535−539.

(9) Lambert, M. P.; Barlow, A. K.; Chromy, B. A.; Edwards, C.; Freed, R.; Liosatos, M.; Morgan, T. E.; Rozovsky, I.; Trommer, B.; Viola, K. L.; et al. Diffusible, Nonfibrillar Ligands Derived from Abeta1−42 Are Potent Central Nervous System Neurotoxins. *Proc. Natl. Acad. Sci. U. S. A.* **1998**, 95 (11), 6448−6453.

(10) Demuro, A.; Mina, E.; Kayed, R.; Milton, S. C.; Parker, I.; Glabe, C. G. Calcium Dysregulation and Membrane Disruption as a Ubiquitous Neurotoxic Mechanism of Soluble Amyloid Oligomers. *J. Biol. Chem.* **2005**, *280* (17), 17294−17300.

(11) Hoshi, M.; Sato, M.; Matsumoto, S.; Noguchi, A.; Yasutake, K.; Yoshida, N.; Sato, K. Spherical Aggregates of β- Amyloid (Amylospheroid) Show High Neurotoxicity and Activate Tau Protein Kinase I/Glycogen Synthase Kinase-3. *Proc. Natl. Acad. Sci. U. S. A.* **2003**, *100* (11), 6370−6375.

(12) Lashuel, H. A.; Hartley, D.; Petre, B. M.; Walz, T.; Lansbury, P. T. Neurodegenerative Disease: Amyloid Pores from Pathogenic Mutations. *Nature* **2002**, *418* (6895), 291.

(13) Laganowsky, A.; Liu, C.; Sawaya, M. R.; Whitelegge, J. P.; Park, J.; Zhao, M.; Pensalfini, A.; Soriaga, A. B.; Landau, M.; Teng, P. K.; et al. Atomic View of a Toxic Amyloid Small Oligomer. *Science* **2012**, *335* (6073), 1228−1231.

(14) Harper, J. D.; Wong, S. S.; Lieber, C. M.; Lansbury, P. T. Observation of Metastable Aβ Amyloid Protofibrils by Atomic Force Microscopy. *Chem. Biol.* **1997**, *4* (2), 119−125.

(15) Glabe, C. G. Structural Classification of Toxic Amyloid Oligomers. *J. Biol. Chem.* **2008**, *283* (44), 29639−29643.

(16) Lesné, S.; Ming, T. K.; Kotilinek, L.; Kayed, R.; Glabe, C. G.; Yang, A.; Gallagher, M.; Ashe, K. H. A Specific Amyloid- β Protein Assembly in the Brain Impairs Memory. *Nature* **2006**, *440* (7082), 352−357.

(17) Nilsberth, C.; Westlind-Danielsson, A.; Eckman, C. B.; Condron, M. M.; Axelman, K.; Forsell, C.; Stenh, C.; Luthman, J.; Teplow, D. B.; Younkin, S. G.; et al. The "Arctic" APP Mutation (E693G) Causes Alzheimer's Disease by Enhanced Aβ Protofibril Formation. *Nat. Neurosci.* **2001**, *4* (9), 887−893.

(18) Gremer, L.; Schölzel, D.; Schenk, C.; Reinartz, E.; Labahn, J.; Ravelli, R. B. G.; Tusche, M.; Lopez-Iglesias, C.; Hoyer, W.; Heise, H.; et al. Fibril Structure of Amyloid-β(1−42) by Cryo-electron Microscopy. *Science* **2017**, *358* (6359), 116−119.

(19) Wälti, M. A.; Böckmann, A.; Meier, B. H.; Arai, H.; Ravotti, F.; Glabe, C. G.; Güntert, P.; Wall, J. S.; Riek, R. Atomic- Resolution Structure of a Disease-Relevant Aβ(1−42) Amyloid Fibril. *Proc. Natl. Acad. Sci. U. S. A.* **2016**, *113* (34), E4976−E4984.

(20) Xiao, Y.; Ma, B.; McElheny, D.; Parthasarathy, S.; Long, F.; Hoshi, M.; Nussinov, R.; Ishii, Y. Aβ(1−42) Fibril Structure Illuminates Self-Recognition and Replication of Amyloid in Alzheimer's Disease. *Nat. Struct. Mol. Biol.* **2015**, *22* (6), 499−505.

(21) Colvin, M. T.; Silvers, R.; Ni, Q. Z.; Can, T. V.; Sergeyev, I.; Rosay, M.; Donovan, K. J.; Michael, B.; Wall, J.; Linse, S.; et al. Atomic Resolution Structure of Monomorphic Aβ42 Amyloid Fibrils. *J. Am. Chem. Soc.* **2016**, *138* (30), 9663−9674.

(22) Lührs, T.; Ritter, C.; Adrian, M.; Riek-Loher, D.; Bohrmann, B.; Döbeli, H.; Schubert, D.; Riek, R. 3D Structure of Alzheimer's Amyloid-beta(1−42) Fibrils. *Proc. Natl. Acad. Sci. U. S. A.* **2005**, *102* (48), 17342−17347.

(23) Urbanc, B.; Betnel, M.; Cruz, L.; Bltan, G.; Teplow, D. B. Elucidation of Amyloid β-Protein Oligomerization Mechanisms: Discrete Molecular Dynamics Study. *J. Am. Chem. Soc.* **2010**, *132* (12), 4266−4280.

(24) Kreutzer, A. G.; Nowick, J. S. Elucidating the Structures of Amyloid Oligomers with Macrocyclic β-Hairpin Peptides: Insights into Alzheimer's Disease and Other Amyloid Diseases. *Acc. Chem. Res.* **2018**, *51* (3), 706−718.

(25) Williams, A. D.; Shivaprasad, S.; Wetzel, R. Alanine Scanning Mutagenesis of Aβ(1−40) Amyloid Fibril Stability. *J. Mol. Biol.* **2006**, *357* (4), 1283−1294.

(26) Williams, A. D.; Portelius, E.; Kheterpal, I.; Guo, J. T.; Cook, K. D.; Xu, Y.; Wetzel, R. Mapping Aβ Amyloid Fibril Secondary Structure Using Scanning Proline Mutagenesis. *J. Mol. Biol.* **2004**, *335* (3), 833−842.

(27) Sandberg, A.; Luheshi, L. M.; Sollvander, S.; Pereira de Barros, T.; Macao, B.; Knowles, T. P. J.; Biverstal, H.; Lendel, C.; Ekholm-Petterson, F.; Dubnovitsky, A.; et al. Stabilization of Neurotoxic Alzheimer Amyloid- Oligomers by Protein Engineering. *Proc. Natl. Acad. Sci. U. S. A.* **2010**, *107* (35), 15595−15600.

(28) Raskatov, J. A.; Teplow, D. B. Using Chirality to Probe the Conformational Dynamics and Assembly of Intrinsically Disordered Amyloid Proteins. *Sci. Rep.* **2017**, *7* (1), 12433.

(29) Warner, C. J. A.; Dutta, S.; Foley, A. R.; Raskatov, J. A. Introduction of D-Glutamate at a Critical Residue of Aβ42 Stabilizes a Prefibrillary Aggregate with Enhanced Toxicity. *Chem. - Eur. J.* **2016**, *22* (34), 11967−11970.

(30) Hayden, E. Y.; Hoi, K. K.; Lopez, J.; Inayathullah, M.; Condron, M. M.; Teplow, D. B. Identification of Key Regions and Residues Controlling Aβ Folding and Assembly. *Sci. Rep.* **2017**, *7* (1), 12434.

(31) Foley, A. R.; Finn, T. S.; Kung, T.; Hatami, A.; Lee, H.-W.; Jia, M.; Rolandi, M.; Raskatov, J. A. Trapping and Characterization of Nontoxic Aβ42 Aggregation Intermediates. *ACS Chem. Neurosci.* **2019**, *10* (8), 3880−3887.

(32) Janek, K.; Rothemund, S.; Gast, K.; Beyermann, M.; Zipper, J.; Fabian, H.; Bienert, M.; Krause, E. Study of the Conformational Transition of Aβ(1−42) Using D-Amino Acid Replacement Analogues. *Biochemistry* **2001**, *40* (18), 5457−5463.

(33) Krause, E.; Bienert, M.; Schmieder, P.; Wenschuh, H. The Helix-Destabilizing Propensity Scale of D-Amino Acids: The Influence of Side Chain Steric Effects. *J. Am. Chem. Soc.* **2000**, *122* (20), 4865−4870.

(34) Hua, Q. X.; Nakagawa, S.; Hu, S. Q.; Jia, W.; Wang, S.; Weiss, M. A. Toward the Active Conformation of Insulin: Stereospecific Modulation of a Structural Switch in the B Chain. *J. Biol. Chem.* **2006**, *281* (34), 24900−24909.

(35) Xie, C.; Prahl, A.; Ericksen, B.; Wu, Z.; Zeng, P.; Li, X.; Lu, W. Y.; Lubkowski, J.; Lu, W. Reconstruction of the Conserved β-Bulge in Mammalian Defensins Using D-Amino Acids. *J. Biol. Chem.* **2005**, *280* (38), 32921−32929.

(36) Masters, P. M.; Bada, J. L.; Samuel Zigler, J. Aspartic Acid Racemisation in the Human Lens during Ageing and in Cataract Formation. *Nature* **1977**, *268* (5615), 71−73.

https://dx.doi.org/10.1021/acs.joc.9b02312
J. Org. Chem. 2020, 85, 1385−1391

(37) Shapira, R.; Austin, G. E.; Mirra, S. S. Neuritic Plaque Amyloid in Alzheimer's Disease Is Highly Racemized. *J. Neurochem.* **1988**, *50*, 69.
(38) Roher, A. E.; Lowenson, J. D.; Clarke, S.; Wolkow, C.; Wang, R.; Cotter, R. J.; Reardon, I. M.; Zurcher-Neely, H. A.; Heinrikson, R. L.; Ball, M. J.; et al. Structural Alterations in the Peptide Backbone of β-Amyloid Core Protein May Account for Its Deposition and Stability in Alzheimer's Disease. *J. Biol. Chem.* **1993**, *268* (5), 3072−3083.
(39) Kubo, T.; Kumagae, Y.; Miller, C. A.; Kaneko, I. β-Amyloid Racemized at the Ser 26 Residue in the Brains of Patients with Alzheimer Disease: Implications in the Pathogenesis of Alzheimer Disease. *J. Neuropathol. Exp. Neurol.* **2003**, *62* (3), 248−259.
(40) Campioni, S.; Mannini, B.; Zampagni, M.; Pensalfini, A.; Parrini, C.; Evangelisti, E.; Relini, A.; Stefani, M.; Dobson, C. M.; Cecchi, C.; et al. A Causative Link between the Structure of Aberrant Protein Oligomers and Their Toxicity. *Nat. Chem. Biol.* **2010**, *6* (2), 140−147.
(41) Yu, L.; Edalji, R.; Harlan, J. E.; Holzman, T. F.; Lopez, A. P.; Labkovsky, B.; Hillen, H.; Barghorn, S.; Ebert, U.; Richardson, P. L.; et al. Structural Characterization of a Soluble Amyloid β-Peptide Oligomer. *Biochemistry* **2009**, *48* (9), 1870−1877.
(42) Foley, A. R.; Raskatov, J. A. A DFT-Assisted Topological Analysis of Four Polymorphic, S-Shaped Aβ42 Fibril Structures. *ChemBioChem* **2019**, *20* (13), 1722−1724.
(43) Grant, M. A.; Lazo, N. D.; Lomakin, A.; Condron, M. M.; Arai, H.; Yamin, G.; Rigby, A. C.; Teplow, D. B. Familial Alzheimer's Disease Mutations Alter the Stability of the Amyloid Beta-Protein Monomer Folding Nucleus. *Proc. Natl. Acad. Sci. U. S. A.* **2007**, *104* (42), 16522−16527.
(44) Lazo, N. D.; Grant, M. A.; Condron, M. C.; Rigby, A. C.; Teplow, D. B. On the Nucleation of Amyloid β-Protein Monomer Folding. *Protein Sci.* **2005**, *14* (6), 1581−1596.
(45) Hatami, A.; Monjazeb, S.; Milton, S.; Glabe, C. G. Familial Alzheimer's Disease Mutations within the Amyloid Precursor Protein Alter the Aggregation and Conformation of the Amyloid-β Peptide. *J. Biol. Chem.* **2017**, *292* (8), 3172−3185.
(46) Yun, S.; Urbanc, B.; Cruz, L.; Bitan, G.; Teplow, D. B.; Stanley, H. E. Role of Electrostatic Interactions in Amyloid β-Protein (Aβ) Oligomer Formation: A Discrete Molecular Dynamics Study. *Biophys. J.* **2007**, *92* (11), 4064−4077.
(47) Baumketner, A.; Bernstein, S. L.; Wyttenbach, T.; Lazo, N. D.; Teplow, D. B.; Bowers, M. T.; Shea, J.-E. Structure of the 21−30 Fragment of Amyloid Beta-Protein. *Protein Sci.* **2006**, *15* (6), 1239−1247.
(48) Sciarretta, K. L.; Gordon, D. J.; Petkova, A. T.; Tycko, R.; Meredith, S. C. Aβ40-Lactam(D23/K28) Models a Conformation Highly Favorable for Nucleation of Amyloid. *Biochemistry* **2005**, *44* (16), 6003−6014.
(49) Krone, M. G.; Baumketner, A.; Bernstein, S. L.; Wyttenbach, T.; Lazo, N. D.; Teplow, D. B.; Bowers, M. T.; Shea, J. E. Effects of Familial Alzheimer's Disease Mutations on the Folding Nucleation of the Amyloid β-Protein. *J. Mol. Biol.* **2008**, *381* (1), 221−228.
(50) Warner, C. J. A.; Dutta, S.; Foley, A. R.; Raskatov, J. A. A Tailored HPLC Purification Protocol That Yields High Purity Amyloid Beta 42 and Amyloid Beta 40 Peptides, Capable of Oligomer Formation. *J. Visualized Exp.* **2017**, No. 121, No. e55482.
(51) Biancalana, M.; Koide, S. Molecular Mechanism of Thioflavin-T Binding to Amyloid Fibrils. *Biochim. Biophys. Acta, Proteins Proteomics* **2010**, *1804* (7), 1405−1412.
(52) Roychaudhuri, R.; Yang, M.; Condron, M. M.; Teplow, D. B. Structural Dynamics of the Amyloid β-Protein Monomer Folding Nucleus. *Biochemistry* **2012**, *51* (19), 3957−3959.
(53) Fawzi, N. L.; Phillips, A. H.; Ruscio, J. Z.; Doucleff, M.; Wemmer, D. E.; Head-Gordon, T. Structure and Dynamics of the Aβ21−30 Peptide from the Interplay of NMR Experiments and Molecular Simulations. *J. Am. Chem. Soc.* **2008**, *130* (19), 6145−6158.
(54) Mithu, V. S.; Sarkar, B.; Bhowmik, D.; Das, A. K.; Chandrakesan, M.; Maiti, S.; Madhu, P. K. Curcumin Alters the Salt Bridge-Containing Turn Region in Amyloid β(1−42) Aggregates. *J. Biol. Chem.* **2014**, *289* (16), 11122−11131.
(55) Ma, B.; Nussinov, R. Stabilities and Conformations of Alzheimer's -Amyloid Peptide Oligomers (A 16−22, A 16−35, and A 10−35): Sequence Effects. *Proc. Natl. Acad. Sci. U. S. A.* **2002**, *99* (22), 14126−14131.
(56) Bitan, G.; Kirkitadze, M. D.; Lomakin, A.; Vollers, S. S.; Benedek, G. B.; Teplow, D. B. Amyloid β-Protein (Aβ) Assembly: Aβ40 and Aβ42 Oligomerize through Distinct Pathways. *Proc. Natl. Acad. Sci. U. S. A.* **2003**, *100* (1), 330−335.
(57) Morimoto, A.; Irie, K.; Murakami, K.; Ohigashi, H.; Shindo, M.; Nagao, M.; Shimizu, T.; Shirasawa, T. Aggregation and Neurotoxicity of Mutant Amyloid β (Aβ) Peptides with Proline Replacement: Importance of Turn Formation at Positions 22 and 23. *Biochem. Biophys. Res. Commun.* **2002**, *295* (2), 306−311.
(58) Irie, K. New Diagnostic Method for Alzheimer's Disease Based on the Toxic Conformation Theory of Amyloid β. *Biosci., Biotechnol., Biochem.* **2020**, *84*, 1−16.
(59) Ladiwala, A. R. A.; Litt, J.; Kane, R. S.; Aucoin, D. S.; Smith, S. O.; Ranjan, S.; Davis, J.; Van Nostrand, W. E.; Tessier, P. M. Conformational Differences between Two Amyloid Boligomers of Similar Size and Dissimilar Toxicity. *J. Biol. Chem.* **2012**, *287* (29), 24765−24773.
(60) Ono, K.; Condron, M. M.; Teplow, D. B. Structure-Neurotoxicity Relationships of Amyloid β-Protein Oligomers. *Proc. Natl. Acad. Sci. U. S. A.* **2009**, *106* (35), 14745−14750.
(61) Jarosz-Griffiths, H. H.; Noble, E.; Rushworth, J. V.; Hooper, N. M. Amyloid-β Receptors: The Good, the Bad, and the Prion Protein. *J. Biol. Chem.* **2016**, *291* (7), 3174−83.
(62) Kostylev, M. A.; Kaufman, A. C.; Nygaard, H. B.; Patel, P.; Haas, L. T.; Gunther, E. C.; Vortmeyer, A.; Strittmatter, S. M. Prion-Protein-Interacting Amyloid-β Oligomers of High Molecular Weight Are Tightly Correlated with Memory Impairment in Multiple Alzheimer Mouse Models. *J. Biol. Chem.* **2015**, *290* (28), 17415−17438.
(63) Limbocker, R.; Chia, S.; Ruggeri, F. S.; Perni, M.; Cascella, R.; Heller, G. T.; Meisl, G.; Mannini, B.; Habchi, J.; Michaels, T. C. T.; et al. Trodusquemine Enhances Aβ 42 Aggregation but Suppresses Its Toxicity by Displacing Oligomers from Cell Membranes. *Nat. Commun.* **2019**, *10* (1), 225.

https://dx.doi.org/10.1021/acs.joc.9b02312
J. Org. Chem. 2020, 85, 1385−1391

ACS Chemical Neuroscience
Cite This: *ACS Chem. Neurosci.* 2019, 10, 3880–3887
Research Article
pubs.acs.org/chemneuro

Trapping and Characterization of Nontoxic Aβ42 Aggregation Intermediates

Alejandro R. Foley,[†] Thomas S. Finn,[†] Timothy Kung,[†] Asa Hatami,[‡] Hsiau-Wei Lee,[†] Manping Jia,[§] Marco Rolandi,[§] and Jevgenij A. Raskatov*[,†]

[†]Department of Chemistry and Biochemistry, University of California Santa Cruz, Santa Cruz, California 95064, United States
[‡]Sangamo Therapeutics, Richmond, California 94804, United States
[§]Department of Electrical Engineering, University of California Santa Cruz, Santa Cruz, California 95064, United States

Supporting Information

ABSTRACT: Amyloid β (Aβ) 42 is an aggregation-prone peptide and the believed seminal etiological agent of Alzheimer's disease (AD). Intermediates of Aβ42 aggregation, commonly referred to as diffusible oligomers, are considered to be among the most toxic forms of the peptide. Here, we studied the effect of the age-related epimerization of Ser26 (i.e., S26s chiral edit) in Aβ42 and discovered that this subtle molecular change led to reduced fibril formation propensity. Surprisingly, the resultant soluble aggregates were nontoxic. To gain insight into the structural changes that occurred in the peptide upon S26s substitution, the system was probed using an array of biophysical and biochemical methods. These experiments consistently pointed to the stabilization of aggregation intermediates in the Aβ42−S26s system. To better understand the changes arising as a consequence of the S26s substitution, molecular level structural studies were performed. Using a combined nuclear magnetic resonance (NMR)- and density functional theory (DFT)-computational approach, we found that the S26s chiral edit induced only local structural changes in the Gly25−Ser26−Asn27 region. Interestingly, these subtle changes enabled the formation of an intramolecular Ser26−Asn27 H-bond, which disrupted the ability of Asn27 to engage in the fibrillogenic side chain-to-side chain H-bonding pattern. This reveals that intermolecular stabilizing interactions between Asn27 side chains are a key element controlling Aβ42 aggregation and toxicity.

KEYWORDS: *Alzheimer's disease, protein aggregation, amyloid β, soluble oligomers, serine epimerization*

INTRODUCTION

Protein misfolding and amyloid accumulation are characteristic of various neurodegenerative disorders.[1] In the case of Alzheimer's disease (AD), age-dependent accumulation of senile plaques, predominantly composed of amyloid β (Aβ), is a hallmark of the disease.[2] Aβ is a 36−43 amino acid peptide, which is proteolytically cleaved from the transmembrane amyloid precursor protein (APP) by β-secretase and γ-secretase.[3] Over the last two decades, soluble oligomers of Aβ42 have emerged as the most neurotoxic species of the amyloid aggregation cascade,[4,5] while insoluble fibrils and amyloid deposits may be comparatively inert, possibly protective.[6−10]

The Aβ42 sequence can formally be partitioned into four domains: (I) N-terminal flexible domain (NTFD, residues 1−16); (II) central hydrophobic domain (CHD, residues 17−20); (III) central flexible domain (CFD, residues 21−30); (IV) C-terminal hydrophobic domain (CTHD, residues 31−42). An important role of the CFD is to orchestrate the relative orientation of the CHD and CTHD, which may underlie the formation of different fibrillary polymorphs of Aβ42.[11] The significance of the CFD is further exemplified by the six AD-causing familial mutations that are harbored by this domain, illuminating the high functional relevance of the CFD and pointing toward this β-turn region as being critical for Aβ aggregation and stability.

Age-related epimerization is an uncatalyzed process that slowly converts naturally occurring L-amino acids to their D-enantiomers. It is particularly well-documented in long-lived proteins including plaque-derived Aβ,[12] crystallins,[13] and elastins.[14] While they are relatively small molecular-level changes (resulting from C_α chirality inversion), they can have profound effects on molecular structure and function[15] and are thought to be significant contributors to age-related disorders.[16] For example, aspartate epimerization has been shown to alter Aβ aggregation properties,[17] and epimerized serine (up to 10%) has been found at the core of amyloid plaques in human AD brains.[18] Similarly, epimerization levels of aspartate and serine residues in α-crystallins were reported to reach 35% by the age of 75 years in cataract human eye lenses found in elderly individuals.[19,20] Aβ42 contains a serine residue (Ser26) located in the center of the CFD. Ser26 is prone to age-related epimerization,[18] which we expected to induce local conformational changes in the CFD. In the present study, we

Received: June 15, 2019
Accepted: July 18, 2019
Published: July 18, 2019

DOI: 10.1021/acschemneuro.9b00340
ACS Chem. Neurosci. 2019, 10, 3880−3887

investigated how the S26s substitution alters the molecular interactions at the β-turn of Aβ42, leading to a drastic difference for both aggregation propensity and biological activity of Aβ42.

RESULTS

Epimerization of Ser26 Delays Aβ42 Fibril Formation and Suppresses Toxicity. We hypothesized that the conformational changes induced by D-Ser replacement at position 26 would alter the aggregation propensity of Aβ42. We thus investigated how the L-Ser26 to D-Ser26 chiral inversion (i.e., S26s) (Figure 1A) altered the fibril formation kinetics of

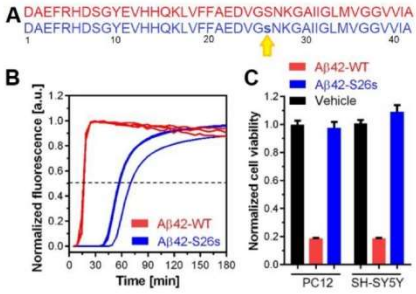

Figure 1. ThT-monitored aggregation kinetics and biological activity of Aβ42−WT and Aβ42−S26s peptides. (A) Amino acid sequence of Aβ42−WT (red) and Aβ42−S26s (blue) peptides. Yellow arrow marks where Ser26 is located and epimerized. Small letter (s) indicates chiral inversion. (B) Aβ42−WT and Aβ42−S26s (20 μM) were monitored by thioflavin T (ThT, 20 μM) fluorescence at 37 °C in 20 mM phosphate buffer (pH 7.4) with continuous shaking. Each curve represents one of three replicates. $t_{1/2}$ is defined as the time required to reach half the maximum fluorescence intensity measured (indicated as the dashed black line). (C) Cellular viability in PC12 and SH-SY5Y cell lines following treatment with 50 μM Aβ42−WT or Aβ42−S26s. Aβ42 peptides were dissolved in culture medium, and the resulting solution was used to incubate the cells for 72 h. Readout of cell viability was measured by using the WST-1 reagent. Each bar represents the average of three replicates with error bars representing standard deviation.

Aβ42 using the thioflavin T (ThT) fluorescence assay, wherein we observed a 4−5-fold delay in amyloid aggregation for the S26s chiral variant. While Aβ42−WT rapidly aggregated with a $t_{1/2}$ of 12.4 ± 0.2 min, the Aβ42−S26s variant displayed a $t_{1/2}$ of 61.6 ± 8.0 min (Figure 1B) in a persistent fashion with different synthetic batches and lower concentrations (Figure S6). This was qualitatively consistent with trends reported in a study of the Aβ40 system.[21] Fibril formation was confirmed by transmission electron microscopy (TEM) for both peptides at the end point of the experiment (TEM Appendix).

Soluble aggregation intermediates of Aβ42 have been shown to be more neurotoxic than Aβ42 fibrils.[7,22] To investigate whether this delayed propensity toward fibril formation influenced the biological activity of the S26s chiral variant, we incubated rat pheochromocytoma cells (PC12) and human neuroblastoma (SH-SY5Y) cells for 72 h with 50 μM Aβ42−WT or Aβ42−S26s and assessed cell viability by the WST-1 assay. Surprisingly, the Aβ42−S26s peptide was not toxic to either of the cell lines, while Aβ42−WT reduced cell viability to approximately 20% in both cases (Figure 1C). To ensure the robustness and the reproducibility of our results, each experiment was performed with 3 different synthetic batches of each peptide, showing consistent results between the three at 50 μM and lower concentrations (Figures S7 and S8).

Epimerization of Ser26 Stabilizes Soluble Aggregation Intermediates. The striking difference in toxicity between these two isoforms, which only differ in one stereocenter out of forty-two, led us to investigate the structural changes that happen when Ser26 is epimerized. Recently, Garai and Frieden[23] showed that incorporating a fluorescent label into the Aβ structure allows one to monitor fibril formation by fluorescence quenching of the dye. This method gives one access to additional information on aggregation steps that are undetectable by ThT fibril formation assays. To test whether we could obtain more information on the Aβ42−S26s aggregation intermediates that are stabilized during the increased lag time period, we fluorescently labeled Aβ42−WT and Aβ42−S26s at the N-terminus with 5(6)-carboxytetramethylrhodamine (TAMRA), which we had previously observed to not alter the biophysical or biological properties of the peptide.[24] Because the labeling was performed using a mixture of two TAMRA diastereomers, this resulted in mixtures of two diastereomeric labeled peptides with both Aβ42−WT and Aβ42−S26s. These mixtures were subsequently purified by HPLC, and only the major diastereomers were used in all the experiments. We found that, apart from displaying the expected delay toward aggregation as observed in the ThT experiments, the TAMRA−Aβ42−S26 peptide showed a double-transition curve, which can be formally partitioned into phase 1 (ϕ_1) and phase 2 (ϕ_2) (Figure 2A). While TAMRA−Aβ42−WT fluorescent intensity rapidly decayed, reaching the final plateau at approximately 60 min, a higher intensity curve was observed for the TAMRA−Aβ42−S26s variant (ϕ_1). This phase, indicative of the presence of metastable species, persisted for approximately 90 min and then decayed again reaching a final plateau at approximately 150 min. This kinetic signature was observed for the 3 synthetic batches that were tested, with minor batch-to-batch variations for the TAMRA−Aβ42−S26s peptide (Figure S9). It is worth noticing that TAMRA−Aβ42−WT also displays a subtle curvature at around the 0.6 intensity value. We also monitored these different stages by TEM to obtain insights into the morphologies of the aggregation intermediates (Figure 2B−G). We observed that both peptides formed spherical oligomers at the initial point of the experiment (t_0) (Figure 2B,E), with a similar average diameter of 11.33 ± 2.10 nm for TAMRA−Aβ42−WT and 11.35 ± 1.97 nm for TAMRA−Aβ42−S26s (Figure S10), consistent with previous observations.[8,25] After 1 h, when TAMRA−Aβ42−WT reached its near-minimum plateau, we observed mostly fibrils with still some residual aggregation intermediates in the TAMRA−Aβ42−WT sample (Figure 2C). However, at the same 1 h time point, the TAMRA−Aβ42−S26s variant was still in its transition phase 1 (ϕ_1) and displayed a heterogeneous mixture of spherical and protofibril-like structures (Figure 2F). At the end point of the experiment (24 h), only fibrils were observed for TAMRA−Aβ42−WT (Figure 2D), while TAMRA−Aβ42−S26s showed a mixture of fibrils and smaller aggregation intermediates (Figure 2G). An additional sample aliquot was taken from the TAMRA−Aβ42−S26s sample as soon as ϕ_1 started its decay ($\phi_1 \rightarrow \phi_2$ transition), showing by TEM that it is in this step

DOI: 10.1021/acschemneuro.9b00340
ACS Chem. Neurosci. 2019, 10, 3880−3887

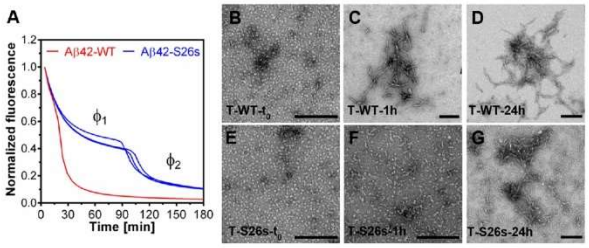

Figure 2. Comparison of TAMRA−Aβ42−WT and TAMRA−Aβ42−S26s aggregation kinetics. (A) Aggregation kinetics of TAMRA−Aβ42−WT and TAMRA−Aβ42−S26s (20 μM) at 37 °C with continuous shaking in 20 mM phosphate buffer (pH 7.4) monitored by TAMRA fluorescence quenching. (B−G) Negative stain TEM images of TAMRA−Aβ42−WT and TAMRA−Aβ42−S26s fibril structures. Samples were collected at three different time points from the TAMRA−quenching experiment (0, 1, and 24 h) and spotted into TEM grids for imaging. TAMRA−Aβ42−WT (B−D); TAMRA−Aβ42−S26s (E−G). Scale bar: 200 nm in all cases.

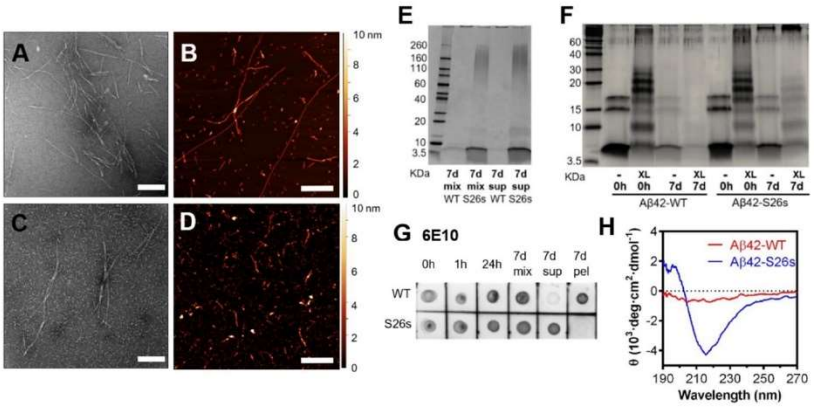

Figure 3. Aβ42−WT and Aβ42−S26s morphology and sizes present after quiescent incubation. (A) Aβ42−WT fibril morphology after a 7-day quiescent incubation at 37 °C by negative stain TEM. (B) Aβ42−WT fibril morphology after a 7-day quiescent incubation at 37 °C by AFM. (C) Aβ42−S26s fibril morphology after a 7-day quiescent incubation at 37 °C by negative stain TEM. (D) Aβ42−S26s fibril morphology after a 7-day quiescent incubation at 37 °C by AFM. TEM scale bar: 200 nm in all cases. AFM scale bar: 1 μm in all cases. (E) SDS-PAGE with 4−20% gradient gel. Samples were incubated for 7 d at 20 μM and mixed 1:1 with loading buffer for either the mixture or supernatant solutions. Twenty μL was loaded into each well. (F) Low MW 16% acrylamide gel with cross-linked Aβ42 peptides. Samples were incubated for the indicated time at 20 μM, cross-linked using PICUP chemistry, and mixed 1:1 with loading buffer, and 20 μL was loaded into each well. "XL" denotes cross-link. (G) 6E10 dot blot results of Aβ42−WT and Aβ42−S26s at a 20 μM peptide concentration. Two μL of solution was spotted onto a nitrocellulose membrane at each time point. The membrane was incubated overnight at 4 °C with 6E10 antibody at a 1:1000 dilution and developed by an Opti-4CN Substrate kit (BioRad). Either a mixture, the supernatant, or the pellet fractions were spotted for the indicated time points. (H) Circular dichroism spectra of the supernatant fractions from the Aβ42−WT (red) and Aβ42−S26s (blue) samples after a 7-day quiescent incubation.

when bigger aggregates started to develop (Figure S11), strongly suggesting that the fibril formation cascade may be initiated at the ϕ_1/ϕ_2 juncture. The aggregation delay for the Aβ42−S26s isoform in both ThT and TAMRA kinetic experiments was consistently observed at lower concentrations (Figure S9).

Stabilized Aggregation Intermediates of Aβ42−S26s Have β-Sheet Structure and Are Comparable to Aβ42−WT Species. We performed a quiescent incubation of Aβ42−WT and Aβ42−S26s (without a TAMRA label) at 37 °C for 7 days in 20 mM phosphate buffer (pH 7.4) and imaged both samples by TEM and atomic force microscopy (AFM; Figure 3A−D). Aβ42−WT yielded mainly elongated fibrils (Figure 3A,B), while in contrast, the Aβ42−S26s chiral variant displayed a mixture of fibrils and smaller, rounded, and protofibril-like structures (Figure 3C,D). We also used gel electrophoresis to determine the size of the aggregates after the 7-day incubation at 37 °C in 20 mM phosphate buffer (pH 7.4) (Figure 3E,F) and compared both the whole mixture fraction (precipitated fibrils + solution) and the isolated supernatant fraction (solution without precipitated fibrils). The supernatant was isolated from fibrils by centrifuging the samples for 20 min

DOI: 10.1021/acschemneuro.9b00340
ACS Chem. Neurosci. 2019, 10, 3880−3887

at 14 000g to remove fibrils from the solution, as previously described.[26] Samples were run on a 4−20% Tgx mini-protean (Bio-Rad) gel and developed by silver staining. Neither the mixed solution nor the supernatant fraction from the Aβ42−WT incubation showed any bands in the 3.5−260 kDa range, with the exception of a faint band at 4.5 kDa (Figure 3E). In contrast, both the mixture and supernatant fraction of the Aβ42−S26s sample displayed a strong band at around 4.5 kDa, corresponding to the Aβ42 monomer size. These samples also contain a diffusely stained area band between 60 and 260 kDa, which corresponds to 13−58 monomeric units. We also analyzed the propensity of both peptides to form low molecular weight oligomers by photoinduced cross-linking of unmodified protein (PICUP) chemistry, which stabilizes oligomers by covalently cross-linking them.[27] We examined the Aβ42−WT and Aβ42−S26s samples either immediately after reconstitution (0 h) or following a 7-day quiescent incubation (37 °C) using a 12% tris-tricine polyacrylamide gel (Figure 3F). The 0 h time point sample shows the expected oligomeric distribution for Aβ42−WT, consistent with previous reports,[27,28] with the Aβ42−S26s chiral variant displaying an indistinguishable distribution, suggesting that there are no apparent differences in the low-n oligomeric species between the two peptides. In contrast, while the Aβ42−WT displays no oligomeric bands after 7 days of incubation, the Aβ42−S26s sample still showed a combination of low-n oligomeric species. The strong band for the higher molecular weight aggregates (960−260 kDa) was also present on the top of the gel. To further characterize the nature of the species remaining in solution for the Aβ42−S26s chiral variant, we performed a dot blot analysis with the commercial mouse monoclonal 6E10 antibody (BioLegend Cat. No. 803001), which reacts with a broad range of Aβ species.[29] Dot blot results (Figure 3G) indicated that, while there was no 6E10-reactive species for Aβ42−WT in the supernatant fraction, the Aβ42−S26s supernatant contained 6E10-positive material, further corroborating the stabilization of soluble oligomeric species that remain in solution. In a complementary manner, the isolated Aβ42−WT pellet was 6E10-reactive, while almost no reactivity was observed for Aβ42−S26s, indicating the absence of precipitated material. Additionally, we analyzed the supernatant fraction by circular dichroism (CD) spectroscopy to elucidate the nature of the species present in solution. While CD spectra showed a curve indicative of the β-sheet structure for the Aβ42−S26s supernatant, a virtually flat line was observed for the Aβ42−WT supernatant, indicating that there was no peptide left in the supernatant at that point (Figure 3H), which is consistent with the higher aggregation propensity of Aβ42−WT than Aβ42−S26s (cf. Figures 1−3). TEM images obtained for the supernatant further corroborated this difference (Figure S12).

Conformational Changes Induced by D-Ser at Position 26 in Aβ42 Are Local but Affect the Overall Aβ42 Fibril Assembly. Given the striking differences in aggregation and biological activity between the Aβ42−S26s isoform and the Aβ42−WT peptide, we investigated the molecular-level interactions that occur when L-Ser26 is replaced by D-Ser. Serine 26 is located in the center of the CFD (residues 21−30) of Aβ42. This region is considered as the folding monomer nucleus of Aβ42 and is typically used as a model segment to study the key interactions involved in the initial folding steps of Aβ42 by solution-state nuclear magnetic resonance (NMR).[30,31] However, while its flexibility and solubility make it a good model to study in solution-state NMR experiments under physiologically relevant conditions, unlike the full-length peptide, the CFD is not aggregation-prone. CFD is flanked by two Phe residues at positions 19 and 20 and by two Ile residues at positions 31 and 32, making it part of the loop I region (17−32) of Aβ42. Given the nature of these Phe and Ile residues, which commonly interact through a hydrophobic steric zipper in mature Aβ fibrils,[32] we hypothesized that incorporating these 4 additional amino acids would result in a 14-mer peptide that might be a better model of full-length Aβ42 that can be studied by solution-state NMR. This choice was further supported by the fact that the 14-mer segment Aβ(19−32) can form a loop domain in Aβ42 fibrils, with the Phe and the Ile residues acting as the hydrophobic sticky ends of the loop.[33−36] As such, we synthesized these Aβ(19−32) fragments, both WT and S26s (Figure 4A), and studied the local changes upon S26s chiral substitution. Interestingly, we found that the increased solubility and decreased aggregation propensity of Aβ42−S26s was also recapitulated in these model peptides. Aβ(19−32)-WT peptide quickly aggregated at 37 °C, reducing the intensity of ^{1}H peak signals, while the Aβ(19−32)−S26s peptide ^{1}H peak signals remained unaltered (Figure 4B). By ^{1}H ^{1}H TOCSY (total correlation spectroscopy) spectra, we observed that chemical shifts were only locally affected following the introduction of the S26s substitution (Figure 4C). Only Gly25, Ser26, and Asn27 displayed a noticeable HA proton shift change.

Epimerization of Serine 26 Interferes with the Asn Intermolecular Side Chain-to-Side Chain H-Bonding, Impairing Fibril Formation. Whereas NMR provided clear evidence of local changes, it did not yield sufficient information about detailed, atomic-level conformational changes that result from S26s. We thus used density functional theory (DFT)-based approaches (see the Supporting Information for computational details) to better understand the molecular nature of the changes induced by the S26s chiral substitution. In Aβ42 fibrils, Asn27 is found to engage in self-intermolecular side chain-to-side chain H-bonding through its side chain amide groups[33−37] (Figure 5A). Because our NMR results pointed to local conformational changes, we first examined how the S26s substitution influenced the local environment, i.e., the Gly25, Ser26, and Asn27 amino acids. The Gly25 residue was modeled as an acetyl cap ($NH3^{+}$ → H), and the Ans 27 terminus was amidated (COO^{-} → $CONH_2$) to eliminate artifactual charge-related issues. DFT molecular modeling revealed that, for the most stable conformer of the D-Ser-L-Asn model peptide, the side chains of D-Ser and L-Asn were able to engage in an *intra*molecular H-bond (Figure 5C), which was not possible in the L-peptide due to conformational reasons (Figure S13). This new intramolecular H-bond takes up the H-bonding capacity of the Asn side chain, so that it can no longer engage in an *inter*molecular Asn side chain-to-side chain H-bond as observed in Aβ42−WT fibrils. Side chain-to-side chain interactions of Asn (as well as Gln) have been reported previously to have fibrillogenic properties.[38,39] The deletion of such an interaction is therefore expected to disfavor fibril formation. To calculate the energy penalty associated with the loss of the interfibrillary H-bond, we calculated the energy of an Asn monomer in stacked pentamer, which was obtained from the most recent high resolution Aβ42 fibril structure 5oqv.[33] Heavy atoms were frozen, and hydrogens were optimized. Stabilization was calculated as 6.7 kcal/mol per monomer in pentamer. The Asn was then truncated to yield Ala (Figure 5B), which can still engage in backbone-to-backbone, but not

DOI: 10.1021/acschemneuro.9b00340
ACS Chem. Neurosci. 2019, 10, 3880−3887

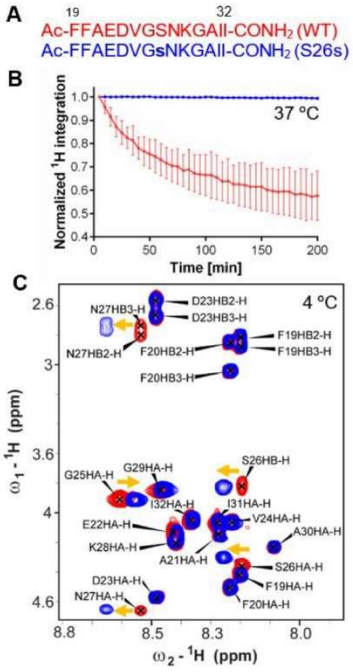

Figure 4. NMR analysis of the model Aβ(19−32) segment for the WT and S26s isoforms. (A) Amino acid sequence for the model 14-mer peptides, with the numbers (19−32) indicating their position in the Aβ42 sequence. (B) Representation of the total integration values of the ^{1}H peaks between 0 and 3.3 ppm at 37 °C in 20 mM phosphate buffer (pH 7.4). Data were normalized by assigning the maximum integration value for t = 5 min for each peptide. Data points show an average of two replicates, with error bars showing SD. (C) ^{1}H ^{1}H TOCSY spectra collected at 4 °C. Orange arrows mark differences in chemical shifts between the two Aβ(19−32) peptides. Red: Aβ(19−32)−WT. Blue: Aβ(19−32)−S26s. All NMR data were acquired on a 600 MHz Varian NMR in 20 mM phosphate buffer (pH 7.4). Orange arrows indicate the chemical shift change between the two Aβ(19−32) model peptides.

side chain-to-side chain H-bonding, yielding the monomer in pentamer stabilization energy of 3.7 kcal/mol (Figure 5D). Therefore, on the basis of our calculations, Asn side chain-to-side chain H-bond contributes 3 kcal/mol to the stabilization of Aβ42 fibrils, which is in good agreement with the published values.[40] We then examined how the replacement of L-Ser with D-Ser might change the conformational fold of this region. Ser26 is located at a central position in the β-hairpin structure of Aβ42, which comprises amino acids 24−29. Folding events occurring in this region have been shown to be critical for Aβ42 aggregation in *in vitro*[41] and *in silico* studies.[42] Furthermore, the neighboring amino acids harbor six familial AD mutations that change the aggregation properties of Aβ42: Flemish (A21G), Arctic (E22G), Dutch (E22Q), Italian (E22K), Osaka (E22Δ), and Iowa (D23N), further corroborating the importance of this loop. To study the conformational rearrangement induced by D-Ser at position 26, we docked the DFT geometry-optimized D-Ser-L-Asn structure into the high-resolution Aβ42 fibril structure 5oqv, using the four heavy atoms of Gly25 (or the model acetyl cap) as points for superposition. By DFT optimizations, we observed that the S26s chiral substitution leads to an "opening" of the β-hairpin loop by as much as 52.3° (Figure 5E). A consistent β-hairpin opening was also observed when the model peptide was docked into all other published Aβ42 structures (Figure S14). This effect, combined with the impairment of Asn cross side chain H-bonding, is likely to be responsible for the reduced propensity of Aβ42−S26s to form fibrils.

DISCUSSION

It is widely accepted that Aβ42 oligomeric species are some of the most, if not the most, neurotoxic species present in the amyloid aggregation cascade.[26,43−45] Some of the observed Aβ42 mechanisms of toxicity include long-term potentiation inhibition, mitochondrial dysfunction, neuroinflammation, calcium dysregulation, generation of reactive oxygen species, membrane poration, or changes in lipid homeostasis, among others.[46,47] However, a molecular-level understanding of Aβ42 oligomers is still lacking, and whether the neurotoxic properties of Aβ42 oligomers are exclusively related to their solubility, structure, and size still requires a better understanding. While terms such as "on-pathway" and "off-pathway" have been used to differentiate oligomers that may or may not proceed toward fibril formation, the transient and dynamic nature of these species allows them to interconvert between monomer, "on-pathway" β-sheet rich, and "off-pathway" unstructured forms.[48] Since Aβ42 oligomers were identified as the most neurotoxic species, the initial research was focused on targeting these oligomeric structures, by blocking the oligomerization process,[49] inhibiting aggregation,[50] or developing antibodies that target these soluble oligomeric structures (Solanezumab, Aducanumab, BAN2401, CAD106, Bapinezumab, SAR228810, Ponezumab).[51] More recently, a diametrically opposed strategy focused on stimulating oligomer-to-fibril conversion by enhancing fibril aggregation has been proposed,[8,25,52,53] with results showing that toxicity can be reduced or completely abolished by promoting aggregation.

Here, we show that the age-related Aβ42−S26s epimerization decreases the fibril formation propensity of Aβ42 and stabilizes β-sheet rich nontoxic species, including oligomers and protofibril-like structures. To the best of our knowledge, this is the first case wherein a physiologically relevant Aβ42 isoform that stabilizes oligomeric species has no toxicity against model cell lines. Our results showed that both Aβ42−WT and Aβ42−S26s form low-n oligomers with similar size distributions at t_0 (Figure 3F) and that the oligomers that were formed by both peptides had similar average diameters (11.33 ± 2.10 and 11.35 ± 1.97 nm, respectively) and size distribution (Figure S10). Both species were recognized by the mouse monoclonal antibody 6E10 (Figure 3G), and the oligomeric species stabilized in the Aβ42−S26s isoform had β-sheet character (Figure 3H), thought to be characteristic for "on-pathway", neurotoxic Aβ species.[54] The fact that the Aβ42−S26s isoform has several key features of toxic oligomers but does not affect cell viability points toward the existence of further subtle factors, such as the dependence on structural motifs or sequence specificity to trigger toxicity. For example, cytosolic

DOI: 10.1021/acschemneuro.9b00340
ACS Chem. Neurosci. 2019, 10, 3880−3887

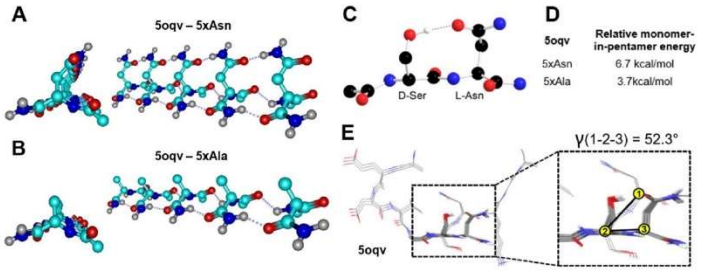

Figure 5. DFT computational analysis. (A) Representation of Asn27 side chain-to-side chain intermolecular H-bonding extracted from the published 5oqv Aβ42 fibril structure.[33] (B) Representation of the substitution of Asn27 by Ala, docked in the published 5oqv Aβ42 fibril structure.[33] (C) DFT results for the most stable calculated conformer of D-Ser-L-Asn, showing a H-bond between −OH from Ser and NH_2 from Asn. (D) Calculated energy difference when Asn27 is substituted by Ala. (E) Aβ42 β-hairpin "opening" induced by S26s mutation. Degraded color structure: Original conformation from 5oqv. Intense color structure: Conformation adopted with D-Ser, which shows an angle difference of 52.3°. Point 1: Asn27 Cα from 5oqv Aβ42 fibril structure. Point 2: Ser26 Cα from D-Ser-L-Asn calculated dimer. Point 3: Asn27 C_α from D-Ser-L-Asn calculated dimer.

chaperonin TRiC and Hsp70 stabilize nontoxic poliQ huntingtin oligomers,[55] and strategies based on stabilizing "off-pathway", nontoxic oligomers of Aβ by the addition of small molecules have been suggested as therapy development against AD.[56] Thus, apart from representing an important region of the central flexible domain of Aβ42, the Gly25−Ser26−Asn27 motif might have additional, fine-tuned structural and functional roles directly related to the toxic effects of Aβ42, representing a potential therapeutic target region.

Additionally, Ser26 and Asn27 are susceptible to additional modifications that change the structure and function of Aβ. Zweckstetter and co-workers[57] showed that phosphorylation of Ser26 in Aβ40 stabilizes nontoxic soluble assemblies, leading to a structural fold that is less prone to adopt the β-turn structure. Interestingly, as observed by NMR, this modification only impacts the neighboring residues of Ser26 but has dramatic consequences on the overall properties of the peptide. Similarly, Teplow and co-workers[58] synthesized an Aβ42 isoform where Gly25 and Ser26 were chemically cross-linked through an ester bond, generating a conformationally constrained peptide that also altered Aβ42 structure, solubility, and aggregation properties. Deamidation of Asn27 to Asp has also been reported to reduce the aggregation propensity of Aβ0 and Aβ42,[59] highlighting the importance of the Asn27 side chain interfibrillar H-bond toward the stabilization and growth of amyloid fibrils.

We found that epimerization of Ser26 led to subtle, local structural changes that prevent fibril formation, and we determined that the lower aggregation propensity was due to two main factors: first, epimerization of Ser26 leads to a rearrangement of the Asn27 side chain, which engages in an intramolecular H-bond with the OH group of Ser26. This prevents Asn27 cross-side chain intermolecular stabilization between Aβ42 strands, as seen in Aβ42 fibrillary structures (Figure 5A). Using DFT, we calculated that this side chain-to-side chain intermolecular H-bond accounted for 3 kcal/mol per Aβ42 monomer unit. Second, the conformational changes induced by the incorporation of D-Ser at position 26 opens the β-hairpin loop, as observed when docking the optimized D-Ser-L-Asp dimer structure into a high-resolution Aβ42 fibril structure (PDB 5oqv) (Figure 5E) and other Aβ42 fibril structures (Figure S14). This leads to attenuated fibril formation propensity, which is likely a consequence of altered relative orientation of the CHD (residues 17−20) and CTHD (residues 31−42).

CONCLUSION

In summary, we described how a very subtle molecular change that arises from epimerization at the serine 26 residue of Aβ42 can profoundly alter both its structure and function, leading to attenuated aggregation propensity and reduced toxicity of the peptide. Subsequent NMR- and DFT-based structural work revealed a pattern consistent with local changes in hydrogen-bonding associated with Ser26 and Asn27. Our results highlight that not all Aβ42 oligomers are toxic per se and that subtle conformational effects and intermolecular H-bond stabilizing interactions are critical for the amyloid fibril formation and biological activity of Aβ42. The Aβ42−S26s chiral variant may become a valuable mechanistic tool to study neuronal toxicity. Furthermore, the Ser26−Asn27 region of Aβ42 may offer a well-defined site for therapeutic intervention with small molecules in the future.

ASSOCIATED CONTENT

Supporting Information

The Supporting Information is available free of charge on the ACS Publications website at DOI: 10.1021/acschemneuro.9b00340.

Sample characterization, preparation, general experimental procedures, batch-to-batch results, and additional experiments and measurements (PDF)

AUTHOR INFORMATION

Corresponding Author

*E-mail: jraskato@ucsc.edu.

ORCID

Alejandro R. Foley: 0000-0002-8644-0546
Marco Rolandi: 0000-0001-7898-2479
Jevgenij A. Raskatov: 0000-0002-0082-9113

DOI: 10.1021/acschemneuro.9b00340
ACS Chem. Neurosci. 2019, 10, 3880−3887

Author Contributions

A.R.F. and J.A.R. designed the study. A.R.F. and J.A.R. wrote the manuscript, and A.R.F made the figures. A.R.F., T.S.F., A.H., T.K., H.-W.L., and M.J. collected the data. A.R.F., T.S.F., A.H., T.K., H.-W.L., M.J., M.R., and J.A.R. participated in data analysis. All authors interpreted the data, provided intellectual contributions, and critically revised the manuscript.

Funding

J.A.R. thanks UC Santa Cruz for unrestricted access to the computational facilities as well as flexible start-up funds, and NIH for funding (R21AG058074). J.A.R. also acknowledges the NIH S10OD016246-01A1 award for the purchase of the JASCO J1500 CD. M.R. and M.J. acknowledge the Office of Naval Research Award N000141612507 (DURIP) for supporting the AFM experiments.

Notes

The authors declare no competing financial interest.

■ ACKNOWLEDGMENTS

The authors thank Dr. Eefei Chen and Dr. Benjamin Abrams for technical support. The authors thank CEM for the independent synthesis of Aβ samples for the validation of key trends. The authors also thank Dr. David S. Kliger, Dr. Eric Y. Hayden, and Dr. Subrata Dutta for helpful comments on the manuscript.

■ DEDICATION

Dedicated to Prof. Samuel H. Gellman on the occasion of his sixtieth birthday.

■ ABBREVIATIONS

AD, Alzheimer's disease; Aβ, amyloid β; Gly, glycine; Ser, serine; Asn, asparagine; NTFD, N-terminal flexible domain; CHD, central hydrophobic domain; CFD, central flexible domain; CTHD, C-terminal hydrophobic domain; ThT, thioflavin T; TAMRA, 5(6)-carboxytetramethylrhodamine; TEM, transmission electron microscopy; AFM, atomic force microscopy; sup, supernatant; pel, pellet; SDS, sodium dodecyl sulfate; PICUP, photoinduced cross-linking of unmodified protein; CD, circular dichroism; NMR, nuclear magnetic resonance; TOCSY, total correlation spectroscopy; DFT, density functional theory

■ REFERENCES

(1) Chiti, F., and Dobson, C. M. (2006) Protein Misfolding, Functional Amyloid, and Human Disease. *Annu. Rev. Biochem. 75* (1), 333−366.

(2) Murphy, M. P., and Levine, H. (2010) Alzheimer's Disease and the Amyloid-β Peptide. *J. Alzheimer's Dis. 1*, 311−323.

(3) O'Brien, R. J., and Wong, P. C. (2011) Amyloid Precursor Protein Processing and Alzheimer's Disease. *Annu. Rev. Neurosci. 34*, 185−204.

(4) Cohen, S. I. A., Linse, S., Luheshi, L. M., Hellstrand, E., White, D. A., Rajah, L., Otzen, D. E., Vendruscolo, M., Dobson, C. M., and Knowles, T. P. J. (2013) Proliferation of Amyloid- 42 Aggregates Occurs through a Secondary Nucleation Mechanism. *Proc. Natl. Acad. Sci. U. S. A. 110* (24), 9758−9763.

(5) Bitan, G., Kirkitadze, M. D., Lomakin, A., Vollers, S. S., Benedek, G. B., and Teplow, D. B. (2003) Amyloid -Protein (Aβ) Assembly: Aβ 40 and Aβ 42 Oligomerize through Distinct Pathways. *Proc. Natl. Acad. Sci. U. S. A. 100* (1), 330−335.

(6) Treusch, S., Cyr, D. M., and Lindquist, S. (2009) Amyloid Deposits: Protection against Toxic Protein Species? *Cell Cycle 8* (11), 1668−1674.

(7) Haass, C., and Selkoe, D. J. (2007) Soluble Protein Oligomers in Neurodegeneration: Lessons from the Alzheimer's Amyloid β-Peptide. *Nat. Rev. Mol. Cell Biol. 8* (2), 101−112.

(8) Dutta, S., Foley, A. R., Warner, C. J. A., Zhang, X., Rolandi, M., Abrams, B., and Raskatov, J. A. (2017) Suppression of Oligomer Formation and Formation of Non-Toxic Fibrils upon Addition of Mirror-Image Aβ42 to the Natural l-Enantiomer. *Angew. Chem., Int. Ed. 56* (38), 11506−11510.

(9) Raskatov, J. A. (2017) Chiral Inactivation: An Old Phenomenon with a New Twist. *Chem. - Eur. J. 23* (67), 16920−16923.

(10) Raskatov, J. A. (2019) What is the "relevant" Amyloid β 42 concentration? *ChemBioChem*, DOI: 10.1002/cbic.201900097.

(11) Foley, A. R., and Raskatov, J. A. (2019) A DFT-assisted topological analysis of four polymorphic, S-shaped Aβ42 fibril structures. *ChemBioChem*, DOI: 10.1002/cbic.201900036.

(12) Shapira, R., Austin, G. E., and Mirra, S. S. (1988) Neuritic Plaque Amyloid in Alzheimer's Disease Is Highly Racemized. *J. Neurochem. 50* (1), 69−74.

(13) Tao, Y., and Julian, R. R. (2014) Identification of Amino Acid Epimerization and Isomerization in Crystallin Proteins by Tandem LC-MS. *Anal. Chem. 86* (19), 9733−9741.

(14) Powell, J. T., Vine, N., and Crossman, M. (1992) On the Accumulation of D-Aspartate in Elastin and Other Proteins of the Ageing Aorta. *Atherosclerosis 97* (2−3), 201−208.

(15) Raskatov, J. A., and Teplow, D. B. (2017) Using Chirality to Probe the Conformational Dynamics and Assembly of Intrinsically Disordered Amyloid Proteins. *Sci. Rep. 7* (1), 12433.

(16) Truscott, R. J. W., Schey, K. L., and Friedrich, M. G. (2016) Old Proteins in Man: A Field in Its Infancy. *Trends Biochem. Sci. 41* (8), 654−664.

(17) Tomiyama, T., Asano, S., Furiya, Y., Shirasawa, T., Endo, N., and Mori, H. (1994) Racemization of Asp23 Residue Affects the Aggregation Properties of Alzheimer Amyloid β Protein Analogues. *J. Biol. Chem. 269* (14), 10205−10208.

(18) Kubo, T., Kumagae, Y., Miller, C. A., and Kaneko, I. (2003) β-Amyloid Racemized at the Ser 26 Residue in the Brains of Patients with Alzheimer Disease: Implications in the Pathogenesis of Alzheimer Disease. *J. Neuropathol. Exp. Neurol. 62* (3), 248−259.

(19) Masters, P. M., Bada, J. L., and Zigler, J. S. (1978) Aspartic Acid Racemization in Heavy Molecular Weight Crystallins and Water Insoluble Protein from Normal Human Lenses and Cataracts. *Proc. Natl. Acad. Sci. U. S. A. 75* (3), 1204−1208.

(20) Hooi, M. Y. S., Raftery, M. J., and Truscott, R. J. W. (2013) Age-Dependent Racemization of Serine Residues in a Human Chaperone Protein. *Protein Sci. 22* (1), 93−100.

(21) Kaneko, I., Morimoto, K., and Kubo, T. (2001) Drastic Neuronal Loss in Vivo by β-Amyloid Racemized at Ser26 Residue: Conversion of Non-Toxic [D-Ser26]β-Amyloid 1−40 to Toxic and Proteinase-Resistant Fragments. *Neuroscience 104* (4), 1003−1011.

(22) Gong, Y., Chang, L., Viola, K. L., Lacor, P. N., Lambert, M. P., Finch, C. E., Krafft, G. A., and Klein, W. L. (2003) Alzheimer's Disease-Affected Brain: Presence of Oligomeric A Ligands (ADDLs) Suggests a Molecular Basis for Reversible Memory Loss. *Proc. Natl. Acad. Sci. U. S. A. 100* (18), 10417−10422.

(23) Garai, K., and Frieden, C. (2013) Quantitative Analysis of the Time Course of Aβ Oligomerization and Subsequent Growth Steps Using Tetramethylrhodamine-Labeled Aβ. *Proc. Natl. Acad. Sci. U. S. A. 110* (9), 3321−3326.

(24) Dutta, S., Finn, T. S., Kuhn, A. J., Abrams, B., and Raskatov, J. A. (2019) Chirality Dependence of Amyloid β Cellular Uptake and a New Mechanistic Perspective. *ChemBioChem 20*, 1023−1026.

(25) Ahmed, M., Davis, J., Aucoin, D., Sato, T., Ahuja, S., Aimoto, S., Elliott, J. I., Van Nostrand, W. E., and Smith, S. O. (2010) Structural Conversion of Neurotoxic Amyloid-B 1−42 Oligomers to Fibrils. *Nat. Struct. Mol. Biol. 17* (5), 561−567.

(26) Kayed, R., Head, E., Thompson, J. L., McIntire, T. M., Milton, S. C., Cotman, C. W., and Glabel, C. G. (2003) Common Structure of Soluble Amyloid Oligomers Implies Common Mechanism of Pathogenesis. *Science 300* (5618), 486−489.

DOI: 10.1021/acschemneuro.9b00340
ACS Chem. Neurosci. 2019, 10, 3880−3887

(27) Bitan, G. (2006) Structural Study of Metastable Amyloidogenic Protein Oligomers by Photo-Induced Cross-Linking of Unmodified Proteins. *Methods Enzymol. 413*, 217−236.
(28) Warner, C. J. A., Dutta, S., Foley, A. R., and Raskatov, J. A. (2016) Introduction of D-Glutamate at a Critical Residue of Aβ42 Stabilizes a Prefibrillary Aggregate with Enhanced Toxicity. *Chem. - Eur. J. 22* (34), 11967−11970.
(29) Hatami, A., Monjazeb, S., Milton, S., and Glabe, C. G. (2017) Familial Alzheimer's Disease Mutations within the Amyloid Precursor Protein Alter the Aggregation and Conformation of the Amyloid-β Peptide. *J. Biol. Chem. 292* (8), 3172−3185.
(30) Roychaudhuri, R., Yang, M., Condron, M. M., and Teplow, D. B. (2012) Structural Dynamics of the Amyloid β-Protein Monomer Folding Nucleus. *Biochemistry 51* (19), 3957−3959.
(31) Fawzi, N. L., Phillips, A. H., Ruscio, J. Z., Doucleff, M., Wemmer, D. E., and Head-Gordon, T. (2008) Structure and Dynamics of the Aβ21−30 Peptide from the Interplay of NMR Experiments and Molecular Simulations. *J. Am. Chem. Soc. 130* (19), 6145−6158.
(32) Colletier, J.-P., Laganowsky, A., Landau, M., Zhao, M., Soriaga, A. B., Goldschmidt, L., Flot, D., Cascio, D., Sawaya, M. R., and Eisenberg, D. (2011) Molecular Basis for Amyloid- Polymorphism. *Proc. Natl. Acad. Sci. U. S. A. 108* (41), 16938−16943.
(33) Gremer, L., Schölzel, D., Schenk, C., Reinartz, E., Labahn, J., Ravelli, R. B. G., Tusche, M., Lopez-Iglesias, C., Hoyer, W., Heise, H., et al. (2017) Fibril Structure of Amyloid-β(1−42) by Cryo−electron Microscopy. *Science 358* (6359), 116−119.
(34) Wälti, M. A., Böckmann, A., Meier, B. H., Arai, H., Ravotti, F., Glabe, C. G., Güntert, P., Wall, J. S., and Riek, R. (2016) Atomic-Resolution Structure of a Disease-Relevant Aβ(1−42) Amyloid Fibril. *Proc. Natl. Acad. Sci. U. S. A. 113* (34), E4976−E4984.
(35) Xiao, Y., Ma, B., McElheny, D., Parthasarathy, S., Long, F., Hoshi, M., Nussinov, R., and Ishii, Y. (2015) Aβ(1−42) Fibril Structure Illuminates Self-Recognition and Replication of Amyloid in Alzheimer's Disease. *Nat. Struct. Mol. Biol. 22* (6), 499−505.
(36) Colvin, M. T., Silvers, R., Ni, Q. Z., Can, T. V., Sergeyev, I., Rosay, M., Donovan, K. J., Michael, B., Wall, J., Linse, S., et al. (2016) Atomic Resolution Structure of Monomorphic Aβ42 Amyloid Fibrils. *J. Am. Chem. Soc. 138* (30), 9663−9674.
(37) Lührs, T., Ritter, C., Adrian, M., Riek-Loher, D., Bohrmann, B., Döbeli, H., Schubert, D., and Riek, R. (2005) 3D Structure of Alzheimer's Amyloid-beta(1−42) Fibrils. *Proc. Natl. Acad. Sci. U. S. A. 102* (48), 17342−17347.
(38) Kurt, T. D., Aguilar-Calvo, P., Jiang, L., Rodriguez, J. A., Alderson, N., Eisenberg, D. S., and Sigurdson, C. J. (2017) Asparagine and Glutamine Ladders Promote Cross-Species Prion Conversion. *J. Biol. Chem. 292* (46), 19076−19086.
(39) Plumley, J. A., and Dannenberg, J. J. (2010) The Importance of Hydrogen Bonding between the Glutamine Side Chains to the Formation of Amyloid VQIVYK Parallel β-Sheets: An ONIOM DFT/AM1 Study. *J. Am. Chem. Soc. 132* (6), 1758−1759.
(40) Sheu, S.-Y., Yang, D.-Y., Selzle, H. L., and Schlag, E. W. (2003) Energetics of Hydrogen Bonds in Peptides. *Proc. Natl. Acad. Sci. U. S. A. 100* (22), 12683−12687.
(41) Hayden, E. Y., Hoi, K. K., Lopez, J., Inayathullah, M., Condron, M. M., and Teplow, D. B. (2017) Identification of Key Regions and Residues Controlling Aβ Folding and Assembly. *Sci. Rep. 7* (1), 12434.
(42) Grant, M. A., Lazo, N. D., Lomakin, A., Condron, M. M., Arai, H., Yamin, G., Rigby, A. C., and Teplow, D. B. (2007) Familial Alzheimer's Disease Mutations Alter the Stability of the Amyloid Beta-Protein Monomer Folding Nucleus. *Proc. Natl. Acad. Sci. U. S. A. 104* (42), 16522−16527.
(43) Lambert, M. P., Barlow, A. K., Chromy, B. A., Edwards, C., Freed, R., Liosatos, M., Morgan, T. E., Rozovsky, I., Trommer, B., Viola, K. L., et al. (1998) Diffusible, Nonfibrillar Ligands Derived from Abeta1−42 Are Potent Central Nervous System Neurotoxins. *Proc. Natl. Acad. Sci. U. S. A. 95* (11), 6448−6453.
(44) Rowan, M. J., Lemere, C. A., Garcia-Munoz, A., Regan, C. M., Sabatini, B. L., Shepardson, N. E., Brett, F. M., Li, S., Shankar, G. M., Selkoe, D. J., et al. (2008) Amyloid-β Protein Dimers Isolated Directly from Alzheimer's Brains Impair Synaptic Plasticity and Memory. *Nat. Med. 14* (8), 837−842.
(45) LaDu, M. J., Baker, L. K., Krafft, G. A., Dahlgren, K. N., Manelli, A. M., and Stine, W. B. (2002) Oligomeric and Fibrillar Species of Amyloid-β Peptides Differentially Affect Neuronal Viability. *J. Biol. Chem. 277* (35), 32046−32053.
(46) Kayed, R., and Lasagna-Reeves, C. A. (2012) Molecular Mechanisms of Amyloid Oligomers Toxicity. *J. Alzheimer's Dis. 33* (s1), S67−S78.
(47) Chiti, F., and Dobson, C. M. (2017) Protein Misfolding, Amyloid Formation, and Human Disease: A Summary of Progress Over the Last Decade. *Annu. Rev. Biochem. 86* (1), 27−68.
(48) Soto, C., and Pritzkow, S. (2018) Protein Misfolding, Aggregation, and Conformational Strains in Neurodegenerative Diseases. *Nat. Neurosci. 21* (10), 1332−1340.
(49) Walsh, D. M. (2005) Certain Inhibitors of Synthetic Amyloid -Peptide (Abeta) Fibrillogenesis Block Oligomerization of Natural Abeta and Thereby Rescue Long-Term Potentiation. *J. Neurosci. 25* (10), 2455−2462.
(50) Begum, A. N., Kayed, R., Cole, G. M., Ubeda, O. J., Frautschy, S. A., Glabe, C. G., Chen, P. P., Lim, G. P., Ambegaokar, S. S., Yang, F., et al. (2005) Curcumin Inhibits Formation of Amyloid β Oligomers and Fibrils, Binds Plaques, and Reduces Amyloid in Vivo. *J. Biol. Chem. 280* (7), 5892−5901.
(51) Knopman, D. S. (2019) Lowering of Amyloid-beta by β-secretase inhibitors - Some informative failures. *N. Engl. J. Med. 380*, 1476−1478.
(52) Bieschke, J., Herbst, M., Wiglenda, T., Friedrich, R. P., Boeddrich, A., Schiele, F., Kleckers, D., Lopez Del Amo, J. M., Grüning, B. A., Wang, Q., et al. (2012) Small-Molecule Conversion of Toxic Oligomers to Nontoxic β-Sheet-Rich Amyloid Fibrils. *Nat. Chem. Biol. 8* (1), 93−101.
(53) Limbocker, R., Chia, S., Ruggeri, F. S., Perni, M., Cascella, R., Heller, G. T., Meisl, G., Mannini, B., Habchi, J., Michaels, T. C. T., et al. (2019) Trodusquemine Enhances Aβ42 Aggregation but Suppresses Its Toxicity by Displacing Oligomers from Cell Membranes. *Nat. Commun. 10* (1), 225.
(54) Chimon, S., Shaibat, M. A., Jones, C. R., Calero, D. C., Aizezi, B., and Ishii, Y. (2007) Evidence of Fibril-like β-Sheet Structures in a Neurotoxic Amyloid Intermediate of Alzheimer's β-Amyloid. *Nat. Struct. Mol. Biol. 14* (12), 1157−1164.
(55) Behrends, C., Langer, C. A., Boteva, R., Böttcher, U. M., Stemp, M. J., Schaffar, G., Rao, B. V., Giese, A., Kretzschmar, H., Siegers, K., et al. (2006) Chaperonin TRiC Promotes the Assembly of PolyQ Expansion Proteins into Nontoxic Oligomers. *Mol. Cell 23* (6), 887−897.
(56) Ehrnhoefer, D. E., Bieschke, J., Boeddrich, A., Herbst, M., Masino, L., Lurz, R., Engemann, S., Pastore, A., and Wanker, E. E. (2008) EGCG Redirects Amyloidogenic Polypeptides into Unstructured, off-Pathway Oligomers. *Nat. Struct. Mol. Biol. 15* (6), 558−566.
(57) Amininasab, M., Schneider, A., Walter, J., Rezaei-Ghaleh, N., Zweckstetter, M., Becker, S., Stündl, A., Giller, K., and Kumar, S. (2014) Turn Plasticity Distinguishes Different Modes of Amyloid-β Aggregation. *J. Am. Chem. Soc. 136* (13), 4913−4919.
(58) Roychaudhuri, R., Lomakin, A., Bernstein, S., Zheng, X., Condron, M. M., Benedek, G. B., Bowers, M., and Teplow, D. B. (2014) Gly25-Ser26 Amyloid β-Protein Structural Isomorphs Produce Distinct Aβ42 Conformational Dynamics and Assembly Characteristics. *J. Mol. Biol. 426* (13), 2422−2441.
(59) Osaki, D., and Hiramatsu, H. (2016) Citrullination and Deamidation Affect Aggregation Properties of Amyloid β-Proteins. *Amyloid 23* (4), 234−241.

DOI: 10.1021/acschemneuro.9b00340
ACS Chem. Neurosci. 2019, 10, 3880−3887

ChemPubSoc Europe

DOI: 10.1002/chem.201601763

CHEMISTRY A European Journal Communication

Neurochemistry

Introduction of D-Glutamate at a Critical Residue of Aβ42 Stabilizes a Prefibrillary Aggregate with Enhanced Toxicity

Christopher J. A. Warner, Subrata Dutta, Alejandro R. Foley, and Jevgenij A. Raskatov*[a]

Dedicated to Professor Dr. Peter B. Dervan on the occasion of his 70th birthday

Abstract: The amyloid beta peptide 42 (Aβ42) is an aggregation-prone peptide that plays a pivotal role in Alzheimer's disease. We report that a subtle perturbation to the peptide through a single chirality change at glutamate 22 leads to a pronounced delay in the β-sheet adoption of the peptide. This was accompanied by an attenuated propensity of the peptide to form fibrils, which was correlated with changes at the level of the fibrillary architecture. Strikingly, the incorporation of D-glutamate was found to stabilize a soluble, ordered macromolecular assembly with enhanced cytotoxicity to PC12 cells, highlighting the importance of advanced prefibrillary Aβ aggregates in neurotoxicity.

Alzheimer's disease (AD) is a major neurodegenerative disorder that affects over 35 million people worldwide.[1] Reflecting the increase in life expectancy, these numbers continue to rise, while no cure exists.[2] Amyloid β (Aβ) is an aggregation-prone peptide of 36–43 amino acids in length and has been strongly implicated in the mechanism of AD.[3] The Aβ42 peptide is widely regarded as the most toxic Aβ entity in AD, which has been attributed to its high aggregation propensity.[4,5] The aggregation profile is complex, with diverse oligomeric, pre-fibrillary, and fibrillary states being formed. Over the past decade, diffusible oligomers have been recognized as particularly neurotoxic species.[4,5]

Familial AD can arise from diverse mutations within the Aβ42 sequence.[6] Over ten Aβ42 mutations have been identified, most of which are disease-causing single amino acid alterations. Strikingly, from those mutations, four AD-accelerating variants are positioned on one specific amino acid—glutamate 22 (E22)—which identifies the residue as particularly important in the context of Aβ42 neurotoxicity. The four E22-borne familial mutations have in common that they alter the charge at that residue, either through amino-acid substitution (E22G, Arctic, G = glycine; E22K, Italian, K = lysine; E22Q, Dutch, Q = glutamine), or amino-acid deletion (E22Δ, Osaka).[6] Biophysical experiments demonstrated that those substitutions enhance the Aβ propensity towards oligomer,[7] or fibril formation.[8] To further examine the role of residue 22 of Aβ42 on structure and function of the peptide, we have created the E22e chiral mutant **2** (e = D-glutamate). This subtle molecular edit enables for an alteration of the sidechain disposition of the peptide without affecting its physical properties, such as size, charge distribution, and polarizability (Figure 1).

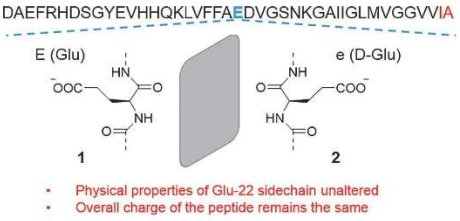

Figure 1. The Aβ sequence with glutamate 22 highlighted in blue. The differences between Aβ40 and Aβ42 are highlighted in red. Replacement of L-glutamate with D-glutamate at position 22 enables for a subtle alteration of the sidechain disposition.

We studied the effect of the introduction of D-glutamate at position 22 on the aggregation propensity of Aβ42 by conducting thioflavin T binding experiments (Figure 2A). Remarkably, the chiral E22e mutant **2** exhibited a fivefold reduction in the fibril-formation rate compared to the wildtype (WT) peptide **1** ($t_{1/2}$[E22e] = 65.6 min; $t_{1/2}$[WT] = 13.4 min). The rate of the fibril formation of **1** was comparable to those previously reported in the literature.[9–11] The aggregation ability of the Aβ42 peptide is believed to stem from its propensity to undertake a secondary structural transition from a random-coil-like structure to a β-sheet configuration.[3] We therefore examined the time-resolved circular dichroism spectra of the peptides **1** and **2** over a period of 24 h. In agreement with the thioflavin T binding results, a delay in the random coil to β-sheet configuration of the Aβ E22e peptide **2** was observed (see Supporting Information). These results demonstrate a reduced

[a] Dr. C. J. A. Warner, Dr. S. Dutta, A. R. Foley, Prof. Dr. J. A. Raskatov
Department of Chemistry and Biochemistry, Physical Science Building
University of California, 1156 High Street, Santa Cruz (USA)
E-mail: jraskato@ucsc.edu

Supporting information and ORCID(s) for the author(s) for this article can be found under http://dx.doi.org/10.1002/chem.201601763.

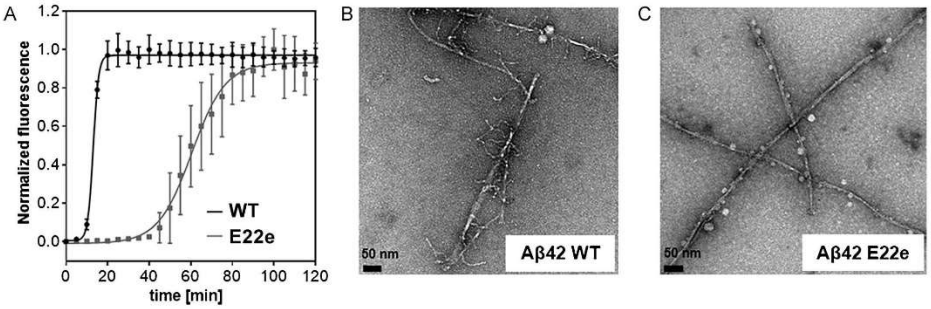

Figure 2. A) Aggregation kinetics of the Aβ42 wildtype peptide **1** (black) and Aβ42 E22e peptide **2** (grey) at 20 μM, monitored by the Thioflavin T (ThT) fluorescence (λ_{em} = 444 nm, λ_{ex} = 485 nm) at 37 °C. B,C) Representative transmission electron microscopy (TEM) images of the fibrillary architectures of the Aβ42 wildtype peptide **1** (B) and the Aβ42 E22e peptide **2** (C). The samples were incubated in phosphate buffer (20 mM, pH = 7.4) at 222 μM before being diluted to 200 nm for imaging.

propensity of the peptide **2** for aggregation at the fibrillary endpoint, as well as at prefibrillary stages.

The delayed aggregation kinetics of the E22e peptide **2** led us to investigate whether the fibrillary assemblies of **2** were altered compared to **1**. To do this, both Aβ42 WT **1** and Aβ42 E22e **2** fibrils were grown for 7 days at 37 °C following protocols by Tycko et al (see Supporting Information for details).[9] Transmission electron microscopy (TEM) images of the wildtype Aβ42 fibrils (Figure 2B) showed a distinct fibrillary architecture, characterized by the presence of numerous branches extending from the main fibril. This is of particular interest, given recent reports suggesting that the Aβ42-fibril formation is a secondary nucleation-dependent process.[10] In contrast, peptide **2** displayed more elongated, organized fibrillary structures devoid of branches (Figure 2C). Analogous TEM experiments were conducted, following an incubation of the peptides **1** and **2** for 2 h. The results were consistent in terms of branching, which was observable for Aβ42 WT, but not for the E22e chiral variant (see Supporting Information for images and further details).

The difference in the fibrillary morphologies between the peptides **1** and **2** led us to further investigate whether alterations in the prefibrillary structural assemblies could account for the striking differences. Photochemically induced crosslinking of unmodified proteins (PICUP) experiments were carried out to gain insight into the distribution of the oligomeric states.[12] Comparative analyses of the wildtype **1** and the E22e Aβ42 peptide **2** were conducted at two time points, either immediately upon reconstitution or following an incubation for 24 h. The oligomerization profiles of the two scaffolds **1** and **2** showed no statistically significant difference in the population states of the oligomers (dimer–heptamer), indicating that any differences in the fibrillary assembly of the two peptides occurred at more advanced stages of the aggregation process (Figure 3A,B, see Supporting Information for details). To investigate these late-stage prefibrillary structures we employed small-angle X-ray scattering (SAXS) analysis. SAXS has been shown to be a powerful technique for monitoring amyloid-related structural features.[13] We examined the SAXS curves of both wildtype **1** and E22e Aβ42 peptide **2** after initial reconstitution and following 24 h incubation at 37 °C (Figure 3C,D). For both time points, SAXS analysis of the peptide **2** demonstrated a Bragg reflection corresponding to a species with a periodicity of 3.7 nm. This value is consistent with the dimensions

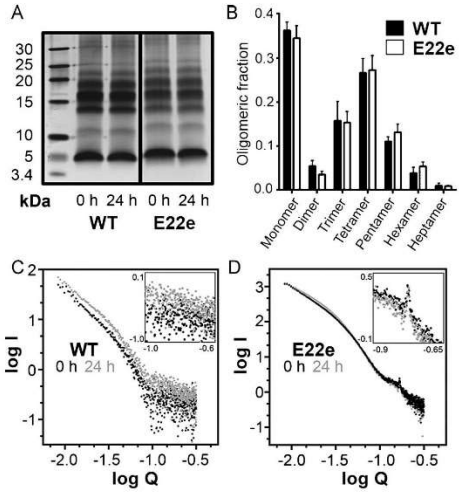

Figure 3. All experiments were carried out in phosphate buffer (20 mM, pH = 7.4) A) Representative PICUP (photochemically induced crosslinking of unmodified proteins) gels at both t = 0 h and t = 24 h. All PICUP experiments were carried out in phosphate buffer at 50 μM, either directly after reconstitution, or following incubation for 24 h. Corresponding experiments were also performed at 20 μM (see the Supporting Information). B) Densitometric analysis of oligomeric band intensity at t = 0 h, (see Supporting Information for t = 24 h). C) Small-angle X-ray scattering (SAXS) measurements of the Aβ42 wildtype peptide **1** at t = 0 h (black) and t = 24 h (grey). D) SAXS measurements of the Aβ42 E22e peptide **2** at t = 0 h (black) and t = 24 h (grey).

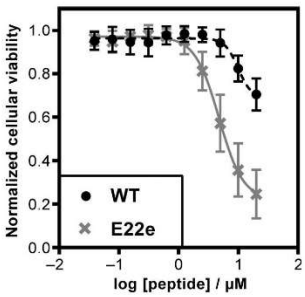

Figure 4. Dose-response curves of both wildtype Aβ42 **1** (black) and Aβ42 E22e **2** (grey) peptides against the rat pheochromocytoma PC12 adhesive cell line. Cells were plated at 5000 cells per well and allowed to adhere for 24 h prior to peptide addition, followed by incubation for additional 72 h. The cellular viability was determined at the endpoint of the assay using the cell proliferation reagent WST-1.

of a single unit of the wildtype Aβ42 sequence found within a fibril using NMR and in silico structural models.[14] No Bragg reflection and an increase in the heterogeneity of the sample was observed for peptide **1**, reflected by the large variance at high Q values.

The mechanism underlying the toxicity of Aβ42 remains a subject of active research. Diverse modes of cytotoxicity have been proposed, including membrane disruption, induction of tau hyperphosphorylation, oxidative stress mediated through copper complexation, brain insulin resistance/signaling, and mitochondrial toxicity.[15] The original (fibril-centric) amyloid-cascade hypothesis was reformulated when diffusible Aβ42 oligomers emerged as the more toxic species.[4c] To test whether the prefibrillary stabilized structure of peptide **2** exhibited an increase in cytotoxicity, we monitored the effects of varying concentrations of the wildtype peptide **1** and the E22e peptide **2** on rat pheochromocytoma PC12 cells (Figure 4). Addition of either peptide resulted in a reduction in the cellular viability, determined by the cell proliferation reagent WST-1. At 20 μM, a 30% reduction in the cellular viability was observed when dosing with the wildtype peptide **1** (Figure 4, WT). However, addition of the same concentration of the E22e peptide **2** resulted in an 80% reduction in the viability (Figure 4, E22e). The cellular viability of the PC12 cells was also found to be lower when peptide **2** was dosed at 10 μM, with a reduction in the cellular viability close to 65%, compared with a 20% reduction when dosing with the same concentration of peptide **1** (for detailed graphical analysis see Supporting Information). Preincubation (2 h or 4 h) of the peptides prior to administration did not affect their cytotoxicity (see Supporting Information). Our E22e variant offers a unique way of trapping an advanced aggregation intermediate of Aβ42 with enhanced toxicity, and highlights how a subtle structural change—a single chiral substitution—can have profound effects on aggregation and neurotoxicity.

In conclusion, incorporation of D-glutamate at position 22 of Aβ42 resulted in a peptide with attenuated propensity for misfolding and aggregation. Transmission electron microscopy showed a striking difference in the fibril morphology. The E22e peptide **2** exhibited elongated, ordered amyloid-beta fibrils. This is in stark contrast to the Aβ42 WT peptide **1**, which displayed a fibrillary architecture, characterized by the presence of a large number of sidechains protruding from the main fibril. No difference in the population density of the oligomers (dimer–heptamer) between the two peptides was observed. However, SAXS analysis of the E22e peptide **2** showed the presence of a unique Bragg reflection corresponding to a soluble species with a periodicity of 3.7 nm. Cell culture studies established a three- to fourfold increase in the cytotoxicity in response to the E22e substitution in Aβ42. This subtle molecular edit therewith offers a tool to improve our understanding of the Aβ42 neurotoxicity.

Acknowledgements

We are grateful to Prof. Maya Koronyo-Hamaoui, Prof. Glenn Millhauser and Prof. James Nowick for helpful discussions, to Prof. David Kliger for his assistance in interpretation of CD spectra, as well as to Rafael Palomino and Kate Markham from the Millhauser laboratory for their help with initial Aβ42 syntheses. Victoria Klein is acknowledged for her assistance with initial gel electrophoresis experiments. We acknowledge the NIH S10OD016246-01A1 award for purchase of the JASCO J1500 CD.

Keywords: aggregation · Alzheimer's disease · amyloid beta peptide · chirality · neurotoxicity

[1] H. W. Querfurth, F. M. LaFerla, *N. Engl. J. Med.* **2010**, *362*, 329–344.
[2] a) J. Hardy, D. J. Selkoe, *Science* **2002**, *297*, 353–356; b) D. J. Selkoe, *Nat. Med.* **2011**, *17*, 1060–1065.
[3] a) F. Chiti, C. M. Dobson, *Annu. Rev. Biochem.* **2006**, *75*, 333–366; b) C. L. Masters, N. A. Weinman, G. Multhaup, B. L. McDonald, K. Beyreuther, *Proc. Natl. Acad. Sci. USA* **1985**, *82*, 4245–4249.
[4] a) Y. S. Gong, L. Chang, K. L. Viola, P. N. Lacor, M. P. Lambert, C. E. Finch, G. A. Krafft, W. L. Klein, *Proc. Natl. Acad. Sci. USA* **2003**, *100*, 10417–10422; b) P. N. Lacor, M. C. Buniel, L. Chang, S. J. Fernandez, Y. S. Gong, K. L. Viola, M. P. Lambert, P. T. Velasco, E. H. Bigio, C. E. Finch, G. A. Krafft, W. L. Klein, *J. Neurosci.* **2004**, *24*, 10191–10200; c) C. Haass, D. J. Selkoe, *Nat. Rev. Mol. Cell. Bio.* **2007**, *8*, 101–112; d) D. J. Selkoe, *Behav. Brain Res.* **2008**, *192*, 106–113.
[5] a) S. Lesné, M. T. Koh, L. Kotilinek, R. Kayed, C. G. Glabe, A. Yang, M. Gallagher, K. H. Ashe, *Nature* **2006**, *440*, 352–357; b) C. Haupt, J. Leppert, R. Röenicke, J. Meinhardt, J. K. Yadav, R. Ramachandran, O. Ohlenschläger, K. G. Reymann, M. Görlach, M. Fändrich, *Angew. Chem. Int. Ed.* **2012**, *51*, 1576–1579; *Angew. Chem.* **2012**, *124*, 1608–1611.
[6] I. Benilova, E. Karran, B. De Strooper, *Nat. Neurosci.* **2012**, *15*, 349–357.
[7] C. Nilsberth, A. Westlind-Danielsson, C. B. Eckman, M. M. Condron, K. Axelman, C. Forsell, C. Stenh, J. Luthman, D. B. Teplow, S. G. Younkin, J. Näslund, L. Lannfelt, *Nat. Neurosci.* **2001**, *4*, 887–893.
[8] A. Baumketner, M. G. Krone, J. E. Shea, *Proc. Natl. Acad. Sci. USA* **2008**, *105*, 6027–6032.
[9] A. T. Petkova, R. D. Leapman, Z. Guo, W.-M. Yau, M. P. Mattson, R. Tycko, *Science* **2005**, *307*, 262–265.
[10] S. I. A. Cohen, S. Linse, L. M. Luheshi, E. Hellstrand, D. A. White, L. Rajah, D. E. Otzen, M. Vendruscolo, C. M. Dobson, T. P. J. Knowles, *Proc. Natl. Acad. Sci. USA* **2013**, *110*, 9758–9763.
[11] V. H. Finder, I. Vodopivec, R. M. Nitsch, R. Glockshuber, *J. Mol. Biol.* **2010**, *396*, 9–18.

[12] a) G. Bitan, A. Lomakin, D. B. Teplow, *J. Biol. Chem.* **2001**, *276*, 35176–35184; b) G. Bitan, M. D. Kirkitadze, A. Lomakin, S. S. Vollers, G. B. Benedek, D. B. Teplow, *Proc. Natl. Acad. Sci. USA* **2003**, *100*, 330–335; c) G. Bitan, D. B. Teplow, *Acc. Chem. Res.* **2004**, *37*, 357–364.
[13] A. E. Langklide, B. Vestergaard, *FEBS Lett.* **2009**, *583*, 2600–2609.
[14] a) M. Coles, W. Bicknell, A. A. Watson, D. P. Fairlie, D. J. Craik, *Biochemistry* **1998**, *37*, 11064–11077; b) T. Lührs, C. Ritter, M. Adrian, D. Riek-Loher, B. Bohrmann, H. Döbeli, D. Schubert, R. Riek, *Proc. Natl. Acad. Sci. USA* **2005**, *102*, 17342–17347; c) W. Qiang, W. M. Yau, Y. Luo, M. P. Mattson, R. Tycko, *Proc. Natl. Acad. Sci. USA* **2012**, *109*, 4443–4448; d) Y. Xiao, B. Ma, S. Parthasarathy, F. Long, M. Hoshi, R. Nussinov, Y. Ishii, *Nat. Struct. Mol. Biol.* **2015**, *22*, 499–505.
[15] a) L. M. Ittner, J. Götz, *Nat. Rev. Neurosci.* **2011**, *12*, 67–72; b) Y. H. Hung, A. I. Bush, R. A. Cherny, *J. Biol. Inorg. Chem.* **2010**, *15*, 61–76.

Received: April 14, 2016
Published online on June 30, 2016

Received: 28 July 2016 | Revised: 18 October 2016 | Accepted: 19 October 2016

DOI 10.1002/chir.22667

WILEY

SPECIAL ISSUE ARTICLE

Using chiral peptide substitutions to probe the structure function relationship of a key residue of Aβ42

Christopher J.A. Warner | Subrata Dutta | Alejandro R. Foley | Eefei Chen | David S. Kliger | Jevgenij A. Raskatov

Department of Chemistry and Biochemistry, University of California, Santa Cruz, CA, USA

Correspondence
Jevgenij A. Raskatov, University of California, Santa Cruz, Department of Chemistry and Biochemistry, Physical Science Building, 1156 High St., Santa Cruz, CA 95064.
Email: jraskato@ucsc.edu

Abstract

Amyloid beta-protein 42 plays an important role in the onset and progression of Alzheimer's disease. Familial mutations have identified the glutamate residue 22 as a hotspot with regard to peptide neurotoxicity. We introduce an approach to study the influence of systematic sidechain modification at this residue, employing chirality as a structural probe. Circular dichroism experiments reveal that charge-preserving alterations of the amino acid sidechain attenuate the characteristic random coil to β-sheet transition associated with the wildtype peptide. Removal of the negative charge from residue 22, a trait observed with all known familial mutations at this residue, gives rise to a peptide with limited random coil propensity and high β-sheet characteristics. Our approach can be extended to other residues of Aβ, as well as further amyloidogenic peptides.

KEYWORDS

Alzheimer's disease, amyloid β, chirality, circular dichroism, familial mutations

1 | INTRODUCTION

Alzheimer's disease (AD) is a neurodegenerative disorder, which affects over 35 million people worldwide today.[1] With life expectancy increasing and no cure available, those numbers are projected to double by 2050.[2] Amyloid beta (Aβ) is a neurotoxic peptide of 36–43 amino acids in length, and is believed to be the disease culprit.[3] The 42 amino acid-long variant, Aβ42, is regarded as the most toxic form of the peptide. This has been attributed, at least in part, to its propensity to form diffusible oligomers, which have emerged as particularly neurotoxic aggregation intermediates.[4]

Familial AD is an accelerated form of the disease, which can arise through single amino acid mutations throughout the Aβ42 sequence.[5] Four of the known AD-causing mutations of the peptide are associated with glutamate (E) 22. This suggests that the residue plays a crucial role in the formation of neurotoxic Aβ42 aggregates. The four mutations have in common that they change the charge of the sidechain (E22G, Arctic, negative → neutral; E22Q, Dutch, negative → neutral; E22K, Italian, negative → positive, and E22Δ, Osaka, negative → neutral).[5] In this study, we systematically probed the influence of sidechain modification on peptide folding. We performed a set of incremental modifications to the E22 residue, gradually removing the sidechain (E → D → A → G) and subsequently reintroducing it with mirror-image connectivity (→ a → d → e).[6]

2 | MATERIALS AND METHODS

All peptides used throughout the course of this study were synthesized and purified, following our published protocols.[6] All peptides displayed a final purity of greater than 95% as determined by analytical high-performance liquid chromatography (HPLC) (see Supporting Information for characterization). Prior to circular dichroism (CD) analysis, peptides were dissolved in an aqueous solution of 0.1% NH_4OH and quantitated by a nanodrop spectrophotometer (280 nm, $\varepsilon = 1490\ M^{-1}\ cm^{-1}$). Samples were fractionated into the

*Dedicated to Prof. Dr. Günter Helmchen, in appreciation of his contributions to the field of molecular chirality.

[This article is part of the Special Issue: Proceedings of 28th International Symposium on Molecular Chirality, Heidelberg 2016.]

appropriate volume required for 90 μg aliquots and lyophilized overnight.

2.1 | CD experiments

CD experiments were performed on a JASCO (Tokyo, Japan) J-1500 circular dichroism spectrometer set to a scan range of 180–280 nm, a DIT of 4 seconds, a scan speed of 50 nm per minute, a bandwidth of 1 nm, and a data pitch of 0.1 nm. Continuous rather than step scan was used in order to make measurements fast enough to monitor the earliest kinetic points. For all experiments, the aliquoted peptides were dissolved in 20 μL of an aqueous solution of 20 mM NaOH and sonicated for 30 sec. Subsequently, 380 μL of freshly prepared 20 mM phosphate buffer solution (pH 7.4; NaCl-free)[7] were added, resulting in a final concentration of 50 μM and a total volume of 400 μl. The solution was then immediately transferred to a 1-mm quartz cuvette and CD measurement undertaken. Following the initial analysis, the solution was removed from the cuvette and transferred to a low-bind Eppendorf tube and incubated at 37°C for the appropriate time. This procedure was repeated for all listed timepoints for peptides **1**–**7** (Figure 1). All experiments were conducted in duplicate and found to be reproducible. All spectra were baseline-corrected through subtraction of the buffer spectrum from each sample spectrum. Spectral smoothing was performed using the Means-Movement method built into the instrument software. Data analysis was performed as described in the Supporting Information.

3 | RESULTS AND DISCUSSION

CD is a powerful tool to monitor structural elements in proteins (random coil, α-helix, β-sheet).[8] The aggregation propensity of the Aβ42 peptide is believed to be triggered by a structural transition of the peptide from random coil to β-sheet.[4] CD was therefore an excellent tool to examine how subtle modification of residue 22 altered this transition.

A total of seven Aβ42 variants were synthesized (Figure 1), comprising a set of incremental changes to the sidechain of amino acid 22, which is normally expressed as glutamate (i.e., Aβ42 wildtype peptide **1**). In the molecular analog **2**, this sidechain was formally shortened by a methylene group, yielding the E22D mutant. Subsequent formal removal of the terminal carboxylate from **2** resulted in the E22A scaffold **3**. The ensuing replacement of the methyl substituent in **3** by hydrogen gave rise to the E22G variant **4**, known as the familial, AD-causing, Arctic mutation.[5] The glutamate sidechain was subsequently reintroduced with the opposite chirality, yielding the frameworks E22a **5**, E22d **6,** and, finally, E22e **7**.

The influence of substituent variation upon the rate of β-sheet formation was explored (Figure 2). The wildtype Aβ42 peptide **1**, initially found in a predominantly random coil

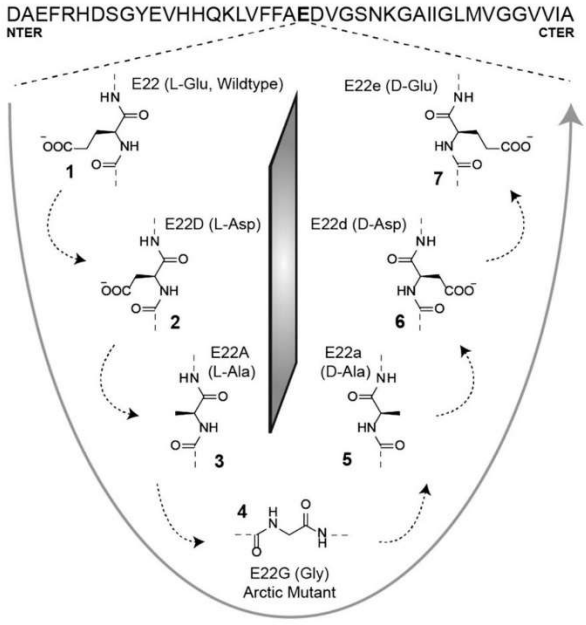

FIGURE 1 Starting with the wildtype Aβ **1**, a set of systematic modifications is performed. Methylene group truncation leads to the analog **2** (E22D). Removal of the carboxylate moiety yields **3** (E22A), and the subsequent replacement of the methyl group with a hydrogen leads to the variant **4** (E22G, the Arctic mutation). The sidechain is then gradually reintroduced with mirror-image connectivity. The lowercase character indicates the use of a D-amino acid; the compounds **5**–**7** correspond to the substitutions E22a, E22d, and E22e, respectively

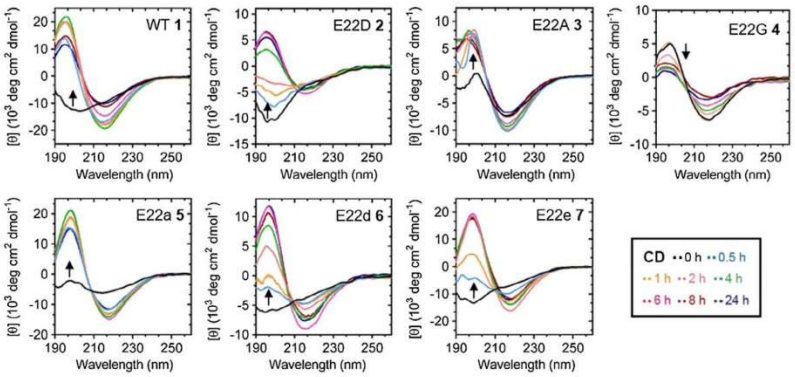

FIGURE 2 CD spectra of Aβ42 variants. Top row, from left to right: variants **1**–**4** bottom row, from left to right: variants **5**–**7**. All sample concentrations were 50 μM; starting points are indicated with arrows; for detailed sample preparation, see Materials and Methods

conformation, began to show a substantial increase in β-sheet characteristics after 30 min of incubation at 37°C, attaining maximal signal strength after 4 h of incubation. These findings are consistent with literature values.[9] Signal intensity subsequently began to decline, presumably due to formation of insoluble (fibrillary) species.[10] The methylene shortening of the sidechain in framework **2** resulted in a pronounced delay in β-sheet formation, with the molecule still exhibiting substantial random coil characteristics after 2 h of incubation. The maximum β-sheet signal was observed following 6 h of incubation. The E22A mutant, **3**, was found as a mixture of random coil and β-sheet following reconstitution, and rapidly reached the maximum β-sheet signature, whereas the Arctic mutant **4** displayed a fully developed β-sheet signature upon reconstitution. The framework **5**, incorporating D-alanine at residue 22, exhibited slightly higher random coil characteristics initially when compared to its L-alanine counterpart, **3**. However, it similarly underwent a rapid transition to a β-sheet motif within 30 min. The D-aspartate analog **6** exhibited a somewhat faster β-sheet transition than the L-aspartate scaffold **2**, whereas the D-glutamate framework **7** showed a delayed β-sheet transition with regard to **1**.

To facilitate visualization of results reported above, a heatmap representation was introduced (Figure 3, left; see also Table SI 1 for numerical values used to create the heatmap). Random coil structure was represented by blue, transitioning to red for β-sheet, and, finally, orange, representing gradual precipitation of sample. The anionic residues contained in scaffolds **1** (wildtype, E), **2** (E22D), **6** (E22d), and **7** (E22e) induced distinct folding properties (Figure 3, right; Table SI 2). Of particular interest, the wildtype variant adopted the β-sheet structure at the fastest rate, followed by E22e **7** and E22d **6**. The E22D mutant **2** was the slowest analog to display β-sheet features by CD. In agreement with previous studies, removal of charge at residue 22 (i.e., scaffolds **3**–**5**) resulted in accelerated β-sheet formation.[11] Previous work has demonstrated that a high random coil structure of the peptide can be formed by dissolution and maintaining of the protein in a high pH solution.[7] Therefore, we examined whether the E22G framework **4,** the most prevalent β-sheet peptide at the onset of the experiment, was capable of adopting a random coil structure at high pH. Dissolution of the peptide in 0.1% NH_4OH (pH 12) and subsequent CD analysis revealed a strong β-sheet signal, comparable to

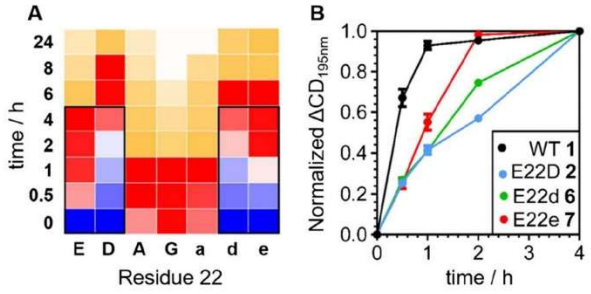

FIGURE 3 **A**, A gradient heatmap (blue: random coil; red: β-sheet; orange with subsequent fading: precipitation) showing the transition of peptide structure. For wildtype, E22D, E22d, and E22e the transition at 195 nm from random coil to β-sheet is depicted in the boxes marked with a black line within the figure; for the mutants E22A, E22G, and E22a, the intensity of β-sheet at 217 nm is plotted. **B**, The rate of change of the wildtype, E22D, E22d, and E22e peptides over the first 4 h of analysis, normalized against $t = 4$ h. Error bars were the result of two independent analyses

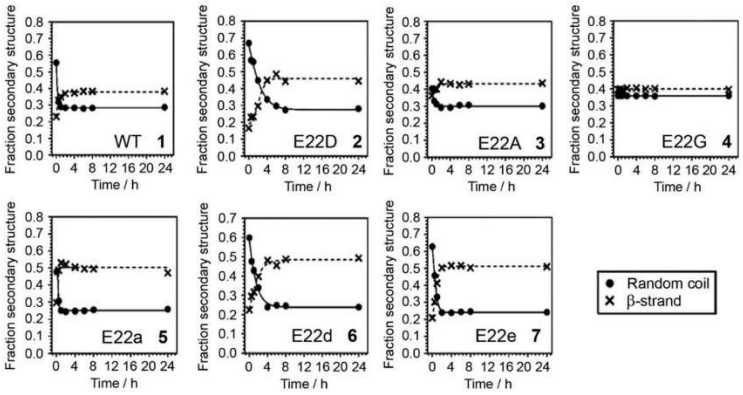

FIGURE 4 The fraction of random coil and β-strand secondary structure of the Aβ42 peptides **1–7**. The spectra were deconvoluted using the CONTINLL dataset 6 and the online program. The values used to plot the above graphs as well as the fractions of turn and α-helical content can be found in the Supporting Information

the one displayed at pH 7.4 (see Supporting Information for spectra and deconvolution analysis). The lack of differentiation between the two conditions suggests the importance of the negative charge associated with position-22 to allow for the peptide to adopt a random coil configuration. The striking 4-fold difference in β-sheet folding between **1** and the E22D mutant **2** was followed up by synthesizing the corresponding Aβ40 analogs **8** (wildtype) and **9** (E22D). The rate of β-sheet formation was attenuated substantially, requiring 4–5 days for the effect to become manifest (Figure SI 2). This is expected, given the known reduction of aggregation propensity of Aβ40, as compared to Aβ42.[11] The differentiation in β-sheet propensity of the two Aβ40 scaffolds was significantly less pronounced than with the corresponding Aβ42 analogs.

To further analyze the effect of how minor perturbations of glutamate 22 within Aβ42 alter the secondary structural features of the peptide, we performed structural deconvolution of the spectra, as shown in Figure 4. Deconvolution was performed using the DichroWeb algorithm and the CONTINLL dataset 6.[12–17] Examination of the wildtype peptide **1** showed that formation of the β-strand secondary structural feature was concurrent with the loss of the random coil structure. The degree of α-helical content and turn structure remained relatively constant through the course of the experiment, although the wildtype peptide **1** did show an increase in α-helical content after 30 min (see Supporting Information for full deconvolution table and graphical analysis of the α-helical and turn content of the CD spectra). This trend in loss of the random coil secondary structural component and an increase in β-strand formation was also found to be true for the E22D **2**, E22d **6,** and E22e **7** Aβ42 analogs. Incorporation of a charge-neutral residue, i.e., the E22A **3** or E22G **4** peptide, resulted in virtually time-invariant β-strand content, whereas the E22a mutant was more similar to the wildtype version.

4 | CONCLUSION

In this study we applied a novel approach to probe the effect of subtle alterations of the amyloid beta peptide at glutamate 22. Replacement of glutamate 22 with either aspartate or the D-amino acid of aspartate or glutamate (E22D **2**, E22d **6**, E22e **7**) resulted in a delay in the transition from random coil secondary structure to β-sheet. Deletion of the negative charge by replacement with either glycine or the two enantiomeric forms of alanine (E22A, **3**; E22G, **4**; E22a, **5**) attenuated the propensity of Aβ42 to adopt a random coil configuration, enhancing β-sheet propensity. In the case of the E22G variant **4**, β-sheet features were clearly observable at high pH, conditions that induce predominantly random coil structure in the wildtype peptide **1**. Our results demonstrate how subtle changes at a single residue of Aβ42 can lead to profound changes in secondary structure. We believe that our approach will be useful for examination of other residues of Aβ42, as well as other Aβ variants. Our approach is general and as such can be applied, in principle, to any peptide.

ACKNOWLEDGMENTS

JAR thanks UCSC for flexible start-up funds and two special research grants, as well as the Hellman Foundation for a Junior Faculty Award. We acknowledge the NIH S10OD016246-01A1 award for purchase of the JASCO J1500 CD.

REFERENCES

1. Qiu C, Kivipelto M, von Strauss E. Epidemiology of Alzheimer's disease: occurrence, determinants, and strategies toward intervention. *Dialogues Clin Neurosci*. 2009;11:111.
2. Prince M, Bryce R, Albanese E, Wimo A, Ribeiro W, Ferri CP. The global prevalence of dementia: a systematic review and metaanalysis. *Alzheimers Dement*. 2013;9:63.
3. Chiti F, Dobson CM. Protein misfolding, functional amyloid, and human disease. *Annu Rev Biochem*. 2006;75:333.
4. Haass C, Selkoe DJ. Soluble protein oligomers in neurodegeneration: lessons from the Alzheimer's amyloid β-peptide. *Nat Rev Mol Cell Biol*. 2007;8:101.
5. Benilova I, Karran E, De Strooper B. The toxic Aβ oligomer and Alzheimer's disease: an emperor in need of clothes. *Nat Neurosci*. 2012;15:349.
6. Warner CJA, Dutta S, Foley AR, Raskatov JA. Introduction of D-glutamate at a critical residue of Aβ42 stabilizes a pre-fibrillary aggregate with enhanced toxicity. *Chem A Eur J*. 2016;22:11967.
7. Fezoui Y, Hartley DM, Harper JD, et al. An improved method of preparing the amyloid β-protein for fibrillogenesis and neurotoxicity experiments. *Amyloid*. 2000;7:166.
8. Greenfield NJ. Using circular dichroism spectra to estimate protein secondary structure. *Nat Protoc*. 2006;1:2876.
9. Finder VH, Vodopivec I, Nitsch RM, Glockshuber R. The recombinant amyloid-beta peptide Abeta1-42 aggregates faster and is more neurotoxic than synthetic Abeta1-42. *J Mol Biol*. 2010;396:9.
10. Kannan R, Santhoshkumar P, Mooney BP, Krishna Sharma K. The αA66–80 peptide interacts with soluble α-crystallin and induces its aggregation and precipitation: a contribution to age-related cataract formation. *Biochemistry*. 2013;52:3638.
11. Norlin N, Hellberg M, Filippov A, et al. Aggregation and fibril morphology of the Arctic mutation of Alzheimer's Aβ peptide by CD, TEM, STEM and in situ AFM. *J Struct Biol*. 2012;180:174.
12. Vandersteen A, Hubin E, Sarroukh R, et al. A comparative analysis of the aggregation behavior of amyloid-β peptide variants. *FEBS Lett*. 2012;586:4088.
13. Whitmore L, Wallace BA. DICHROWEB, an online server for protein secondary structure analyses from circular dichroism spectroscopic data. *Nucleic Acids Res*. 2004;32:W668.
14. Whitmore L, Wallace BA. Protein secondary structure analyses from circular dichroism spectroscopy: Methods and reference databases. *Biopolymers*. 2008;89:392.
15. Sreerama N, Woody RW. Estimation of protein secondary structure from circular dichroism spectra: comparison of CONTIN, SELCON, and CDSSTR methods with an expanded reference set. *Anal Biochem*. 2000;287:252.
16. Lobley A, Whitmore L, Wallace BA. DICHROWEB: an interactive website for the analysis of protein secondary structure from circular dichroism spectra. *Bioinformatics*. 2002;18:211.
17. Bokvist M, Lindström F, Watts A, Gröbner G. Two types of Alzheimer's β-amyloid (1–40) peptide membrane interactions: aggregation preventing transmembrane anchoring versus accelerated surface fibril formation. *J Mol Biol*. 2004;335:1039.

SUPPORTING INFORMATION

Additional Supporting Information may be found online in the supporting information tab for this article.

How to cite this article: Warner CJA, Dutta S, Foley AR, Chen E, Kliger DS, Raskatov JA. Using chiral peptide substitutions to probe the structure function relationship of a key residue of Aβ42. *Chirality* 2017;29:5–9. doi: 10.1002/chir.22667

CHAPTER 3:

Mirror-image peptides as structural modifiers of amyloidogenic peptides and proteins and as mechanistic tools to study cellular interactions

Introduction to Chapter 3

In addition to introducing chiral point mutations within the Aβ sequence, using full-length D-amino acid Aβ (D-Aβ), i.e. mirror-image Aβ, also provided with a powerful strategy to modulate Aβ aggregation and to determine how Aβ interacts with biological systems. In this sense, the use of D-Aβ in the work performed in this thesis has resulted valuable to develop novel mechanistic approaches to accelerate Aβ fibril formation, and to understand how Aβ peptides are uptaken into cells.

Mixtures of enantiomeric proteins or polymers can result in the generation of structurally different systems. For example, enantiomeric peptide assemblies can lead to distinct hydrogels when compared to its homochiral counterparts, originated from different interaction patters at the nanoscale level, which also leads to changes in hydrogel rigidity.(49) This phenomenon has also been observed in self-assembling, fibrillary-prone peptides, where a mixture of (poly(D-lysine) and poly(L-lysine)), which adopt α-helical structures when enantiopure, resulted in the generation racemic β-sheet aggregates.(50) These observations led us to hypothesize that Aβ aggregation could be modulated by the addition of mirror-image Aβ. Upon mixing L- and D-Aβ at equimolar ratios, we observed that the generated new system led to rapid Aβ aggregation with an accompanied loss of cellular toxicity.(51) This strategy, which we termed Chiral Inactivation (CI), relies on the principles of molecular chirality, and it is a clear example of how racemic mixtures exhibit reduced solubility when compared to the enantiopure counterparts.(52) This approach, as discussed in the reprinted manuscript (Dutta et. al. 2019), also highlights that acceleration of fibril formation can be an alternative strategy to inhibit oligomer formation and Aβ toxicity.

The results discussed above also exemplify how enantiomeric Aβ can also be used as a mechanistic probe to study biological interactions. Enantiomeric peptides are typically used to discern between receptor mediated mechanisms (where the stereochemistry of the peptide play a critical role), and non-receptor-mediated mechanisms, i.e. lipid membrane-based uptake such as pinocytosis, where chiral interactions play a minor role.(53–55) The work in this chapter describes how using mirror-image Aβ can unveil cellular interactions leading to Aβ cell internalization. Specifically, by adopting a mirror-

image, fragment-based approach, in this chapter (Foley et. al. 2020) we show that a specific region within the Aβ sequence may be majorly responsible for Aβ cellular uptake, and that it is also dependent on receptor-mediated interactions (i.e. cellular prion protein (PrP^C), also showing for the first time that Aβ uptake may not be dependent on its aggregation state, as believed thus far.

GDCh **Communications** Angewandte International Edition Chemie

VIP Amyloid β-Peptides Very Important Paper

International Edition: DOI: 10.1002/anie.201706279
German Edition: DOI: 10.1002/ange.201706279

Suppression of Oligomer Formation and Formation of Non-Toxic Fibrils upon Addition of Mirror-Image Aβ42 to the Natural L-Enantiomer

*Subrata Dutta, Alejandro R. Foley, Christopher J. A. Warner, Xiaolin Zhang, Marco Rolandi, Benjamin Abrams, and Jevgenij A. Raskatov**

Abstract: *Racemates often have lower solubility than enantiopure compounds, and the mixing of enantiomers can enhance the aggregation propensity of peptides. Amyloid beta (Aβ) 42 is an aggregation-prone peptide that is believed to play a key role in Alzheimer's disease. Soluble Aβ42 aggregation intermediates (oligomers) have emerged as being particularly neurotoxic. We hypothesized that the addition of mirror-image* D-*Aβ42 should reduce the concentration of toxic oligomers formed from natural* L-*Aβ42. We synthesized* L- *and* D-*Aβ42 and found their equimolar mixing to lead to accelerated fibril formation. Confocal microscopy with fluorescently labeled analogues of the enantiomers showed their colocalization in racemic fibrils. Owing to the enhanced fibril formation propensity, racemic Aβ42 was less prone to form soluble oligomers. This resulted in the protection of cells from the toxicity of* L-*Aβ42 at concentrations up to 50 μM. The mixing of Aβ42 enantiomers thus accelerates the formation of non-toxic fibrils.*

Enantiomers and racemates of the same molecule may exhibit drastically different properties upon aggregation, which can lead to pronounced differences in both the structure and reactivity of the resultant molecular assemblies.[1] In 1953, Pauling and Corey proposed that racemic peptide mixtures should be able to form stable structures with alternating L- and D-amino acid derived peptide units. The authors referred to this arrangement as the "rippled sheet" configuration.[2a] Recent studies have shown that such heterochiral interfaces can indeed be formed from biologically relevant peptides.[2b] Mixing of the enantiomers of certain intrinsically disordered peptides was also found to lead to the formation of peptidic frameworks with enhanced stability.[3]

Amyloid beta (Aβ) is a hydrophobic, intrinsically disordered, aggregation-prone peptide that is believed to play a pivotal role in Alzheimer's disease.[4] Aβ is produced as a cleavage product of the transmembrane protein APP and can range from 36 to 43 amino acids in length.[4a] The 40 amino acid long variant (Aβ40) is the most abundant form of the peptide, but its 42 amino acid long analogue (Aβ42) is substantially more neurotoxic; this property has been attributed to the higher aggregation propensity of the latter.[5] Although Aβ42 fibrils were initially believed to be the disease culprit, intermediates of aggregation (commonly referred to as diffusible oligomers) have been recognized as being significantly more harmful.[5b] Aβ peptides can form diverse fibrillary aggregates,[6] and cases exist where Aβ42 fibrils were found to be non-toxic.[7]

Racemates often have lower solubility than their enantiopure counterparts.[1a] As Aβ42 fibrils are believed to act as (potentially protective) reservoirs that scavenge the toxic oligomers,[8] we hypothesized that mixing of the Aβ42 enantiomers should accelerate fibril formation and attenuate the toxicity of the native L-peptide.

We synthesized the natural L-Aβ42 as well as its mirror image, the D-enantiomer (see the Supporting Information, Figure S1 and associated material for preparative procedures). As expected, the two peptides had reciprocal circular dichroism (CD) spectra,[9] and equimolar mixing of L- and D-Aβ42 led to disappearance of the CD signal (Figure S2). We employed the thioflavin T (ThT) assay to measure the kinetics of fibril formation of the two enantiomers of Aβ42 and their racemic mixture. In agreement with previous reports,[9b] both enantiopure compounds exhibited a sigmoidal fibril growth profile.

Both enantiomers had a lag phase of 20–30 min (Figure 1 A, B). Consistent with recent reports, longer incubation times were needed at lower concentrations.[10] The racemic mixture showed a qualitatively different fibril formation profile that was devoid of any lag phase (Figure 1 C). The induction period in the enantiopure cases was followed by a rapid increase in fluorescence, diagnostic for fibril formation. The time required to reach half of the maximum fluorescence ($t_{1/2}$) was comparable for the two enantiomers, but substantially shorter with the racemate, which exhibited a three- to fourfold acceleration of fibril formation (31.4 ± 2.6 min, L-Aβ42, 20 μM; 37.6 ± 0.5 min, D-Aβ42, 20 μM; 9.8 ± 0.4 min, *rac*-Aβ42, 20 μM). Racemic Aβ42 also exhibited

[*] Dr. S. Dutta, A. R. Foley, Dr. C. J. A. Warner, Prof. Dr. J. A. Raskatov
Dept. of Chemistry and Biochemistry, UCSC
1156 High Street, Santa Cruz, CA (USA)
E-mail: jraskato@ucsc.edu
X. Zhang, Prof. Dr. M. Rolandi
Dept. of Electrical Engineering, UCSC
1156 High Street, Santa Cruz, CA (USA)
X. Zhang
Dept. of Materials Science and Engineering
University of Washington, Seattle, WA (USA)
Dr. B. Abrams
Dept. of Biomolecular Engineering
Life Sciences Microscopy Center, UCSC
1156 High Street, Santa Cruz, 95064 CA (USA)
Supporting information and the ORCID identification number(s) for the author(s) of this article can be found under: https://doi.org/10.1002/anie.201706279.

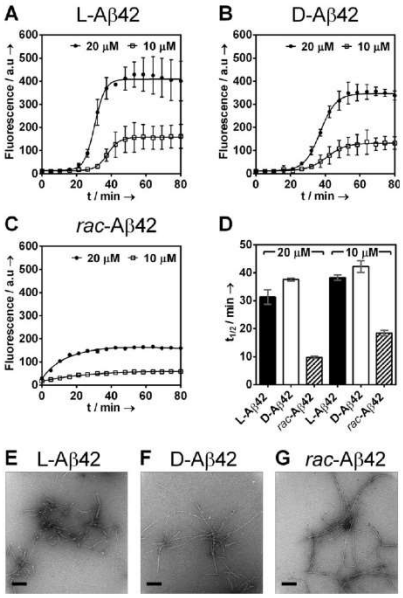

Figure 1. Aggregation kinetics of A) L-Aβ42 (10, 20 μM), B) D-Aβ42 (10, 20 μM), and C) *rac*-Aβ42 (20, 10 μM total concentration) monitored by thioflavin T (ThT, 20 μM) fluorescence at 37 °C in PBS (pH 7.4) in the presence of 0.02% NaN_3. Racemic Aβ42 was prepared by mixing equal amounts of L-Aβ42 and D-Aβ42 in 20 mM NaOH before diluting with PBS. Each data point is an average of three replicates with error bars representing the standard deviations. D) Half-times ($t_{1/2}$) of Aβ42 fibril formation; $t_{1/2}$ is defined as the time required to reach half of the maximum fluorescence intensity measured in the ThT assays (A–C). See the Supporting Information for details. TEM images of fibrils of E) L-Aβ42, F) D-Aβ42, and G) racemic Aβ42. Samples were taken directly from the ThT assay (20 μM) at the endpoint of the experiment. Scale bars: 200 nm. See Appendix A in the Supporting Information for further TEM images.

lower final fluorescence (ca. twofold reduction at 20 μM total concentration; see Figure 1). Consistent trends were observed at lower concentrations (Figure 1A–D) but the racemic mixture prepared from 20 μM each of L- and D-Aβ42 (40 μM in total) resulted in fibril formation that was too rapid to be monitored (Figure S3).[11] Fibrils formed in the ThT experiments were readily observed by TEM, both for the two enantiopure samples as well as for the racemate (for representative images, see Figure 1E–G; Appendix A of the Supporting Information displays all TEM images obtained, 100 per condition).

The results from the ThT experiments suggested that fibrils obtained from *rac*-Aβ42 were distinct from those formed by enantiopure materials. To better understand the composition of the racemic fibrils, we synthesized fluorescently labeled analogues of the two Aβ42 enantiomers. L-Aβ42 was N-terminally labeled with 5(6)-carboxyfluorescein (denoted as L-Aβ42-FAM) and D-Aβ42 was N-terminally labeled with 5(6)-carboxytetramethylrhodamine (denoted as D-Aβ42-TAMRA). Chemical modifications were performed as described in the Supporting Information, Figure S6. The use of the conditions employed in the ThT experiments was found to yield fibrils of the fluorescently labeled peptides (Figure S7). Two-channel confocal imaging was performed (channel 1, FAM: $\lambda_{ex} = 476$ nm, $\lambda_{em} = 484$–514 nm; channel 2, TAMRA: $\lambda_{ex} = 543$ nm; $\lambda_{em} = 630$–690 nm). Under these conditions, we found the L-Aβ42-FAM fluorescence to be detectable exclusively by channel 1 (Figure 2A) whereas D-Aβ42-TAMRA was seen via channel 2 only (Figure 2B). Importantly, fibrils grown from an equimolar (i.e., "racemic") mixture of L-Aβ42-FAM and D-Aβ42-TAMRA were fluorescent in both channels (Figure 2C), and the two signals had a high degree of colocalization (Pearson correlation coefficient, PCC = 0.93; see the Supporting Information for details). On the other hand, when mature fibrils that had been grown from either L-Aβ42-FAM or D-Aβ42-TAMRA

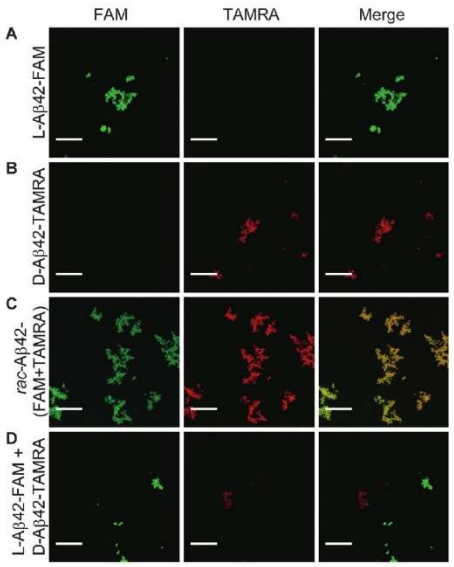

Figure 2. Two-channel confocal microscopy imaging (channel 1, left panel, monitors FAM: $\lambda_{ex} = 476$ nm, $\lambda_{em} = 484$–514 nm; channel 2, middle panel, monitors TAMRA: $\lambda_{ex} = 543$ nm; $\lambda_{em} = 630$–690 nm; right panel: merging of channels 1 and 2 allows to probe for colocalization of the fluorescent labels). L-Aβ42-FAM fibrils were fluorescent in channel 1, but not in channel 2 (A) whereas D-Aβ42-TAMRA fibrils were active via channel 2 only (B). Fibrils grown from an equimolar mixture of L-Aβ42-FAM and D-Aβ42-TAMRA were fluorescently active in both channels 1 and 2, with robust signal colocalization (C). In a control experiment (D), fibrils grown from either L-Aβ42-FAM or D-Aβ42-TAMRA were subsequently mixed and were fluorescently active either in channel 1 or channel 2, with very low colocalization. Scale bars: 20 μm.

were subsequently mixed, we found that these mixtures were fluorescently active via either channel 1 (L-Aβ42-FAM) or channel 2 (D-Aβ42-TAMRA), with very low signal colocalization (Figure 2D; PCC = 0.03).

The acceleration of fibril formation from racemic Aβ42 (Figure 1) and the colocalization of L- and D-Aβ42 in fibrils grown from the racemic mixture (Figure 2C) prompted us to investigate earlier stages of aggregation. To measure the abundance of oligomers in solution, we conducted PICUP experiments.[5c] Performed with either enantiopure Aβ42 (L or D, 50 μM) or their racemic mixture (50 μM L and 50 μM D), the experiment revealed that oligomer formation was suppressed with *rac*-Aβ42 (Figure 3A), which was accompanied by an increase in the formation of a high-molecular-weight band (see arrow in Figure 3A). Indicating increased formation of larger aggregates, this is consistent with the enhancement of fibril formation upon mixing of the two enantiomers (Figure 1). The oligomer distribution obtained from L-Aβ42 was consistent with previous reports by us and others,[5c,12] and D-Aβ42 showed a virtually identical oligomerization pattern, as expected for a mirror-image peptide. The suppression of oligomer formation from L-Aβ42 showed dose dependence upon addition of substoichiometric amounts of D-Aβ42 above a 4:1 ratio.

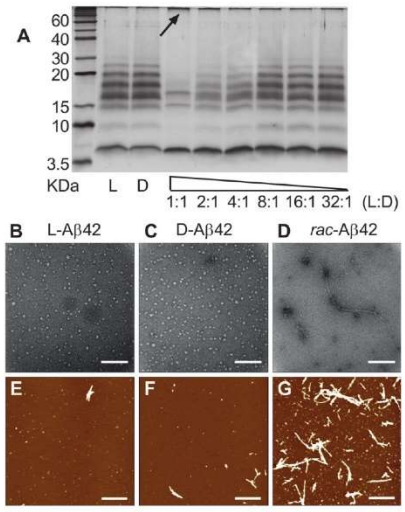

Figure 3. A) A PICUP gel of L- and D-Aβ42 (50 μM), as well as various mixtures of the two enantiomers. In mixtures, L-Aβ42 was always kept at 50 μM and the D-Aβ42 concentration covered the range between 50 μM and 1.56 μM, as indicated. B–D) Representative TEM images of L-, D-, and *rac*-Aβ42 aggregation intermediates. Scale bars: 200 nm. Samples were prepared as described in Appendix B in the Supporting Information; the method was adopted from Ref. [13]. E–G) Representative AFM images of L-, D-, and *rac*-Aβ42 aggregation intermediates. Sample preparation as for TEM analysis. Scale bars: 1000 nm. See the Supporting Information for further TEM and AFM images.

We explored the inhibition of oligomer formation further by conducting TEM experiments on aggregation intermediates following recently published protocols (see Appendix B in the Supporting Information).[13] These experiments revealed that both L- and D-Aβ42 were forming spherical oligomers with diameters of 12.9 ± 3.7 nm and 13.6 ± 4.1 nm, respectively (Figure 3B,C), which is consistent with literature values (see Appendix B in the Supporting Information for further images and a histogram analysis of the oligomer size distribution).[13] With *rac*-Aβ42, we observed a more heterogeneous mixture of aggregation intermediates, which frequently contained advanced (fibrillary) aggregates. Atomic force microscopy (AFM) confirmed the presence of these aggregation intermediates (Figure 3E–G; see Figure S8 for further images). From AFM imaging, both L- and D-Aβ42 were more likely to form oligomers and only few fibrils (Figure 3E,F). By comparison, *rac*-Aβ42 produced more fibrils with a high aspect ratio (Figure 3G). Oligomers obtained from enantiopure (L- or D-)Aβ42 were disc-shaped and had an average height of about 0.2–0.3 nm, which is in agreement with previous reports.[13] With *rac*-Aβ42, on the other hand, the average height of the oligomers was higher at 0.4 nm, and the average height of the high-aspect-ratio fibers was approximately 3 nm, reflecting the enhanced aggregation propensity upon mixing of the two enantiomers. Overall, the results from AFM imaging were in qualitative agreement with the TEM studies.

Taken together, our findings on Aβ42 aggregation intermediates (Figure 3) are consistent with the observation that mixing of the enantiomers accelerates fibril formation (Figure 1) and that the enantiomers colocalize in fibrils grown from *rac*-Aβ42 (Figure 2).

Diffusible Aβ42 oligomers have been recognized as particularly toxic,[5] and we found their concentration to be substantially reduced in the racemate. Hence, we hypothesized that *rac*-Aβ42 should exhibit reduced cytotoxicity in comparison to (natural) L-Aβ42. Incubation of PC12 neuron-like cells with 20 μM L-Aβ42 reduced the cell viability (measured in an WST-1 assay; see the Supporting Information for details) by approximately 25%, which is in agreement with our previous findings (Figure 4A).[12] The D-enantiomer was non-toxic under those conditions. The addition of one equivalent D-Aβ42 to L-Aβ42 prior to dosing the PC12 resulted in full suppression of toxicity (final concentration of L-Aβ42 in the racemate: 20 μM). As the cytotoxicity observed with L-Aβ42 at 20 μM was modest, we also conducted the experiment at 50 μM. At that concentration, L-Aβ42 reduced the PC12 viability by 60%, whereas D-Aβ42 again showed no toxicity. Remarkably, in the racemic mixture (50 μM L-Aβ42 and 50 μM D-Aβ42), the toxicity of L-Aβ42 was completely suppressed. We also measured the partial toxicity reduction against PC12 cells by WST-1 in the mixture of 50 μM L-Aβ42/25 μM D-Aβ42, but not 50 μM L-Aβ42/12.5 μM D-Aβ42 (Figure S9).

Consistent observations were made when the MTT cytotoxicity assay was employed in place of WST-1 (Figure 4B and Figure S10) and when the SH-SY5Y cell line was used instead of PC12 (Figure 4B). We did note marginal toxicity of D-Aβ42 against SH-SY5Y cells (ca. 14% viability reduction).

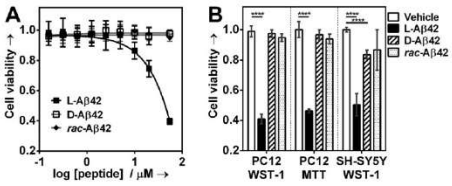

Figure 4. A) Cellular viability of the PC12 adhesive cell line in response to dosing in of varied concentrations of enantiopure (L- or D-) or racemic Aβ42. B) Cell viability (PC12 or SH-SY5Y) in response to treatment with either enantiopure (L or D; 50 μM in both cases) or *rac*-Aβ42 (50 μM L-Aβ42 and 50 μM D-Aβ42). Cells were plated and allowed to adhere for 24 h. Peptides were then added and cells incubated for further 72 h. The cell viability was determined using the cell proliferation reagent WST-1 or MTT, as shown. Data are represented as mean ± standard deviation; $^{****}P < 0.0001$, calculated by an unpaired t-test.

We are aware of two independent studies that compared L- and D-Aβ42, with apparently contradictory results.[9] The investigation by Cribbs and co-workers reported comparable toxicity for both L- and D-Aβ42,[9a] whereas the study by Ciccotosto et al. found D-Aβ42 to be non-toxic.[9b] The first study used hippocampal neurons while the second one used cortical neurons. The different cell model systems chosen in those studies may underlie the apparent contradiction. We also measured the LDH release induced by L-, D-, and racemic Aβ42 in PC12 cells. We found L-Aβ42 to induce about 40% maximum LDH release, whereas with D- or *rac*-Aβ42, it was less than 10% (Figure S11). The amount of LDH released upon exposing PC12 cells to D- or *rac*-Aβ42 is comparable to that recently reported for scrambled Aβ42, which the authors also found to be non-toxic against rat brain endothelial cells by MTT.[14]

Examples of enhancing Aβ42 fibrillization as a strategy to protect from toxicity are scarce.[7] Tailored D-peptides have previously been employed to attenuate Aβ42 aggregation,[15] but not to promote fibril formation. Our approach to induce non-toxic fibril formation through the addition of mirror-image Aβ42 ("chiral inactivation") is based on fundamentals of molecular stereochemistry, and we were able to recapitulate the trend of accelerated fibril formation upon enantiomer mixing with the Aβ40 system (Figure S4). Of relevance to our work, Kar et al. found that mirror-image D-polyglutamine can recruit L-polyglutamine and induce the formation of potentially toxic inclusion bodies in cell-based assays.[16] We therefore note that although there appears to be some generality in terms of the stereochemical aspects underlying the formation of homo- and heterochiral aggregates from intrinsically disordered peptides, biological consequences will be specific to the system under study.

In summary, we have shown that racemic Aβ42 forms fibrils substantially more rapidly than enantiopure Aβ42, and that the fluorescently labeled derivatives of the two enantiomers colocalize in racemic fibrils. Acceleration of fibrillization is accompanied by a suppression of oligomer formation with racemic Aβ42. These changes in the aggregation properties lead to the inhibition of toxicity against PC12 and SH-SY5Y cells.

Acknowledgements

J.A.R. thanks the UCSC for flexible start-up funds, special research grants, and the Hellman Foundation for a fellowship. We acknowledge the NIHS10OD016246-01A1 award for the purchase of the JASCO J1500 CD. M.R. and X.Z. acknowledge Office of Naval Research Awards (N000141410724 and N000141612507 (DURIP)) for the purchase of the AFM.

Conflict of interest

The authors declare no conflict of interest.

Keywords: aggregation · amyloid β-peptides · oligomers · D-peptides · racemates

How to cite: *Angew. Chem. Int. Ed.* **2017**, *56*, 11506–11510
Angew. Chem. **2017**, *129*, 11664–11668

[1] a) J. Jacques, A. Collet, S. H. Wilen, *Enantiomers, Racemates and Resolutions*, Wiley, New York, **1981**; b) I. Weissbuch, R. A. Illos, G. Bolbach, M. Lahav, *Acc. Chem. Res.* **2009**, *42*, 1128–1140; c) J. A. Raskatov, A. L. Thompson, A. R. Cowley, T. D. W. Claridge, J. M. Brown, *Chem. Sci.* **2013**, *4*, 3140–3147; d) K. Soai, T. Kawasaki, A. Matsumoto, *Acc. Chem. Res.* **2014**, *47*, 3643–3654.

[2] a) L. Pauling, R. B. Corey, *Proc. Natl. Acad. Sci. USA* **1953**, *39*, 253–256; b) V. Torbeev, M. Grogg, J. Ruiz, R. Boehringer, A. Schirer, P. Hellwig, G. Jeschke, D. Hilvert, *J. Pept. Sci.* **2016**, *22*, 290–304.

[3] a) K. J. Nagy, M. C. Giano, A. Jin, D. J. Pochan, J. P. Schneider, *J. Am. Chem. Soc.* **2011**, *133*, 14975–13977; b) R. J. Swanekamp, J. T. DiMaio, C. J. Bowerman, B. L. Nilsson, *J. Am. Chem. Soc.* **2012**, *134*, 5556–5559.

[4] a) H. W. Querfurth, F. M. LaFerla, *N. Engl. J. Med.* **2010**, *362*, 329–344; b) F. Chiti, C. M. Dobson, *Annu. Rev. Biochem.* **2006**, *75*, 333–366.

[5] a) Y. S. Gong, L. Chang, K. L. Viola, P. N. Lacor, M. P. Lambert, C. E. Finch, G. A. Krafft, W. L. Klein, *Proc. Natl. Acad. Sci. USA* **2003**, *100*, 10417–10422; b) C. Haass, D. J. Selkoe, *Nat. Rev. Mol. Cell Biol.* **2007**, *8*, 101–112; c) G. Bitan, M. D. Kirkitadze, A. Lomakin, S. S. Vollers, G. B. Benedek, D. B. Teplow, *Proc. Natl. Acad. Sci. USA* **2003**, *100*, 330–335.

[6] a) M. Schmidt, A. Rohou, K. Lasker, J. K. Yadav, C. Schiene-Fischer, M. Fandrich, N. Grigorieff, *Proc. Natl. Acad. Sci. USA* **2015**, *112*, 11858–11863; b) Y. Xiao, B. Ma, D. McElheny, S. Parthasarathy, F. Long, M. Hoshi, R. Nussinov, Y. Ishii, *Nat. Struct. Mol. Biol.* **2015**, *22*, 499–505; c) M. T. Colvin, R. Silvers, Q. Z. Ni, T. V. Can, I. Sergeyev, M. Rosay, K. J. Donovan, B. Michael, J. Wall, S. Linse, R. G. Griffin, *J. Am. Chem. Soc.* **2016**, *138*, 9663–9674; d) M. A. Wälti, F. Ravotti, H. Arai, C. G. Glabe, J. S. Wall, A. Bockmann, P. Guntert, B. H. Meier, R. Riek, *Proc. Natl. Acad. Sci. USA* **2016**, *113*, E4976–4984; e) M. Fändrich, J. Meinhardt, N. Grigorieff, *Prion* **2009**, *3*, 89–93.

[7] a) J. Ghanta, C. L. Shen, L. L. Kiessling, R. M. Murphy, *J. Biol. Chem.* **1996**, *271*, 29525–29528; b) J. Bieschke, M. Herbst, T. Wiglenda, R. P. Friedrich, A. Boeddrich, F. Schiele, D. Kleckers, J. M. Lopez del Amo, B. A. Grüning, Q. Wang, M. R. Schmidt, R. Lurz, R. Anwyl, S. Schnoegl, M. Fändrich, R. F. Frank, B.

Reif, S. Günther, D. M. Walsh, E. E. Wanker, *Nat. Chem. Biol.* **2011**, *8*, 93 – 101.
[8] a) L. Jiang, C. Liu, D. Leibly, M. Landau, M. Zhao, M. P. Hughes, D. S. Eisenberg, *eLife* **2013**, *2*, e00857; b) D. J. Selkoe, J. Hardy, *EMBO Mol. Med.* **2016**, *8*, 595 – 608.
[9] a) D. H. Cribbs, C. J. Pike, S. L. Weinstein, P. Velazquez, C. W. Cotman, *J. Biol. Chem.* **1997**, *272*, 7431 – 7436; b) G. D. Ciccotosto, D. J. Tew, S. C. Drew, D. G. Smith, T. Johanssen, V. Lal, T. L. Lau, K. Perez, C. C. Curtain, J. D. Wade, F. Separovic, C. L. Masters, J. P. Smith, K. J. Barnham, R. Cappai, *Neurobiol. Aging* **2011**, *32*, 235 – 248.
[10] G. Meisl, J. B. Kirkegaard, P. Arosio, T. C. Michaels, M. Vendruscolo, C. M. Dobson, S. Linse, T. P. Knowles, *Nat. Protoc.* **2016**, *11*, 252 – 272.
[11] We performed the corresponding ThT fibril formation experiments with the Aβ40 isoform and observed accelerated fibril formation for the racemic mixture there as well (Figure S4). Our racemic fibril formation experiment has to be distinguished from the seeding experiment performed by Esler and co-workers where preformed fibrils of L-Aβ40 were found to seed stereospecifically the fibrillization of the L-enantiomer (but not the D-enantiomer); see: W. P. Esler, E. R. Stimson, J. R. Fishman, J. R. Ghilardi, H. V. Vinters, P. W. Mantyh, J. E. Maggio, *Biopolymers* **1999**, *49*, 505 – 514. We found their results to qualitatively hold true for the Aβ42 system as well (Figure S5).
[12] C. J. Warner, S. Dutta, A. R. Foley, J. A. Raskatov, *Chem. Eur. J.* **2016**, *22*, 11967 – 11970.
[13] M. Ahmed, J. Davis, D. Aucoin, T. Sato, S. Ahuja, S. Aimoto, J. I. Elliott, W. E. Van Nostrand, S. O. Smith, *Nat. Struct. Mol. Biol.* **2010**, *17*, 561 – 567.
[14] M. A. Deli, S. Veszelka, B. Csiszar, A. Toth, A. Kittel, M. Csete, A. Sipos, A. Szalai, L. Fulop, B. Penke, C. S. Abraham, M. Niwa, *J. Alzheimer's Dis.* **2010**, *22*, 777 – 794.
[15] a) K. Wiesehan, J. Stohr, L. Nagel-Steger, T. van Groen, D. Riesner, D. Willbold, *Protein Eng. Des. Sel.* **2008**, *21*, 241 – 246; b) S. A. Sievers, J. Karanicolas, H. W. Chang, A. Zhao, L. Jiang, O. Zirafi, J. T. Stevens, J. Munch, D. Baker, D. Eisenberg, *Nature* **2011**, *475*, 96 – 100.
[16] K. Kar, I. Arduini, K. W. Drombosky, P. C. A. van der Wel, R. Wetzel, *J. Mol. Biol.* **2014**, *426*, 816 – 829.

Manuscript received: June 20, 2017
Accepted manuscript online: July 6, 2017
Version of record online: July 19, 2017

Received: 2 August 2019 | Revised: 10 September 2019 | Accepted: 12 September 2019
DOI: 10.1002/pep2.24139

FULL PAPER

PeptideScience WILEY

New insights into differential aggregation of enantiomerically pure and racemic Aβ40 systems

Subrata Dutta[1] | Alejandro R. Foley[1] | Ariel J. Kuhn[1] | Benjamin Abrams[2] | Hsiau-Wei Lee[1] | Jevgenij A. Raskatov[1]

[1]Department of Chemistry and Biochemistry, University of California Santa Cruz, Santa Cruz, California

[2]Department of Biomolecular Engineering, Life Sciences Microscopy Center, University of California Santa Cruz, Santa Cruz, California

Correspondence
Jevgenij A. Raskatov, Department of Chemistry and Biochemistry, University of California Santa Cruz, Santa Cruz, CA 95064.
Email: jraskato@ucsc.edu

Funding information
National Institutes of Health, Grant/Award Numbers: S10OD016246-01A1, R21AG058074

Abstract

Racemic mixtures frequently display properties that are different from those associated with their enantiopure counterparts, and are often characterized by higher propensity to form aggregates. Our previous research established that mixing of the enantiomers of Alzheimer amyloid β (Aβ) 42 peptides is an effective strategy to induce an oligomer-to-fibril conversion, which puts Aβ42 into a substantially less toxic state. Here, new insights into this chiral inactivation effect are presented. In addition to the commonly used Thioflavin T fibril formation assays, the use of the less aggregation-prone Aβ40 system allowed us to monitor peptide aggregation by NMR. Whereas enantiopure peptide was well soluble under the chosen experimental conditions and showed no sign of precipitation, addition of one equivalent of the mirror-image peptide triggered an instant and rapid aggregation, observable through the attenuation of the NMR signal. The racemic Aβ40 fibrils were found by transmission electron microscopy to be distinct in morphology, exhibiting a ~2-fold narrowing as compared with their enantiopure counterparts.

KEYWORDS
amyloid beta, chiral inactivation, rippled beta-sheets

1 | INTRODUCTION

The aggregation-prone, intrinsically disordered amyloid β (Aβ) peptide was initially characterized in 1984, and has since continuously attracted widespread interest of the chemical, biological, and medicinal communities alike, due to its believed principal role in Alzheimer disease.[1–6] It has also served as an inspiration for reductionist studies, which established new design principles for amyloid-based materials.[7]

In 2017, we reported that the mixing of the two Aβ42 enantiomers led to acceleration in fibril formation with a concomitant removal of oligomeric aggregation intermediates from solution and toxicity suppression in two model neuron-like cell lines.[8,9] A striking feature observed in that study was the complete disappearance of the incubation phase that is the characteristic for enantiopure Aβ fibril formation kinetics (in Thioflavin T [ThT] assays) upon mixing of enantiomers. This pointed to a fundamentally different mechanism of assembly. We hypothesized this to be due to the formation of a new and unique type of cross-β configuration in the racemic Aβ mixture, which was termed rippled β-sheets by Pauling and Corey in 1953,[10] and is not available to the enantiopure peptide. Our hypothesis was further validated in 2019 by Nilsson and coworkers, who used the Aβ (16-22) segment, that is, the KLVFFAE peptide, which represents the key central hydrophobic domain of Aβ, and found, using IR-based structural analysis, that the racemic mixture of this peptide showed a signature consistent with the formation of rippled β-sheets.[11] The authors also noted a substantial solubility reduction upon mixing of enantiomers, in agreement with our study on the full-length system. Other short hydrogel-forming peptides with propensity to form

Subrata Dutta, Alejandro R. Foley, and Ariel J. Kuhn contributed equally to this study.

rippled β-sheet networks with enhanced stability and mechanical rigidity upon mixing of enantiomers have also been reported.[12,13]

2 | MATERIALS AND METHODS

2.1 | Solid phases Aβ40 synthesis

Peptides were synthesized by Fmoc HOBt//DIC/Piperidine chemistry on a Liberty One CEM peptide synthesizer equipped with a CEM discovery microwave, as previously described.[8] All syntheses were performed at a 0.1-mmol scale. Resins were cleaved by using a cocktail solution of trifluoroacetic acid (10 mL), 1, 2-diethanethiol (0.5 mL), triisopropylsilane (1 mL), and liquefied phenol (0.5 mL). The cocktail solution was added to the resins, mixtures agitated for 2 h, cocktail solution then evaporated to 2 mL under nitrogen gas, and peptides precipitated with cold diethyl ether and centrifuged at 6000 rpm. The peptide pellet was washed with cold diethyl ether, dried, dissolved in 1:1 acetonitrile:water, flash frozen in liquid nitrogen, and lyophilized. Peptides were than purified by HPLC as before to afford 95% purity or greater Aβ40 peptides.

2.2 | Circular dichroism experiments

L-Aβ40 or D-Aβ40 peptide of 0.1 mg was dissolved in 20 μL of 20-mM NaOH and sonicated for 30 s; 440 μL of 20-mM phosphate buffer solution (pH 7.4) was added to yield 50-μM final concentration of L-Aβ40 or D-Aβ40 peptide. For the racemic mixture, 0.1 mg of L-Aβ40 and 0.1 mg of D-Aβ40 were dissolved separately in 20 μL of 20-mM NaOH solution each, and then mixed to yield racemic Aβ40. Subsequently, 880 μL of freshly prepared 20-mM phosphate buffer solution (pH 7.4) were added to yield a final concentration of 50-μM rac-Aβ40 in a final volume of 920 μL. Spectra were recorded using a Jasco 1500 circular dichroism (CD) spectrophotometer at room temperature, set to a scan range of 180 to 280 nm, a DIT of 4 s, and a scan speed of 50 nm per minute.

2.3 | Thioflavin T assay

Lyophillized L- or D-Aβ40 was dissolved in 20-mM NaOH (~15 μL of 20-mM NaOH per 0.1 mg of peptide) and sonicated for 30 s and concentration was measured by nanodrop (ε = 1490 M^{-1} cm^{-1} at 280 nm). Enantiomers were mixed in a 1:1 ratio for rac-Aβ40. L-and D-Aβ40 were then diluted with PBS containing 0.02% (w/v) NaN_3 and 20 μM ThT, yielding 20 μM L- or D-Aβ40 solutions. For rac-Aβ40, two solutions were made (20 μM L and 20 μM D-Aβ40, 40 μM total; 10 μM L- and 10 μM D-Aβ40, 20 μM total). ThT experiments were conducted in black, clear bottom 96-well plates using a Molecular Device Gemini EM fluorescence plate reader (λ_{em} = 444 nm, λ_{ex} = 485 nm). Each well contained 200 μL of peptide solution and was sealed with optically clear adhesive film. Three replicates were obtained per condition. Each ThT assay was conducted for 24 h at 37 °C. Readings were collected every 5 min with 5 s shaking before reading and 295 s shaking in between readings.

2.4 | ^{1}H NMR experiments

For the enantiopure samples in aqueous conditions, NH_4OH-treated, lyophilized Aβ40 (L- or D-) was dissolved in 0.6 mL of 50 mM phosphate buffer containing the internal standard 4,4-dimethyl-4-silapentane-1-sulfonic acid (DSS) with 10% D_2O (pH 7.4), yielding 160-μM peptide solutions. For the racemic samples, the two peptides (L- and D-Aβ40) were prepared as described above and then mixed at a 1:1 M ratio prior to spectra acquisition. For the experiments conducted in DMSO, NH_4OH-treated, lyophilized Aβ (L-, D-, or rac-) was dissolved in 0.6 mL of d_6-DMSO containing the internal standard DSS to give a 160-μM peptide solution. The exact concentration of the peptide solutions was determined with a Nanodrop by absorbance at 280 nm (ε = 1490 M^{-1} cm^{-1}). Time points were collected every minute for a total of ~40 min. The NMR data were processed using MestreNova.

2.5 | TEM experiments

The samples of Aβ40 (L-, D-, or racemic) for transmission electron microscopy (TEM) were taken directly from ThT assays (20 μM total concentration of Aβ40) after 24 h. For specimen preparation, 3 μL of sample was spotted onto a freshly glow-discharge carbon-coated electron microscopy grid (Ted Pella, Catalog No. 01701-F). Grids were rinsed with 30 μL of milliQ water after 1 min incubation, followed by staining with 30 μL 1% uranyl acetate. All fibrils were imaged by using a Tecnai 12 microscope at an accelerating voltage of 120 kV. Images taken at 23000× were quantitatively analyzed as follows. The fibril width was measured at the thickest point where the fibril appeared to be a single fiber rather than a bundle using the FIJI/ImageJ software (https://fiji.sc/). Between 18 and 36 fibrils were measured per chiral form and pairwise two-sample *t* tests with unequal variance were performed between each condition using Microsoft Excel.

2.6 | Structural DFT-computational analysis

The peptidic backbone for the heterochiral, parallel, "rippled" dimeric interface was generated using the distances and symmetry operations published by Pauling and Corey.[10] Substituents of the LVFFA sequence were positioned using the standard geometric parameters defined in the Molden program package, the peptide N-terminally acetylated and C-terminally amidated. The resultant structure was imported into the SPARTAN program package, the backbone heavy atoms (C,N,O) are frozen, and the side chains are optimized using the SPARTAN MM/MD search engine. The lowest energy structure thus obtained was optimized for ~20 cycles using Gaussian 09 at the M062X/6-31G* level of theory, with solvent modeled via PCM.[14–17] The resultant structure was exported back into SPARTAN, backbone atoms frozen again, and sidechains reoptimized by MM/MD, and the lowest energy structure was imported back into Gaussian to repeat the DFT optimization cycle. The SPARTAN-Gaussian iteration was then repeated once more, yielding a total of three MM/MD-DFT back-and-forth iterations. The thus obtained refined structural guess

was then fully optimized at the M062X/6-31G* level of theory, with water contribution included via PCM (same as above), using an ultrafine integration grid and tight SCF convergence criteria, as defined in Gaussian 09.[14] Cartesian force constants were calculated explicitly via frequency calculation and used in structural optimization to facilitate energy minimization. A structure was considered converged based on negligible forces (10-fold below the standard threshold defined in Gaussian 09) and energy changes $\Delta E < 0.01$ kcal/mol over 10 consecutive geometry optimization cycles. Cartesian coordinates have been deposited as part of the Supporting Information.

3 | RESULTS AND DISCUSSION

In continuation of our research efforts on the racemic aggregating Aβ system, we performed experiments with the two enantiopure Aβ40 peptides and their racemic mixture. The two Aβ40 enantiomers were synthesized and purified, using our previously published protocols and procedures.[8] The two peptides displayed reciprocal CD bands of comparable intensity, as expected for mirror-image peptides, and mixing of the enantiomers in a 1:1 ratio led to disappearance of that band (Figure 1A). The aggregation $t_{1/2}$ values were measured for the two enantiopure peptide in ThT fibril formation assays as $t_{1/2,\text{L-A}\beta40}$ = 104 ± 15 min and $t_{1/2,\text{D-A}\beta40}$ = 116 ± 13 min at 20-μM peptide concentration (Figure 1B,C). Mixing of the two enantiomers resulted in an acceleration of fibril formation to $t_{1/2,\text{rac-A}\beta40}$ = 19.1 ± 0.5 min when 20 μM each L- and 20 μM D-peptide (40 μM total racemic Aβ40) were used (Figure 1D). It was slightly higher at 20 μM total racemic Aβ40, with $t_{1/2,\text{rac-A}\beta40}$ = 26.2 ± 0.3 min (Figure 1E). Consistent with our previously reported findings, the racemic aggregating Aβ40 system was characterized by a lack of lag phase, much smaller error bars, and a lower final fluorescence output than the two enantiopure counterparts, all indicating that the fibrils formed were of a distinctly different polymorph for the racemic Aβ40 mixture.

To probe further the acceleration of fibril formation upon enantiomer mixing, ^{1}H NMR experiments were conducted. It was anticipated that the relatively high solubility of Aβ40, as compared with Aβ42, which had been the subject of the majority of our experiments in the past,[8] would be an asset for these experiments. An enantiopure aqueous solution of L-Aβ40 displayed a well-defined ^{1}H NMR spectrum, and showed no evidence of precipitation (298 K; 160 μM L-Aβ40; 9:1 H_2O/D_2O mixture, phosphate-buffered to pH 7.4; Figure 2A). Mixing of L- and D-Aβ40 in a 1:1 ratio initiated rapid precipitation, which could be readily monitored via loss of ^{1}H NMR signal intensity (Figure 2B), and was found to be consistent with the enhanced precipitation tendency of *rac*-Aβ40 observed by ThT (Figure 1). Within 40 min of incubation, the ^{1}H NMR signal intensity was reduced to ~39% with the Aβ40 racemate, corresponding to a loss of 61% of soluble species due to precipitation. Conversely, signal intensity remained invariant over the same time window with

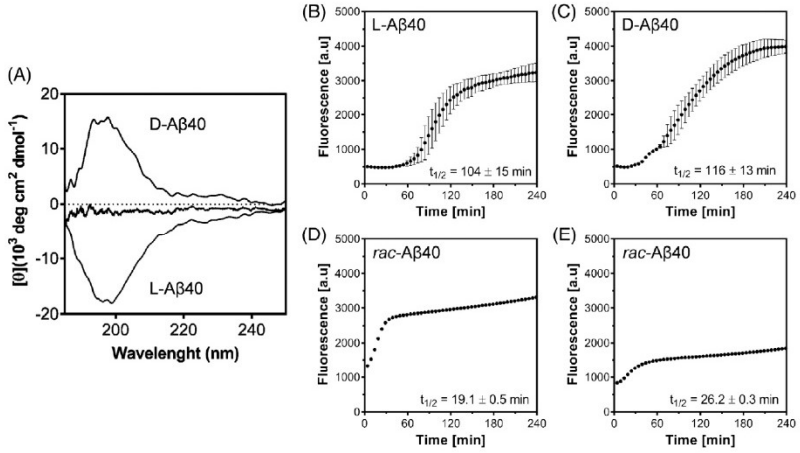

FIGURE 1 A, CD spectra of enantiopure (L- or D-) Aβ40, and the racemic mixture of the two peptides; spectra were obtained immediately upon reconstitution. Samples were dissolved in 20-mM NaOH and diluted to 50 μM in 20-mM phosphate buffer (pH 7.4). For rac-Aβ40, the mixture was composed of 25 μM L- and 25 μM D-Aβ40 (total peptide concentration of 50 μM). All CD spectra were obtained at room temperature. B, ThT fibril formation assay performed for L-Aβ40 (20 μM). L-Aβ40 was dissolved in 20-mM NaOH and diluted to 20 μM in 1xPBS (pH 7.4) along with 20-μM ThT. Samples were monitored by ThT fluorescence (λ_{em} = 444 nm, λ_{ex} = 485 nm) under shaking at 37 °C with data acquisition every 5 min. Curves show an average of three technical replicates with error bars as SD. C, ThT assay with D-Aβ40 (same conditions). D, ThT assay with rac-Aβ40 (20-μM L- and 20-μM D-Aβ40, otherwise the same conditions). E, ThT assay with rac-Aβ40 (10-μM L- and 10-μM D-Aβ40, otherwise the same conditions)

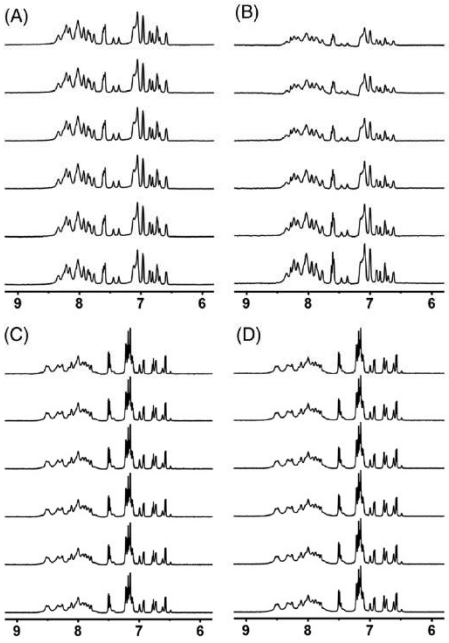

FIGURE 2 A, Enantiopure (L-)Aβ40 in a 9:1 H_2O/D_2O mixture, phosphate-buffered to pH 7.4. B, rac-Aβ40 in a 9:1 H_2O/D_2O mixture, phosphate-buffered to pH 7.4. C, L-Aβ40 in d_6-DMSO. D, rac-Aβ40 in d_6-DMSO. All ^{1}H NMR experiments were performed at 298 K with 160 μM total Aβ40 in all cases. The stacked spectra correspond, from lowest up, to *t* = 1, 9, 17, 25, 33, and 41 min. Racemic Aβ40 loses 61% signal in water over that time period, whereas signal intensity is invariant in all other cases. Aromatic ^{1}H NMR spectral regions are shown; full spectra can be found in the Supporting Information (Supporting Information Figure S1)

enantiopure L-Aβ40. To test for solvent influence, analogous experiments were also performed in DMSO. In stark contrast to the observations made with aqueous Aβ40 solutions, mixing of Aβ40 enantiomers did not trigger precipitation in DMSO, highlighting the importance of solvent for the effect (Figure 2C,D).

Because the findings made via ThT fibril formation assays (Figure 1) and ^{1}H NMR (Figure 2) indicated a significant mechanistic difference between fibril formation from enantiopure and racemic Aβ40 in aqueous solution, TEM imaging experiments were conducted. Mimicking conditions of ThT fibril formation assays, L-, D-, or *rac*-Aβ40 was incubated for 24 h with shaking at 37 °C. Samples were subsequently transferred onto TEM grids, stained with uranyl acetate and imaged, following previously published protocols and procedures.[8] Fibrils obtained from L- or D-Aβ40 had an appearance that was distinct from those derived from racemic Aβ40. As such, fibrils

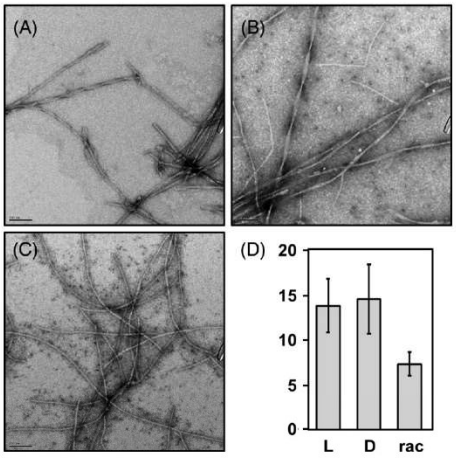

FIGURE 3 A, Fibrils grown from L-Aβ40. B, Fibrils grown from D-Aβ40. C, Fibrils grown from rac-Aβ40. Fibrils were obtained by incubating 20-μM Aβ40 with 20-μM ThT in phosphate buffer (pH 7.4) for 24 h at 37 °C, transferred to TEM grids, stained with uranyl acetate, and imaged (magnification: 23 k; scale bar corresponds to 100 nm). D, Statistical analysis of fibril widths. Fibrils used in the analysis are shown in Supporting Information Figures S2-S4

derived from enantiopure material were wider than the ones formed from the racemate and also often displayed a twist, whereas the racemic ones did not (Figure 3A-C).

To determine whether there was in fact a statistically significant difference in width, measurements were made using FIJI/ImageJ. Six fibril TEM images were selected per condition. Representative images are shown in Figure 3; the full collection images used for the analysis can be found in the Supporting Information. Fibrils derived from enantiopure Aβ40 were measured to have a width of 13.9 ± 3.0 nm (L-Aβ40; 37 datapoints) and 14.6 ± 3.8 nm (D-Aβ40; 18 datapoints). Because the mature fibrils made from enantiopure Aβ40 frequently displayed a periodic twisting, care was taken to take measurements at their widest points. Fibril widths were found to be comparable and statistically indistinguishable ($P > 0.05$, two-tailed *t* test with unequal variance), as expected for the two mirror-image systems.[18] A notable difference in width was apparent between fibrils formed from enantiopure Aβ40 and those formed from the racemate. The width of rac-Aβ40 fibrils was determined as 7.4 ± 1.3 nm (30 datapoints), and the difference with fibrils formed from both L- and D-Aβ40 was statistically significant ($P < 0.05$, two-tailed *t* test with unequal variance).

Because racemic Aβ40 fibrils were clearly different and because mixing of enantiomers of the much smaller peptidic segment KLVFFAE that comprises the central hydrophobic domain of Aβ recapitulated the key trends,[11] the hydrophobic rippled interface LVFFA was constructed using the parallel rippled Pauling-Corey cross-β coordinates,[10] and analyzed through the combination of MM/MD

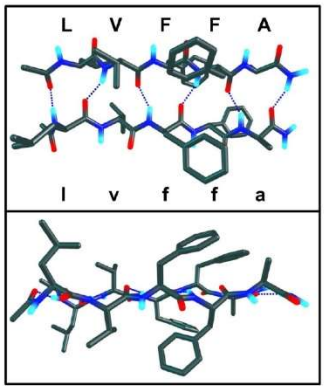

FIGURE 4 A DFT-optimized low-energy structure of the rippled parallel cross-β interface formed in the racemic LVFFA:lvffa dimer peptide (two orthogonal projections). See Section 2 for details on how the structure has been obtained. Cartesian coordinates for the structure have been provided as part of the Supporting Information

and DFT computational methods (see Section 2 for further technical details). The LVFFA segment is well suited for DFT analysis because of the lack of charges, which can complicate DFT calculations that model solvent contributions as a continuum.

A low-energy structure of the dimeric-rippled parallel LVFFA:lvffa cross-β structure is shown in Figure 4. The opposite chirality sense of the two layers projects the bulky hydrophobic sidechains onto opposing sides, thus minimizing steric clashes between residues and yielding a stable structure. The LVFFA:lvff interface qualitatively recapitulates the rippled cross-β backbone topology found by Urban *et al.*[11] It should be noted that Urban *et al.* reported an antiparallel arrangement of KLVFFAE:klvffae in the racemic mixture, which is reasonable to assume due to the better positioning of the opposite charges (K close to E as opposed to K close to K and E close to E). We believe that the parallel arrangement chosen in our study, on the other hand, would allow for better rippled cross-β interactions for the long, hydrophobic C-terminal domain IIGLMVGGVVIA, as found in full-length enantiopure Aβ40 fibrils,[19] and is, therefore, more relevant here.

4 | CONCLUSIONS

Taken together, findings presented here corroborate our initial observations made with the Aβ42 system,[8] further supporting the notion that the racemic Aβ system is fundamentally different from the enantiopure one. The morphological differences determined for the Aβ40 isoform using TEM were more pronounced and well defined than those observed with Aβ42.[8] This allowed for a quantitative fibril analysis, revealing an approximately 2-fold narrowing of *rac*-Aβ40 fibrils along with the disappearance of the helical twisting that was often present with enantiopure Aβ40. DFT calculations supported the viability of rippled cross-β interactions as a likely underlying driving force for accelerated fibril formation upon Aβ40 enantiomer mixing. Future experimental structural work on *rac*-Aβ40 would be of interest as it may give insights into packing and molecular-level interactions of the Aβ40 enantiomers in racemic fibrils.

Whereas strong experimental evidence has been provided by the Schneider and the Nillson laboratories that racemic mixtures of short peptides likely assemble to form rippled cross-β configurations,[11–13,20,21] there is, to the best of our knowledge, not a single high-resolution rippled cross-β structure available yet. The *rac*-Aβ40 system may offer a unique opportunity to obtain the first such structure in the future. There is a broad significance in the heterochiral molecular recognition phenomena that underlie the formation of rippled cross-β structures, ranging from materials,[11–13,20] as well as biomedical applications,[8] to phenomena related to origins of life and chirality of biospheres.[9,22,23]

ACKNOWLEDGMENTS

J.A.R. thanks UCSC for flexible start-up funds and the National Institutes of Health for funding (R21AG058074). UCSC and Dr. Nikolaos Sgourakis are gratefully acknowledged for access to computational facilities. Mr. Stephen Hauskins and the UCSC computing team are acknowledged for help and support. We also acknowledge the National Institutes of Health S10OD016246-01A1 award for the purchase of the JASCO J1500 CD.

ORCID

Alejandro R. Foley https://orcid.org/0000-0002-8644-0546
Jevgenij A. Raskatov https://orcid.org/0000-0002-0082-9113

REFERENCES

[1] G. G. Glenner, C. W. Wong, *Biochem. Biophys. Res. Commun.* **1984**, *120*, 885.
[2] D. J. Selkoe, J. Hardy. *EMBO Mol. Med.* **2016**, *8*, 595.
[3] J. Hardy, D. J. Selkoe, *Science* **2002**, *297*, 353.
[4] G. Bitan, M. D. Kirkitadze, A. Lomakin, S. S. Vollers, G. B. Benedek, D. B. Teplow, *Proc. Natl. Acad. Sci. U.S.A.* **2003**, *100*, 330.
[5] C. L. Masters, G. Simms, N. A. Weinman, G. Multhaup, B. L. McDonald, K. Beyreuther, *Proc. Nat. Acad. Sci. U.S.A.* **1985**, *82*, 4245.
[6] J. Hardy, G. Higgins, *Science* **1992**, *256*, 184.
[7] I. Cherny, E. Gazit, *Angew. Chem. Int. Ed.* **2008**, *47*, 4062.
[8] S. Dutta, A. R. Foley, C. J. A. Warner, X. Zhang, M. Rolandi, B. Abrams, J. A. Raskatov, *Angew. Chem. Int. Ed.* **2017**, *56*, 11506.
[9] J. A. Raskatov, *Chem. Eur. J.* **2017**, *23*, 16920.
[10] L. Pauling, R. B. Corey, *Proc. Natl. Acad. Sci. U.S.A.* **1953**, *39*, 253.
[11] J. M. Urban, J. Ho, G. Piester, R. Fu, B. L. Nilsson, *Molecules* **2019**, *24*, 1983.
[12] R. J. Swanekamp, J. T. M. DiMaio, C. J. Bowerman, B. L. Nilsson, *J. Am. Chem. Soc.* **2012**, *134*, 5556.
[13] K. J. Nagy, M. C. Giano, A. Jin, D. J. Pochan, J. P. Schneider, *J. Am. Chem. Soc.* **2011**, *133*, 14975.
[14] M. J. Frisch, G. W. Trucks, H. B. Schlegel, G. E. Scuseria, M. A. Robb, J. R. Cheeseman, G. Scalmani, V. Barone, B. Mennucci, G. A. Petersson, H. Nakatsuji, M. Caricato, X. Li, H. P. Hratchian,

A. F. Izmaylov, J. Bloino, G. Zheng, J. L. Sonnenberg, M. Hada, M. Ehara, K. Toyota, R. Fukuda, J. Hasegawa, M. Ishida, T. Nakajima, Y. Honda, O. Kitao, H. Nakai, T. Vreven Jr., J. E. Peralta, F. Ogliaro, M. Bearpark, J. J. Heyd, E. Brothers, K. N. Kudin, V. N. Staroverov, R. Kobayashi, J. Normand, K. Raghavachari, A. Rendell, J. C. Burant, S. S. Iyengar, J. Tomasi, M. Cossi, N. Rega, J. M. Millam, M. Klene, J. E. Knox, J. B. Cross, V. Bakken, C. Adamo, J. Jaramillo, R. Gomperts, R. E. Stratmann, O. Yazyev, A. J. Austin, R. Cammi, C. Pomelli, J. W. Ochterski, R. L. Martin, K. Morokuma, V. G. Zakrzewski, G. A. Voth, P. Salvador, J. J. Dannenberg, S. Dapprich, A. D. Daniels, J. B. Farkas, J. V. Foresman, J. Ortiz, Cioslowski, D. J. Fox, *Gaussian 09 Revision A.02*, Gaussian Inc, Wallingford, CT **2009**.

[15] W. J. Hehre, R. Ditchfield, J. A. Pople, *J. Chem. Phys.* **1972**, *56*, 2257.

[16] R. Ditchfield, W. J. Hehre, J. A. Pople, *J. Chem. Phys.* **1971**, *54*, 724.

[17] Y. Zhao, D. G. Truhlar, *Theor. Chem. Acc.* **2008**, *120*, 215.

[18] A. J. Kuhn, J. A. Raskatov, *Prog. Mol. Biol. Transl. Sci.* **2019** *In print*.

[19] R. Tycko, *Neuron* **2015**, *86*, 632.

[20] K. Nagy-Smith, P. J. Beltramo, E. Moore, R. Tycko, E. M. Furst, J. P. Schneider, *ACS Cent. Sci.* **2017**, *3*, 586.

[21] D. M. Raymond, B. L. Nilsson, *Chem. Soc. Rev.* **2018**, *47*, 3659.

[22] I. Weissbuch, R. A. Illos, G. Bolbach, M. Lahav, *Acc. Chem. Res.* **2009**, *42*, 1128.

[23] I. Weissbuch, M. Lahav, L. Leiserowitz, *Cryst. Growth Des.* **2003**, *3*, 125.

SUPPORTING INFORMATION

Additional supporting information may be found online in the Supporting Information section at the end of this article.

How to cite this article: Dutta S, Foley AR, Kuhn AJ, Abrams B, Lee H-W, Raskatov JA. New insights into differential aggregation of enantiomerically pure and racemic Aβ40 systems. *Peptide Science*. 2019;e24139. https://doi.org/10.1002/pep2.24139

Evidence for aggregation-independent, PrP^C-mediated Aβ cellular internalization

Alejandro R. Foley[a,1], Graham P. Roseman[a,1], Ka Chan[a], Amanda Smart[a], Thomas S. Finn[a], Kevin Yang[a], R. Scott Lokey[a], Glenn L. Millhauser[a,2], and Jevgenij A. Raskatov[a,2]

[a]Department of Chemistry and Biochemistry, University of California, Santa Cruz, CA 95064

Edited by Samuel H. Gellman, University of Wisconsin–Madison, Madison, WI, and approved October 8, 2020 (received for review May 8, 2020)

Evidence linking amyloid beta (Aβ) cellular uptake and toxicity has burgeoned, and mechanisms underlying this association are subjects of active research. Two major, interconnected questions are whether Aβ uptake is aggregation-dependent and whether it is sequence-specific. We recently reported that the neuronal uptake of Aβ depends significantly on peptide chirality, suggesting that the process is predominantly receptor-mediated. Over the past decade, the cellular prion protein (PrP^C) has emerged as an important mediator of Aβ-induced toxicity and of neuronal Aβ internalization. Here, we report that the soluble, nonfibrillizing Aβ (1–30) peptide recapitulates full-length Aβ stereoselective cellular uptake, allowing us to decouple aggregation from cellular, receptor-mediated internalization. Moreover, we found that Aβ (1–30) uptake is also dependent on PrP^C expression. NMR-based molecular-level characterization identified the docking site on PrP^C that underlies the stereoselective binding of Aβ (1–30). Our findings therefore identify a specific sequence within Aβ that is responsible for the recognition of the peptide by PrP^C, as well as PrP^C-dependent cellular uptake. Further uptake stereodifferentiation in PrP^C-free cells points toward additional receptor-mediated interactions as likely contributors for Aβ cellular internalization. Taken together, our results highlight the potential of targeting cellular surface receptors to inhibit Aβ cellular uptake as an alternative route for future therapeutic development for Alzheimer's disease.

Alzheimer's disease | amyloid β | prion protein (PrP) | mirror-image peptides | receptor-mediated internalization

Amyloid β (Aβ) is an aggregation-prone peptide, typically ranging in length from 36 to 43 amino acids, released into the extracellular matrix by the proteolytic cleavage of the transmembrane amyloid precursor protein (APP) (1). Formation of amyloid plaques is a hallmark of Alzheimer's disease (AD); however, it is the soluble Aβ aggregation intermediates, often referred to as oligomers, that are the most neurotoxic species (2, 3). While Aβ degradation is facilitated by cellular uptake via glial cells (4), increasing evidence suggests that intracellular accumulation of Aβ may play an early role in AD pathogenesis (5–7), including mitochondrial dysfunction (8), synaptic impairment (7), and increased seeding and prion-like cellular propagation (9). Cellular uptake of soluble, nanomolar concentrations of Aβ leads to intracellular endosomal and lysosomal Aβ concentration, facilitating the formation of high-molecular-weight species capable of seeding amyloid fibril growth (10). This cell-uptake-induced aggregation has been shown to contribute to cellular death, ultimately leading to the release of amyloid species to the extracellular matrix (11). Thus, elucidating the mechanisms by which Aβ is internalized and accumulated inside the cells becomes critical to better understanding the early development of AD.

Various Aβ cellular internalization mechanisms have been reported, such as pore formation (3, 12), endocytosis (13), and receptor-mediated uptake (14). Over the past decade, numerous cell-surface receptors of Aβ have been proposed for the uptake of Aβ. These include the α7 nicotinic acetylcholine receptor (15) and the low-density lipoprotein receptor-related protein-1 (LRP1) (16, 17). Inhibition of soluble Aβ species interacting with the cell surface (18), membrane receptors (19), or blocking Aβ uptake (16) have been shown to reduce Aβ-induced toxicity. Over 400 clinical trials targeting Aβ aggregation have failed (20). In late 2019, the Aducanumab antibody that binds soluble Aβ aggregates showed some limited benefit in a phase III clinical trial (21), supporting the hypothesis that Aβ aggregation is important in AD. Targeting soluble, toxic forms of oligomeric Aβ remains the most promising avenue for AD therapeutic development, but it needs to be substantially improved to make real impact on lives of AD patients. Targeting interactions of Aβ with high-affinity receptors that lead to Aβ cellular internalization may offer a promising alternative for therapeutic development.

Using a cell-based screen of 225,000 clones from a mouse brain complementary DNA library, Strittmatter and coworkers found the cellular prion protein (PrP^C) binds to Aβ oligomers with the highest affinity as compared to the clones screened, displaying a dissociation constant less than 100 nM (22), leading to a PrP^C-dependent inhibition of long-term potentiation (LTP) in neurons (22) and memory impairment in AD mouse models (23). Subsequent work demonstrated that the PrP^C–Aβ interaction occurs in AD patients (24) and drives an aberrant signaling cascade mediated by mGluR5 (25, 26) leading to Fyn kinase phosphorylation in neurons. Additional research has demonstrated that PrP^C, in

Significance

Amyloid β (Aβ) aggregation has been the therapeutic target of several Alzheimer's disease (AD) clinical trials. Aβ exists in many different aggregated forms, making it exceedingly challenging to target. Evidence links intracellular Aβ accumulation and AD pathogenesis. We report that amino acids 1 to 30 of Aβ, Aβ (1–30), do not aggregate yet display cellular uptake stereospecificity when compared to its mirror image, suggesting that Aβ uptake is predominantly receptor-mediated and may be independent from its aggregation state. Additionally, we found Aβ (1–30) internalization to depend on PrP^C expression. Aβ (1–30) thus represents a powerful tool to study mechanisms of Aβ cellular internalization and suggests that Aβ uptake could be modulated by therapeutically targeting high-affinity Aβ receptors.

Author contributions: A.R.F., G.P.R., T.S.F., R.S.L., G.L.M., and J.A.R. designed research; A.R.F., G.P.R., K.C., A.S., and K.Y. performed research; A.R.F., G.P.R., K.C., A.S., K.Y., R.S.L., G.L.M., and J.A.R. contributed new reagents/analytic tools; A.R.F., G.P.R., K.C., A.S., T.S.F., K.Y., R.S.L., G.L.M., and J.A.R. analyzed data; and A.R.F., G.P.R., G.L.M., and J.A.R. wrote the paper.

The authors declare no competing interest.

This article is a PNAS Direct Submission.

[1]A.R.F. and G.P.R. contributed equally to this work.

[2]To whom correspondence may be addressed. Email: glennm@ucsc.edu or jraskato@ucsc.edu.

This article contains supporting information online at https://www.pnas.org/lookup/suppl/doi:10.1073/pnas.2009238117/-/DCSupplemental.

conjunction with LRP1, facilitates cellular uptake of Aβ (16), causing an increase in Fyn kinase phosphorylation.

In previous experiments we compared toxicity of L- and D-Aβ42. We found that, under conditions where L-Aβ42 reduced cell viability over 50%, D-Aβ42 was either nontoxic (PC12) or under 20% toxic (SH-SY5Y) (27). We later showed that L-Aβ is taken up approximately fivefold more efficiently than D-Aβ (28), suggesting that neuronal Aβ uptake and toxicity are linked. Here, we used the mirror-image strategy to pinpoint specific sites within Aβ that are responsible for this stereodifferentiation. Furthermore, we used PrP^C-transfected cells as a high-affinity receptor of Aβ to showcase the relevance of receptor-mediated mechanisms leading to cellular internalization.

Results

We first examined how PrP^C expression influenced Aβ uptake in HEK293T cells, which do not naturally express PrP^C (29). We chose the Aβ40 system for its lower propensity to form pores in cellular membranes (30) and lipid bilayers (12), therefore making it suitable to study receptor-mediated interactions. We synthesized Aβ peptides by solid-phase peptide chemistry, yielding purities exceeding 96% (*SI Appendix*, Figs. S1–S5). For uptake studies, we N-terminally labeled Aβ (1–40) peptides with 5(6)-carboxytetramethylrhodamine (TAMRA), which we have shown previously does not change Aβ aggregation and toxicity (28). As quantitated by flow cytometry (Fig. 1 *B* and *C*), there is a 3.8-fold difference between L- and D-Aβ. When PrP^C is transfected and expressed, both L-Aβ40 and D-Aβ40 values increase (fourfold and 2.2-fold, respectively), and the difference between L-Aβ40 and D-Aβ40 rises to 7.3-fold. Transfection buffer had no effect on cellular association (*SI Appendix*, Fig. S7*A*) and increased PrP^C expression levels result in a dose-dependent behavior (*SI Appendix*, Fig. S7*B*). Z stacks obtained from confocal imaging reveal that Aβ40 peptides are mostly internalized rather than bound to the cellular membrane (Fig. 1 *D*–*G*), qualitatively showing an increase in cellular uptake for L-Aβ40 compared to D-Aβ40 (green color indicated with arrows) (Fig. 1 *D* and *F*). Furthermore, PrP^C-expressing HEK293T cells display an increase in internalized TAMRA-L-Aβ40 (Fig. 1 *E* and *G*) relative to untransfected cells, which is consistent with the flow cytometry results. While L-Aβ40 uptake increases fourfold upon PrP^C expression, D-Aβ40 uptake also increases (2.2-fold), suggesting that both stereospecific and nonspecific interactions between PrP^C–Aβ40 might be involved in increased Aβ uptake, with stereospecific interactions contributing at a higher degree. Additionally, Aβ40 uptake is reduced for PrP^C constructs that delete (ΔCR and Δ100–109 PrP^C) or mutate (G5 PrP^C) the putative binding site of Aβ on wild-type (WT) PrP^C (*SI Appendix*, Fig. S8) (22). Intriguingly, QCR PrP^C, which mutates four conserved lysines between residues 100 and 109 known to influence a PrP^C–Aβ interaction (31) to glutamines, does not result in a decrease in uptake.

Enantiomeric peptides are usually employed to differentiate receptor-mediated from achiral-based toxicity and uptake mechanisms, such as pore formation or passive permeability (32). However, recent work performed by Craik and coworkers demonstrated that the chirality of membrane phospholipids can also modulate interactions of peptides with membranes (33). To address this effect, we performed liposome association controls in lipid unilamellar vesicles composed of 99% phosphatidylcholine (PC) (achiral headgroups) and 1% brain-derived phosphatidylserine (PS) (chiral headgroups). Our results show that both TAMRA-L-Aβ40 and TAMRA-D-Aβ40 associate to liposomes at similar levels, establishing that the observed stereoselectivity of cellular uptake of Aβ is not due to chiral interactions with the lipid bilayer itself (*SI Appendix*, Fig. S9).

We then sought to investigate sequences within Aβ responsible for these stereospecific interactions. Thus, we synthesized truncated variants of Aβ including the flexible N-terminal region

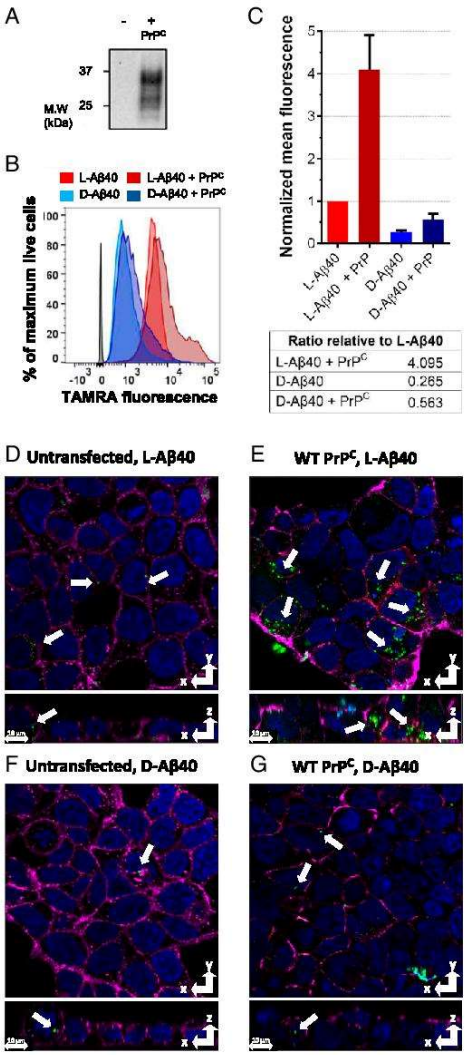

Ratio relative to L-Aβ40	
L-Aβ40 + PrP^C	4.095
D-Aβ40	0.265
D-Aβ40 + PrP^C	0.563

Fig. 1. Aβ40 uptake in HEK293T cells (5 μM peptide, 2-h incubation). (*A*) Western blot showing PrP^C expression. (*B*) Representative FACS diagram. (*C*) Mean FACS quantitation, with error bars showing SD from three biological replicates, and table below showing relative ratios. (*D*–*G*) Representative confocal images from Z stacks. Magenta: membrane dye; green: TAMRA-Aβ; red: PrP^C dye; blue: nuclear dye. (*D*) L-Aβ40 (no PrP^C). (*E*) L-Aβ40 + PrP^C. (*F*) D-Aβ40 (no PrP^C). (*G*) D-Aβ40 + PrP^C. White arrows mark TAMRA-Aβ peptides. (Scale bars, 10 μm.)

(Fig. 2*A*), which we hypothesized to be more available for intermolecular interactions given its greater flexibility when compared to the hydrophobic C terminus of Aβ (34). We observed in SH-SY5Y cells that Aβ (1–16) sequence retained little stereoselectivity (1.4-fold of L over D). In contrast, substantial stereodifferentiation arose with amino acids 16 to 30, where Aβ (16–30) and Aβ (1–30) sequence showed a 4.2-fold and 4.3-fold L vs. D difference, respectively (Fig. 2*B*). These differences are comparable to full-length Aβ40. We then tested these sequences in PrP^C-transfected HEK293T cells (Fig. 2*C*). While stereodifferentiation for the different Aβ fragments in untrasfected cells followed the same trend as in SH-SY5Y cells, surprisingly we did not observe a PrP^C-dependent uptake for Aβ (16–30). However, L-Aβ (1–30) showed a PrP^C-dependent increase in uptake, with trends similar to full-length L-Aβ40. Importantly, the Aβ (1–30) segment is soluble, does not aggregate, and retains a random-coil conformation for at least 24 h (*SI Appendix*, Figs. S10 and S11), which is consistent with previous studies on the Aβ (1–28) system (35). These properties of Aβ (1–30) pointed to the existence of a specific site, responsible, at least in part, for Aβ interactions with PrP^C, as well as its cellular internalization.

Since the nonaggregating Aβ (1–30) was sufficient to recapitulate the trends in PrP^C-dependent uptake stereoselectivity, we studied its interaction with PrP^C using NMR. We collected ^1H-^{15}N heteronuclear single quantum coherence (HSQC) spectra on uniformly ^{15}N-labeled PrP^C with or without L- or D-Aβ (1–30). Intensity ratios (I/I_o) and weighted averaged chemical shifts (Δ) were calculated for each assigned amino acid (data in *SI Appendix*, Tables S1 and S2) and then plotted as bar graphs (Fig. 3). For D-Aβ (1–30), we observed minimal changes in I/I_o throughout the assigned amino acids, indicating little interaction. In contrast, L-Aβ (1–30) displayed a decrease in I/I_o values for assigned amino acids between residues 94 and 125, with the largest decrease between residues 94 and 110. This region also displayed small changes in Δ, indicating an overall intermediate exchange, or moderate affinity for the PrP^C-L-Aβ (1–30) interaction (36). There is additional change in chemical shifts for the structured C terminus [N-terminal side of Helix 1 (H1) and N-terminal end of Helix 2 (H2)] for both L- and D-Aβ (1–30); however, the Δs are not accompanied by appreciable decreases in I/I_o, indicating a fast exchange regime and perhaps nonspecific interactions. Overall, these results correlate with other studies showing oligomeric Aβ (1–42) binds to residues 94 to 110 on PrP^C (22, 37). Furthermore, our NMR results are consistent with our cell studies demonstrating a decrease in uptake when this region is deleted or mutated from full-length WT PrP^C (*SI Appendix*, Fig. S8).

Discussion

Previous studies have shown that PrP^C preferentially interacts with oligomeric Aβ over nonaggregated Aβ (22, 38). In contrast, we have shown that nonaggregating Aβ (1–30) can interact with PrP^C and lead to increased cellular uptake. Importantly, soluble L-Aβ (1–30) interacts with PrP^C between residues 94 and 110, which is the known docking site of oligomeric Aβ (22, 37), thus demonstrating that the absence of Aβ residues 31 to 40 does not affect the locus of binding to PrP^C. We also observed higher PrP^C-dependent uptake of the natural L-isoforms of both Aβ (1–30) and Aβ40 when compared to the D-enantiomers, suggesting a docking site on PrP^C facilitating this interaction.

It has been proposed that an Aβ binding partner relevant to synaptic dysfunction in AD will be 1) oligomer-specific, 2) high-affinity, and 3) present in adult synapses (39). Previous studies have demonstrated that PrP^C contains these three characteristics (16, 22, 25, 26, 38–40). However, our results demonstrate that PrP^C can bind to Aβ (1–30), which is highly soluble, does not aggregate, and remains stable as a single species with a random-coil conformation. This conceivably points to Aβ (1–30)'s not being a higher-order oligomer while still retaining stereoselective uptake and PrP^C binding. This implies that Aβ (1–30) may be the amino acid sequence within full-length Aβ that allows for a PrP^C–Aβ interaction, whereas residues 31 to 40 in full-length Aβ could have a major and main role in promoting Aβ oligomerization. Furthermore, oligomerization could potentially enrich for the preferred conformation of Aβ (1–30) that facilitates an interaction with PrP^C, which is in agreement with our results showing higher PrP^C-dependent cellular uptake levels of Aβ40 when compared to Aβ (1–30) (Fig. 2). This is supported by recent evidence showing that different oligomeric Aβ conformations, measured by accessibility of conformational antibodies, bind with different affinities to PrP^C (41).

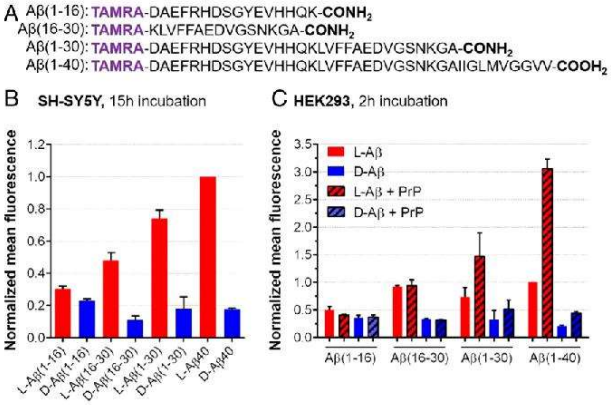

Fig. 2. Cellular uptake of the Aβ peptides studied in this work. (*A*) Sequence of Aβ peptides tested. (*B*) Mean FACS results in SH-SY5Y cells normalized against L-Aβ40 (5 μM peptide, 15-h incubation). Bars show mean fluorescence with error bars for SD of three biological replicates. (*C*) Mean FACS results in HEK293T cells with and without PrP^C expression, normalized against L-Aβ40 (5 μM peptide, 2-h incubation). Bars show mean fluorescence with error bars for SD of two biological replicates.

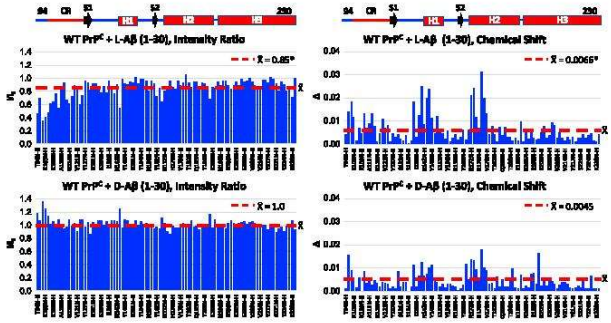

Fig. 3. Effect of 200 μM L-Aβ (1–30) or D-Aβ (1–30) on the intensities ratios (I/I_0) or chemical shifts (Δ) of 100 μM WT-PrP^C resonances recorded in a ^1H- ^{15}N HSQC spectrum at room temperature in 10 mM MES (pH 6.6). Linear schematics above line up with bar graphs. CR: central region (amino acids 105 to 125). The red lines on the intensity ratio and chemical shift graphs are centered at the average value ($\bar{X}$) for the respective data set. The asterisk (*) next to the $\bar{X}$ values denotes a statistically significant difference when comparing the $\bar{X}$ values for the intensity ratios or chemical shifts induced by either L-Aβ (1–30) or D-Aβ (1–30) using the nonparametric Wilcoxon matched- pairs signed rank test ($P < 0.0001$), as appropriate for non-Gaussian distributions.

Mounting evidence shows physiological relevance to a PrP^C–Aβ interaction. For example, monoclonal antibodies directed to target PrPC–Aβ binding sites protected against the Aβ-mediated block of LTP in C57BL/6J mice in vitro and in vivo (42). However, other studies have exhibited PrP^C-independent neurotoxicity in AD models (43, 44). From our results, we observed a PrP^C-independent, but still stereoselective, uptake of L-Aβ (16–30). While PrP^C–Aβ binding seems to require amino acids (1–30), the (16–30) sequence may be sufficient for other chiral interactions with cells, and resolving these chiral interactions may reveal novel receptors as targets to develop therapeutics to inhibit Aβ cellular uptake beyond PrP^C. For example, Aβ oligomers have been shown to bind to the neuronal cell surface receptor LilrB2, producing deleterious effects on hippocampal LTP in mice, resulting from impaired neuronal signaling and thus generating synaptotoxicity (45). Further studies of Aβ–LilrBr2 interactions led to the identification of Aβ moiety 16–21 (^{16}KLVFFA^{21}) as responsible for the interaction with LilrBr2, and small molecules designed to block this interaction were shown to reduce Aβ toxicity in in vitro models (19). Additionally, the tyrosine kinase EphB2 receptor, which modulates the activity of *N*-methyl-D-aspartate–type glutamate receptors, has been reported to interact with Aβ oligomers (46), and blocking this interaction with small peptides results in the rescue of impaired synaptic plasticity and memory deficits in AD APPswe/PS1dE9 (APP/PS1) transgenic mice (47). Other receptors linked in AD pathogenesis include α7 nicotinic acetylcholine receptor (15) or LRP1 (16, 17).

While receptor-mediated interactions of Aβ can lead to downstream neurotoxicity, there are additional mechanisms by which Aβ–membrane interactions may be deleterious. Lipid membranes themselves are known to bind Aβ by either the phospholipid head groups (48) or through the interaction of additional membrane components such as cholesterol, the later reported to catalyze Aβ aggregation in synthetic lipid membranes (49). Cellular plasma membranes also promote Aβ self-assembly, aggregation, and internalization, in a process that generates cytotoxic Aβ species (50). In contrast, Aβ (1–30) does not aggregate, yet we showed it can participate in cell-surface interactions that lead to stereoselective cellular uptake. An increase in intracellular Aβ can create local gradients of particularly high concentrations of Aβ which may favor intracellular Aβ aggregation, ultimately leading to increased pathogenicity and extracellular release of Aβ aggregates which can further act as a seed for fibril growth (10, 11). Abnormally high concentrations of intracellular Aβ resulting from Aβ uptake can also result in decreased Aβ solubility, promoting a homeostatic intracellular imbalance that could trigger amyloid formation (51). Factors controlling Aβ trafficking into cells are therefore of seminal importance to prevent AD pathogenesis (52), and modulating receptor-mediated Aβ uptake could represent a promising strategy for AD disease prevention. In addition, sporadic AD and resulting dementia may be associated with infections of brain tissue with pathogens that are known to enter into neurons, such as herpes simplex virus 1 (HSV-1) and porphyromonas gingivalis (53, 54). As a result, those HSV-1–infected cells produce more Aβ (55), a mechanism that has recently been exploited for the development of brain-tissue models of AD (56).

Taken together, we found that the soluble, nonfibrillizing Aβ (1–30) peptide recapitulates uptake stereoselectivity of full-length Aβ (28). Our findings show that molecular cell-surface recognition of Aβ underlying its internalization is largely due to the amino acid sequence and not the state of aggregation. We found that the soluble Aβ (1–30) peptide segment is both necessary and sufficient to recapitulate stereospecific and PrP^C-dependent uptake. Solution NMR demonstrated that L-Aβ (1–30) interacts with WT-PrP^C between residues 94 and 110, in agreement with previous studies (22, 37), thus validating L-Aβ (1–30) as model system to study this disease-relevant interaction. Deletion of this PrP^C site resulted in a decrease in PrP^C-dependent uptake of Aβ40, further demonstrating a functional interaction between PrP^C and the (1–30) segment of Aβ. These results are consistent with a model in which the relatively flexible segment (1–30) is responsible for cell-surface recognition, whereas the hydrophobic C terminus orchestrates Aβ aggregation and may act in membrane docking and/or perforation activity (12, 30). Future efforts targeting this specific sequence, as well as its cellular binding partners, may hold therapeutic potential to inhibit Aβ toxicity.

Materials and Methods

Synthesis of Aβ Peptides. Aβ and derived peptides were synthesized by solid-phase chemistry, following our previously reported protocols (27). L-Aβ40 and D-Aβ40 were synthesized using Tentagel PHB resin (Rapp Polymere) to achieve carboxyl C terminus, while Aβ fragments were synthesized using Rink Amide resin (Creosalus) to yield amidated C terminus. All syntheses were performed on a CEM Liberty Blue automated microwave-assisted peptide synthesizer at 0.1 mM scale relative to resin loading. Thirty percent

piperidine (Spectrum) in dimethylformamide (DMF) was used for deprotection steps, and 1-hydroxybenzotriazole hydrate (Oakwood Chemical) and *N,N′*-diisopropylcarbodiimide (Chem-Impex) were used as coupling reagents. Peptides were cleaved and deprotected with a mixture solution consisting of trifluoroacetic acid (10 mL), 1, 2-diethanethiol (0.5 mL), tri-isopropylsilane (1 mL), and liquefied phenol (0.5 mL). Peptides were purified by reverse-phase high-performance liquid chromatography (HPLC) as previously described (27), yielding peptides with purities exceeding 97% (*SI Appendix*, Figs. S3 and S4).

N-Terminal TAMRA Labeling of Aβ Peptides. One hundred milligrams of resin (1 eq.) with deprotected N terminus Aβ40 and derived peptides resin were swelled in 2 mL of DMF. Then, a mixture of TAMRA (10 eq.), benzotriazol-1-yl-oxytripyrrolidinophosphonium hexafluorophosphate (PyBOP, 10 eq.), 1-hydroxy-7-azabenzotriazole (HOAt, 16 mg, 20 eq.), and diisopropylethylamine (10 eq.), was dissolved in 5 mL of DMF and added to the resin. The TAMRA–resin mixture was agitated on a rotational shaker for 24 h protected from light. The resin was then washed with DMF (three times) and DCM (two times) and vacuum-dried for 30 min. Reaction completion was confirmed by a cleavage and mass spectrometry analysis of a small fraction of reacted resin. Purification of the peptides was performed as described above, yielding peptides with purity exceeding 96% (*SI Appendix*, Figs. S3–S5). TAMRA $\lambda_{ex/em}$ was 550/580 nm.

Cellular Cultures.

SH-SY5Y cells. Human neuroblastoma SH-SY5Y cells (ATCC) were cultured in 1:1 Dulbecco's Modified Eagle's Medium (DMEM):F12 K media supplemented with 10% fetal bovine serum and 1% penicillin–streptomycin.

SH-SY5Y cell preparation for flow cytometry experiments. Cells were seeded into six-well plates at a density of 5×10^4 cells per well (2 mL) and allowed to adhere for 24 h before performing experiments.

HEK 293T cells. Human embryonic kidney HEK293T cells (ATCC) were cultured in high-glucose DMEM supplemented with 10% fetal bovine serum (Life Technologies) and GlutaMAX (Gibco).

HEK293T cell preparation for flow cytometry, Western blotting, and confocal microscopy experiments. Cells were first seeded into six-well plates at a density of 4×10^5 cells per well, where cells for confocal microscopy were first seeded into eight-well chamber slides (ibidi) at a density of 8×10^4 cells per well. Twenty-four hours after plating, the cells were transiently transfected using LipoD293 In Vitro DNA Transfection Reagent (SignaGEN Laboratories) with 1 μg (for fluorescence-activated cell sorting [FACS] experiments) or 0.25 μg (for confocal microscopy) of PrP^C encoding pcDNA3.1(+)Hygro plasmids. The media was changed 24 h after transfection with fresh DMEM and incubated overnight before starting dosing experiments.

Protein Expression. Recombinant PrP^C was prepared using previously established methods (57). In brief, recombinant PrP^C constructs encoding the various mouse PrP^C(23–230) constructs in the pJ414 vector (DNA 2.0) were transformed into and expressed using *Escherichia coli* (BL21 [DE3]; Invitrogen) (58).

Bacteria were grown in M9 minimal media supplemented with $^{15}NH_4Cl$ (1 g/L) (Cambridge Isotopes) for ^1H-^{15}N HSQC experiments or in Luria broth media (Research Product International). Cells were grown at 37 °C until reaching an optical density of 1 to 1.2, at which point expression was induced with 1 mM isopropyl-1-thio-D-galactopyranoside. PrP^C constructs were purified as previously described (59). Briefly, proteins were extracted from inclusion bodies with extraction buffer (8 M guanidium chloride (GdnHCl), 100 mM Tris, and 100 mM sodium acetate, pH 8) at room temperature and were purified by Ni^{2+}-immobilized metal-ion chromatography (IMAC). Proteins were eluted from the IMAC column using elution butter (5 M GdnHCl, 100 mM Tris, and 100 mM sodium acetate, pH 4.5) and were brought to pH 8 with 6 M potassium hydroxide (KOH) and left at 4 °C for 2 d to oxidize the native disulfide bond. Proteins were then desalted into 50 mM potassium acetate buffer (pH 4.5) and purified by reverse-phase HPLC on a C_4 column (Grace). Pure protein was lyophilized and stored at −20 °C until needed. The purity and identity of all constructs were verified by analytical HPLC and electrospray ionization mass spectrometry (ESI-MS). Disulfide oxidation was confirmed by reaction with *N*-ethylmaleimide and subsequent ESI-MS analysis.

Western Blotting Experiments. Whole-cell lysates were prepared by washing cells two times with phosphate-buffered saline (PBS). Cells were then lysed with lysis buffer [50 mM Tris(hydroxymethyl)aminomethane (Tris) (pH 8), 150 mM sodium chloride (NaCl), 1 mM ethylenediaminetetraacetic acid (EDTA), 1% Triton X-100, and 10% glycerol] supplemented with Halt Protease Inhibitor Mixture (Thermo Fisher Scientific) and quantified using Pierce BCA Protein Assay Kit (Thermo Fisher Scientific). To remove N-linked glycans, cell lysates were treated with recombinant PNGase F (New England Biolabs) under denaturing conditions according to the manufacturer's protocol. Completed PNGaseF reactions were boiled in sodium dodecyl sulfate polyacrylamide gel electrophoresis (SDS-PAGE) buffer and run on a 4 to 20% Mini-PROTEAN TGX Precast Protein Gels (Bio-Rad) along with Precision Plus Protein WesternC Blotting Standards (Bio-Rad). SDS-PAGE gels were subsequently washed with water three times totaling 15 min and transferred to a nitrocellulose membrane using Trans-Blot Turbo Transfer System (Bio-Rad). Membranes were blocked using 5% bovine serum albumin (BSA) in TBS-T. PrP^C constructs were probed with PrP^C Antibody (M-20) (sc-7694, goat origin; Santa Cruz Biotechnology) whose epitope matches near the C terminus of PrP^C. The PrP^C antibody was then detected with horseradish peroxidase (HRP) rabbit anti-goat immunoglobulin G (ab6741; Abcam) and the ladder was detected with Precision Protein StrepTactin-HRP Conjugate (Bio-Rad). Blots were exposed to Pierce ECL Western Blotting Substrate (Thermo Fisher Scientific) and images were taken using ChemiDoc XRS+ System (Bio-Rad) and analyzed using Image Lab Software (Bio-Rad).

Flow Cytometry Experiments. Flow cytometry experiments were performed as previously described (28). Briefly, lyophilized TAMRA-labeled peptides were dissolved in 20 mM NaOH and diluted to a final concentration of 5 μM using SH-SY5Y cell media. Original seeding media was removed from cells and replaced with the freshly prepared 5 μM TAMRA-labeled peptide solution. For control cells, original seeding media was replaced by fresh cell media with no peptide. Cells were then incubated for the desired amount of time at 37 °C. Following incubation time, cells were washed twice with 1× PBS, pH 7.4, trypsinized for 5 min, resuspended in cell culture media, centrifuged at $120 \times g$ for 10 min, resuspended in 1× PBS, pH 7.4, centrifuged at $120 \times g$ for 10 min, and then incubated for 20 min with 1× PBS, pH 7.4, containing 0.1% live/dead fixable violet dye (Thermo Fisher Scientific). Cells were then centrifuged and resuspended in FACS buffer solution (5 mM EDTA and 0.5% BSA in 1× Dulbecco's PBS [DPBS]). A population of 1×10^4 cells was analyzed on a BD FACS Aria II flow cytometer. Live/dead cell dye was excited at 405 nm and fluorescence was detected through a 450/30 nm filter. TAMRA was excited at 571 nm and fluorescence was detected through a 580/10-nm filter. Collected data were processed and analyzed using FlowJo software.

Confocal Microscopy Experiments. HEK293T cells were plated in an eight-well chamber slide (ibidi) as described in *Cellular Cultures*. Cells were dosed with TAMRA-Aβ peptides at 5 μM concentration, following the same sample reconstitution procedures as detailed for FACS. Cells were incubated for 2 h at 37 °C. After incubation, cells were washed twice with 1× DPBS (HyClone) and incubated for 20 min with a solution containing 5 μg/mL Hoechst 33342 dye (nuclear stain, $\lambda_{ex/em}$ 350/461 nm; ThermoFisher), 5 μg/mL wheat germ agglutinin Alexa Fluor dye (membrane stain, $\lambda_{ex/em}$ 650/668 nm; ThermoFisher), and 5 μg/mL PrP^C(8B4) Alexa Fluor dye (PrP^C-specific stain, $\lambda_{ex/em}$ 490/525 nm; Santa Cruz Biotechnology) in DPBS. After incubation, dye-containing solution was removed and cells were washed twice with 1× DPBS and resuspended again in 1× DPBS. Confocal images were acquired on a Leica SP5 confocal microscope using a 63×/1.4 to 0.6 oil immersion objective. Z stacks were collected by three sequential scans (PrP^C-Alexa Fluor & wheat germ agglutinin Alexa Fluor/TAMRA/Hoechst 33342) to avoid spectral overlapping. Images were analyzed using Imaris software.

NMR Experiments. Lyophilized uniformly ^{15}N-labeled PrP^C constructs were first suspended in water until fully solubilized and concentrations were checked using the absorbance at 280 nm (A_{280}) with the proper extinction coefficient. L- or D- Aβ (1–30) was first dissolved to 4 mM in 20 mM potassium hydroxide (KOH) and sonicated for 30 s in a bath sonicator until fully solubilized. The Aβ (1–30) solution was then subsequently diluted to 400 μM with 10 mM 2-(*N*-morpholino)ethanesulfonic acid (MES) at pH 6. NMR samples were contained 100 μM WT PrP^C with or without 200 μM L- or D-Aβ (1–30) in 10 mM MES buffer with 10% D_2O and the pH was adjusted to 6.6 using 600 mM KOH. Samples were loaded into a Shigemi NMR tube (BMS-005B; Wilmad Glass) and a ^1H- ^{15}N HSQC spectrum was collected at 25 °C on an 800-MHz spectrometer (Bruker) at the University of California, Santa Cruz NMR Facility. NMR spectra were analyzed with NMRPipe (60) and Sparky. Protein assignments were achieved using previously determined values (58). Intensity ratios (I/I_o) were calculated by dividing the peak intensity with Aβ (1–30) (I) by the peak intensity of WT PrP^C alone (I_o). The weighted average chemical shifts (Δ) were calculated by the equation $\Delta = [\Delta\delta_{HN}^2 + (0.17\ \Delta\delta_N^2)]^{1/2}$, where $\Delta\delta_{HN}$ and $\Delta\delta_N$ are the Aβ (1–30)–induced differences amide proton and nitrogen chemical shifts, respectively.

Synthetic Liposomes Experiments. A solution of 10 mg/mL 99:1 L-α-phosphatidylcholine (PC):L-α-phosphatidylserine (PS)-brain (Avanti Polar Lipids) in

DCM was blown down with N_2 to create a lipid film, which was then covered with a wipe and vacuum-desiccated for 3 h. The film was then rehydrated with 1× PBS, pH 7.4, and the liposome solution was rotated for 30 min. After mixing, unilamellar vesicles were extruded on a mini extruder with a 0.2-μm polycarbonate membrane over a heating block. The liposome crude solution was passed through the membrane a minimum of 40 times.

Dynamic light scattering characterization. Extruded liposomes diameter was measured on a Malvern Zetasizer Nano ZS90 particle analyzer using 1-cm path length cuvettes, with five runs of 10 s of run duration per run. Three measurements were taken per run with 0-s delay between measurements.

Incubation of liposomes with L-Aβ40-TAMRA and D-Aβ40-TAMRA. Confirmed-diameter liposomes were incubated in the dark for 2 h at room temperature with a 5 μM solution of either L-Aβ40-TAMRA or D-Aβ40-TAMRA in 1× PBS, pH 7.4. Association of TAMRA-Aβ samples to liposomes was determined by flow cytometry on a FACS Aria II flow cytometer, with excitation at 571 nm and fluorescence detection through a 580/10-nm filter. Liposomes incubated with 1× PBS, pH 7.4, only were used as a control.

TAMRA Quenching Kinetic Assays. Lyophilized Aβ peptides were dissolved in 20 mM NaOH, sonicated for 30 s, and diluted with 20 mM phosphate buffer, pH 7.4. Concentration was determined by Nanodrop (ε = 99,000 $M^{-1}{\cdot}cm^{-1}$) at 555 nm. As soon as samples were dissolved to the desired concentration, 200 μL were added to each well in a clear-bottom, black 96-well plate (Corning). Samples were monitored in a Biotek synergy HTX fluorescence plate reader (λ_{ex} = 550 nm, λ_{em} = 580 nm) at 37 °C with continuous shaking. All experiments were run in triplicate and the plate was sealed with optically clear adhesive film. Readings were collected every 5 min with 5 s of shaking before reading and 295 s of shaking in between readings.

Circular Dichroism Spectroscopy Experiments. Aβ (1–30) peptides were dissolved to 200 μM concentration (same as for NMR experiments) in 20 mM phosphate buffer (pH 7.4). To obtain the circular dichroism (CD) spectra, 400 μL of peptide-containing solution were placed in a quartz 1-mm cell. Spectra were then recorded using a Jasco 1500 CD spectrophotometer, set to a scan range of 180 to 280 nm, a digital integration time of 4 s, and a scan speed of 50 nm/min. Samples were incubated at 37 °C in between measurements.

Size-Exclusion Chromatography Experiments. Aβ (1–30) lyophilized peptides were reconstituted to 200 μM in 20 mM phosphate buffer, pH 7.4, as previously described. The solution was injected to a Yarra SEC-2000 column at 0.6 mL/min flow rate on a 1260 Agilent Infinity II LC system, using 20 mM phosphate buffer, pH 7.4, as running buffer. Absorbance at 214 nm was used as method of detection. Peptides were incubated at 37 °C for time = 24-h measurements.

Data Availability. All study data are included in the paper and *SI Appendix*.

ACKNOWLEDGMENTS. J.A.R. thanks University of California, Santa Cruz (UCSC) for start-up funds. We thank NIH for funding: J.A.R. (R21AG058074), A.R.F. (2R25GM058903-20-IMSD), G.L.M. (R35GM131781, S10OD024980, and S10OD018455), and R.S.L and K.Y. (GM131135). We thank Prof. M. Vendruscolo, Prof. D. Kliger, and Dr. E. Chen for helpful comments, UCSC NMR facility, and UCSC microscopy facility and Dr. Benjamin Abrams for help with confocal imaging and critical discussions. We thank B. Nazario for the help with flow cytometry experiments and Phenomenex for the generous donation of a size-exclusion chromatography column.

1. R. J. O'Brien, P. C. Wong, Amyloid precursor protein processing and Alzheimer's disease. *Annu. Rev. Neurosci.* **34**, 185–204 (2011).
2. C. Haass, D. J. Selkoe, Soluble protein oligomers in neurodegeneration: Lessons from the Alzheimer's amyloid beta-peptide. *Nat. Rev. Mol. Cell Biol.* **8**, 101–112 (2007).
3. R. Kayed *et al.*, Common structure of soluble amyloid oligomers implies common mechanism of pathogenesis. *Science* **300**, 486–489 (2003).
4. M. Ries, M. Sastre, Mechanisms of Aβ clearance and degradation by glial cells. *Front. Aging Neurosci.* **8**, 160 (2016).
5. G. K. Gouras *et al.*, Intraneuronal Abeta42 accumulation in human brain. *Am. J. Pathol.* **156**, 15–20 (2000).
6. F. M. LaFerla, K. N. Green, S. Oddo, Intracellular amyloid-beta in Alzheimer's disease. *Nat. Rev. Neurosci.* **8**, 499–509 (2007).
7. S. Oddo *et al.*, Triple-transgenic model of Alzheimer's disease with plaques and tangles: Intracellular Abeta and synaptic dysfunction. *Neuron* **39**, 409–421 (2003).
8. H. Du *et al.*, Cyclophilin D deficiency attenuates mitochondrial and neuronal perturbation and ameliorates learning and memory in Alzheimer's disease. *Nat. Med.* **14**, 1097–1105 (2008).
9. T. T. Olsson, O. Klementieva, G. K. Gouras, Prion-like seeding and nucleation of intracellular amyloid-β. *Neurobiol. Dis.* **113**, 1–10 (2018).
10. X. Hu *et al.*, Amyloid seeds formed by cellular uptake, concentration, and aggregation of the amyloid-beta peptide. *Proc. Natl. Acad. Sci. U.S.A.* **106**, 20324–20329 (2009).
11. R. P. Friedrich *et al.*, Mechanism of amyloid plaque formation suggests an intracellular basis of Abeta pathogenicity. *Proc. Natl. Acad. Sci. U.S.A.* **107**, 1942–1947 (2010).
12. M. Serra-Batiste *et al.*, Aβ42 assembles into specific β-barrel pore-forming oligomers in membrane-mimicking environments. *Proc. Natl. Acad. Sci. U.S.A.* **113**, 10866–10871 (2016).
13. E. Wesén, G. D. M. Jeffries, M. Matson Dzebo, E. K. Esbjörner, Endocytic uptake of monomeric amyloid-β peptides is clathrin- and dynamin-independent and results in selective accumulation of Aβ(1-42) compared to Aβ(1-40). *Sci. Rep.* **7**, 2021 (2017).
14. H. H. Jarosz-Griffiths, E. Noble, J. V. Rushworth, N. M. Hooper, Amyloid-β receptors: The good, the bad, and the prion protein. *J. Biol. Chem.* **291**, 3174–3183 (2016).
15. R. G. Nagele, M. R. D'Andrea, W. J. Anderson, H. Y. Wang, Intracellular accumulation of beta-amyloid(1-42) in neurons is facilitated by the alpha 7 nicotinic acetylcholine receptor in Alzheimer's disease. *Neuroscience* **110**, 199–211 (2002).
16. J. V. Rushworth, H. H. Griffiths, N. T. Watt, N. M. Hooper, Prion protein-mediated toxicity of amyloid-β oligomers requires lipid rafts and the transmembrane LRP1. *J. Biol. Chem.* **288**, 8935–8951 (2013).
17. C. V. Zerbinatti *et al.*, Apolipoprotein E and low density lipoprotein receptor-related protein facilitate intraneuronal Abeta42 accumulation in amyloid model mice. *J. Biol. Chem.* **281**, 36180–36186 (2006).
18. R. Limbocker *et al.*, Trodusquemine enhances $Aβ_{42}$ aggregation but suppresses its toxicity by displacing oligomers from cell membranes. *Nat. Commun.* **10**, 225 (2019).
19. Q. Cao *et al.*, Inhibiting amyloid-β cytotoxicity through its interaction with the cell surface receptor LilrB2 by structure-based design. *Nat. Chem.* **10**, 1213–1221 (2018).
20. P. P. Liu, Y. Xie, X. Y. Meng, J. S. Kang, History and progress of hypotheses and clinical trials for Alzheimer's disease. *Signal Transduct. Target. Ther.* **4**, 29 (2019).
21. L. Schneider, A resurrection of aducanumab for Alzheimer's disease. *Lancet Neurol.* **19**, 111–112 (2020).
22. J. Laurén, D. A. Gimbel, H. B. Nygaard, J. W. Gilbert, S. M. Strittmatter, Cellular prion protein mediates impairment of synaptic plasticity by amyloid-beta oligomers. *Nature* **457**, 1128–1132 (2009).
23. D. A. Gimbel *et al.*, Memory impairment in transgenic Alzheimer mice requires cellular prion protein. *J. Neurosci.* **30**, 6367–6374 (2010).
24. F. Dohler *et al.*, High molecular mass assemblies of amyloid-β oligomers bind prion protein in patients with Alzheimer's disease. *Brain* **137**, 873–886 (2014).
25. L. T. Haas *et al.*, Metabotropic glutamate receptor 5 couples cellular prion protein to intracellular signalling in Alzheimer's disease. *Brain* **139**, 526–546 (2016).
26. J. W. Um *et al.*, Metabotropic glutamate receptor 5 is a coreceptor for Alzheimer aβ oligomer bound to cellular prion protein. *Neuron* **79**, 887–902 (2013).
27. S. Dutta *et al.*, Suppression of oligomer formation and formation of non-toxic fibrils upon addition of mirror-image Aβ42 to the natural l-enantiomer. *Angew. Chem. Int. Ed. Engl.* **56**, 11506–11510 (2017).
28. S. Dutta, T. S. Finn, A. J. Kuhn, B. Abrams, J. A. Raskatov, Chirality dependence of amyloid β cellular uptake and a new mechanistic perspective. *ChemBioChem* **20**, 1023–1026 (2019).
29. Z. Y. Wang *et al.*, Knockdown of prion protein (PrP) by RNA interference weakens the protective activity of wild-type PrP against copper ion and antagonizes the cytotoxicity of fCJD-associated PrP mutants in cultured cells. *Int. J. Mol. Med.* **28**, 413–421 (2011).
30. D. C. Bode, M. D. Baker, J. H. Viles, Ion channel formation by amyloid-β42 oligomers but not amyloid-β40 in cellular membranes. *J. Biol. Chem.* **292**, 1404–1413 (2017).
31. M. A. Kostylev *et al.*, Liquid and hydrogel phases of PrP(C) linked to conformation shifts and triggered by Alzheimer's amyloid-beta oligomers. *Mol. Cell* **72**, 426–443.e12 (2018).
32. D. Wade *et al.*, All-D amino acid-containing channel-forming antibiotic peptides. *Proc. Natl. Acad. Sci. U.S.A.* **87**, 4761–4765 (1990).
33. S. T. Henriques, H. Peacock, A. H. Benfield, C. K. Wang, D. J. Craik, Is the mirror image a true reflection? Intrinsic membrane chirality modulates peptide binding. *J. Am. Chem. Soc.* **141**, 20460–20469 (2019).
34. J. P. Colletier *et al.*, Molecular basis for amyloid-beta polymorphism. *Proc. Natl. Acad. Sci. U.S.A.* **108**, 16938–16943 (2011).
35. M. F. Knauer, B. Soreghan, D. Burdick, J. Kosmoski, C. G. Glabe, Intracellular accumulation and resistance to degradation of the Alzheimer amyloid A4/beta protein. *Proc. Natl. Acad. Sci. U.S.A.* **89**, 7437–7441 (1992).
36. I. R. Kleckner, M. P. Foster, An introduction to NMR-based approaches for measuring protein dynamics. *Biochim. Biophys. Acta* **1814**, 942–968 (2011).
37. N. D. Younan, K. F. Chen, R. S. Rose, D. C. Crowther, J. H. Viles, Prion protein stabilizes amyloid-β (Aβ) oligomers and enhances Aβ neurotoxicity in a *Drosophila* model of Alzheimer's disease. *J. Biol. Chem.* **293**, 13090–13099 (2018).
38. B. R. Fluharty *et al.*, An N-terminal fragment of the prion protein binds to amyloid-β oligomers and inhibits their neurotoxicity in vivo. *J. Biol. Chem.* **288**, 7857–7866 (2013).
39. A. H. Brody, S. M. Strittmatter, Synaptotoxic signaling by amyloid beta oligomers in Alzheimer's disease through prion protein and mGluR5. *Adv. Pharmacol.* **82**, 293–323 (2018).
40. A. Aguzzi, C. Sigurdson, M. Heikenwaelder, Molecular mechanisms of prion pathogenesis. *Annu. Rev. Pathol.* **3**, 11–40 (2008).

41. P. Madhu, S. Mukhopadhyay, Preferential recruitment of conformationally distinct amyloid-β oligomers by the intrinsically disordered region of the human prion protein. *ACS Chem. Neurosci.* **11**, 86–98 (2020).
42. D. B. Freir *et al.*, Interaction between prion protein and toxic amyloid β assemblies can be therapeutically targeted at multiple sites. *Nat. Commun.* **2**, 336 (2011).
43. C. Balducci *et al.*, Synthetic amyloid-beta oligomers impair long-term memory independently of cellular prion protein. *Proc. Natl. Acad. Sci. U.S.A.* **107**, 2295–2300 (2010).
44. I. J. Whitehouse *et al.*, Ablation of prion protein in wild type human amyloid precursor protein (APP) transgenic mice does not alter the proteolysis of APP, levels of amyloid-β or pathologic phenotype. *PLoS One* **11**, e0159119 (2016).
45. T. Kim *et al.*, Human LilrB2 is a β-amyloid receptor and its murine homolog PirB regulates synaptic plasticity in an Alzheimer's model. *Science* **341**, 1399–1404 (2013).
46. M. Cissé *et al.*, Ablation of cellular prion protein does not ameliorate abnormal neural network activity or cognitive dysfunction in the J20 line of human amyloid precursor protein transgenic mice. *J. Neurosci.* **31**, 10427–10431 (2011).
47. X. D. Shi *et al.*, Blocking the interaction between EphB2 and ADDLs by a small peptide rescues impaired synaptic plasticity and memory deficits in a mouse model of Alzheimer's disease. *J. Neurosci.* **36**, 11959–11973 (2016).
48. E. Terzi, G. Hölzemann, J. Seelig, Interaction of Alzheimer beta-amyloid peptide(1-40) with lipid membranes. *Biochemistry* **36**, 14845–14852 (1997).
49. J. Habchi *et al.*, Cholesterol catalyses Aβ42 aggregation through a heterogeneous nucleation pathway in the presence of lipid membranes. *Nat. Chem.* **10**, 673–683 (2018).
50. S. Jin *et al.*, Amyloid-β(1-42) aggregation initiates its cellular uptake and cytotoxicity. *J. Biol. Chem.* **291**, 19590–19606 (2016).
51. R. Freer *et al.*, A protein homeostasis signature in healthy brains recapitulates tissue vulnerability to Alzheimer's disease. *Sci. Adv.* **2**, e1600947 (2016).
52. R. Kundra, P. Ciryam, R. I. Morimoto, C. M. Dobson, M. Vendruscolo, Protein homeostasis of a metastable subproteome associated with Alzheimer's disease. *Proc. Natl. Acad. Sci. U.S.A.* **114**, E5703–E5711 (2017).
53. T. Fülöp, R. F. Itzhaki, B. J. Balin, J. Miklossy, A. E. Barron, Role of microbes in the development of Alzheimer's disease: State of the art–An international symposium presented at the 2017 IAGG congress in San Francisco. *Front. Genet.* **9**, 362 (2018).
54. T. Fülöp *et al.*, Targeting infectious agents as a therapeutic strategy in Alzheimer's disease. *CNS Drugs* **34**, 673–695 (2020).
55. G. Ill-Raga *et al.*, Activation of PKR causes amyloid ß-peptide accumulation via derepression of BACE1 expression. *PLoS One* **6**, e21456 (2011).
56. D. M. Cairns *et al.*, A 3D human brain-like tissue model of herpes-induced Alzheimer's disease. *Sci. Adv.* **6**, eaay8828 (2020).
57. G. P. Roseman, "The central region of the cellular prion protein attenuates the intrinsic toxicity of N-terminus," PhD thesis, University of California, Santa Cruz, CA (2019).
58. E. G. Evans, M. J. Pushie, K. A. Markham, H. W. Lee, G. L. Millhauser, Interaction between prion protein's copper-bound octarepeat domain and a charged C-terminal pocket suggests a mechanism for N-terminal regulation. *Structure* **24**, 1057–1067 (2016).
59. A. R. Spevacek *et al.*, Zinc drives a tertiary fold in the prion protein with familial disease mutation sites at the interface. *Structure* **21**, 236–246 (2013).
60. F. Delaglio *et al.*, NMRPipe: A multidimensional spectral processing system based on UNIX pipes. *J. Biomol. NMR* **6**, 277–293 (1995).

CHAPTER 4:

Conclusions

More than 12,000 documents mentioning “amyloid beta aggregation” have been published since Dr. Alois Alzheimer filled the first reported case of Alzheimer’s disease (AD) based on his observations on the *postmortem* brain of August Deter in 1906, with this number exponentially increasing year by year. While our understanding about the mechanisms of AD progression has vastly increased over the years, a successful therapy to prevent and slowdown its progress remains elusive, highlighting the huge challenge that represents to decipher this system.

While this thesis has been focused on studying structure-activity relationships of the Aβ peptide from a biophysical and cellular activity perspective, it is important to note that AD pathology involves much more than Aβ. In fact, the tau protein, usually expressed and found in brain cells, is considered the second pathological hallmark of AD, where toxic, modified (hyperphosphorylated) versions of the tau protein are found forming neurofibrillary tangles in AD patients. Additional proteins and genetic components are also believed to play an important role, such as the apolipoprotein E4 (ApoE4), whose carriers have a 4-fold increased risk factor for AD. Additionally, patients of another amyloidogenic protein-causing disease, type II diabetes, have also been hypothesized to be predisposed for AD development. But it is not proteins that are considered to be the only disease culprits. Brain inflammation is thought to have major influence on disease progression, mitochondrial failure and generation of reactive oxygen species (ROS) are typically observed in diseased neurons, and additional factors such as imbalances in calcium homeostasis, impairment on metal ion transport, and a compromised blood-brain barrier, are also pathologies observed in AD patients. What is a cause and what is a symptom in AD is still a hard question to answer. Perhaps the reason why we have not still disentangled this system is because, surprisingly, we still have limited knowledge about some of the main components of this disease. Quoting my mentor Prof. Jevgenij Raskatov, “the fact that the amyloid precursor protein (APP) is named after its proteolytic by-product (Aβ) already tells us how little we understand the system”. And this is in fact true. How come we have put so much focus and resources on studying the Aβ peptide, when we still do not know what the functions of APP are? Asking this question is undoubtedly much easier than studying APP. Nonetheless, it seems that the Aβ peptide, at least for nowconclussions, is

offering us the most plausible working hypothesis; molecules and antibodies targeting Aβ aggregation and toxicity have proven to be successful *in vitro* and in animal studies, and although still not reaching phase IV of clinical trials, phase III has been reached by several Aβ and β-site amyloid precursor protein cleaving enzyme 1 (BACE1) targeting drugs.

The work from this thesis has focused on studying the mechanisms of Aβ oligomer and fibril formation. Because of its aggregation-prone properties and unstructured nature, the Aβ peptide is not a trivial system to study. Consequently, research performed on Aβ needs to be exceptionally particularly rigorous, so meaningful results can be obtained and reproduced by other laboratories. It seems an obvious statement, but as stated in Chapter 1 (Foley and Raskatov, ChemBioChem 2020), this issue has been pointed as one of the possible main reasons on why drugs targeting Aβ fail when taken from the bench to clinical trials. Aβ aggregation and toxicity levels are exquisitely dependent on experimental conditions, and thus, results obtained for this system should always be benchmarked against different sources (laboratory purified, expressed, or synthetic) and even testing multiple synthetic batches of Aβ to ensure reproducible results. The latter was an approach consistently applied on the work performed in this thesis.

The aggregating nature of Aβ is also a major hindrance for Aβ research. While mounting studies show high-resolution Aβ fibrillar structures (Chapter 1: Foley and Raskatov ChemBioChem 2019), high-resolution structures of the most neurotoxic, intermediate oligomeric species remain elusive. In the Raskatov laboratory, and as main theme of this thesis, we thought on molecular chirality as a tool to obtain novel structure-activity relationships of Aβ aggregation intermediates. Our hypothesis was that, by introducing chiral point mutations, we would be able to stabilize and characterize toxic Aβ aggregation intermediates. We based this hypothesis on the fact that chiral mutations only modify the side chain functional groups orientation (Ramachandran space) of Aβ, and therefore the size, charge, polarity, hydropathy, and flexibility of the resultant Aβ mutant peptide remain the same. Thus, this allows to introduce mutations that solely focus on conformational changes. To achieve this, in Chapter 2 we designed a focused chiral mutant library (FCML) of Aβ, and introduced D-amino acid mutations

at specific regions of the Aβ sequence which we hypothesized to have an important role on Aβ aggregation and toxicity (Foley et al. J. Org. Chem. 2020). The obtained results supported our hypothesis, with the chiral mutant peptides all having different aggregation propensity and/or biological activity compared to wild-type Aβ. A further and extended analysis on one of the chiral variants, which had D-Ser at position 26 (S26s) of Aβ provided with important molecular interactions leading to Aβ amyloidogenesis (Foley et al. ACS Chem. Neurosci. 2019). Specifically, we showed that upon S26s, Aβ slowed aggregation (approximately 4-fold), and also became non-toxic. By NMR and computational (DFT) calculations, we observed that this was due to the formation of an intramolecular H-bond interaction between Ser26 and the neighbor amino acid Asn27. This disrupted the ability of Asn27 to engage in the fibrillogenic side chain-to-side chain H-bonding, revealing that intermolecular stabilizing interactions between Asn27 side chains are a key element controlling Aβ aggregation and toxicity. It will thus be important to further study this effect within Aβ, for example, by mutating the remaining Asn amino acids of the Aβ sequence, to probe this stabilizing interaction. A distinctly interesting position would be Asn27, given that it is located within the electrostatic-rich and loop region of Aβ, which has been postulated to be particularly important for the generation of Aβ toxic species. Asn27 cannot only be mutated to D-Asn, but also to amino acids with side chains which could provide with destabilizing interactions. Fox example, by mutating Asn to Asp, which would turn the stabilizing Asn intermolecular H-bond to negatively charged, repulsive carboxylate electrostatic interactions. Evaluating the impact of Asn sidechain interactions as an amyloidogenic-promoting interaction would not only important for Aβ, but for fibrillogenic systems in general. Finally, generating the Aβ-S26s system and stabilizing aggregation intermediates through this mutation has also allowed us to start advanced structural studies in collaboration with the Eisenberg laboratory at the University of California Los Angeles. A successful outcome would provide a breakthrough finding, since it would lead to the first atomic-level structure of Aβ oligomers ever reported, with many implications for the structural and biological understanding of Aβ aggregation and pathology in AD.

The use of chirality as a molecular probe is not only limited to introducing point D-amino acid substitutions. Chapter 3 focuses on using mirror-image Aβ as a structural modifier and mechanistic tools to study cellular interactions. On a project led by Dr. Subrata Dutta, we developed a novel mechanism to prevent Aβ toxicity, which we termed the chiral inactivation strategy (Dutta et al. Angew. Chem. Int. Ed. 2017). We showed that this approach, based on enhancing the aggregation of the peptide by mixing L- and D- enantiomers of Aβ, can drastically reduce its toxicity. A morphological and structural analysis on the obtained racemic fibrils revealed that racemic fibrils had distinct morphology when compared to enantiopure fibrils, exhibiting a ~2-fold narrowing in fibril diameter (Dutta et al. Pept. Sci. 2019). Additionally, racemic fibrils appeared flat, in contrast to enantiopure fibrils, which exhibited a twist, suggesting that the fibril architecture of racemic fibrils may be different. This was indeed already proposed by Pauling and Corey in 1953, which hypothesized that a heterochiral polypeptide system should adopt a rippled β-sheet structure, rather than the pleated β-sheet structure usually adopted in homochiral systems (see Chapter 3: Dutta et al. Pept. Sci. 2019). However, a high-resolution experimental structure confirming this arrangement has not been obtained thus far. In this regard, our laboratory and my late work as a PhD student has been focused on establishing a collaboration with Dr. Robert Tycko (NIH). For this ongoing collaboration, I synthesized D-Aβ with point ^{15}N-Gly labels, and Dr. Tycko is personally growing racemic fibrils along his own ^{15}N-L-Aβ. By performing solid-state NMR experiments, our goal here is to obtain the first in vitro, high-resolution, rippled cross-β structure ever reported, which will allow the understanding of the structural elements that lead to the suppression of Aβ toxicity.

Lastly, also in Chapter 3, we employed the mirror-image strategy to study the mechanisms of uptake of Aβ and its interaction with cellular membranes, in particular with the cellular prion protein (PrP^C) (Foley et al. Proc. Natl. Acad. Sci. USA 2020). PrP^C has been reported to be a high-affinity receptor of Aβ, and its interactions with Aβ have proven to cause toxic effects. In collaboration with the Millhauser and Lokey labs at University of California Santa Cruz, we investigated how Aβ is uptaken into cells, since this is a mechanism reported to initiate its toxicity. By using enantiomeric Aβ, we were

able to determine a specific domain within the Aβ sequence (amino acids 1 to 30) that is responsible for stereospecific interactions with potential cellular membrane receptors. This was an important finding, since this Aβ(1-30) domain does not fibrillize, unlike full-length Aβ, yet it recapitulates its uptake properties. We could then use this domain as a model to look for cellular Aβ receptors that could be novel targets for drug development. For example, PrP^C had been shown to mediate Aβ uptake and toxicity. By using this Aβ(1-30) peptide, we were also been able to obtain Aβ-PrP^C binding insights through flow cytometry, confocal microscopy, and solution state NMR. This was the first time that Aβ aggregation and its cellular, receptor-mediated neuronal uptake were disentangled.

Overall, the work performed on this thesis has proven the potential of chiral editing and the use mirror-image peptides/proteins to provide with novel mechanistic information of Aβ and AD pathogenesis. This work shows how molecular chirality can be used as a tool to either control the aggregation state, to stabilize oligomeric intermediates, or to elucidate the nature of the cellular interactions of amyloidogenic peptides and proteins, thus being a powerful tool for studying aggregation-prone systems. The concepts and results presented here should be broadly applicable to many other proteins and peptides involved in amyloidogenic diseases.

REFERENCES

1. Chiti F, Dobson CM (2006) Protein Misfolding, Functional Amyloid, and Human Disease. *Annu Rev Biochem* 75(1):333–366.

2. Eisenberg D, Jucker M (2012) The amyloid state of proteins in human diseases. *Cell* 148(6):1188–1203.

3. Murphy MP, Levine H (2010) Alzheimer's disease and the amyloid-β peptide. *J Alzheimer's Dis* 19(1):311–323.

4. Araki K, et al. (2019) Parkinson's disease is a type of amyloidosis featuring accumulation of amyloid fibrils of α-synuclein. *Proc Natl Acad Sci U S A* 116(36):17963–17969.

5. Hull RL, Westermark GT, Westermark P, Kahn SE (2004) Islet amyloid: A critical entity in the pathogenesis of type 2 diabetes. *J Clin Endocrinol Metab* 89(8):3629–3643.

6. Uversky VN (2019) Intrinsically disordered proteins and their "Mysterious" (meta)physics. *Front Phys* 7(FEB). doi:10.3389/fphy.2019.00010.

7. Fink AL (1998) Protein aggregation: Folding aggregates, inclusion bodies and amyloid. *Fold Des* 3(1). doi:10.1016/S1359-0278(98)00002-9.

8. Dobson CM (2003) Protein folding and misfolding. *Nature* 426(6968):884–890.

9. Nelson R, et al. (2005) Structure of the cross-β spine of amyloid-like fibrils. *Nature*. doi:10.1038/nature03680.

10. Greenwald J, Riek R (2010) Biology of amyloid: Structure, function, and regulation. *Structure* 18(10):1244–1260.

11. Jahn TR, Radford SE (2008) Folding versus aggregation: Polypeptide conformations on competing pathways. *Arch Biochem Biophys* 469(1):100–117.

12. Eichner T, Radford SE (2011) A Diversity of Assembly Mechanisms of a Generic Amyloid Fold. *Mol Cell* 43(1):8–18.

13. Baldwin AJ, et al. (2011) Metastability of native proteins and the phenomenon of amyloid formation. *J Am Chem Soc* 133(36):14160–14163.

14. Knowles TPJ, Vendruscolo M, Dobson CM (2014) The amyloid state and its association with protein misfolding diseases. *Nat Rev Mol Cell Biol* 15(6):384–396.

15. Koo EH, Lansbury J, Kelly JW (1999) Amyloid diseases: Abnormal protein aggregation in neurodegeneration. *Proc Natl Acad Sci U S A* 96(18):9989–9990.

16. Bucciantini M, et al. (2002) Inherent toxicity of aggregates implies a common mechanism for protein misfolding diseases. *Nature* 416(6880):507–511.

17. Kayed R, et al. (2003) Common structure of soluble amyloid oligomers implies common mechanism of pathogenesis. *Science (80-)* 300(5618):486–489.

18. Haass C, Selkoe DJ (2007) Soluble protein oligomers in neurodegeneration: Lessons from the Alzheimer's amyloid β-peptide. *Nat Rev Mol Cell Biol* 8(2):101–112.

19. Choi ML, Gandhi S (2018) Crucial role of protein oligomerization in the pathogenesis of Alzheimer's and Parkinson's diseases. *FEBS J* 285(19):3631–3644.

20. Lotz GP, Legleiter J (2013) The role of amyloidogenic protein oligomerization in neurodegenerative disease. *J Mol Med* 91(6):653–664.

21. Rodriguez JA, et al. (2015) Structure of the toxic core of α-synuclein from invisible crystals. *Nature* 525(7570):486–490.

22. Tuttle MD, et al. (2016) Solid-state NMR structure of a pathogenic fibril of full-length human α-synuclein. *Nat Struct Mol Biol* 23(5):409–415.

23. Iadanza MG, et al. (2018) The structure of a β2-microglobulin fibril suggests a molecular basis

for its amyloid polymorphism. *Nat Commun* 9(1). doi:10.1038/s41467-018-06761-6.

24. Radamaker L, et al. (2019) Cryo-EM structure of a light chain-derived amyloid fibril from a patient with systemic AL amyloidosis. *Nat Commun* 10(1). doi:10.1038/s41467-019-09032-0.

25. Cao Q, Boyer DR, Sawaya MR, Ge P, Eisenberg DS (2020) Cryo-EM structure and inhibitor design of human IAPP (amylin) fibrils. *Nat Struct Mol Biol* 27(7):653–659.

26. Krotee P, et al. (2017) Atomic structures of fibrillar segments of hIAPP suggest tightly mated β-sheets are important for cytotoxicity. *Elife* 6. doi:10.7554/eLife.19273.

27. Kreutzer AG, Nowick JS (2018) Elucidating the Structures of Amyloid Oligomers with Macrocyclic β-Hairpin Peptides: Insights into Alzheimer's Disease and Other Amyloid Diseases. *Acc Chem Res* 51(3):706–718.

28. Pham JD, Chim N, Goulding CW, Nowick JS (2013) Structures of oligomers of a peptide from β-amyloid. *J Am Chem Soc* 135(33):12460–12467.

29. Buchanan LE, et al. (2013) Mechanism of IAPP amyloid fibril formation involves an intermediate with a transient β-sheet. *Proc Natl Acad Sci U S A* 110(48):19285–19290.

30. Shea D, et al. (2019) α-Sheet secondary structure in amyloid β-peptide drives aggregation and toxicity in Alzheimer's disease. *Proc Natl Acad Sci U S A* 116(18):8895–8900.

31. Ciudad S, et al. (2020) Aβ(1-42) tetramer and octamer structures reveal edge conductivity pores as a mechanism for membrane damage. *Nat Commun* 11(1). doi:10.1038/s41467-020-16566-1.

32. Chen SW, et al. (2015) Structural characterization of toxic oligomers that are kinetically trapped during α-synuclein fibril formation. *Proc Natl Acad Sci U S A* 112(16):E1994–E2003.

33. Marina GB, et al. (2003) Amyloid β-protein (Aβ) assembly: Aβ40 and Aβ42 oligomerize through distinct pathways. *Proc Natl Acad Sci U S A* 100(1):330–335.

34. Cummings J, Lee G, Ritter A, Sabbagh M, Zhong K (2019) Alzheimer's disease drug

development pipeline: 2019. *Alzheimer's Dement Transl Res Clin Interv* 5:272–293.

35. Alzheimer A (1906) Über einen eigenartigen schweren Erkrankungsprozeß der Hirnrinde. *Neurol Zentralblatt*. doi:10.1145/1658550.1658558.

36. Glenner GG, Wong CW (1984) Alzheimer's disease: Initial report of the purification and characterization of a novel cerebrovascular amyloid protein. *Biochem Biophys Res Commun* 120(3):885–890.

37. Liu P-P, Xie Y, Meng X-Y, Kang J-S (2019) History and progress of hypotheses and clinical trials for Alzheimer's disease. *Signal Transduct Target Ther* 4(1). doi:10.1038/s41392-019-0063-8.

38. Bhadbhade A, Cheng DW (2012) Amyloid Precursor Protein Processing in Alzheimer's Disease. *Iran J Child Neurol* 6(1):1–4.

39. Hardy JA, Higgins GA (1992) Alzheimer's disease: The amyloid cascade hypothesis. *Science (80-)* 256(5054):184–185.

40. Selkoe DJ (1991) The molecular pathology of Alzheimer's disease. *Neuron* 6(4):487–498.

41. Kayed R, et al. (2003) Common structure of soluble amyloid oligomers implies common mechanism of pathogenesis. *Science (80-)* 300(5618):486–489.

42. Teplow DB, et al. (2003) Amyloid -protein (A) assembly: A 40 and A 42 oligomerize through distinct pathways. *Proc Natl Acad Sci* 100(1):330–335.

43. Hoshi M, et al. (2003) Spherical aggregates of -amyloid (amylospheroid) show high neurotoxicity and activate tau protein kinase I/glycogen synthase kinase-3 . *Proc Natl Acad Sci* 100(11):6370–6375.

44. Lashuel HA, Hartley D, Petre BM, Walz T, Lansbury PT (2002) Neurodegenerative disease: Amyloid pores from pathogenic mutations. *Nature* 418(6895):291.

45. Laganowsky A, et al. (2012) Atomic view of a toxic amyloid small oligomer. *Science (80-* 335(6073):1228–1231.

46. Harper JD, Wong SS, Lieber CM, Lansbury PT (1997) Observation of metastable Aβ amyloid protofibrils by atomic force microscopy. *Chem Biol* 4(2):119–125.

47. Lesné S, et al. (2006) A specific amyloid-β protein assembly in the brain impairs memory. *Nature* 440(7082):352–357.

48. Nilsberth C, et al. (2001) The "Arctic" APP mutation (E693G) causes Alzheimer's disease by enhanced Aβ protofibril formation. *Nat Neurosci* 4(9):887–893.

49. Nagy KJ, Giano MC, Jin A, Pochan DJ, Schneider JP (2011) Enhanced mechanical rigidity of hydrogels formed from enantiomeric peptide assemblies. *J Am Chem Soc* 133(38):14975–14977.

50. Dzwolak W, Ravindra R, Nicolini C, Jansen R, Winter R (2004) The Diastereomeric Assembly of Polylysine is the Low-Volume Pathway for Preferential Formation of β-Sheet Aggregates. *J Am Chem Soc* 126(12):3762–3768.

51. Dutta S, et al. (2017) Suppression of Oligomer Formation and Formation of Non-Toxic Fibrils upon Addition of Mirror-Image Aβ42 to the Natural l-Enantiomer. *Angew Chemie - Int Ed* 56(38):11506–11510.

52. Jacques J, Collet A, Wilen S (1994) Enantiomers, Racemates and Resolutions. *Krieger Publ Malabar, FL*:1994.

53. Yao Z, et al. (2019) Use of a Stereochemical Strategy to Probe the Mechanism of Phenol-Soluble Modulin α3 Toxicity. *J Am Chem Soc* 141(19):7660–7664.

54. Wade D, et al. (1990) All-D amino acid-containing channel-forming antibiotic peptides. *Proc Natl Acad Sci U S A* 87(12):4761–4765.

55. Veach RA, et al. (2004) Receptor/Transporter-independent Targeting of Functional Peptides

across the Plasma Membrane. *J Biol Chem* 279(12):11425–11431.

APPENDIX

CHEMBIOCHEM

Supporting Information

A DFT-Assisted Topological Analysis of Four Polymorphic, S-Shaped Aβ42 Fibril Structures

Alejandro R. Foley and Jevgenij A. Raskatov*[a]

cbic_201900036_sm_miscellaneous_information.pdf

SUPPORTING INFORMATION

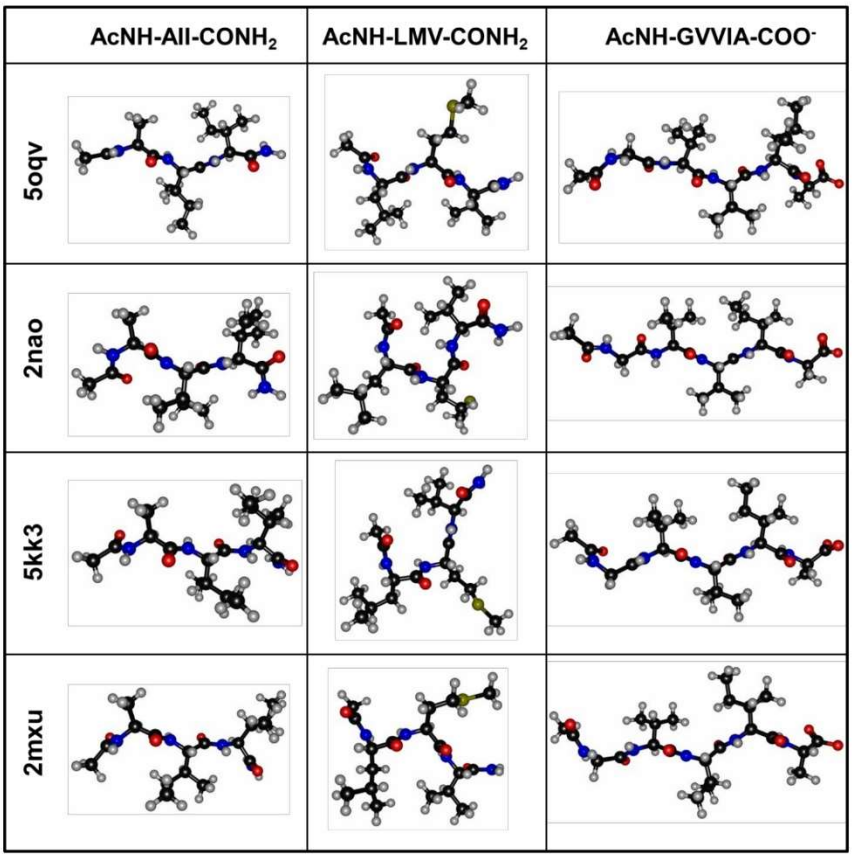

Figure S1. Segments used in calculations associated with Figure 3, in which a partition analysis of loop 2 was performed. All segments are projected to follow the NTER to CTER orientation and to be displayed in a consistent relative disposition to facilitate comparison.

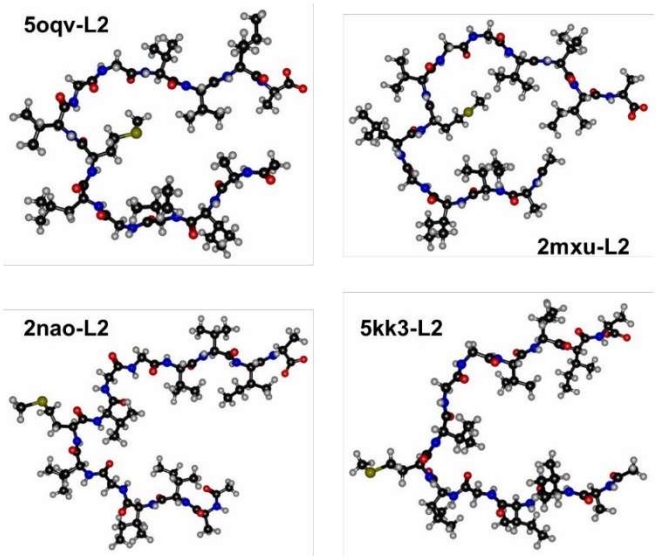

Figure S2. Fragments of the four Aβ42 peptides that correspond to the hydrophobic loop 2 that were used in DFT calculations.

COORDINATES USED IN FINAL SINGLE POINT ENERGY CALCULATIONS

2mxu loop 2

189
symmetry c1

C	10.257283000	-2.407636000	-2.356911000
C	9.504690000	-2.874367000	-1.110075000
C	10.342073000	-3.879593000	-0.318979000
C	6.911463000	-1.200222000	-1.288695000
C	8.260593000	-0.620579000	-0.843510000
C	8.173684000	8.515698000	-1.119635000
C	7.111398000	-5.471844000	-0.378401000
C	9.128208000	-1.705059000	-0.191178000
C	3.751714000	-0.932627000	-1.553206000
C	2.363134000	-1.511463000	-1.838283000
C	4.631109000	-3.217524000	-0.909898000
C	8.006055000	1.788045000	-0.453500000
C	7.522043000	7.162708000	-0.840809000
C	5.942878000	-7.631526000	0.219388000
C	4.581111000	-1.722833000	-0.536085000
C	5.990645000	-6.117928000	0.429463000
C	4.635290000	-5.492242000	0.057586000
C	1.230232000	-3.741194000	-0.513672000
C	7.731174000	2.865353000	0.587338000
C	6.193710000	7.271781000	-0.081419000

C	5.505682000	5.891275000	-0.021842000
C	6.351472000	4.853409000	0.715741000
C	3.550781000	-6.018097000	0.995094000
C	3.053768000	5.639579000	0.022860000
C	0.234849000	-7.303212000	0.362254000
C	1.542002000	-7.418871000	1.142440000
C	6.367887000	7.904604000	1.299738000
C	-2.189881000	-7.514370000	0.442770000
C	1.871433000	5.353863000	0.942530000
C	1.730580000	3.819511000	1.122727000
C	3.035622000	3.173907000	1.600957000
C	-4.484081000	2.013705000	-1.614502000
C	-1.579469000	6.833373000	0.265603000
C	-0.281392000	6.525257000	1.010568000
C	-1.900146000	8.323876000	0.331101000
C	-2.862629000	-6.338816000	1.147662000
C	-2.882424000	-2.988161000	0.665033000
C	-1.663977000	-3.278170000	1.540886000
C	-3.472831000	5.250249000	0.224773000
C	-5.161853000	-3.867897000	-0.031179000
C	0.546018000	3.460903000	2.033130000
C	-3.911089000	-4.136901000	0.803420000
C	-5.650769000	1.380101000	-0.860164000
C	-7.026126000	1.735003000	-1.434620000
C	-3.482733000	-1.627565000	1.017337000
C	-7.354429000	3.220481000	-1.273223000
C	-4.266898000	4.270678000	1.059302000
C	-7.367654000	-2.788400000	-0.083238000
C	-8.504595000	-5.022595000	-0.117984000
C	-8.126048000	0.883212000	-0.767461000
C	-9.482541000	1.109397000	-1.439358000
C	0.718019000	3.854955000	3.499301000
C	-7.490405000	-1.288796000	0.191668000
C	-8.634672000	-3.567074000	0.328744000
C	-11.757098000	2.030165000	-1.132674000
C	-12.110797000	3.521783000	-0.862535000
C	-8.916331000	-3.478524000	1.828353000
C	-12.730697000	1.103349000	-0.407639000
H	10.616228000	-3.269446000	-2.928720000
H	9.616188000	-1.816105000	-3.016321000
H	11.128356000	-1.800263000	-2.081414000
H	8.584321000	-3.369333000	-1.441083000
H	10.573818000	-4.759965000	-0.926987000
H	8.735303000	-0.270222000	-1.762863000
H	6.930351000	-5.578694000	-1.454788000
H	4.307228000	-0.891705000	-2.496043000
H	9.059887000	8.397359000	-1.749220000
H	7.477296000	9.183457000	-1.638588000
H	2.449317000	-2.425023000	-2.429145000
H	5.727642000	-7.867279000	-0.829634000
H	7.347595000	6.643427000	-1.792611000
H	1.782597000	-0.790735000	-2.418029000
H	8.074038000	-5.937549000	-0.145352000
H	11.290583000	-3.425858000	-0.006652000
H	4.403724000	-5.722042000	-0.987558000
H	7.186907000	-4.403790000	-0.151336000
H	9.816868000	-4.215970000	0.581427000
H	6.913050000	3.915600000	-1.045240000
H	10.049511000	-1.219038000	0.157053000
H	6.905481000	-8.083049000	0.475862000
H	3.664116000	0.091435000	-1.173559000
H	8.487067000	9.008560000	-0.195006000

H	5.311602000	5.557856000	-1.046130000
H	2.526630000	-6.805920000	-0.602527000
H	0.352190000	-4.001419000	-1.107659000
H	2.125222000	-4.158455000	-0.981390000
H	8.609694000	-2.089016000	0.699175000
H	8.217388000	6.535331000	-0.265902000
H	5.513447000	7.904614000	-0.668833000
H	5.174332000	-8.105596000	0.839022000
H	6.083176000	-0.619126000	0.472187000
H	8.682927000	3.254219000	0.973185000
H	8.216173000	0.399915000	1.034362000
H	4.101986000	-1.645069000	0.441817000
H	6.154040000	-5.912774000	1.495677000
H	4.670804000	-3.656580000	1.102570000
H	1.126569000	-4.171354000	0.484835000
H	7.177636000	2.455762000	1.437047000
H	-2.063312000	-7.347751000	-0.626310000
H	0.585363000	5.734188000	-0.681756000
H	1.785063000	-8.479389000	1.284152000
H	6.700205000	8.941753000	1.205373000
H	1.508282000	3.426664000	0.120679000
H	3.811741000	3.209171000	0.829145000
H	-3.350051000	-5.515769000	-0.673120000
H	-4.530225000	1.753592000	-2.678365000
H	7.106630000	7.356881000	1.892841000
H	-1.531388000	6.498730000	-0.773462000
H	-2.569565000	-2.973434000	-0.388697000
H	5.424222000	7.915117000	1.853761000
H	4.252593000	5.878228000	1.657797000
H	1.452014000	-6.958210000	2.129641000
H	-2.797491000	-8.411452000	0.595954000
H	-1.128384000	8.908097000	-0.178604000
H	-1.206971000	-4.240279000	1.291316000
H	-3.530308000	1.642771000	-1.223819000
H	-7.031982000	1.480643000	-2.505098000
H	-0.833179000	-7.861793000	2.021445000
H	2.859397000	2.121867000	1.847825000
H	-2.862872000	8.513303000	-0.149608000
H	1.993216000	5.848278000	1.910093000
H	-4.468478000	3.104216000	-1.531447000
H	-0.908403000	-2.497210000	1.406773000
H	-0.367921000	3.918593000	1.634188000
H	3.433420000	3.664254000	2.496980000
H	-5.534666000	0.291330000	-0.888620000
H	-6.583544000	3.849263000	-1.728364000
H	0.398612000	2.375905000	1.963859000
H	-7.188031000	-2.953960000	-1.149494000
H	-8.109327000	-0.976559000	-1.744114000
H	-8.336310000	-5.096954000	-1.196906000
H	-5.270983000	4.177720000	0.641576000
H	-2.712796000	-0.852965000	0.947010000
H	-4.303589000	-1.344514000	0.352259000
H	-1.951983000	8.644727000	1.374890000
H	-8.313467000	3.480961000	-1.733250000
H	-1.949482000	-3.300811000	2.598849000
H	-4.169711000	-4.268336000	1.859804000
H	-7.661841000	-5.502189000	0.392472000
H	-2.535920000	5.942461000	1.922026000
H	-5.622597000	1.668733000	0.200768000
H	-3.780294000	3.291640000	0.993602000
H	0.827510000	4.937980000	3.608317000
H	-4.328808000	4.560476000	2.110248000

H	-9.411686000	-5.582142000	0.129151000
H	-7.416548000	3.480775000	-0.208438000
H	-3.863293000	-1.623901000	2.046762000
H	1.588725000	3.367143000	3.948753000
H	-11.815998000	1.850747000	-2.209771000
H	-9.468223000	-3.102754000	-0.215729000
H	-6.035024000	-2.890645000	1.545309000
H	-0.161729000	3.554574000	4.076229000
H	-8.171542000	1.123531000	0.299552000
H	-10.090893000	2.354104000	0.066302000
H	-12.508449000	0.053865000	-0.623519000
H	-8.101721000	-3.939330000	2.399191000
H	-9.835353000	-4.021701000	2.067768000
H	-9.028115000	-2.444767000	2.164454000
H	-13.751613000	1.325901000	-0.727049000
H	-12.663837000	1.255750000	0.675147000
N	8.146494000	0.532949000	0.031940000
N	5.914309000	-1.146064000	-0.373927000
N	6.952358000	3.911744000	-0.032313000
N	4.631338000	-4.043451000	0.166917000
N	2.572161000	-6.731696000	0.406072000
N	4.217371000	5.929879000	0.645568000
N	-0.874890000	-7.709447000	1.021106000
N	0.687757000	5.904946000	0.311516000
N	-3.344721000	-5.382984000	0.331251000
N	-2.602895000	6.029008000	0.915041000
N	-7.842382000	-0.537138000	-0.869805000
N	-6.175097000	-3.246022000	0.606324000
N	-10.386286000	1.785156000	-0.721007000
O	6.812139000	-1.739549000	-2.382865000
O	4.567823000	-3.627298000	-2.060632000
O	8.002719000	2.048503000	-1.649976000
O	2.929427000	5.553900000	-1.194201000
O	0.228447000	-6.907880000	-0.797464000
O	6.419989000	4.865480000	1.943782000
O	3.611243000	-5.803717000	2.201957000
O	-3.578091000	5.308906000	-0.997058000
O	-5.200995000	-4.205274000	-1.210990000
O	-9.701415000	0.593040000	-2.538041000
O	-0.198909000	6.777647000	2.210916000
O	-2.880746000	-6.273683000	2.372126000
O	-7.233123000	-0.828557000	1.301933000
O	-13.188921000	3.912695000	-1.358857000
O	-11.303099000	4.159853000	-0.143653000
S	1.405554000	-1.934799000	-0.329218000

2nao loop 2

189
symmetry c1

C	-9.775806000	1.217429000	3.558931000
C	-10.303322000	1.260773000	2.124226000
C	-9.354644000	2.014040000	1.185558000
C	-7.962869000	1.388293000	1.010141000
N	-7.191745000	2.227356000	0.119996000
C	-5.846940000	2.175094000	0.042678000
O	-5.155824000	1.431333000	0.732140000
C	-11.681142000	1.923367000	2.088635000
C	-8.110000000	-0.020230000	0.424393000
O	-8.335359000	-0.204482000	-0.764635000
C	-5.238900000	3.146828000	-0.957834000
N	-4.126936000	3.846452000	-0.350363000

C	-3.837378000	5.107349000	-0.741348000
O	-4.462842000	5.666902000	-1.637332000
C	-2.648486000	5.784102000	-0.052449000
N	-1.436556000	5.424444000	-0.774995000
C	-0.263926000	5.184080000	-0.145632000
O	-0.124322000	5.255917000	1.071073000
C	0.904015000	4.818035000	-1.058566000
N	2.064508000	5.534620000	-0.566298000
C	2.917168000	6.179747000	-1.390130000
O	2.788824000	6.221478000	-2.609640000
C	-2.808394000	7.305137000	0.134108000
C	-2.736665000	8.103773000	-1.168650000
C	-4.081330000	7.601408000	0.936282000
C	-4.188114000	9.056529000	1.388274000
C	4.090322000	6.886107000	-0.696743000
N	5.305126000	6.133587000	-0.960440000
C	5.587267000	5.006897000	-0.264005000
O	4.835339000	4.591237000	0.615797000
C	6.877333000	4.306351000	-0.624073000
C	4.226899000	8.306420000	-1.224916000
C	1.133121000	3.286706000	-1.141863000
C	2.388159000	3.011508000	-1.972597000
N	-7.959236000	-1.039272000	1.302297000
C	-8.076791000	-2.426422000	0.882134000
C	-6.985357000	-2.817458000	-0.125005000
O	-7.204793000	-3.621927000	-1.025260000
C	1.227291000	2.603226000	0.236797000
C	-0.097359000	2.020482000	0.727251000
C	-9.478252000	-2.781557000	0.363106000
C	-9.778962000	-4.270190000	0.511064000
S	-11.406351000	-4.757003000	-0.142413000
C	-12.496214000	-3.877075000	1.013227000
N	-5.747228000	-2.343317000	0.141440000
C	-4.630159000	-2.651281000	-0.745748000
C	-3.775243000	-1.419803000	-1.050166000
C	-2.517346000	-1.813820000	-1.827821000
C	-4.595717000	-0.409806000	-1.852078000
C	-3.852344000	-3.773960000	-0.052716000
O	-2.923334000	-3.575986000	0.723946000
N	-4.302867000	-5.013154000	-0.361966000
C	-3.671525000	-6.184910000	0.212388000
C	-2.544709000	-6.646477000	-0.709501000
O	-2.740213000	-7.359081000	-1.683918000
N	-1.334061000	-6.165021000	-0.345958000
C	-0.110909000	-6.457485000	-1.061102000
C	0.610150000	-5.147072000	-1.368518000
O	0.140113000	-4.330650000	-2.152154000
N	1.797100000	-4.986140000	-0.748028000
C	2.615104000	-3.797814000	-0.926588000
C	3.880513000	-4.049643000	-0.110941000
O	3.806233000	-4.385098000	1.069065000
N	5.041850000	-3.966486000	-0.787906000
C	6.334304000	-4.177201000	-0.158284000
C	7.011052000	-5.468427000	-0.647491000
C	6.142510000	-6.679614000	-0.314175000
C	7.169635000	-2.949744000	-0.515495000
O	7.264298000	-2.587994000	-1.686112000
N	7.721836000	-2.303377000	0.525362000
C	8.550309000	-1.118744000	0.398771000
C	9.828848000	-1.393332000	1.190755000
O	9.740222000	-1.869588000	2.323672000
N	10.986898000	-1.154139000	0.563414000

C	12.274931000	-1.367931000	1.199589000
C	13.335527000	-1.637783000	0.138098000
C	12.700508000	-0.184228000	2.129481000
O	13.824352000	-0.333225000	2.663000000
O	11.903055000	0.770501000	2.258473000
C	7.813981000	0.118999000	0.949418000
C	6.521124000	0.366869000	0.161742000
C	5.525135000	1.268332000	0.887519000
C	8.733939000	1.341141000	0.938253000
C	1.932329000	-2.469895000	-0.504621000
C	2.960112000	-1.335687000	-0.508817000
C	1.218858000	-2.560963000	0.841956000
C	8.405504000	-5.601508000	-0.033840000
H	-10.488584000	0.710289000	4.216177000
H	-12.387690000	1.385935000	2.728443000
H	-3.299152000	9.355201000	1.954691000
H	-10.414227000	0.230148000	1.758231000
H	-9.628655000	2.234976000	3.939983000
H	-12.086695000	1.943887000	1.072199000
H	-4.105081000	6.948063000	1.818965000
H	-8.819866000	0.691211000	3.645078000
H	-4.287273000	9.735662000	0.536395000
H	-0.868774000	2.791411000	0.814329000
H	3.937881000	6.888114000	0.386281000
H	1.621830000	3.308497000	0.977829000
H	-5.061043000	9.201773000	2.031128000
H	-11.617492000	2.956660000	2.449601000
H	-1.944832000	7.590558000	0.752636000
H	-2.529691000	5.346769000	0.945606000
H	2.273286000	5.481441000	0.423093000
H	5.091967000	8.796262000	-0.771641000
H	7.503141000	4.247999000	0.270024000
H	-7.430149000	1.340802000	1.965615000
H	0.017593000	1.554205000	1.710430000
H	-7.752937000	-0.839911000	2.271753000
H	1.963216000	1.793170000	0.171120000
H	-4.953171000	7.339028000	0.324582000
H	5.943903000	2.247215000	1.138566000
H	7.431921000	4.809643000	-1.417962000
H	-3.606252000	3.374751000	0.378750000
H	-9.219491000	3.038984000	1.554702000
H	-7.871682000	-3.024405000	1.778389000
H	3.330949000	8.885052000	-0.987284000
H	-9.812230000	2.081685000	0.189157000
H	7.553527000	-0.120399000	1.991443000
H	-0.460914000	1.255672000	0.031413000
H	1.919131000	-2.816387000	1.642431000
H	5.898920000	6.422504000	-1.725971000
H	-5.640019000	-1.587204000	0.809665000
H	-1.867097000	7.809987000	-1.765459000
H	5.188891000	0.795273000	1.817229000
H	3.278618000	3.339100000	-1.422579000
H	0.756560000	-1.596920000	1.078795000
H	8.238361000	2.198130000	1.404141000
H	6.647227000	3.284080000	-0.937426000
H	4.345786000	8.288972000	-2.311555000
H	-2.631678000	9.170678000	-0.952109000
H	-10.197515000	-2.197948000	0.947561000
H	4.641753000	1.451548000	0.265749000
H	12.163218000	-2.248881000	1.840149000
H	0.424931000	-3.314496000	0.823862000
H	7.661474000	-2.695892000	1.458217000

H	-7.698617000	2.832041000	-0.512717000
H	-3.477700000	-0.970038000	-0.093367000
H	-3.305604000	-5.933517000	1.209368000
H	-1.457709000	5.431624000	-1.786934000
H	0.726278000	5.193018000	-2.070504000
H	3.672427000	-1.445645000	0.318969000
H	-9.721482000	-4.575380000	1.562396000
H	0.262902000	2.877914000	-1.675076000
H	-9.050360000	-4.855624000	-0.053986000
H	-5.960593000	3.893585000	-1.292053000
H	-3.636506000	7.952408000	-1.768420000
H	6.156962000	-4.237532000	0.919669000
H	-1.296757000	-5.541003000	0.451234000
H	8.344584000	-5.618622000	1.061077000
H	2.484030000	1.937620000	-2.162331000
H	9.675160000	1.155870000	1.468351000
H	-5.554544000	-0.184788000	-1.374933000
H	2.365154000	3.539267000	-2.930554000
H	6.786343000	0.799039000	-0.814170000
H	6.025879000	-6.779800000	0.771331000
H	-4.919383000	2.576841000	-1.839618000
H	-4.404345000	-6.989419000	0.286761000
H	8.977021000	1.618624000	-0.096241000
H	-1.875465000	-2.489109000	-1.257628000
H	14.296161000	-1.795257000	0.629068000
H	-4.034860000	0.523257000	-1.960834000
H	-9.569230000	-2.480354000	-0.682460000
H	6.030433000	-0.590235000	-0.050247000
H	2.054526000	-5.605390000	0.011336000
H	10.964855000	-0.675442000	-0.327586000
H	2.456415000	-0.372111000	-0.385897000
H	1.184454000	-2.265680000	-1.276519000
H	13.435235000	-0.777442000	-0.534593000
H	8.759995000	-0.984244000	-0.667578000
H	0.521526000	-7.144885000	-0.489716000
H	3.529617000	-1.299540000	-1.445175000
H	8.875494000	-6.534256000	-0.358418000
H	-5.108610000	-5.113171000	-0.967222000
H	-5.059341000	-3.033944000	-1.677210000
H	-12.249890000	-4.139757000	2.044897000
H	9.062250000	-4.775040000	-0.324740000
H	6.604484000	-7.596610000	-0.691981000
H	13.086262000	-2.517293000	-0.462835000
H	-2.791103000	-2.310632000	-2.766907000
H	-4.797678000	-0.802616000	-2.855797000
H	-1.938902000	-0.920092000	-2.082454000
H	5.146243000	-6.592294000	-0.758129000
H	-12.434753000	-2.795143000	0.882099000
H	5.055455000	-3.649026000	-1.750274000
H	2.867517000	-3.716422000	-1.990774000
H	7.110101000	-5.382464000	-1.738093000
H	-0.387086000	-6.931181000	-2.005206000
H	-13.517210000	-4.198311000	0.799607000

5kk3 loop 2

189
symmetry c1

C	0.525753000	2.859911000	4.136006000
C	0.215708000	4.090999000	0.499674000
C	0.288915000	2.024346000	2.877894000
C	-0.575792000	-6.933589000	0.640687000

C	-1.259432000	-5.599139000	0.979412000
C	9.958274000	3.638573000	-1.969566000
C	10.209716000	-2.440211000	0.247389000
C	11.269656000	-2.001678000	-0.755774000
C	-0.874208000	3.897246000	1.551594000
C	0.862651000	7.515109000	0.420816000
C	-12.267484000	-0.214981000	-0.640023000
C	-12.901861000	0.921033000	-1.504373000
C	-12.896938000	-0.255157000	0.749745000
C	-0.941118000	2.433178000	2.056820000
C	-1.177210000	1.452311000	0.910174000
C	13.911131000	-1.867835000	-1.550262000
C	-1.285352000	-2.906684000	-1.877534000
C	-1.900137000	-2.615597000	-0.508724000
C	1.830990000	6.905037000	-0.594112000
C	1.763064000	-6.121662000	0.848753000
C	-2.690801000	-3.820531000	0.062674000
C	-2.792917000	-1.374705000	-0.572020000
C	2.611192000	4.604950000	0.158338000
C	2.987391000	6.089385000	0.019112000
C	3.121483000	-6.074454000	0.141251000
C	-3.195101000	4.662171000	1.664077000
C	3.684549000	-2.537357000	2.808344000
C	3.719536000	3.816549000	0.854650000
C	-4.030496000	-3.979279000	-0.649797000
C	3.958798000	-1.229688000	0.671746000
C	4.258444000	6.209159000	-0.825926000
C	-4.427595000	5.083135000	0.869533000
C	-4.545850000	6.608817000	0.850469000
C	4.671355000	-2.052613000	1.745117000
C	4.562273000	-4.103164000	0.257107000
C	5.446882000	2.103312000	0.615232000
C	5.459792000	-3.246009000	1.148491000
C	-5.697297000	1.701245000	-2.575259000
C	-6.471893000	-3.757587000	-0.416247000
C	6.296502000	1.631255000	-0.551232000
C	-6.392406000	0.676910000	-1.681299000
C	-6.682798000	4.115677000	0.823872000
C	-7.348013000	-4.915076000	1.693402000
C	-7.127321000	-2.408025000	-0.108460000
C	-7.258854000	-4.948279000	0.168285000
C	7.757513000	-2.428394000	0.841738000
C	-7.879335000	0.473178000	-2.003302000
C	-7.781473000	3.468094000	1.638626000
C	-8.475194000	-0.554511000	-1.016684000
C	-8.649512000	-5.018724000	-0.464269000
C	8.496202000	1.520068000	-1.584576000
C	8.656509000	-0.006229000	-1.591169000
C	8.807644000	-2.039009000	-0.207015000
C	-8.654242000	1.791808000	-1.978161000
C	9.062267000	4.600963000	-1.186647000
C	9.684164000	3.748525000	-3.470255000
C	9.874997000	2.182981000	-1.478210000
C	-9.964079000	-0.820891000	-1.268901000
H	-0.573090000	-7.524191000	1.561365000
H	0.811980000	3.894463000	3.916293000
H	0.145938000	0.978314000	3.174167000
H	-0.311465000	1.409316000	0.239377000
H	0.111595000	8.129655000	-0.084832000
H	-0.726777000	-2.032406000	-2.225973000
H	0.332953000	6.754719000	1.001249000
H	1.327353000	2.428286000	4.741257000

H	1.182992000	2.036375000	2.239865000
H	-1.085687000	-2.431700000	0.204705000
H	-1.129734000	-7.476461000	-0.125016000
H	-0.689998000	4.556517000	2.406863000
H	10.235124000	-3.529084000	0.373101000
H	10.219021000	2.114776000	-0.437078000
H	9.877503000	4.767671000	-3.819182000
H	-10.455637000	0.665508000	0.016442000
H	-0.379956000	2.899667000	4.750763000
H	10.319821000	3.065825000	-4.043637000
H	11.069079000	-2.430085000	-1.743313000
H	10.399409000	-1.993969000	1.229247000
H	10.566851000	1.579753000	-2.078020000
H	10.999458000	3.941612000	-1.798802000
H	11.275116000	-0.910718000	-0.851797000
H	1.280605000	6.273447000	-1.303239000
H	-12.525834000	-1.103668000	1.331901000
H	-12.457260000	-1.160548000	-1.155760000
H	1.570303000	4.498046000	1.984377000
H	-12.670918000	0.665241000	1.301359000
H	13.803287000	-0.782017000	-1.602721000
H	13.617338000	-2.313540000	-2.503262000
H	0.975427000	-7.013448000	-0.799826000
H	-13.980319000	-0.330818000	0.647127000
H	14.954797000	-2.113457000	-1.347155000
H	-0.590860000	-3.750981000	-1.832902000
H	-1.345663000	0.447026000	1.308520000
H	-1.993590000	-5.533021000	-0.949567000
H	1.400045000	8.156972000	1.127090000
H	-2.206572000	-0.500005000	-0.867030000
H	-2.053697000	1.731505000	0.316797000
H	2.265483000	7.721789000	-1.182827000
H	-1.812748000	2.413348000	2.724505000
H	-2.149812000	4.290903000	-0.074818000
H	-2.062677000	-3.135292000	-2.612910000
H	2.387468000	4.190929000	-0.829768000
H	2.903739000	-3.170428000	2.370083000
H	-2.853576000	-3.652089000	1.130977000
H	-3.584922000	-1.508756000	-1.318925000
H	3.030240000	-5.717678000	-0.886726000
H	3.192683000	-1.683974000	3.284421000
H	-3.267099000	-1.156669000	0.391920000
H	3.199305000	6.466311000	1.029676000
H	3.458591000	-0.370909000	1.133039000
H	3.190714000	-1.823427000	0.165011000
H	4.190124000	-3.113328000	3.591552000
H	-4.609136000	6.988365000	1.874126000
H	3.542337000	-7.086012000	0.119917000
H	4.088458000	5.812784000	-1.834397000
H	4.552168000	7.258036000	-0.921193000
H	4.049822000	2.712834000	-0.844990000
H	4.053507000	-5.280516000	1.853839000
H	-3.678095000	7.058452000	0.358593000
H	-4.376306000	4.701321000	-0.153863000
H	-5.005139000	-3.241341000	1.000985000
H	-4.615011000	1.682011000	-2.411509000
H	5.064872000	1.220165000	1.140579000
H	4.653105000	-0.853999000	-0.087715000
H	5.098787000	5.662928000	-0.385042000
H	5.430338000	-1.426353000	2.231674000
H	-5.449182000	6.894758000	0.306316000
H	-6.356484000	-4.867688000	2.154736000

H	5.855041000	-3.844389000	1.977458000
H	6.015769000	2.700935000	1.331369000
H	-5.511695000	4.337922000	2.513577000
H	-5.879710000	-0.288527000	-1.760306000
H	-5.880213000	1.487706000	-3.634828000
H	-6.388968000	-3.893371000	-1.498641000
H	-6.304119000	0.994246000	-0.631508000
H	-6.050241000	2.713199000	-2.359166000
H	-6.691730000	-5.840494000	-0.127837000
H	6.430503000	-2.859660000	-0.674899000
H	-7.841812000	-5.822158000	2.054877000
H	-7.925697000	-4.050762000	2.034480000
H	-8.008676000	-2.373302000	-1.956019000
H	-7.758891000	2.387505000	1.463702000
H	7.969056000	2.515493000	0.237260000
H	8.001625000	4.409556000	-1.385636000
H	-7.964989000	0.034182000	-3.009480000
H	8.021967000	1.757219000	-2.542082000
H	-8.323346000	-0.202073000	0.008789000
H	-8.287049000	2.456756000	-2.765291000
H	8.510731000	-0.034621000	0.450309000
H	-8.744299000	3.846246000	1.290993000
H	-8.592593000	-5.057999000	-1.557760000
H	-7.679831000	3.649554000	2.710289000
H	8.579456000	-2.489745000	-1.176766000
H	-8.492791000	2.313644000	-1.025734000
H	-9.179180000	-5.912085000	-0.121364000
H	8.638907000	3.517443000	-3.704407000
H	-9.253300000	-4.145862000	-0.188619000
H	9.230171000	4.522262000	-0.106126000
H	9.271045000	5.634528000	-1.479893000
H	-9.730403000	1.652510000	-2.124809000
N	-10.823248000	-0.100398000	-0.534175000
N	0.791715000	-6.767657000	0.163786000
N	1.435480000	4.384603000	0.985915000
N	-1.971880000	-5.072325000	-0.048014000
N	-2.117455000	4.318620000	0.938169000
N	3.992496000	-5.170665000	0.849535000
N	4.372885000	2.920253000	0.092293000
N	-5.115821000	-3.670385000	0.090000000
N	-5.567068000	4.455248000	1.509342000
N	6.580156000	-2.834917000	0.327461000
N	7.610263000	1.931596000	-0.507439000
N	-7.793059000	-1.831240000	-1.126778000
N	8.666783000	-0.598884000	-0.376430000
O	-0.035732000	3.979311000	-0.697858000
O	-1.214959000	-5.088541000	2.087939000
O	-10.300004000	-1.677317000	-2.089252000
O	-12.126456000	1.752471000	-2.027626000
O	-14.151277000	0.872020000	-1.580842000
O	1.627965000	-5.686267000	1.981823000
O	-3.213025000	4.661046000	2.893401000
O	3.975146000	4.015950000	2.038193000
O	-4.088453000	-4.413969000	-1.797389000
O	4.439805000	-3.842379000	-0.937017000
O	5.792166000	1.014542000	-1.484385000
O	-6.788633000	4.297767000	-0.387031000
O	-6.962216000	-1.878760000	0.989330000
O	7.979872000	-2.335889000	2.044080000
O	8.843229000	-0.610768000	-2.639364000
S	12.914673000	-2.544801000	-0.192937000

5oqv loop 2

189
symmetry c1

C	0.844642000	-5.813120000	-0.675465000
C	-2.000174000	7.800191000	-1.648517000
C	-2.847279000	8.869381000	-2.335296000
C	-1.875257000	5.843005000	-0.100621000
C	1.674940000	-6.633861000	0.312371000
C	-2.748613000	7.028770000	-0.554168000
C	-0.506699000	6.250498000	0.450202000
C	-9.767303000	0.423483000	-1.176140000
C	-9.737709000	-4.195468000	0.140153000
C	10.217550000	2.384035000	-1.680013000
C	10.249776000	0.999314000	-1.027672000
C	-10.314571000	-5.448187000	0.795703000
C	-11.321900000	0.387217000	-1.297936000
C	11.495394000	3.154998000	-1.349781000
C	1.824025000	-2.631313000	-0.820312000
C	-3.203683000	7.936269000	0.588589000
C	1.004285000	2.931500000	3.177772000
C	0.905221000	4.178340000	2.297767000
C	-1.445639000	-4.956987000	-0.986515000
C	-3.344271000	4.032366000	0.667152000
C	-2.231142000	-0.404642000	-0.257778000
C	2.093975000	4.355166000	1.336243000
C	-1.753942000	-7.334908000	-1.798295000
C	-2.133355000	-3.769630000	-0.309480000
C	4.047615000	-6.120762000	0.332664000
C	1.880437000	5.606338000	0.419124000
C	-2.442534000	-6.129182000	-1.161504000
C	3.731136000	-1.562360000	0.888288000
C	-3.318531000	2.225648000	2.411151000
C	-4.086669000	3.427884000	1.858772000
C	3.409784000	4.425497000	2.118387000
C	-3.613227000	-0.746219000	-0.812377000
C	-3.110036000	-6.509463000	0.160211000
C	2.816859000	5.574074000	-0.803958000
C	4.311867000	-0.513697000	-0.060539000
C	5.407894000	-6.406557000	-0.318189000
C	-4.002045000	-2.196704000	-0.442854000
C	-4.663571000	0.261185000	-0.340237000
C	5.837194000	-0.380600000	0.084311000
C	6.830577000	-4.803557000	0.869887000
C	-6.544574000	3.377350000	2.137370000
C	-5.400773000	-2.487186000	-0.978545000
C	6.488396000	-1.724098000	-0.250355000
C	5.151081000	5.395024000	-1.532661000
C	7.780526000	-3.620522000	0.643129000
C	6.060866000	4.314250000	-0.956205000
C	-7.813055000	2.779905000	1.561731000
C	7.248177000	1.573881000	-0.420753000
C	8.960858000	-3.602765000	1.611936000
C	7.660887000	2.519833000	-1.572767000
C	-7.774330000	-2.723603000	-0.312993000
C	-8.107072000	-3.719201000	2.033374000
C	9.815771000	-4.855071000	1.414134000
C	-8.279068000	-3.911096000	0.525925000
C	9.799848000	-2.338993000	1.414917000
C	-8.561411000	-1.426399000	-0.072794000
C	8.991893000	3.215976000	-1.276048000
C	-9.152629000	1.242101000	-2.308235000

H	1.168937000	-7.597174000	0.439540000
H	0.783635000	-2.936382000	-0.954136000
H	-2.305020000	9.316561000	-3.173108000
H	-1.746712000	5.175399000	-0.957390000
H	-2.359631000	8.484253000	1.014872000
H	-1.638039000	7.087717000	-2.401590000
H	-3.114351000	9.675653000	-1.646143000
H	1.230050000	2.043434000	2.575476000
H	0.054951000	2.753698000	3.691396000
H	1.738125000	-6.146742000	1.287310000
H	-1.108491000	8.267627000	-1.206967000
H	-9.344973000	0.767196000	-3.277412000
H	-9.334274000	-1.492761000	-1.950671000
H	-9.522455000	0.887512000	-0.216776000
H	-9.609517000	2.233588000	-2.316694000
H	-9.674097000	-6.316709000	0.606168000
H	10.173074000	2.243401000	-2.770110000
H	-9.798286000	-4.299449000	-0.951326000
H	-10.409530000	-5.329510000	1.878802000
H	-10.357024000	-3.325446000	0.401165000
H	10.251590000	1.087312000	0.063941000
H	11.151342000	0.457868000	-1.332967000
H	-11.308999000	-5.669945000	0.398453000
H	-0.456266000	-5.309471000	0.829562000
H	11.499391000	4.141781000	-1.824494000
H	-3.775749000	8.438730000	-2.725877000
H	11.582492000	3.300789000	-0.266478000
H	-0.016884000	4.105485000	1.712788000
H	12.382361000	2.609685000	-1.687890000
H	2.449129000	-3.528010000	-0.791015000
H	-2.451154000	5.411234000	1.887642000
H	-3.942607000	8.656549000	0.226480000
H	2.120817000	-1.996070000	-1.657155000
H	0.414769000	5.107400000	-0.987494000
H	-3.640901000	6.570550000	-1.005180000
H	3.139663000	-7.384070000	-1.018173000
H	-1.067636000	-4.660874000	-1.971099000
H	-3.678849000	7.360134000	1.388985000
H	-1.462874000	-1.066961000	-0.666933000
H	1.775264000	3.020919000	3.947351000
H	-1.022274000	-7.771077000	-1.108839000
H	-1.231519000	-7.060113000	-2.719210000
H	2.119069000	3.474116000	0.676508000
H	-1.965114000	0.627298000	-0.511192000
H	-2.347957000	2.546008000	2.802380000
H	0.811006000	5.076464000	2.922030000
H	-2.215235000	-0.507376000	0.833389000
H	2.030411000	6.517571000	1.009425000
H	-2.363282000	-6.834685000	0.893772000
H	-3.148019000	1.484397000	1.627274000
H	4.176032000	-2.551142000	0.725040000
H	-4.199333000	4.178136000	2.646717000
H	-2.491293000	-8.108949000	-2.030636000
H	3.929172000	-1.282431000	1.928298000
H	3.455252000	3.616925000	2.851177000
H	4.090638000	-0.782190000	-1.100865000
H	3.857683000	0.462349000	0.137296000
H	5.290453000	-6.732223000	-1.352871000
H	-3.571973000	-0.710656000	-1.909767000
H	-3.313598000	-3.460890000	-1.975335000
H	-3.218022000	-5.773319000	-1.852288000
H	-3.889547000	1.763266000	3.220461000

H	-3.956856000	-2.325128000	0.643111000
H	-3.673199000	-5.674443000	0.590783000
H	-4.304258000	1.275262000	-0.545042000
H	3.479482000	5.371858000	2.670639000
H	5.885553000	-7.215099000	0.246498000
H	4.293106000	4.315846000	1.487338000
H	-3.804962000	-7.339839000	0.005763000
H	-5.510339000	2.637827000	0.523721000
H	-4.839441000	0.173286000	0.740606000
H	6.314093000	-4.645437000	-1.096876000
H	4.453405000	5.955536000	0.368891000
H	6.097658000	-0.065382000	1.098181000
H	-5.624931000	0.128895000	-0.848096000
H	4.645201000	5.069025000	-2.442803000
H	6.888554000	-2.023003000	1.726969000
H	6.071263000	0.581704000	-1.781380000
H	-6.162546000	-2.045576000	0.863255000
H	-7.901432000	2.991364000	0.491536000
H	6.332019000	3.588684000	-2.835200000
H	5.776218000	6.260752000	-1.780315000
H	8.135930000	-3.616141000	-0.392101000
H	-7.801942000	1.691362000	1.685228000
H	-7.074578000	-3.461970000	2.291235000
H	8.549623000	-3.618866000	2.629760000
H	-8.674291000	3.194050000	2.085663000
H	9.237046000	-5.764367000	1.595017000
H	7.767293000	1.909212000	-2.476173000
H	-7.668822000	-4.772551000	0.218465000
H	-7.826375000	-3.001063000	-1.369940000
H	-8.069963000	1.343938000	-2.183986000
H	9.217723000	-1.424103000	1.563235000
H	-8.345947000	-4.646514000	2.561076000
H	-8.760044000	-2.925087000	2.404830000
H	10.213820000	-4.890744000	0.393157000
H	9.030786000	3.455323000	-0.207943000
H	10.664579000	-4.847340000	2.104102000
H	10.215558000	-2.311831000	0.400186000
H	9.386644000	0.384674000	-1.310521000
H	9.009962000	4.160538000	-1.831217000
H	10.635253000	-2.325864000	2.121028000
N	-0.301301000	-5.301085000	-0.171319000
N	-2.483166000	5.034982000	0.946946000
N	0.540713000	5.632379000	-0.130466000
N	3.012123000	-6.828441000	-0.184065000
N	-3.085119000	-3.148487000	-1.037735000
N	-5.426316000	3.104827000	1.417777000
N	6.262232000	-5.245827000	-0.281694000
N	4.134417000	5.750134000	-0.568721000
N	6.932653000	-2.437907000	0.803702000
N	6.360416000	0.624704000	-0.812188000
N	-6.386157000	-2.385687000	-0.063781000
N	6.568139000	3.449619000	-1.861633000
N	-9.192248000	-0.910246000	-1.135854000
O	1.156176000	-5.736469000	-1.856929000
O	-11.854614000	-0.733160000	-1.458981000
O	-11.870193000	1.512496000	-1.240528000
O	-0.409866000	6.979531000	1.433928000
O	-1.866493000	-3.459701000	0.847891000
O	-3.525269000	3.601395000	-0.468582000
O	3.902598000	-5.291506000	1.219465000
O	2.375499000	5.295405000	-1.914731000
O	6.703669000	-5.350234000	1.954702000

O	-6.517246000	3.997438000	3.194618000
O	6.552537000	-2.127274000	-1.408844000
O	-5.567951000	-2.810784000	-2.150436000
O	6.319890000	4.281658000	0.239985000
O	7.707533000	1.634125000	0.708045000
O	-8.462844000	-0.856320000	1.017943000
S	1.923797000	-1.750919000	0.764062000

A Focused Chiral Mutant Library of the Amyloid β 42 Central Electrostatic Cluster as a Tool to Stabilize Aggregation Intermediates

Alejandro R. Foley[†], Hsiau-Wei Lee[†], Jevgenij A. Raskatov*[,†]

[†] Department of Chemistry and Biochemistry, University of California Santa Cruz, Santa Cruz, California 95064

Email: jraskato@ucsc.edu

SUPPORTING INFORMATION

TABLE OF CONTENTS

ADDITIONAL EXPERIMENTAL PROCEDURES

Photo-Induced crosslinking (PICUP) and SDS-PAGE analysis. Lyophilized Aβ42 peptides were each dissolved in 20 mM NaOH (less than 3% v/v in final dilution volume) and diluted to a final concentration of 20 μM in 20 mM phosphate buffer pH 7.4. After the desired peptide incubation time, for the crosslinking reaction, 4 μL of 1 mM [Ru(bipy)3]2+and 4 μL of 20 mM ammonium persulfate were added to 32 μL of peptide-containing solution. Peptide concentration was 20 μM in the final solution. The sample was then irradiated for 1.2 seconds with light, using our previously reported setup.[1] Following irradiation, the solution was quenched with 40 μL of loading buffer with 5% 2-mercaptoethanol. Samples were then run on SDS-page 12% tris-tricine polyacrylamide gel. Gels were developed by common silver staining procedures.

NMR experiments. Sample preparation and NMR acquisition were performed at 4°C. 1.0 mg of either Aβ(19–32)-WT, Aβ(19–32)-S26s, Aβ(19–32)- D23d -S26s, and Aβ(19–32)-D23d-S26s-K28k peptides were saturated in 0.6 mL of 10% D_2O pH 7.4 20 mM phosphate buffer. Samples were centrifuged for 1 minute at 15,000g and the supernatant solution was transferred to an NMR tube. NMR experiments were performed on a Varian INOVA 600 MHz spectrometer equipped with a triple resonance cryoprobe. Data were collected at 4 °C. ^{1}H-^{1}H TOCSY spectra were acquired with 65ms mixing time.

Aβ42-WT

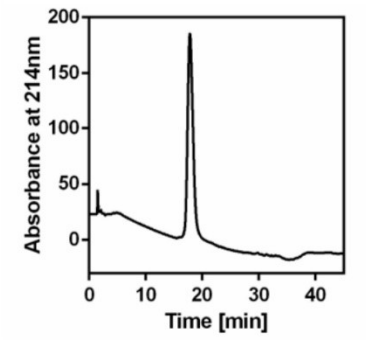

Peak	Time	Area	% Area
1	16.927	24.2	0.196
2	17.871	1237.1	99.804

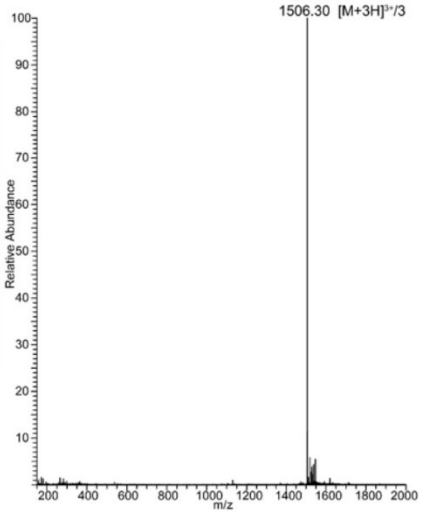

Aβ42-E22e

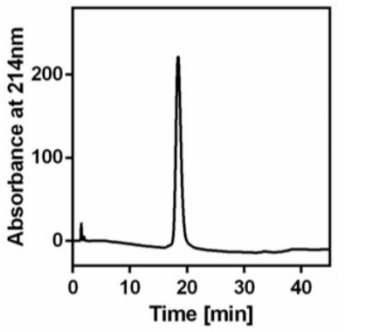

Peak	Time	Area	% Area
1	17.202	70.3	0.481
2	18.433	14543.8	99.519

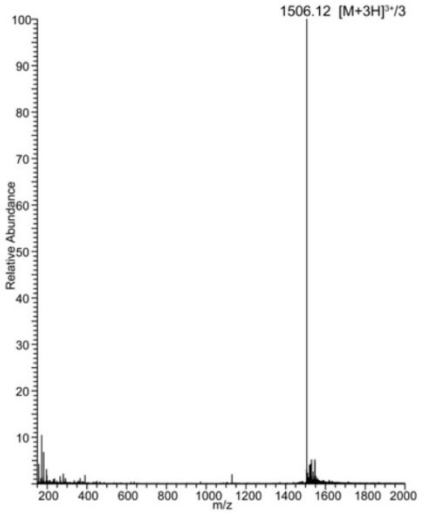

S3

Aβ42-D23d

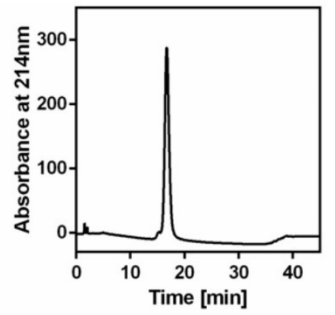

Peak	Time	Area	% Area
1	16.86	381.6	2.2278
2	17.763	16743.7	97.772

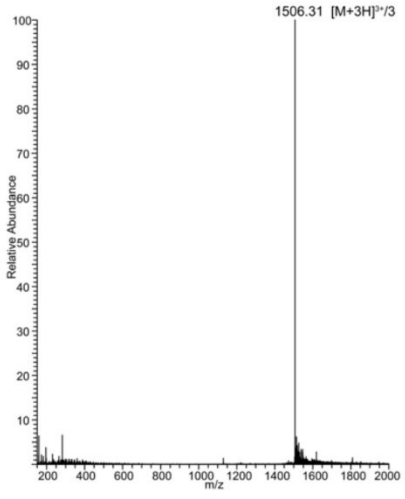

Aβ42-S26s

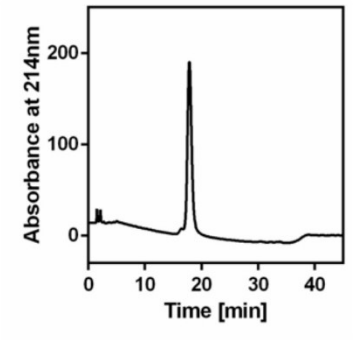

Peak	Time	Area	% Area
1	16.422	294.5	2.703
2	17.846	10597.8	97.297

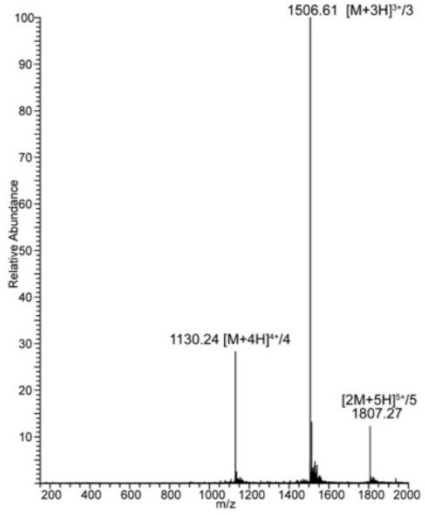

S4

Aβ42-K28k

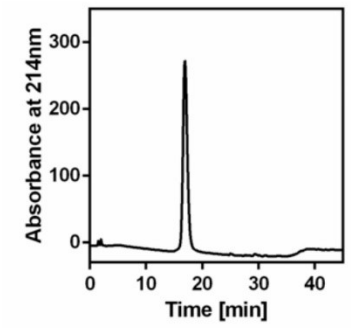

Peak	Time	Area	% Area
1	15.871	136.2	0.85
2	16.903	15893	99.15

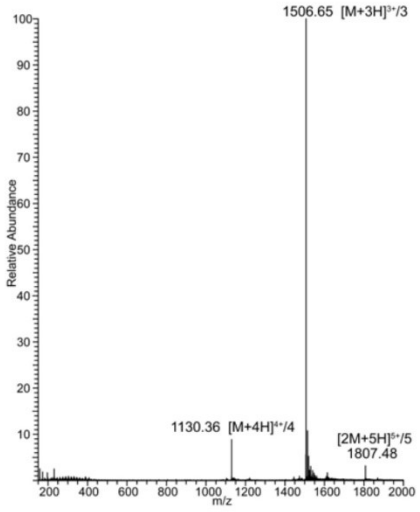

Aβ42-E22eD23d

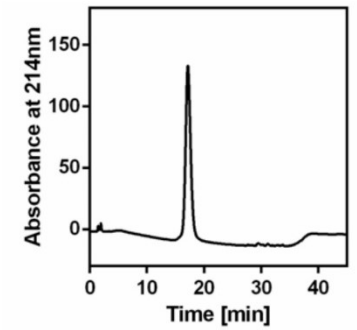

Peak	Time	Area	% Area
1	15.964	89.6	1.005
2	17.164	8824.7	98.995

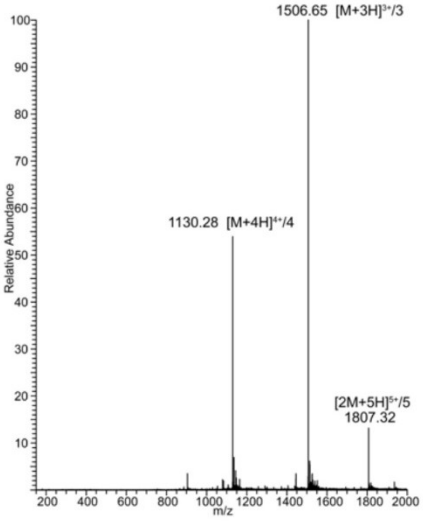

S5

Aβ42-E22eS26s

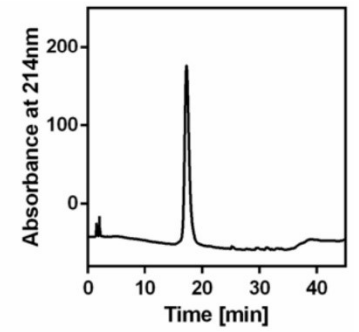

Peak	Time	Area	% Area
1	17.688	94.4	0.893
2	18.945	10468.5	99.107

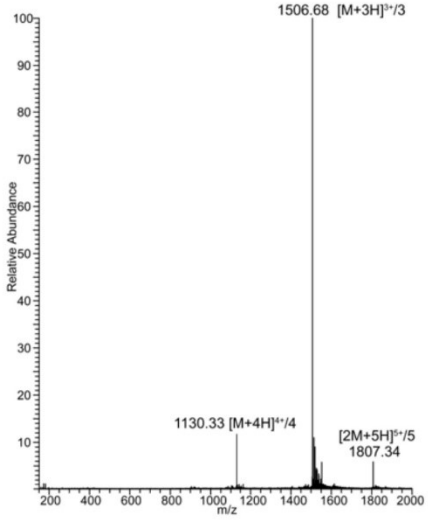

Aβ42-E22eK28k

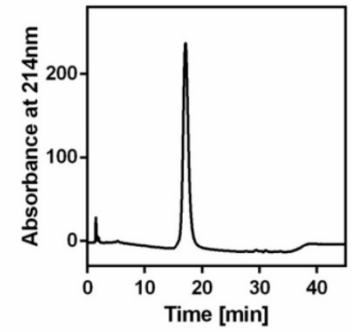

Peak	Time	Area	% Area
1	17.688	94.4	0.893
2	18.945	10468.5	99.107

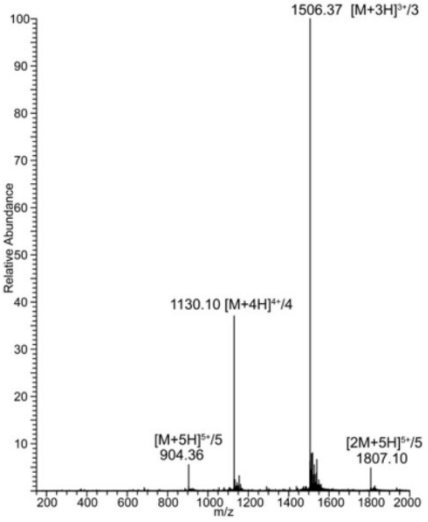

S6

Aβ42-D23dS26s

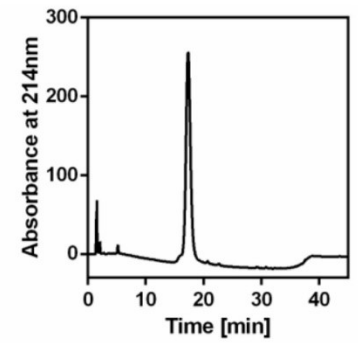

Peak	Time	Area	% Area
1	16.291	378.9	2.46
2	17.324	15022.8	97.54

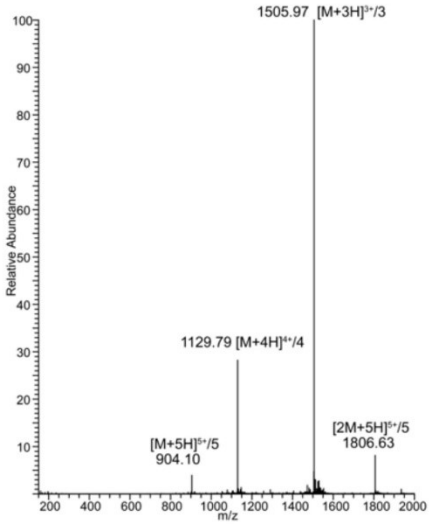

Aβ42-D23dK28k

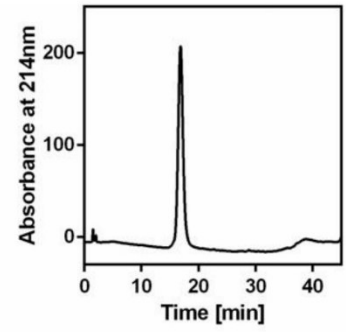

Peak	Time	Area	% Area
1	16.849	604.7	0.417
2	17.651	13887.8	99.583

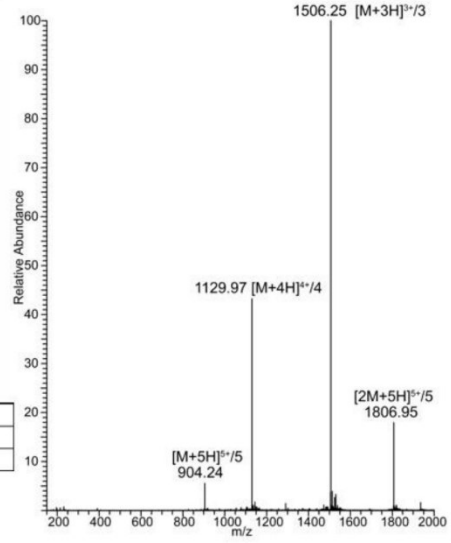

S7

Aβ42-S26sK28k

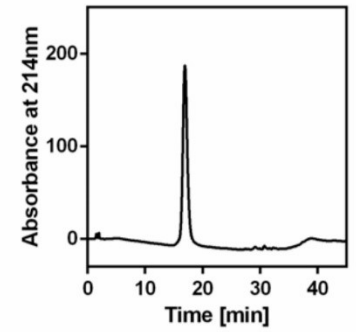

Peak	Time	Area	% Area
1	15.976	92	0.844
2	16.92	10797.3	99.156

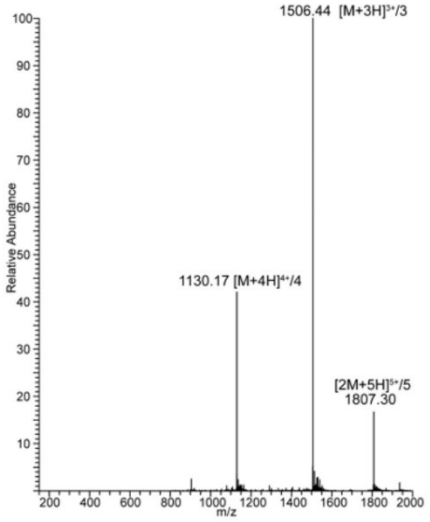

Aβ42-E22eD23dS26s

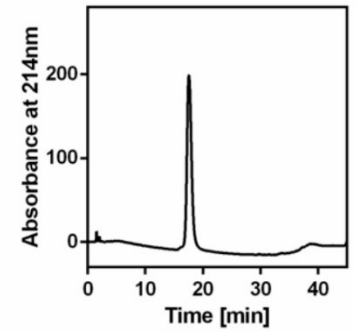

Peak	Time	Area	% Area
1	16.575	122.5	1.040
2	17.561	11653.9	98.960

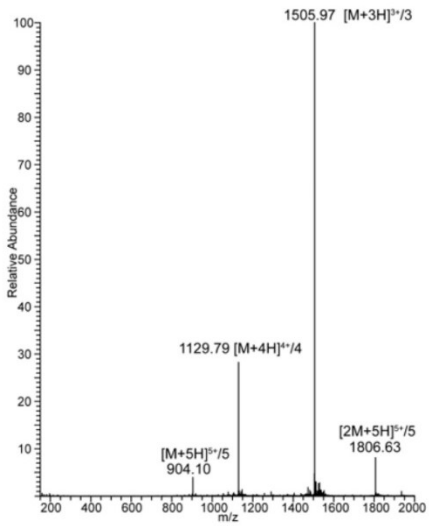

S8

Aβ42-E22eD23dK28k

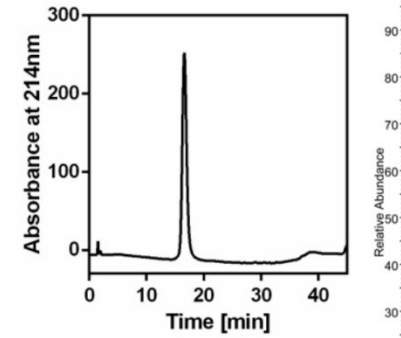

Peak	Time	Area	% Area
1	15.452	66.4	0.455
2	16.589	14529.8	99.545

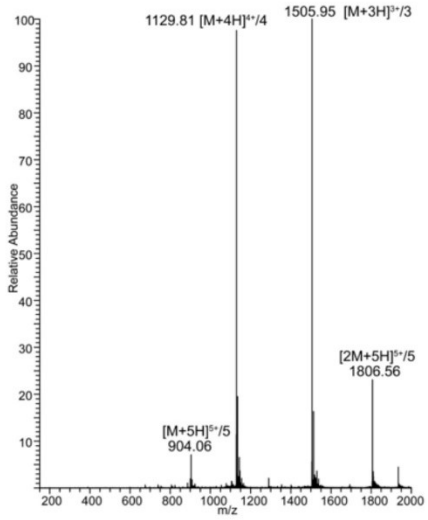

Aβ42-E22eS26sK28k

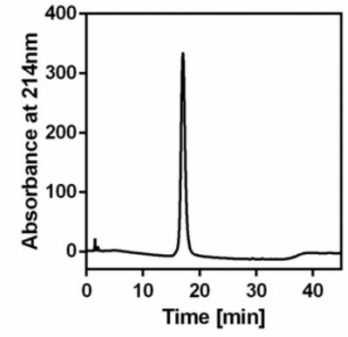

Peak	Time	Area	% Area
1	16.087	210.1	1.171
2	17.048	17737.7	98.829

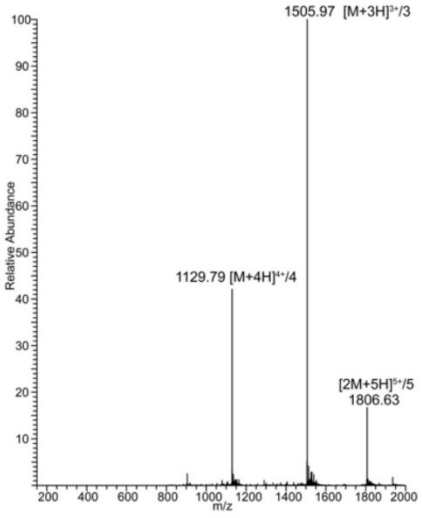

Aβ42-D23dS26sK28k

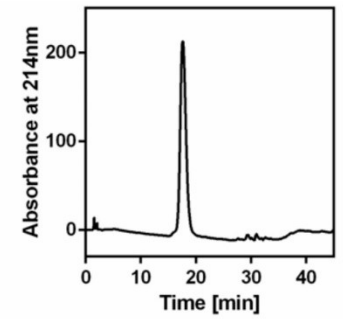

Peak	Time	Area	% Area
1	16.628	359	2.179
2	17.606	16114.2	97.821

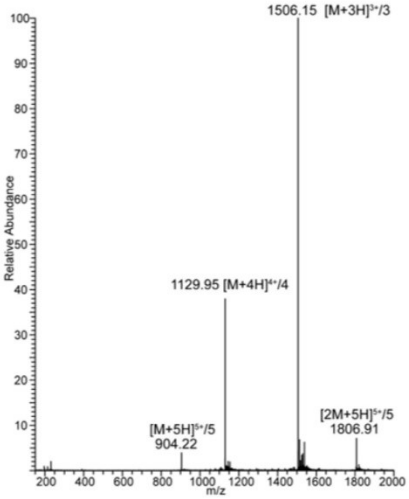

Aβ42-E22eD23dS26sK28k

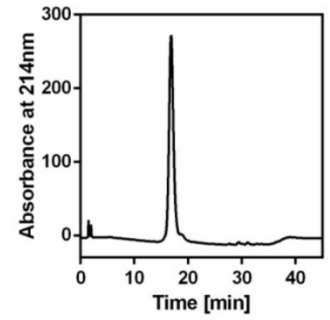

Peak	Time	Area	% Area
1	16.855	16915.4	96.54
2	16.683	604.7	3.452

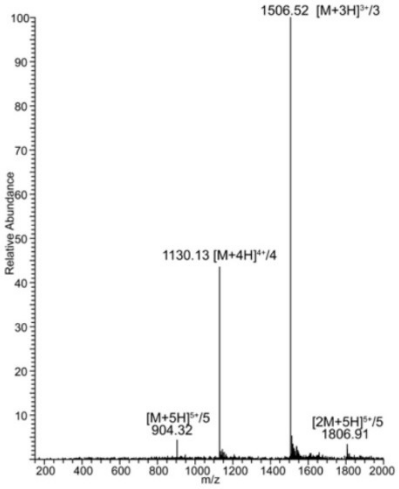

S10

Aβ(19-32)-WT

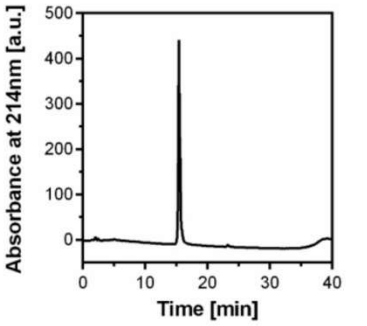

Peak	Time	Area	% Area
1	15.4	8655	96.6
2	16.14	302	3.4

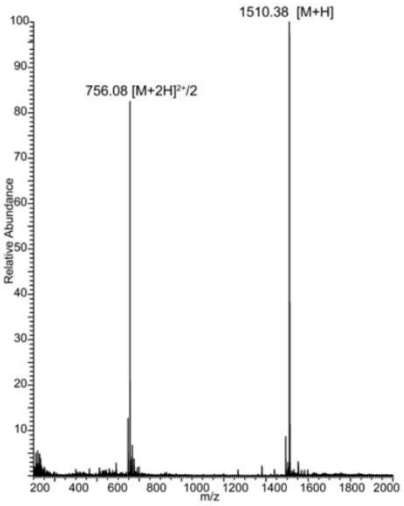

Aβ(19-32)-D23d-S26s (ds)

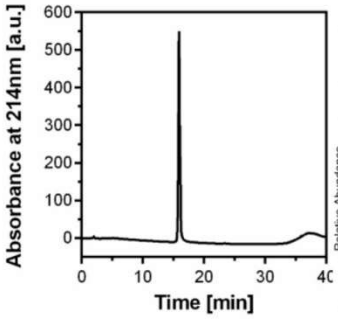

Peak	Time	Area	% Area
1	15.9	9723	98.1
2	16.5	184	1.9

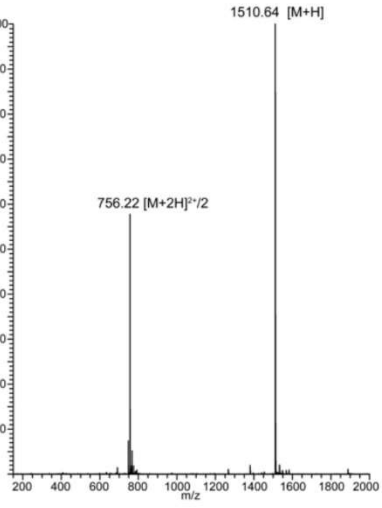

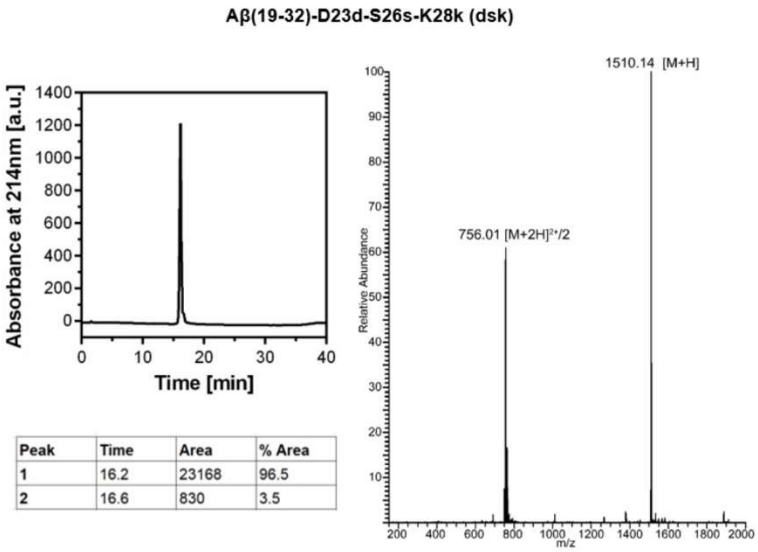

Peak	Time	Area	% Area
1	16.2	23168	96.5
2	16.6	830	3.5

Figure S1. HPLC and LTQ-MS characterization of the Aβ42 and Aβ(19-32) peptides. The purity of each peptide was >96 %, as determined by integration of signals at 214 nm.

Peptide	Mean $t_{1/2}$ ± SD [min]
Aβ42-WT	11.8 ± 0.3
Aβ42-E22e	46.8 ± 0.7
Aβ42-D23d	15.7 ± 0.7
Aβ42-S26s	99.2 ± 4.2
Aβ42-K28k	92.0 ± 3.4
Aβ42-E22e D23d	45.6 ± 1.7
Aβ42-E22e S26s	142.0 ± 15.7
Aβ42-E22e K28k	27.6 ± 1.7
Aβ42-D23d S26s	326.0 ± 73.8
Aβ42-D23d K28k	183.5 ± 4.6
Aβ42-S26s K28k	159.6 ± 10.1
Aβ42-E22e D23d S26s	172.4 ± 3.4
Aβ42-E22e D23d K28k	47.9 ± 17.5
Aβ42-E22e S26s K28k	63.4 ± 10.1
Aβ42-D23d S26s K28k	596.5 ± 45.6
Aβ42-E22e D23d S26s K28k	109.6 ± 4.9

Figure S2. Mean $t_{1/2}$ and standard deviation (SD) for the aggregation curves from the ThT kinetics experiment (main text Figure 2). $t_{1/2}$ is defined as the time required for each curve to reach ½ of maximum intensity values. Mean and SD were calculated from 3 technical replicates for each peptide.

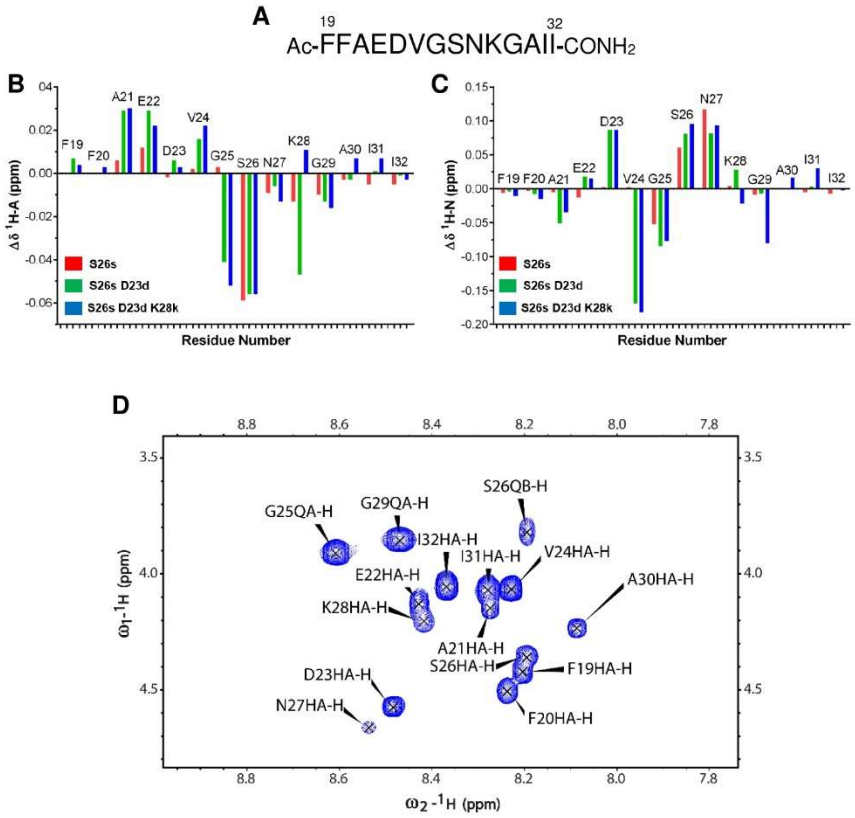

Figure S3. NMR analysis of the model Aβ(19–32) segment for the WT and chiral variants. Aβ(19–32) peptides were acetylated at the N-terminus and amidated at C-terminus. (A) Aβ(19–32) region of the Aβ sequence. Numbers (19–32) indicate their position in the Aβ42 sequence. (B) Residue chemical shift increment of Aβ(19–32)-S26s, Aβ(19–32)- D23d -S26s, Aβ(19–32)-D23d-S26s-K28k peptides after Aβ(19–32)-WT shifts subtraction for α-Hydrogen (H-A). (C) Residue chemical shift increment of Aβ(19–32)-S26s, Aβ(19–32)- D23d -S26s, Aβ(19–32)-D23d-S26s-K28k peptides after Aβ(19–32)-WT shifts subtraction for N-Hydrogen (H-N). (D) Representative ^{1}H-^{1}H TOCSY spectra of Aβ(19–32)-WT. A denotes α-hydrogen, B denotes β-hydrogen, Q denotes degenerate hydrogen. Chemical shifts were obtained by ^{1}H-^{1}H TOCSY and assigned using Sparky.[2] Aβ(19–32)-S26s data was processed from previously reported results[3] for comparison purposes. Chemical shifts values are shown in Table S1 and Table S2.

Δδ ^{1}H-A (ppm)				
Amino Acid	**Aβ(19-32)-WT**	**Aβ(19-32)-S26s**	**Aβ(19-32)-D23dS26s**	**Aβ(19-32)-D23dS26sK28k**
F19	4.421	4.421	4.428	4.425
F20	4.506	4.505	4.506	4.509
A21	4.147	4.153	4.176	4.177
E22	4.130	4.142	4.159	4.152
D23	4.575	4.573	4.581	4.578
V24	4.066	4.068	4.082	4.088
G25	3.911	3.914	3.870	3.859
S26	4.361	4.302	4.305	4.305
N27	4.662	4.653	4.656	4.649
K28	4.206	4.193	4.159	4.217
G29	3.856	3.846	3.843	3.840
A30	4.234	4.231	4.231	4.241
I31	4.070	4.065	4.071	4.077
I32	4.055	4.050	4.054	4.052

Table S1. Amino acid ^{1}H-A chemical shift values (ppm) of the Aβ(19–32) segment for the WT and chiral variants. Data were collected at 4 °C in 10% D_2O pH 7.4 20 mM phosphate buffer in a Varian INOVA 600 MHz spectrometer equipped with a triple resonance cryoprobe.

Δδ ^{1}H-N (ppm)				
Amino Acid	**Aβ(19-32)-WT**	**Aβ(19-32)-S26s**	**Aβ(19-32)-D23dS26s**	**Aβ(19-32)-D23dS26sK28k**
F19	8.204	8.198	8.200	8.193
F20	8.236	8.233	8.228	8.221
A21	8.274	8.269	8.223	8.239
E22	8.428	8.415	8.446	8.443
D23	8.484	8.486	8.571	8.571
V24	8.228	8.230	8.059	8.046
G25	8.608	8.556	8.523	8.531
S26	8.195	8.256	8.276	8.291
N27	8.536	8.653	8.618	8.629
K28	8.418	8.422	8.446	8.396
G29	8.469	8.460	8.462	8.389
A30	8.087	8.087	8.088	8.103
I31	8.279	8.274	8.282	8.309
I32	8.369	8.362	8.369	8.367

Table 2. Amino acid ^{1}H-N chemical shift values (ppm) of the Aβ(19–32) segment for the WT and chiral variants. Data were collected at 4 °C in 10% D_2O pH 7.4 20 mM phosphate buffer in a Varian INOVA 600 MHz spectrometer equipped with a triple resonance cryoprobe.

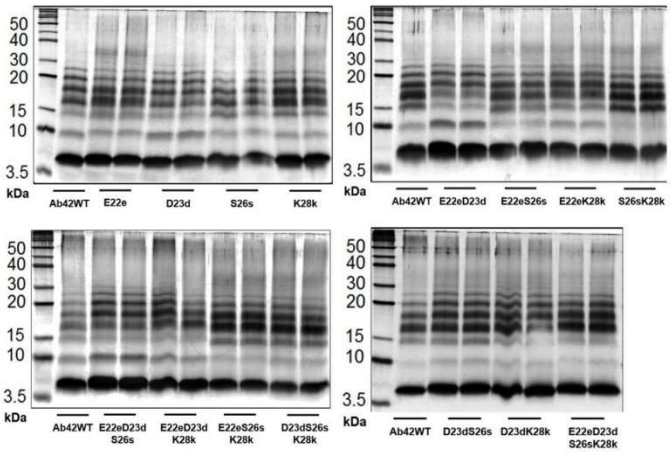

Figure S4. Oligomerization of Aβ42-WT and Aβ42 chiral mutant peptides. Samples were crosslinked using PICUP at 20 μM peptide concentration. Two technical replicates for each chiral mutant peptide were crosslinked and loaded into each gel. Aβ42-WT was performed in quadruplicates and one of each is showed in each gel. Samples were run on 12% tris-tricine polyacrylamide gel and gels were developed by silver staining.

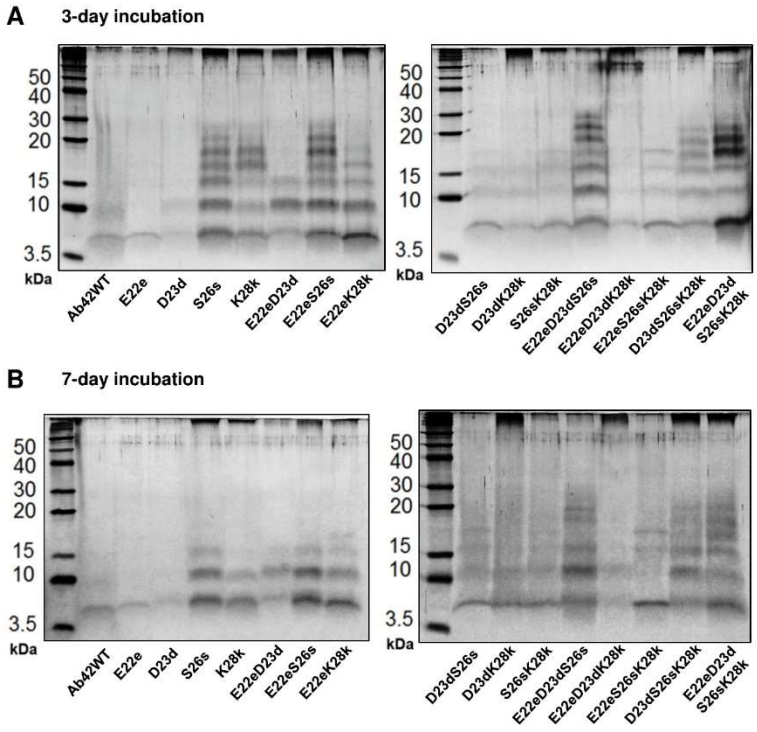

Figure S5. Oligomerization of Aβ42-WT and Aβ42 chiral mutant peptides after extended incubation times. Samples were crosslinked using PICUP at 20 μM peptide concentration. Samples were run on 12% tris-tricine polyacrylamide gel and gels were developed by silver staining. (A) Crosslinking after 3-day incubation in 20 mM phosphate buffer at 20 μM concentration. (B) Crosslinking after 7-day incubation in 20 mM phosphate buffer at 20 μM concentration.

TEM ANNEX

All scalebars: 200nm

Aβ42-WT

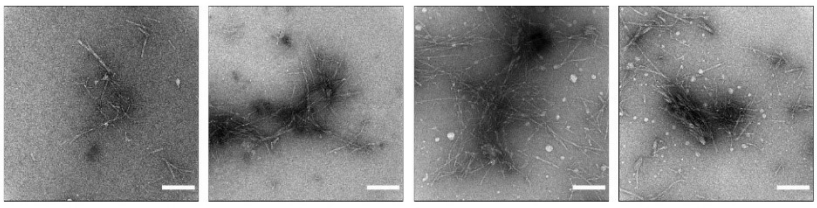

Aβ42-E22e (e)

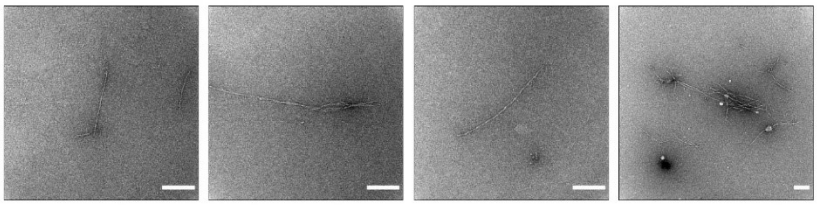

Aβ42-D23d (d)

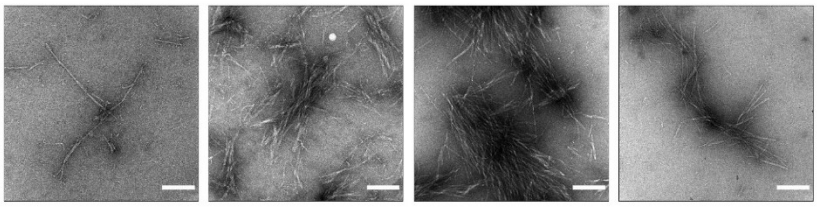

Aβ42-S26s (s)

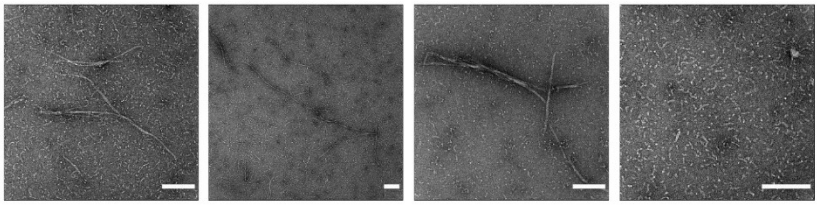

Aβ42-K28k (k)

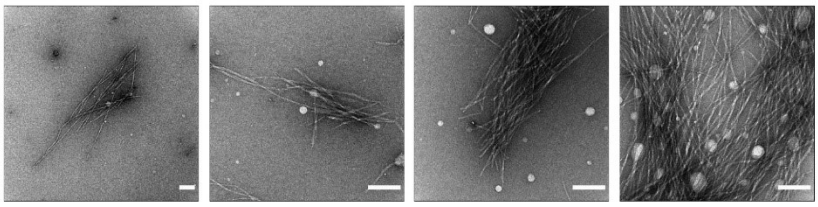

Aβ42-E22eD23d (ed)

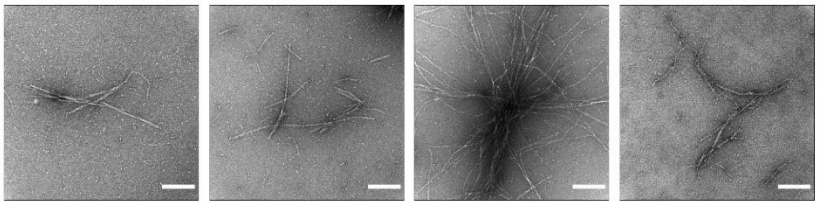

Aβ42-E22eS26s (es)

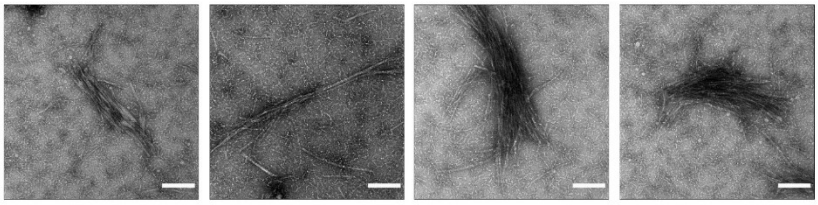

Aβ42-E22eK28k (ek)

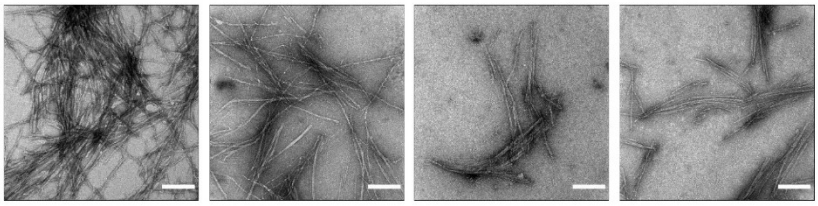

Aβ42-D23dS26s (ds)

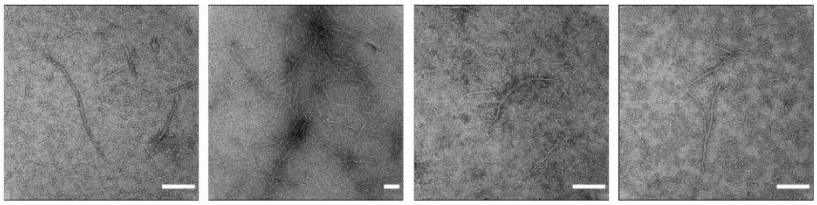

Aβ42-D23dK28k (dk)

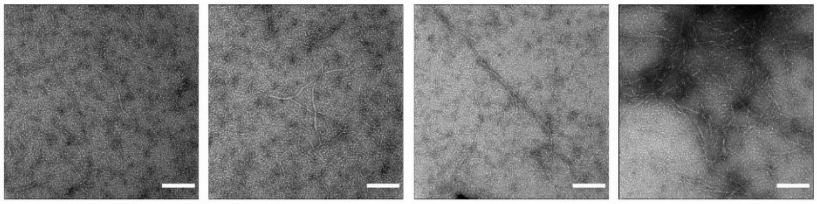

Aβ42-S26sK28k (sk)

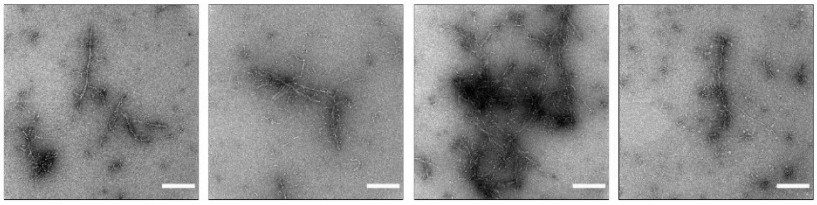

Aβ42-E22eD23dS26s (eds)

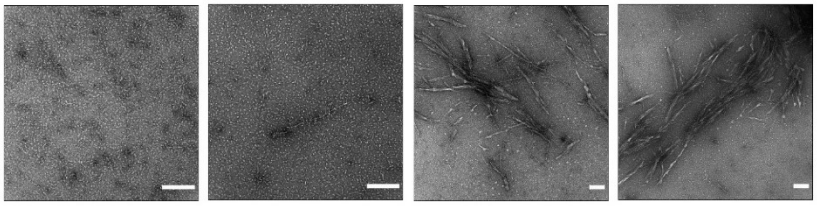

S19

Aβ42-E22eD23dK28k (edk)

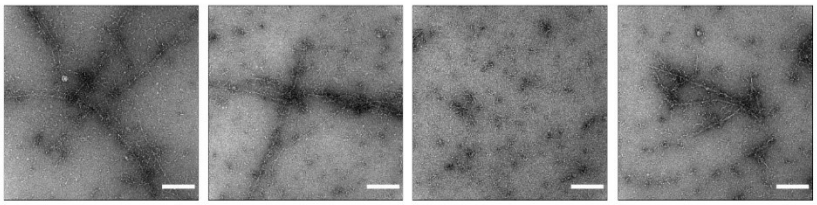

Aβ42-E22eS26sK28k (esk)

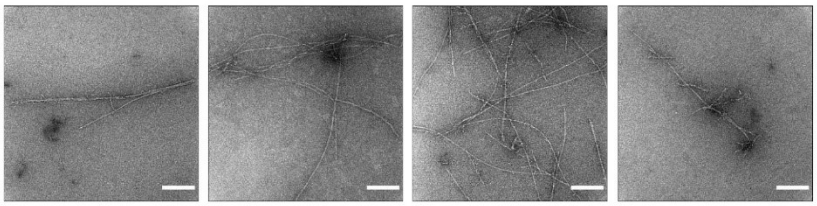

Aβ42-D23dS26sK28k (dsk)

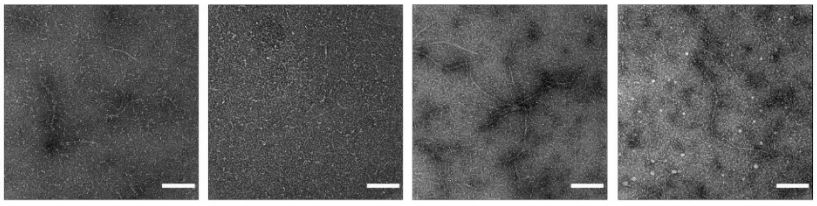

Aβ42-E22eD23dS26sK28k (edsk)

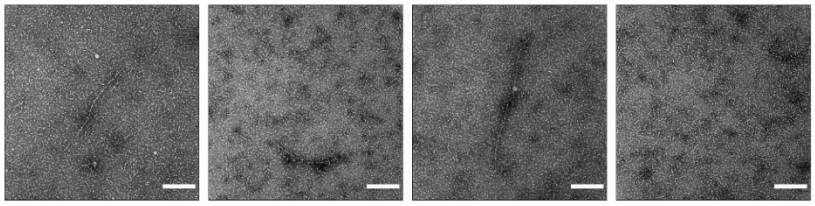

TEM annex. Negative-stain TEM images of Aβ42-WT and Aβ42 diastereomers at 20 μM peptide concentration after incubation in pH 7.4, 20 mM phosphate buffer. 3 μL of peptide-containing solution were aliquoted into carbon type-B, 200 mesh copper grids and stained with 1% uranyl acetate solution. Images were acquired in a JEOL 1230 TEM microscope.

REFERENCES

1 Warner, C. J. A.; Dutta, S.; Foley, A. R.; Raskatov, J. A. Introduction of D-Glutamate at a Critical Residue of Aβ42 Stabilizes a Prefibrillary Aggregate with Enhanced Toxicity. Chem. - A Eur. J. 2016, 22 (34), 11967 11970

2 T. D. Goddard and D. G. Kneller, SPARKY 3,University of California, San Francisco.

3 Alejandro R. Foley, Thomas S. Finn, Timothy Kung, Asa Hatami, Hsiau-Wei Lee, Manping Jia, Marco Rolandi, J. A. Raskatov. Trapping and Characterization of Nontoxic Aβ42 Aggregation Intermediates. ACS Chem. Neurosci. 2019, 10, 8, 3880-3887

Trapping and Characterization of Non-Toxic Aβ42 Aggregation Intermediates

Alejandro Foley[†], Thomas Finn[†], Timothy Kung[†], Asa Hatami[‡], Hsiau-Wei Lee[†], Manping Jia[§], Marco Rolandi[§], Jevgenij Raskatov[*,†].

SUPPORTING INFORMATION

[†] Department of Chemistry and Biochemistry, University of California Santa Cruz, Santa Cruz, CA 95064
[‡] Sangamo Therapeutics, Richmond, CA 94804
[§] Department of Electrical Engineering, University of California Santa Cruz, Santa Cruz, CA 95064
* correspondence should be addressed to: jraskato@ucsc.edu

CONTENTS PAGE

GENERAL EXPERIMENTAL PROCEDURES

Synthesis of Aβ42 and 14-mer peptides.

Peptides were synthesized by solid-phase Fmoc chemistry in a CEM Liberty automated microwave-assisted peptide synthesizer. Aβ42-WT and Aβ42-S26s peptides were synthesized using HMPB ChemMatrix® resin, pre-loaded with L-alanine (Sigma-Aldrich, cat no. 727822). 14-mer peptides were synthesized using Rink Amide resin (Creosalus, cat no. 501141107). All syntheses were performed on a 0.1 mM scale relative to resin loading. A solution of 30% piperidine (Spectrum, cat no. P1146) in DMF was employed for deprotection steps, and 1-Hydroxybenzotriazole hydrate (Oakwood Chemical, cat no. M02875) and N,N'-Diisopropylcarbodiimide (Chem-Impex, cat no. 00110) were used as coupling reagents. The peptides were cleaved from resin and deprotected with a cocktail solution containing trifluoroacetic acid (10 mL), 1, 2-diethanethiol (0.5 mL), tri-isopropylsilane (1 mL) and liquefied phenol (0.5 mL). Peptides were purified by reverse-phase HPLC, as previously described by us (1), yielding peptides with purities exceeding 97 % (Fig. S1, Fig. S2, Fig. S5).

N-terminal TAMRA labeling of Aβ42-WT and Aβ42-S26s peptides. Aβ42-WT and Aβ42-S26s peptides were synthesized using solid phase peptide synthesis as described above. 1 equivalent of loaded resin (fully protected except the terminal amino group) was swelled with 2 mL of DMF for 15 minutes. Then, a mixture of 5(6)-carboxy tetramethylrhodamine (TAMRA-COOH, 10 eq.), benzotriazol-1-yl-oxytripyrrolidinophosphonium hexafluoro phosphate (PyBOP, 10 eq.) and 1-Hydroxy-7-azabenzotriazole (HOAt, 16 mg, 20 eq.), was dissolved in 3 mL of DMF. Finally, diisopropylethylamine (10 eq.) was added to the mixture and combined to the swelled resin. The TAMRA-resin mixture was allowed to react at room temperature for 24 hours protected from light. The resin was then washed with DMF (3x), DCM (2x), and dried *in vacuo* for 30 minutes. Cleavage and purification were performed as described above, yielding peptides with purity exceeding 97% (Figure S3, Figure S4).

Thioflavin T (ThT) kinetic assays

Thioflavin T (Acros Organics, 2390-54-7) was dissolved in 10 mL of pH 7.4 20 mM phosphate buffer containing 0.02% (w/v) NaN_3. The solution was filtered through a 0.22 microns filter and the concentration of the filtrated solution was determined by Nanodrop at 412 nm ($\varepsilon = 36000 M^{-1}cm^{-1}$). The concentration was then adjusted with pH 7.4 20 mM phosphate buffer to obtain a 100 μM ThT stock solution. *Preparation of Aβ solution:* Lyophilized samples were dissolved in cold 20 mM NaOH (20 mM NaOH should not exceed more than 3% v/v in the final solution), sonicated for 30s, and then the concentration was measured by Nanodrop ($\varepsilon = 1490 M^{-1} cm^{-1}$) at 280 nm. Samples were then dissolved to the desired concentration in pH 7.4 20 mM phosphate buffer. *Reading of ThT experiments:* As soon as samples were dissolved to the desired concentration, 200 μL were added in each well (final ThT centration of 20 μM). All experiments were conducted in black, clear bottom 96-well plates with shaking in Biotek synergy HTX fluorescence plate reader ($\lambda_{ex} = 444$ nm, $\lambda_{em} = 485$ nm) at 37 °C with continuous shaking. All experiments were run in triplicates and the plate was sealed with optically clear adhesive film. Readings were collected every 5 minutes with 5 seconds of shaking before reading and 295 seconds of shaking in between readings. The experiment was monitored for a total of 24 hours. Results for the 3 synthetic batches tested for each peptide are shown in Figure S6.

TAMRA quenching kinetic assays

Preparation of Aβ solution: Lyophilized Aβ42-WT and Aβ42-S26s were dissolved in cold 20 mM NaOH, and sonicated for 30 seconds, as described above. However, the concentration was determined by Nanodrop ($\varepsilon = 99000 M^{-1} cm^{-1}$) at 550 nm. Samples were then dissolved to the desired concentration in pH 7.4 20 mM phosphate buffer. *Reading of ThT experiments:* As soon as samples were dissolved to the desired concentration, 200 μL were added in each well. All experiments were conducted in black, clear bottom 96-well plates with shaking in Biotek synergy HTX fluorescence plate reader ($\lambda_{ex} = 550$ nm, $\lambda_{em} = 580$ nm) at 37 °C with continuous shaking. All experiments were run in triplicates and the plate was sealed with optically clear adhesive film. Readings were collected every 5 minutes with 5 seconds of shaking before reading and 295 seconds of shaking in between readings. The experiment was monitored for a total of 24 hours. Results for the 3 synthetic batches tested for each peptide are shown in Figure S9.

Preparation of quiescent samples.

Lyophilized Aβ42-WT and Aβ42-S26s were dissolved in 20 mM NaOH (1.5% final v/v of NaOH) and diluted to a final concentration of 20 μM in pH 7.4 20 mM phosphate buffer. Samples remined immobile for 7 days at 37 C. *Preparation of mixed and supernatant fractions.* After 7 days of incubation, samples were gently agitated to obtain the mixed fraction and then centrifuged at 14,000 g for 20 minutes to separate the pellet from the supernatant (sup) fractions, as previously described (2). The resulting supernatant was carefully isolated from the pellet. *Preparation of the pellet fraction.* After centrifugation at 14,000 g, the isolated pellet fraction was washed with Milli Q water and centrifuged again. This process was repeated 2 more times. After the 3 washed with Milli Q water, the pellet was re-dissolved in 4M Guanidine HCl for dot-blot experiments.

TEM sample preparation and imaging

Samples of Aβ42-WT and Aβ42-S26s were taken directly from either the endpoint of the kinetic experiments (ThT and TAMRA kinetic assays completed at 24 hours) or from the 7-day quiescent incubation samples. For grid preparation, 3 μL of sample were spotted onto freshly glow-discharge carbon-coated electron microscopy grid (Ted Pella, Catalog No. 01701-F) and allowed to adhere for 1 minute. Excess solution was then removed, and the grid was stained with 30 μL 1% uranyl acetate (3x10 μL). Finally, the grid was allowed to dry at room temperature for 2 minutes. All fibrils were imaged by using JEOL 1230 microscope at an accelerating voltage of 120 kV. All TEM images collected are available as a TEM Appendix in the Supplemental Information.

AFM sample preparation and imaging

5 μL of incubated Aβ42-WT and Aβ42-S26s samples were drop-casted onto freshly taped mica substrate. The solution was left on the substrate for 5 min, and then rinsed with a constant stream of miliQ water for 2 minutes. The substrate was then dried with a stream of filtered nitrogen gas. AC Air Tapping mode Atomic Force Microscopy (AFM) was performed on an Asylum MFP-3D Infinity System. Bruker Sb-doped Si cantilevers (ρ = 0.01-0.025 Ω-cm, k = 42 N/m, v ~ 320 kHz) were used in all cases.

SDS-PAGE

The mixed and supernatant fractions were combined 1:1 with SDS-free sample buffer and separated on a 4-20% Mini-Protean TGX gel (Bio-Rad, cat no. 456-1093). 20 μL of each sample were placed in each well. Gels were run at 100 V for approximately 2 hours using 1x Tris/Glycine/SDS Buffer (Bio-rad, cat no. 1610732), and then developed by silver staining.

Photochemically induced crosslinking of unmodified proteins (PICUP)

4 μL of 1 mM $[Ru(bipy)_3]^{2+}$ and 4 μL of 20 mM ammonium persulfate were added to 32 μL of the desired Aβ42-WT and Aβ42-S26s samples in pH 7.4 20 mM phosphate buffer. The mixture was then irradiated for 1.2 seconds with white light using our previously described setup (3). Following irradiation, the solution was immediately quenched with 40 μL of loading buffer containing 5% 2-mercaptoethanol. Crosslinked oligomers were separated by SDS-PAGE gel electrophoresis using a 12% tris-tricine polyacrylamide gel. The voltage of the system was kept constant at 100 V for approximately 2 hours. Following electrophoresis, gels were developed by silver staining.

Dot Blot Assay

Sample preparation. Lyophilized Aβ42-WT and Aβ42-S26s were dissolved in 20 mM NaOH (1.5% final v/v of 20 mM NaOH) and diluted to a final concentration of 20 μM in 20 mM phosphate buffer (pH 7.4). Samples remined immobile for 7 days at 37 °C. After 7 days of incubation, samples were gently agitated to obtain "mixed" fraction and then centrifuged at 14,000 g for 20 minutes to separate any precipitate from solution, as previously described (2). Once the supernatant was extracted, fibril pellet was washed 3 times with Milli Q water, and then resuspended in 4M Guanidine HCl. 2 μL of peptide solution were used for each blot. *Blot Development.* Once the blot had completely dried, the membrane was blocked with 10% non-fat dry milk in TBST for 1h at room temperature on an orbital shaker. After 1h, the non-fat dry milk was removed and 6E10 antibody (Biolegend, cat no. 803001) was diluted 1:1000 in 5% non-fat dry milk in TBST, added to the membrane, and incubated overnight at 4 °C according to previously published protocols (4). The membrane was then washed three times with TBST for 5 minutes each and then incubated with HRP-conjugated secondary antibody diluted 1:1000 in 10% non-fat dry milk TBST for 1h at RT on an orbital shaker. The membrane was washed again three times, 5 minutes each, with TBST and developed with an Opti-4CN Substrate Kit (Bio-Rad, cat no. 1708235) for 5 minutes.

Circular dichroism (CD) experiment

400 μL of the 7 days incubated Aβ42-WT and Aβ42-S26s supernatant solutions in 20mM phosphate buffer (pH 7.4) were placed in a quartz 1 mm cell. Spectra were then recorded using a Jasco 1500 CD spectrophotometer, set to a scan range of 180 to 280 nm, a DIT of 4 seconds and a scan speed of 50 nm per minute at room temperature.

Cell viability experiments.

Cell cultures. Adherent PC12 and adherent human neuroblastoma SH-SY5Y cells were purchased from ATCC. PC12 cells were cultured in F12K media supplemented with 2.5% fetal bovine serum, 12.5 % horse serum and 1% penicillin-streptomycin. Human neuroblastoma SH-SY5Y cells were cultured in 1:1 DMEM: F12 K media supplemented with 10% fetal bovine serum and 1% penicillin-streptomycin. All incubations were kept at 37 ℃ with 5% CO2. *Preparation of plates.* PC12 cells were plated in a 96-well plate at a density of 5,000 cells/well (100 μL total volume per well) and allowed to adhere for 24 h before dosing. SH-SY5Y cells were plated in a 96-well plate at a density of 50,000 cells/well (100 μL total volume per well) and allowed to adhere for 24 h before dosing.

Cell dosing. Lyophilized Aβ42-WT and Aβ42-S26s peptides were dissolved in 15 μL of 20 mM NaOH (1.5% final v/v), and the solutions were diluted to a final concentration of 50 μM with media (F12-K media containing 2.5% Fetal Bovine Serum and 15% Horse Serum for PC12 cells, and 1:1 DMEM: F12 K media supplemented with 10% fetal bovine serum and 1% penicillin-streptomycin for SH-SY5Y cells). After 72 h incubation at 37 C, 10 μL of WST-1 (Roche) were added to each well and incubated for 3 hours. Then, absorbance was measured at λ = 490 nm for the WST-1 assay reading. All the experiments were performed with 3 technical replicates, and cell viability assays were reproduced with 3 biological replicates for each cell line (Figure S7, Figure S8). Results are shown normalized against vehicle (cells and media only).

NMR experiments

37 °C experiments (time monitoring of ^{1}H integration). 1.0 mg of either 14-mer-WT and 14-mer-S26s peptides were saturated in 0.6 mL of 10% D_2O pH 7.4 20 mM phosphate buffer. Immediately after, the sample was placed on a Varian INOVA 600 MHz spectrometer equipped with a triple resonance cryoprobe at 37 °C. Each ^{1}H proton spectra acquisition was 5 minutes for a total of 200 min (40 ^{1}H total spectra). After data was collected, the spectra were processed and integrated between the 0-3.3 ppm region using Mestrenova. Data were normalized by assigning maximum integration value for t = 5 min for each peptide.

4 °C experiments (^{1}H-^{13}C HSQC, TOCSY, and NOESY). 1.0 mg of either 14-mer-WT and 14-mer-S26s peptides were saturated in 0.6 mL of 10% D_2O pH 7.4 20 mM phosphate buffer. Temperature was kept constant at 4 °C during sample preparation by keeping the solutions on a water/ice bath and using pre-cooled 4 °C solutions. NMR experiments for resonance assignment were performed on a Varian INOVA 600 MHz spectrometer equipped with a triple resonance cryoprobe. Data were collected at 4 °C. Sequence-specific assignment was performed by using ^{1}H-13C HSQC, TOCSY (65 ms), and NOESY (350 ms) spectra.

DFT computational analysis

DFT calculations were conducted with the Gaussian 09 program suite (5), using the M062X functional, which is recommended for molecular modeling of compounds made of main group elements, including peptides (6). All geometry optimizations were conducted at the M062X/6-311++G** level of theory (7). Certain coordinates were frozen, where indicated. Solvent (water) was modeled using the polarizable continuum model (PCM), as implemented in Gaussian 09 (ε_r = 78.3553). All geometry-optimized coordinate sets have been deposited as part of the Supporting Information.

Aβ42-WT
Batch 1

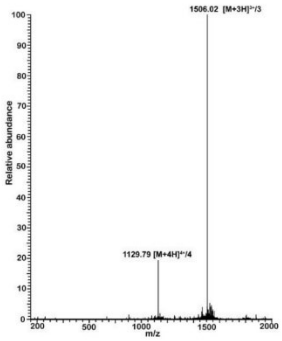

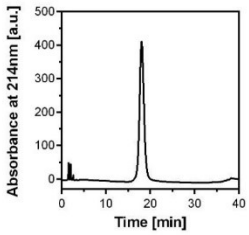

Peak #	Time [min]	Area	% Area
1	3.4	156.5	0.5
2	**18**	**29957.1**	**99.5**

Aβ42-WT
Batch 2

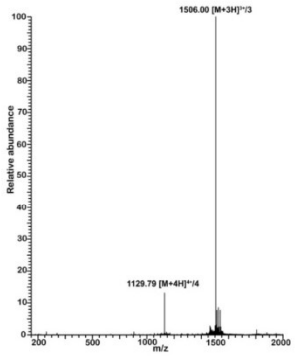

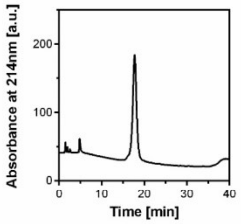

Peak #	Time [min]	Area	% Area
1	4.847	304.2	3.0
2	**17.7**	**9975.3**	**97.0**

Aβ42-WT
Batch 3

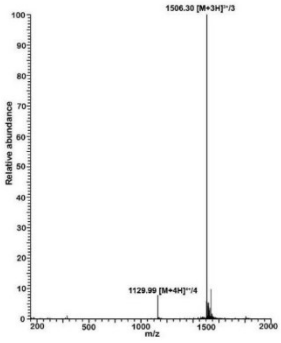

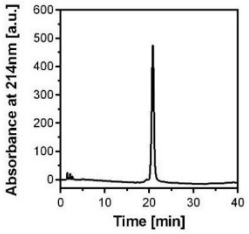

Peak #	Time [min]	Area	% Area
1	19.4	226.3	1.3
2	**20.8**	**17080.4**	**98.7**

Figure S1. Mass spectrometry and HPLC characterization for Aβ42-WT synthetic batches.

Aβ42-S26s
Batch 1

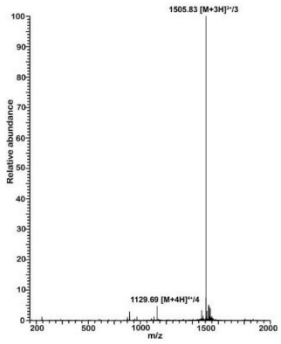

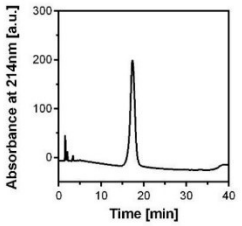

Peak #	Time [min]	Area	% Area
1	15.8	168.9	1.8
2	**17.3**	**16485.8**	**98.2**

Aβ42-S26s
Batch 2

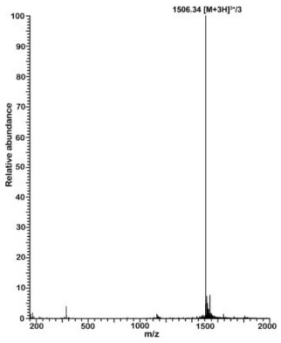

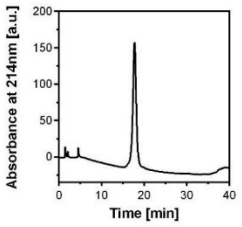

Peak #	Time [min]	Area	% Area
1	4.6	253.6	2.5
2	**17.8**	**9771.6**	**97.5**

Aβ42-S26s
Batch 3

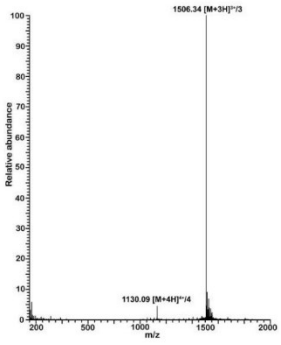

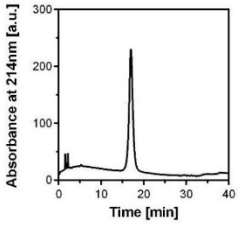

Peak #	Time [min]	Area	% Area
1	4.6	45.6	0.8
2	**16.6**	**5573.4**	**99.2**

Figure S2. Mass spectrometry and HPLC characterization for Aβ42-S26s synthetic batches.

Aβ42-TAMRA
Batch 1

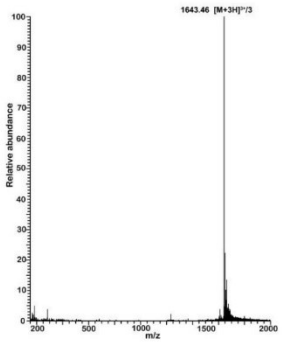

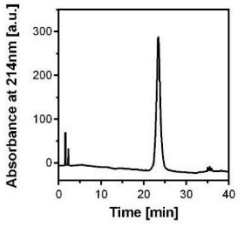

Peak #	Time [min]	Area	% Area
1	22.3	449.8	2.3
2	**23.4**	**19449**	**97.7**

Aβ42-TAMRA
Batch 2

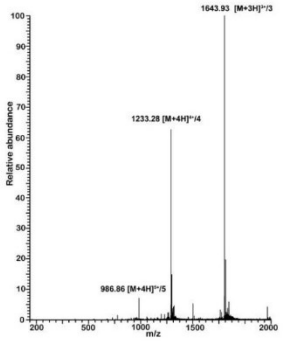

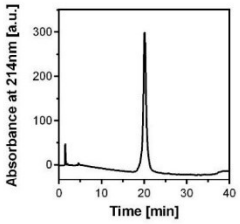

Peak #	Time [min]	Area	% Area
1	19.0	313	1.9
2	**20.1**	**16042.4**	**98.1**

Aβ42-TAMRA
Batch 3

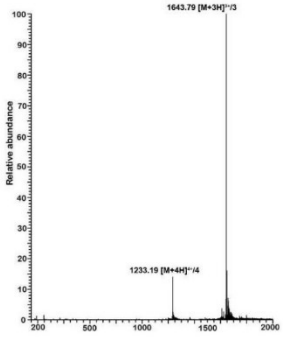

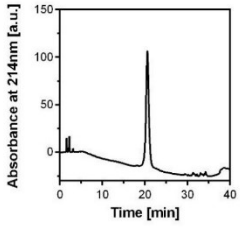

Peak #	Time [min]	Area	% Area
1	**20.567**	**61.547**	**99.7**
2	22.021	19.2	0.3

Figure S3. Mass spectrometry and HPLC characterization for TAMRA-Aβ42-WT synthetic batches.

Aβ42-S26s-TAMRA
Batch 1

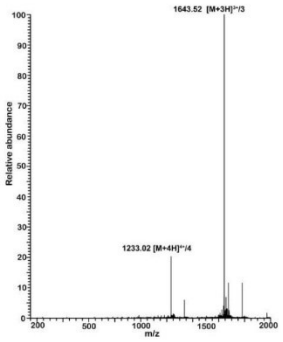

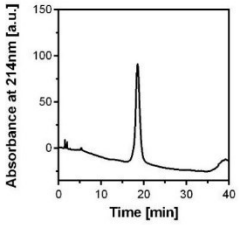

Peak #	Time [min]	Area	% Area
1	17.3	164.3	2.3
2	**18.5**	**7131.6**	**97.7**

Aβ42-S26s-TAMRA
Batch 2

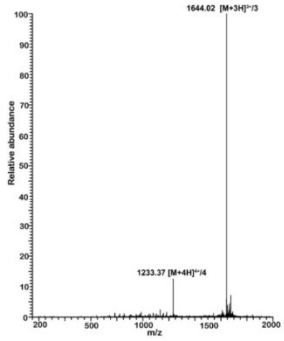

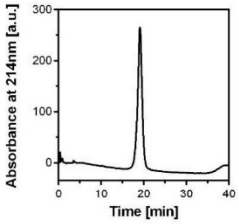

Peak #	Time [min]	Area	% Area
1	17.3	124.8	0.6
2	**19**	**20427.1**	**99.4**

Aβ42-S26s-TAMRA
Batch 3

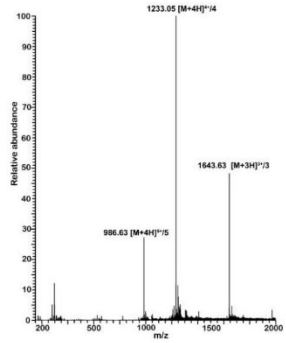

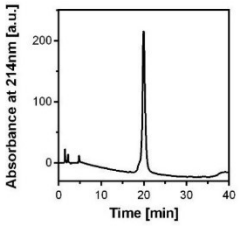

Peak #	Time [min]	Area	% Area
1	18.9	310.6	2.8
2	**19.9**	**10633**	**97.2**

Figure S4. Mass spectrometry and HPLC characterization for TAMRA-Aβ42-S26s synthetic batches.

Ac-FFAEDVGSNKGAII-CONH$_2$ (WT)

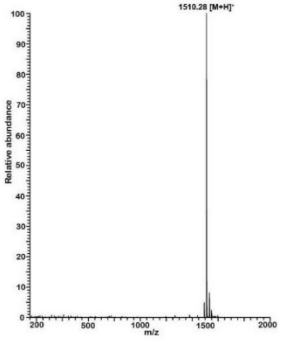

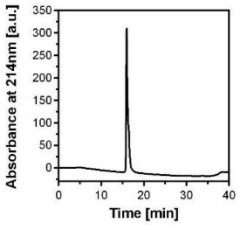

Peak #	Time [min]	Area	% Area
1	**16.0**	**8834.6**	**97.6**
2	17.0	214	2.4

Ac-FFAEDVGsNKGAII- CONH$_2$ (S26s)

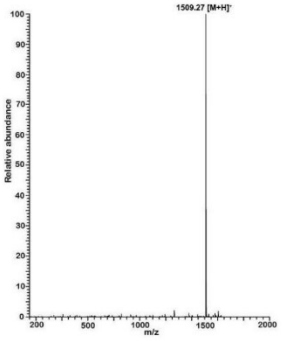

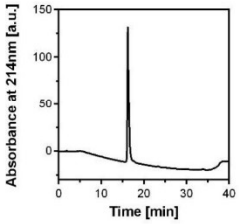

Peak #	Time [min]	Area	% Area
1	**16.3**	**3405.6**	**97.2**
2	17.5	99.2	2.8

Figure S5. Mass spectrometry and HPLC characterization for Ac-FFAEDVGSNKGAII-CONH$_2$ (Aβ19-32) WT and S26s peptides.

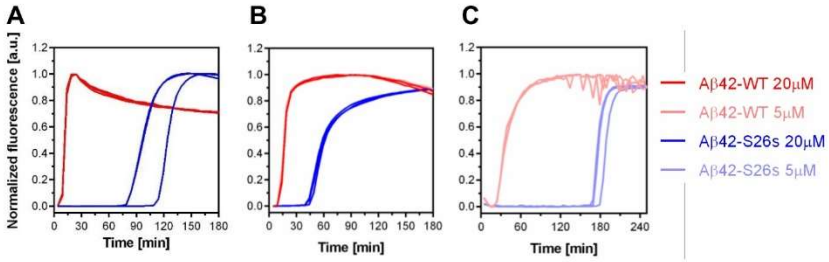

Figure S6. Aggregation kinetics monitored by ThT fluorescence for different synthetic batches. At least 3 technical replicates were run per peptide in each case, shown as individual curves. Samples were run for at 37 °C in presence of 20 μM ThT solution in 20mM phosphate buffer (pH 7.4) with continuous shaking. (A-C) represents an independent synthetic batch each.

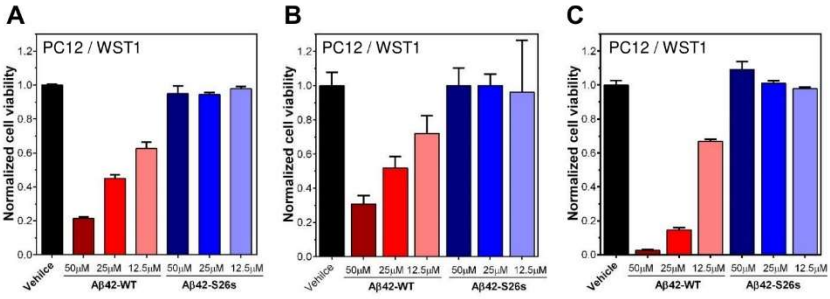

Figure S7. Cell viability assays of the three synthetic batches for both Aβ42-WT and Aβ42-S26s in PC12 cell line for three different synthetic batches (A-C). Cells were incubated with the peptides at three different concentrations (50, 25, 12.5 μM) for 3 days. Cell viability readout was performed by the WST1 assay. Columns show mean and SD for three technical replicates.

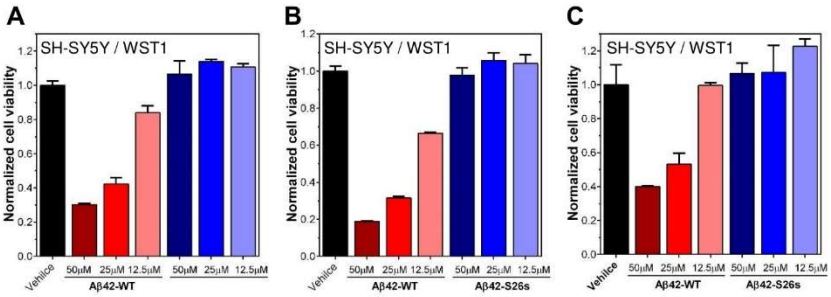

Figure. S8. Cell viability assays of the three synthetic batches for both Aβ42-WT and Aβ42-S26s in SH-SY5Y cell line for three different synthetic batched (A-C). Cells were incubated with the peptides at three different concentrations (50, 25, 12.5 μM) for 3 days. Cell viability readout was performed by the WST1 assay. Columns show mean and SD for three technical replicates.

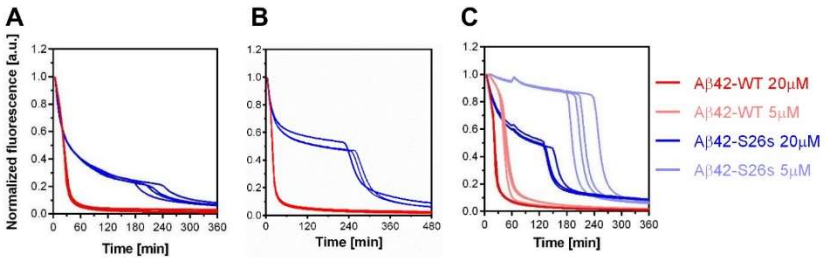

Figure. S9. Aggregation kinetics monitored by TAMRA fluorescence for different synthetic batches (A-C). At least 3 technical replicates were run per peptide in each case, shown as individual curves. Samples were run for at 37 °C in in 20mM phosphate (pH 7.4) buffer with continuous shaking.

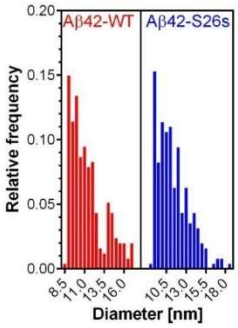

Figure S10. Distribution of oligomer diameter of TAMRA-Aβ42-WT and TAMRA-Aβ42-S26s, calculated from 250 oligomer spheres from TEM images in TEM appendix-Fig. S18 and Fig. S21, as previously described (8).

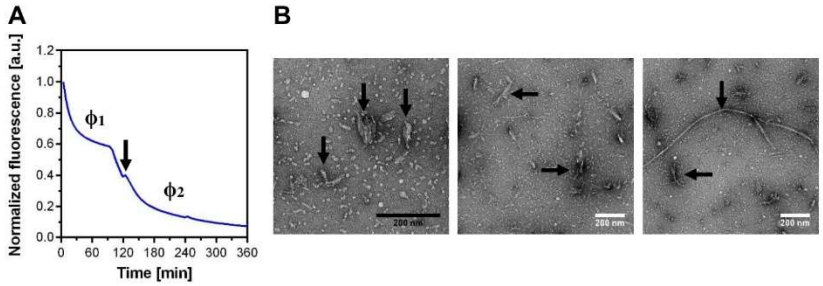

Figure. S11. (A) Aggregation kinetics monitored by TAMRA fluorescence for Aβ42-S26s at 20 μM in 20mM phosphate buffer (pH 7.4), 37 °C with continuous shaking. The experiment was stopped at 120 minutes and a 5 μL of solution were aliquoted out for TEM imaging. (B) Negative-stain images showing small aggregation clusters structures and fibrils starting to form. Black arrows show bigger aggregates and fibrils starting to form.

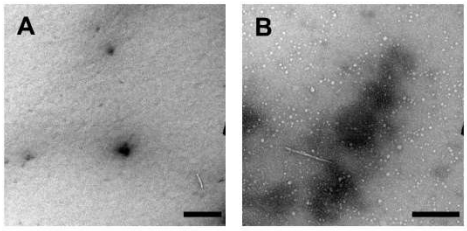

Figure S12. Negative-stain TEM images of supernatant solutions of Aβ42-WT (A) and Aβ42-S26s (B) after 7-day incubation at 37 °C in 20 mM phosphate buffer (pH 7.4). Scalebar: 200 nm in all cases.

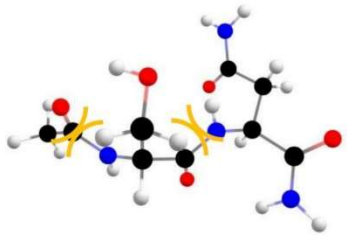

Figure S13. Representation of steric clash between D-Ser 27 and L-Asn 27 before DFT optimization.

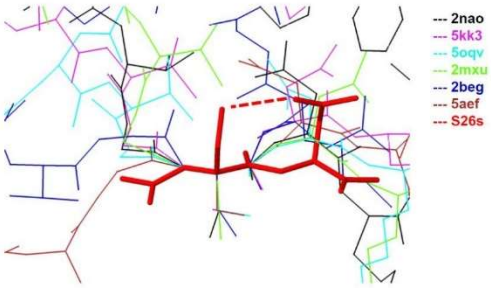

Figure S14. Docking of D-Ser26-L-Asn27 DFT-optimized structure into published Aβ42 fibril structures. S26s adopts an "open" conformation when compared to the rest of the structures. A H-bond between Ser and Asn side chains is shown with a dashed red line.

TEM APPENDIX

Aβ42-WT 24h ThT

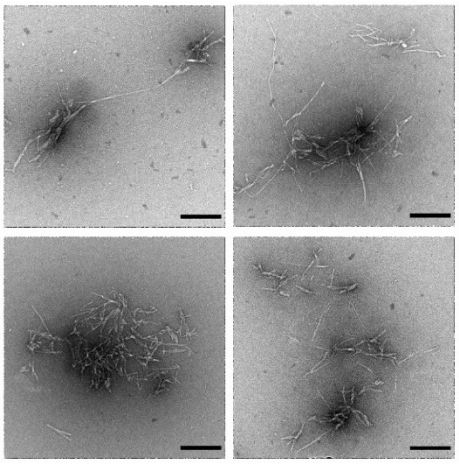

Figure S15. Negative-stain TEM images of Aβ42-WT at the endpoint (24h) of ThT experiment. Scalebar: 200 nm in all cases.

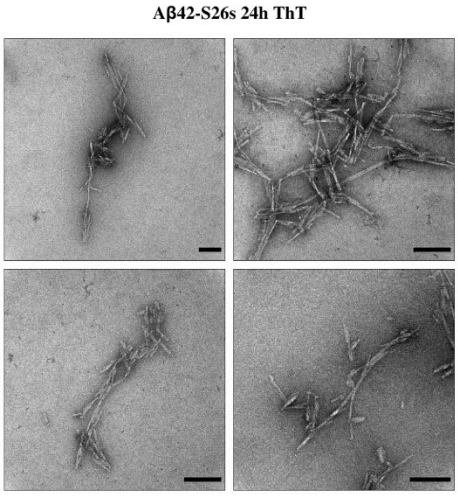

Figure S16. Negative-stain TEM images of Aβ42-S26s at the endpoint (24h) of ThT experiment. Scalebar: 200 nm in all cases.

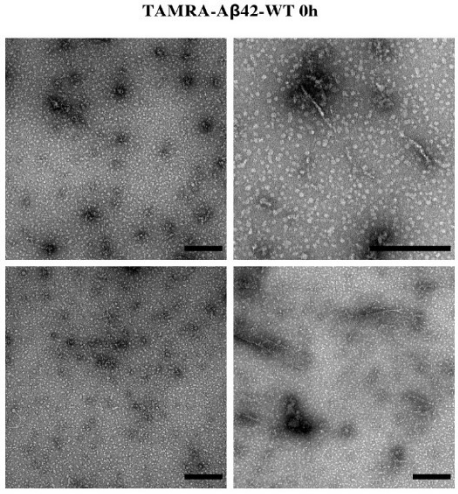

Figure S17. Negative-stain TEM images of TAMRA-Aβ42-WT at the initial time point (t_0) of the TAMRA-kinetics experiment (Figure 2). Scalebar: 200 nm in all cases.

TAMRA-Aβ42-WT 1h

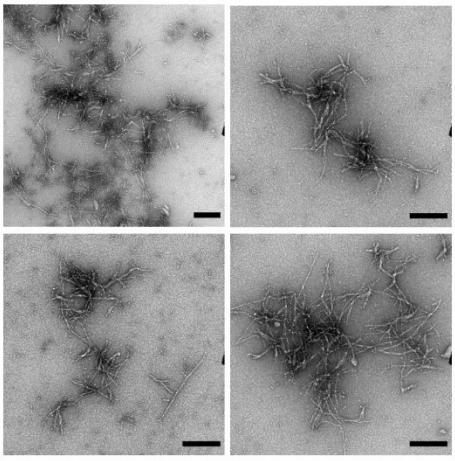

Figure S18. Negative-stain TEM images of TAMRA-Aβ42-WT 1h after starting the TAMRA-kinetics experiment (Figure 2). Scalebar: 200 nm in all cases.

TAMRA-Aβ42-WT 24h

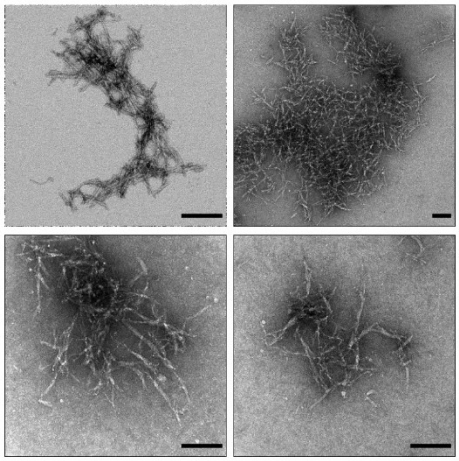

Figure S19. Negative-stain TEM images of TAMRA-Aβ42-WT upon completion (24h) of the TAMRA-kinetics experiment (Figure 2). Scalebar: 200 nm in all cases.

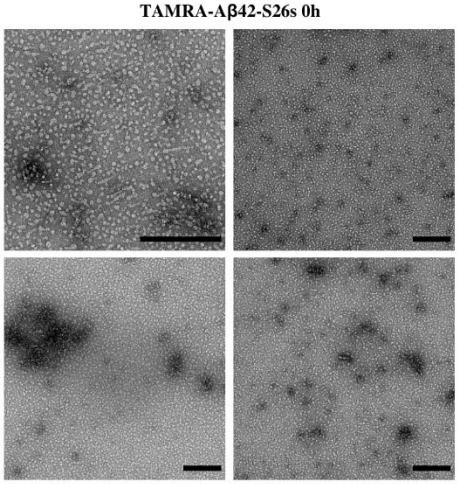

Figure S20. Negative-stain TEM images of TAMRA-Aβ42-S26s at the initial time point (t_0) of the TAMRA-kinetics experiment (Figure 2). Scalebar: 200 nm in all cases.

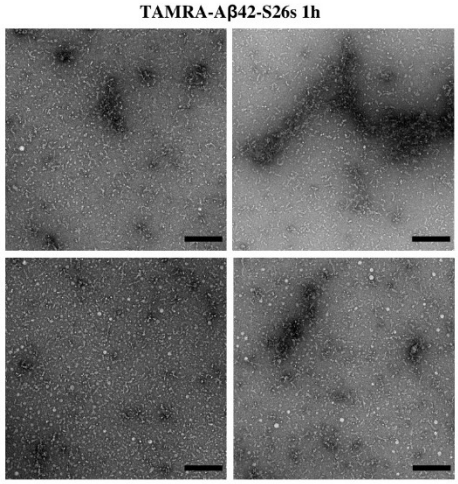

Figure S21. Negative-stain TEM images of TAMRA-Aβ42-S26s 1h after starting the TAMRA-kinetics experiment (Figure 2). Scalebar: 200 nm in all cases.

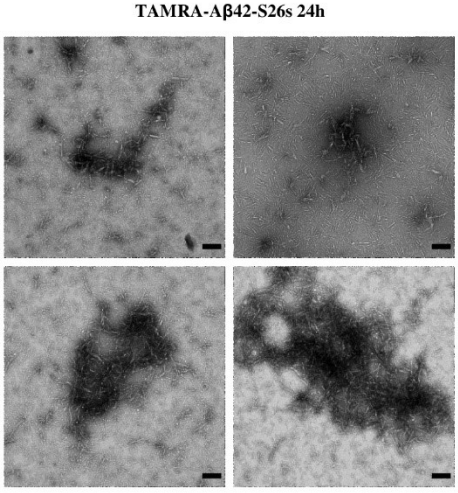

Figure S22. Negative-stain TEM images of TAMRA-Aβ42-S26s upon completion (24h) of the TAMRA-kinetics experiment (Fig. 2). Scalebar: 200 nm in all cases.

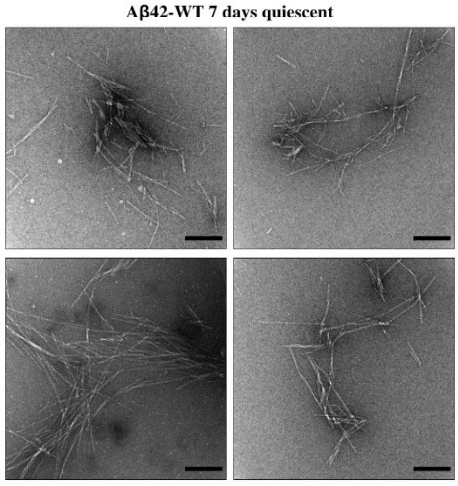

Figure S23. Negative-stain TEM images of Aβ42-WT after 7-day quiescent incubation at 37 °C. Scalebar: 200 nm in all cases.

Aβ42-S26s 7 days quiescent

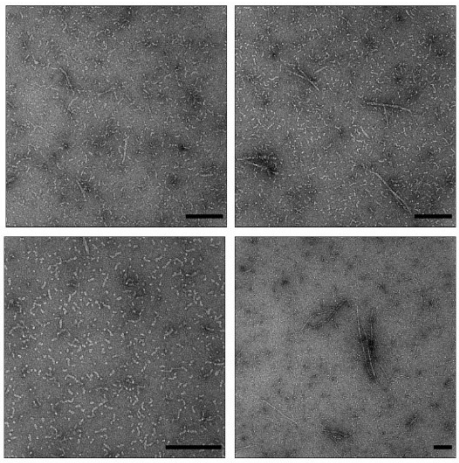

Figure S24. Negative-stain TEM images of Aβ42-S26s after 7-day quiescent incubation at 37 °C. Scalebar: 200 nm in all cases

DFT APPENDIX – COORDINATES USED IN FINAL SINGLE POINT ENERGY CALCULATIONS

Ala monomer

19

symmetry c1

C	0.000518000	2.157171000	-0.196145000
C	-0.037070000	0.764137000	-0.799573000
C	0.170238000	-0.554467000	-2.852615000
C	-1.105982000	-0.730829000	-3.649996000
C	1.346441000	-0.583270000	-3.806099000
H	0.304443000	1.543048000	-2.645532000
H	0.262353000	-1.348615000	-2.111083000
H	0.080187000	2.946723000	-0.942087000
H	-0.904069000	2.303217000	0.394104000
H	-1.092757000	-1.671841000	-4.204330000
H	0.856194000	2.211403000	0.478555000
H	-1.220361000	0.090267000	-4.360743000
H	-1.964653000	-0.735750000	-2.977357000
H	1.807951000	-2.516485000	-3.287463000
H	2.802646000	-1.808197000	-4.515282000
N	0.142738000	0.698751000	-2.113583000
N	2.057705000	-1.712341000	-3.840602000
O	-0.214439000	-0.224367000	-0.084265000
O	1.615454000	0.412992000	-4.476279000

Asn monomer
23
symmetry c1
C 0.000515000 2.157177000 -0.196138000
C -0.037067000 0.764123000 -0.799613000
C -0.298063000 -1.627961000 -0.345314000
C 0.974676000 -2.370953000 0.006637000
C -1.462831000 -2.305853000 0.345471000
C 2.097842000 -2.073606000 -0.929884000
H -0.321415000 -0.038873000 1.045620000
H -0.421631000 -1.633714000 -1.429306000
H 0.936253000 2.634279000 -0.488528000
H -0.084012000 2.158954000 0.889832000
H 0.795191000 -3.450158000 -0.070501000
H -0.820482000 2.734097000 -0.623553000
H 1.239535000 -2.168350000 1.046656000
H -2.050308000 -3.228662000 -1.395283000
H -2.984248000 -3.607670000 0.013513000
H 3.408363000 -1.875956000 0.618158000
H 4.070693000 -1.683184000 -0.966825000
N -0.205271000 -0.233562000 0.060399000
N -2.238935000 -3.079566000 -0.416731000
N 3.266208000 -1.844048000 -0.378315000
O 0.073526000 0.605215000 -2.017272000
O -1.664986000 -2.105757000 1.542602000
O 1.916135000 -2.030688000 -2.145097000

D-Ser-L-Asp DFT-optimized dipeptide
34
symmetry c1
C -0.661000000 0.594000000 -2.300000000
C -1.040000000 0.702000000 -0.839000000
O -2.156000000 0.372000000 -0.422000000
N -0.080000000 1.196000000 -0.018000000
C -0.273000000 1.282000000 1.411000000
C 1.105000000 1.271000000 2.069000000
N 1.084000000 1.230000000 3.418000000
C 2.287000000 1.401000000 4.199000000
C 1.963000000 0.991000000 5.637000000
N 3.041000000 0.797000000 6.431000000
C -1.026000000 2.565000000 1.807000000
H -1.343000000 2.499000000 2.855000000
O 2.149000000 1.340000000 1.415000000
C 2.800000000 2.863000000 4.156000000
C 1.781000000 3.811000000 4.755000000
O 0.790000000 4.194000000 4.116000000
N 2.004000000 4.188000000 6.030000000
O 0.798000000 0.940000000 6.031000000
H -0.857000000 0.417000000 1.749000000
H 0.857000000 1.362000000 -0.362000000
H -0.758000000 -0.450000000 -2.608000000
H -1.366000000 1.187000000 -2.887000000
H 0.355000000 0.937000000 -2.501000000
H 0.211000000 1.206000000 3.933000000
H 3.075000000 0.760000000 3.790000000
H 3.954000000 0.642000000 6.031000000

H	2.882000000	0.467000000	7.374000000
H	3.757000000	2.925000000	4.682000000
H	2.957000000	3.133000000	3.110000000
H	1.317000000	4.760000000	6.502000000
H	2.785000000	3.833000000	6.558000000
O	-0.236000000	3.722000000	1.588000000
H	-1.921000000	2.636000000	1.183000000
H	0.234000000	3.902000000	2.422000000

5xAsn (from pdb 5oqv)

115

symmetry c1

C	-0.014513000	2.164489000	-0.190011000
C	-0.083280000	-1.311757000	-1.697101000
C	0.154566000	0.660089000	-0.168162000
C	0.233643000	-0.790873000	1.803996000
C	-0.490112000	-1.232398000	3.063734000
C	-0.535204000	0.074722000	-1.383429000
C	4.157824000	0.007310000	-1.393631000
C	4.210044000	-1.188088000	3.084871000
C	-4.466448000	-0.834275000	1.783268000
C	-4.541509000	0.663758000	-0.152426000
C	4.614219000	-1.384878000	-1.672940000
C	4.673851000	2.128564000	-0.252691000
C	-4.705830000	2.169119000	-0.137986000
C	-4.784606000	-1.269715000	-1.729262000
C	4.846839000	0.624777000	-0.193530000
C	4.931863000	-0.776527000	1.813900000
C	-5.191081000	-1.304882000	3.032073000
C	-5.232993000	0.111404000	-1.382235000
C	8.870231000	0.002500000	-1.406990000
C	8.924352000	-1.079826000	3.100688000
C	-9.178555000	-0.865879000	1.760195000
C	-9.250414000	0.682013000	-0.137758000
C	9.331105000	-1.396196000	-1.650977000
C	9.380417000	2.152553000	-0.319563000
C	-9.410661000	2.186996000	-0.084039000
C	-9.498390000	-1.209678000	-1.762463000
C	9.557421000	0.651153000	-0.222324000
C	9.645382000	-0.697760000	1.819695000
C	-9.904227000	-1.364745000	2.996254000
C	-9.943347000	0.162729000	-1.379900000
H	-0.392923000	-2.313713000	3.155768000
H	-0.290455000	0.681470000	-2.263921000
H	0.014240000	-0.772035000	3.916251000
H	-0.746835000	-3.117306000	-2.228365000
H	0.955087000	3.883746000	-0.561937000
H	-10.203085000	-2.983164000	-2.405686000
H	10.353873000	3.846969000	-0.876904000
H	10.612864000	0.376466000	-0.229656000
H	-10.704526000	0.421944000	1.370784000
H	-10.895148000	-0.929618000	3.118302000
H	-11.025225000	0.221484000	-1.247443000
H	11.308458000	2.402925000	-0.979855000
H	-11.419383000	-1.790633000	-2.102166000
H	1.209426000	0.385593000	-0.188678000

H	-1.363087000	0.331413000	1.285779000
H	-1.543229000	-0.957417000	3.062291000
H	-1.620444000	0.107803000	-1.263627000
H	1.990744000	2.503365000	-0.548808000
H	-2.017875000	-1.949838000	-1.946829000
H	2.681178000	-2.034436000	-1.904943000
H	-2.698537000	2.514412000	-0.482052000
H	3.072654000	0.039544000	-1.273202000
H	3.158871000	-0.906177000	3.082562000
H	3.329743000	0.323515000	1.266410000
H	-3.487709000	0.386093000	-0.178674000
H	-3.732073000	3.894407000	-0.465642000
H	3.955536000	-3.204662000	-2.159566000
H	4.721361000	-0.714662000	3.926013000
H	4.399850000	0.592967000	-2.289079000
H	4.300269000	-2.268057000	3.198068000
H	-5.077413000	-2.385589000	3.109453000
H	-4.985233000	0.738343000	-2.247495000
H	-4.700309000	-0.848522000	3.894636000
H	-5.454512000	-3.059250000	-2.306126000
H	5.642056000	3.839996000	-0.670355000
H	5.902117000	0.351165000	-0.208398000
H	-6.056835000	0.311577000	1.297548000
H	-6.248334000	-1.045469000	3.027393000
H	-6.318138000	0.146156000	-1.262038000
H	6.676027000	2.460782000	-0.633246000
H	-6.718694000	-1.894185000	-1.998557000
H	7.400524000	-2.060521000	-1.863693000
H	-7.403323000	2.537532000	-0.415323000
H	7.784407000	0.038095000	-1.286497000
H	7.867459000	-0.819859000	3.082882000
H	8.040732000	0.382704000	1.243879000
H	-8.196785000	0.402624000	-0.171546000
H	-8.433959000	3.916046000	-0.359847000
H	8.678520000	-3.228645000	-2.088928000
H	9.418680000	-0.567344000	3.928743000
H	9.107720000	0.566490000	-2.317385000
H	-9.293094000	-1.123198000	3.867333000
H	9.035355000	-2.153093000	3.251384000
H	-9.688832000	0.808114000	-2.229376000
H	-9.987337000	-2.449904000	2.932915000
N	-0.404124000	0.101611000	1.053901000
N	-1.026900000	-2.176698000	-1.988315000
N	10.437540000	2.849683000	-0.740015000
N	-10.446690000	-2.052771000	-2.096562000
N	1.046796000	2.876830000	-0.574005000
N	-3.642509000	2.887917000	-0.504781000
N	3.672700000	-2.259421000	-1.942265000
N	4.291396000	0.095905000	1.042819000
N	-5.101339000	0.077442000	1.055979000
N	-5.729965000	-2.123656000	-2.042200000
N	5.733002000	2.833075000	-0.655546000
N	-8.346194000	2.911577000	-0.431877000
N	8.391725000	-2.279417000	-1.898106000
N	9.003070000	0.152772000	1.026705000
N	-9.811517000	0.067329000	1.055731000

O	-10.475254000	2.676246000	0.292256000
O	10.522945000	-1.689288000	-1.598102000
O	10.760905000	-1.157111000	1.567095000
O	-1.081354000	2.665669000	0.162224000
O	1.107724000	-1.613785000	-1.659108000
O	1.347038000	-1.243475000	1.529309000
O	-3.354131000	-1.282841000	1.497284000
O	-3.593955000	-1.574643000	-1.698865000
O	3.605916000	2.635167000	0.087707000
O	-5.771532000	2.664928000	0.226091000
O	5.804983000	-1.683769000	-1.627906000
O	6.045255000	-1.232729000	1.549701000
O	-8.068320000	-1.309058000	1.462520000
O	-8.308777000	-1.518170000	-1.739972000
O	8.310196000	2.665379000	0.007221000

5x ala (modified from pdb 5oqv)

115

symmetry c1

C	-0.014513000	2.164489000	-0.190011000
C	-0.083280000	-1.311757000	-1.697101000
C	0.154566000	0.660089000	-0.168162000
C	0.233643000	-0.790873000	1.803996000
C	-0.490112000	-1.232398000	3.063734000
C	-0.535204000	0.074722000	-1.383429000
C	4.157824000	0.007310000	-1.393631000
C	4.210044000	-1.188088000	3.084871000
C	-4.466448000	-0.834275000	1.783268000
C	-4.541509000	0.663758000	-0.152426000
C	4.614219000	-1.384878000	-1.672940000
C	4.673851000	2.128564000	-0.252691000
C	-4.705830000	2.169119000	-0.137986000
C	-4.784606000	-1.269715000	-1.729262000
C	4.846839000	0.624777000	-0.193530000
C	4.931863000	-0.776527000	1.813900000
C	-5.191081000	-1.304882000	3.032073000
C	-5.232993000	0.111404000	-1.382235000
C	8.870231000	0.002500000	-1.406990000
C	8.924352000	-1.079826000	3.100688000
C	-9.178555000	-0.865879000	1.760195000
C	-9.250414000	0.682013000	-0.137758000
C	9.331105000	-1.396196000	-1.650977000
C	9.380417000	2.152553000	-0.319563000
C	-9.410661000	2.186996000	-0.084039000
C	-9.498390000	-1.209678000	-1.762463000
C	9.557421000	0.651153000	-0.222324000
C	9.645382000	-0.697760000	1.819695000
C	-9.904227000	-1.364745000	2.996254000
C	-9.943347000	0.162729000	-1.379900000
H	-0.392923000	-2.313713000	3.155768000
H	-0.290455000	0.681470000	-2.263921000
H	0.014240000	-0.772035000	3.916251000
H	-0.746835000	-3.117306000	-2.228365000
H	0.955087000	3.883746000	-0.561937000
H	-10.203085000	-2.983164000	-2.405686000
H	10.353873000	3.846969000	-0.876904000

H	10.612864000	0.376466000	-0.229656000
H	-10.704526000	0.421944000	1.370784000
H	-10.895148000	-0.929618000	3.118302000
H	-11.025225000	0.221484000	-1.247443000
H	11.308458000	2.402925000	-0.979855000
H	-11.419383000	-1.790633000	-2.102166000
H	1.209426000	0.385593000	-0.188678000
H	-1.363087000	0.331413000	1.285779000
H	-1.543229000	-0.957417000	3.062291000
H	-1.620444000	0.107803000	-1.263627000
H	1.990744000	2.503365000	-0.548808000
H	-2.017875000	-1.949838000	-1.946829000
H	2.681178000	-2.034436000	-1.904943000
H	-2.698537000	2.514412000	-0.482052000
H	3.072654000	0.039544000	-1.273202000
H	3.158871000	-0.906177000	3.082562000
H	3.329743000	0.323515000	1.266410000
H	-3.487709000	0.386093000	-0.178674000
H	-3.732073000	3.894407000	-0.465642000
H	3.955536000	-3.204662000	-2.159566000
H	4.721361000	-0.714662000	3.926013000
H	4.399850000	0.592967000	-2.289079000
H	4.300269000	-2.268057000	3.198068000
H	-5.077413000	-2.385589000	3.109453000
H	-4.985233000	0.738343000	-2.247495000
H	-4.700309000	-0.848522000	3.894636000
H	-5.454512000	-3.059250000	-2.306126000
H	5.642056000	3.839996000	-0.670355000
H	5.902117000	0.351165000	-0.208398000
H	-6.056835000	0.311577000	1.297548000
H	-6.248334000	-1.045469000	3.027393000
H	-6.318138000	0.146156000	-1.262038000
H	6.676027000	2.460782000	-0.633246000
H	-6.718694000	-1.894185000	-1.998557000
H	7.400524000	-2.060521000	-1.863693000
H	-7.403323000	2.537532000	-0.415323000
H	7.784407000	0.038095000	-1.286497000
H	7.867459000	-0.819859000	3.082882000
H	8.040732000	0.382704000	1.243879000
H	-8.196785000	0.402624000	-0.171546000
H	-8.433959000	3.916046000	-0.359847000
H	8.678520000	-3.228645000	-2.088928000
H	9.418680000	-0.567344000	3.928743000
H	9.107720000	0.566490000	-2.317385000
H	-9.293094000	-1.123198000	3.867333000
H	9.035355000	-2.153093000	3.251384000
H	-9.688832000	0.808114000	-2.229376000
H	-9.987337000	-2.449904000	2.932915000
N	-0.404124000	0.101611000	1.053901000
N	-1.026900000	-2.176698000	-1.988315000
N	10.437540000	2.849683000	-0.740015000
N	-10.446690000	-2.052771000	-2.096562000
N	1.046796000	2.876830000	-0.574005000
N	-3.642509000	2.887917000	-0.504781000
N	3.672700000	-2.259421000	-1.942265000
N	4.291396000	0.095905000	1.042819000

N	-5.101339000	0.077442000	1.055979000
N	-5.729965000	-2.123656000	-2.042200000
N	5.733002000	2.833075000	-0.655546000
N	-8.346194000	2.911577000	-0.431877000
N	8.391725000	-2.279417000	-1.898106000
N	9.003070000	0.152772000	1.026705000
N	-9.811517000	0.067329000	1.055731000
O	-10.475254000	2.676246000	0.292256000
O	10.522945000	-1.689288000	-1.598102000
O	10.760905000	-1.157111000	1.567095000
O	-1.081354000	2.665669000	0.162224000
O	1.107724000	-1.613785000	-1.659108000
O	1.347038000	-1.243475000	1.529309000
O	-3.354131000	-1.282841000	1.497284000
O	-3.593955000	-1.574643000	-1.698865000
O	3.605916000	2.635167000	0.087707000
O	-5.771532000	2.664928000	0.226091000
O	5.804983000	-1.683769000	-1.627906000
O	6.045255000	-1.232729000	1.549701000
O	-8.068320000	-1.309058000	1.462520000
O	-8.308777000	-1.518170000	-1.739972000
O	8.310196000	2.665379000	0.007221000

1 Warner, C. J. A.; Dutta, S.; Foley, A. R.; Raskatov, J. A. A tailored HPLC purification protocol that yields high-purity amyloid beta 42 and amyloid beta 40 peptides, capable of oligomer formation. *J. Vis. Exp.*, **2017**, *e55482*

2 Kayed, R.; Head, E.; Thompson, J. L.; McIntire, T. M.; Milton, S. C.; Cotman, C. W.; Glabel, C. G. Common Structure of Soluble Amyloid Oligomers Implies Common Mechanism of Pathogenesis. *Science* **2003**, *300* (5618), 486–489.

3 Warner, C. J. A.; Dutta, S.; Foley, A. R.; Raskatov, J. A. Introduction of D-Glutamate at a Critical Residue of Aβ42 Stabilizes a Prefibrillary Aggregate with Enhanced Toxicity. *Chem. - A Eur. J.* **2016**, *22* (34), 11967–11970.

4 Hatami, A.; Monjazeb, S.; Milton, S.; Glabe, C. G. Familial Alzheimer's Disease Mutations within the Amyloid Precursor Protein Alter the Aggregation and Conformation of the Amyloid-β Peptide. *J. Biol. Chem.* **2017**, *292* (8), 3172–3185.

5 Frisch M. J. et al. Gaussian 09 Revision A.02 (Gaussian Inc. Wallingford, CT 2009)

6 Zhao, Y.; Truhlar, D. G. The M06 suite of density functionals for main group thermochemistry, thermochemical kinetics, noncovalent interactions, excited states, and transition elements: two new functionals and systematic testing of four M06-class functionals and 12 other functionals. *Theor. Chem. Acc.* **2008**, *120*, 215-241.

7 a) Harihara P. C.; Pople, J. A. Influence of Polarization Functions on Molecular-Orbital Hydrogenation Energies. *Theo. Chim. Acta* **1973**, *28*, 213-222. b) Hehre W. J.; Ditchfield, R.; Pople, J. Self—Consistent Molecular Orbital Methods. XII. Further Extensions of Gaussian—Type Basis Sets for Use in Molecular Orbital Studies of Organic Molecules *J. Chem. Phys.* **1972**, *56*, 2257-2261. c) Ditchfield R.; Hehre, W. J.; J. Pople, A; Self-Consistent Molecular-Orbital Methods. IX. An Extended Gaussian-Type Basis for Molecular-Orbital Studies of Organic Molecules *J. Chem. Phys.* **1971**, *54*, 724-728.

8 Dutta, S.; Foley, A. R.; Warner, C. J. A.; Zhang, X.; Rolandi, M.; Abrams, B.; Raskatov, J. A. Suppression of Oligomer Formation and Formation of Non-Toxic Fibrils upon Addition of Mirror-Image Aβ42 to the Natural l-Enantiomer. *Angew. Chemie - Int. Ed.* **2017**, *56* (38), 11506–11510.

CHEMISTRY
A European Journal

Supporting Information

Introduction of D-Glutamate at a Critical Residue of Aβ42 Stabilizes a Prefibrillary Aggregate with Enhanced Toxicity

Christopher J. A. Warner, Subrata Dutta, Alejandro R. Foley, and Jevgenij A. Raskatov*[a]

chem_201601763_sm_miscellaneous_information.pdf

Introduction of D-glutamate at a critical residue of Aβ42 stabilizes a pre-fibrillary aggregate with enhanced toxicity

SUPPORTING INFORMATION

Christopher J. A. Warner,[†] Subrata Dutta[†], Alejandro R. Foley and Jevgenij A. Raskatov[†,*]

†Department of Chemistry and Biochemistry, University of California Santa Cruz, Santa Cruz, CA 95064

* To whom correspondence should be addressed: jraskato@ucsc.edu

CONTENTS PAGE

Aβ synthesis, purification and reconstitution: Compounds **1** and **2** were synthesized on HMPB ChemMatrix resin, pre-loaded with L-Ala, employing standard Fmoc coupling chemistry conditions. Cleavage under acidic conditions with subsequent ether precipitation was followed by

HPLC purification, employing a PLRP-S column (8 µm, 300 Å) under basic conditions, as recommended by Agilent to attenuate on-column aggregation. The aqueous buffer (A) consisted of 20 mM ammonium hydroxide, whereas the organic buffer was composed of 80 % acetonitrile and 20 % 20 mM aqueous ammonium hydroxide. Following existing protocols by Teplow and co-workers[1], samples were lyophilized and taken up in 20 mM NaOH, adjusted to represent 5 % of the final volume, and diluted with either phosphate buffer or PBS, depending on the nature of the experiment (final pH was 7.4 in all cases).

Thioflavin T aggregation studies. Preparation of Thioflavin T solution: A ThT solution was freshly prepared before use. 4 mg of ThT was dissolved in 10 mL of commercially bought 1X-PBS buffer (pH 7.4, 10 mM) containing 0.02% (w/v) NaN_3. The solution was filtered through a 0.22 micron filter and the concentration of a 1/20 dilution of the filtrated solution was determined by Nanodrop (ε = 36000M^{-1} cm^{-1} at 412 nm). An aliquot of this stock solution was combined with 1X-PBS (10 mM, pH 7.4) containing 0.02% NaN_3 (w/v) to obtain a 100 µM ThT stock solution. Preparation of Aβ42 solution: 0.5 mg of 0.1% NH_4OH pretreated Aβ42 WT **1** or E22e **2** were freshly dissolved separately in 50 µL of 20 mM NaOH solution. The mixtures were sonicated for 30 s. Aβ42 solutions were then diluted by adding 450 µL of cold 1X-PBS (10 mM, pH 7.4) and filtered through 100 kDa MWCO spin filter (Corning® Spin-XR UF 500, catalog number: 431481) at 4 °C at 16200 rcf for 5 min. The filter was washed three times with cold 1X-PBS (pH 7.4) before use. The concentration of filtered Aβ42 solutions was measured by Nanodrop (ε = 1490 M^{-1} cm^{-1} at 280 nm). Preparation of ThT experiments: All experiments were conducted in black, clear bottom 96-well plates with shaking in a Molecular Device Gemini EM fluorescence plate reader (λem = 444 nm, λex = 485 nm) at 37 °C. Each well contained 200 µL of reaction solution containing 20 µM of peptide **1** or **2**, 20 µM ThT and 1X-PBS buffer (10 mM, pH 7.4) in presence of 0.02% (w/v) NaN_3. The wells were prepared in quintuplicate or greater and the plate was sealed with optically clear adhesive film. Each ThT assay was conducted for 2 hours at 37 °C. Readings were collected every 5 min with 5 s shaking before reading and 295 s shaking in between readings.

Circular Dichroism studies. Circular dichroism experiments were performed on a Jasco 1500 circular dichroism spectrometer set to a scan range of 180 to 280 nm, a DIT of 4 seconds and a scan speed of 50 nm per minute. For experiments involving wildtype Aβ42 **1**, 90 µg of NH_4OH pre-treated protein was dissolved in 20 µl of an aqueous solution of 20 mM NaOH and sonicated for 30 seconds. 380 µl of freshly prepared 20 mM phosphate buffer solution at a pH 7.4 not containing sodium chloride was then added resulting in a final concentration of 50 µM and final volume of 400 µl. The solution was immediately transferred to the cuvette and CD analysis undertaken. Following the initial analysis, the solution was removed from the cuvette and transferred to a low-bind 1.5 ml eppendorf tube and incubated in a mini-dry bath at 37 ºC for the appropriate time. This procedure was repeated for all time points collected. For the E22e **2** peptide the same procedure as described above was applied.

Photochemically induced crosslinking of unmodified proteins (PICUP): 4 µL of 1 mM $[Ru(bipy)_3]^{2+}$ and 4 µL of 20 mM ammonium persulfate were added to 32 µL of either a 50 µM or 20 µM solution of the reconstituted peptide in 20 mM phosphate buffer. The sample was irradiated for 1 s using the setup as shown in Image SI 1. Following irradiation the solution was immediately quenched with 40 µL of loading buffer containing 5% 2-mercaptoethanol. The oligomeric distribution of the peptide was determined by SDS-page gel electrophoresis using a 12% tris-tricine polyacrylamide

[1] Y. Fezoui, D. M. Hartley, J. D. Harper, R. Khurana, D. M. Walsh, M. M. Condron, D. J. Selkoe, P. T. Lansbury, A. L. Fink, D. B. Teplow, *Amyloid* **2000**, 7, 166–178.

gel. The voltage of the system was kept constant at 100V for 2 hours. Following electrophoresis the gels were silver stained and the oligomeric bands analyzed as previously reported.[2]

*Transmission electron microscopy (TEM) of wild-type **1** and E22e **2**.* Aβ42 wild-type **1** or Aβ42 E22e **2** fibrils were grown for 0h, 2h or 7 days at 37 ° C in 20 mM phosphate buffer (pH 7.4) at a concentration of 222 µM. At the appropriate time point, 1 µl of the fibril sample was added to 999 µl of milliQ water in order to obtain an imaging concentration of 200 nM. 3 µl aliquots of this material were adsorbed to activated carbon-coated Formvar 200 mesh copper grids for 1 minute and then negatively stained with 30 µl 1% (w/v) uranyl acetate. All fibrils were imaged by using FEI Tecnai 12 microscope at 120 kV.

*Small angle X-ray scattering (SAXS) of wild-type **1** and E22e **2**.* Small angle x-ray scattering was collected at the SIBYLS beamline at the Advanced Light Source (Berkeley, CA). All samples were ran at a concentration of 1 mg / ml (222 µM). Samples were exposed to the beamline for either 0.5, 1, 2 or 4 seconds. Samples were placed 1.5 m from a MAR165 CCD detector arranged coaxial with the 12 keV monochromatic beam; 10^{12} photons/second were impingent on the sample. Scattering data were plotted on log of x-ray intensity scale versus momentum transfer (q) in inverse Å, where $q = (4\pi \sin(\theta/2))/\lambda$, θ is the scattering angle relative to the incident beam, and λ is the wavelength.

Cytotoxicity analysis of peptides against the rat pheochromocytoma (PC12) cell line: Adhesive PC12 cells were purchased from ATCC (1721.1) and cultured in accordance with the supplier's instructions. For cytotoxicity experiments, cells were plated at a density of 5000 cells / well and incubated for 24 hours before dosing. Each well contained 100 µl total volume. For dosing, 100 µg of 0.1% NH_4OH pre-treated peptide was dissolved in 20 µl of 20 mM NaOH. The solution was diluted to a final concentration of 20 µM using 980 µl of F12-K media containing 2.5% FBS and 15% HS. 500 µl of this solution was removed to allow for serial dilution of the peptide concentration. Following 72 hour incubation, 10 µl of WST-1 (Roche) was added to each well and incubated for a further 2 hours. The absorbance at λ = 490 nm was used to determine cellular viability. For pre-incubation experiments the same protocol was used, except that samples were pre-incubated for indicated time periods in the cell culture media before dosing.

[2] G. Yamin, T.-P. V. P. Huynh, D. B. Teplow, *Biochemistry* **2015**, *54*, 5315–5321.

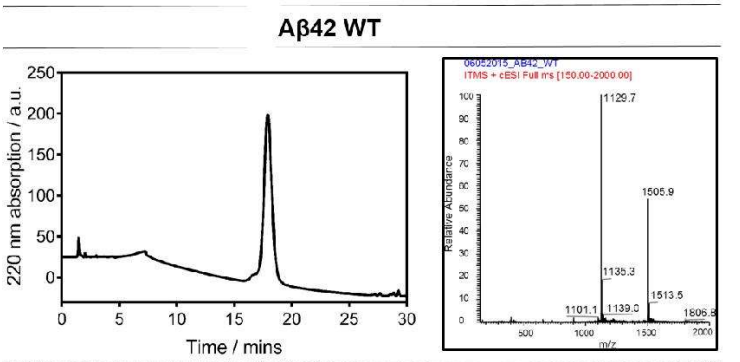

#	Time Start	Time End	Height	Area	Width	% Area
1	1.25395	1.9324156	24.501301	201.58136	1.4812154	1.84
2	1.9339499	2.2672834	5.63586	27.255154	2.0366676	0.2489
3	15.847283	20.787283	206.6098	10719.455	17.91662	97.909843

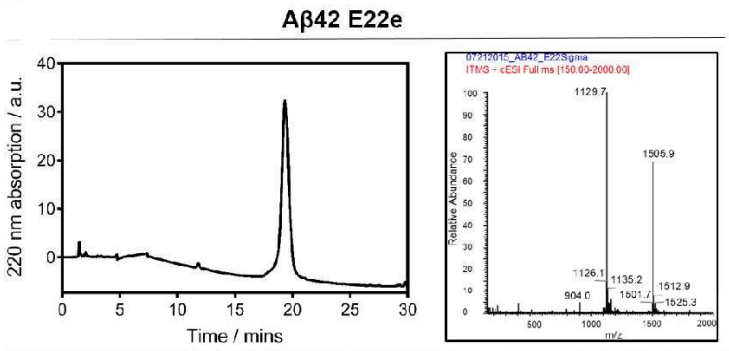

#	Time Start	Time End	Height	Area	Width	% Area
1	11.628821	12.074709	0.9981354	13.883545	0.2318247	0.8
2	17.2327	20.946033	36.508011	1719.9103	0.7056224	99.2

Figure S1, HPLC and mass spectrum analysis of the Aβ42 wildtype **1** and E22e **2** peptide. The purity of each peptide was >95% as determined by integration of signals at 220 nm.

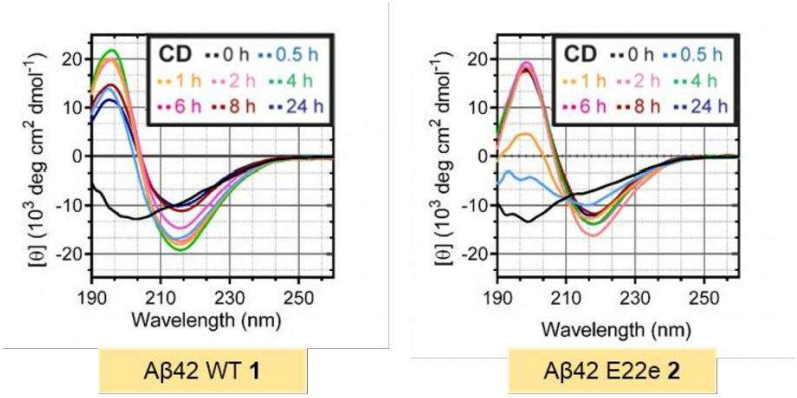

Figure S2, Circular Dichroism (CD) spectra of wildtype Aβ42 **1** and the E22e peptide **2**. The E22e peptide shows a delay in β-sheet formation compared to the wildtype.

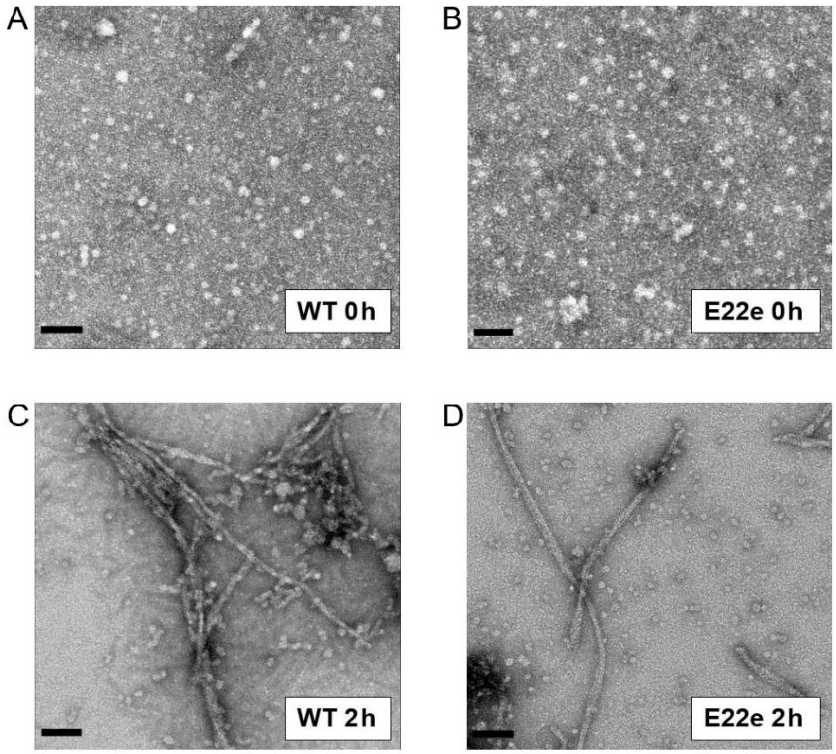

Figure S3, Transmission electron microscopy (TEM) images of the fibrillary architecture of Aβ42 wild-type peptide **1** (A, C) and Aβ42 E22e peptide **2** (B, D). Samples were taken for imaging immediately following reconstitution (A, B) or following 2 h of incubation (C, D) at 37 °C. In all instances samples were incubated in 20 mM phosphate buffer at a concentration of 222 μM before being diluted to 200 nM for imaging. Scale bar corresponds to 50 nm in all instances.

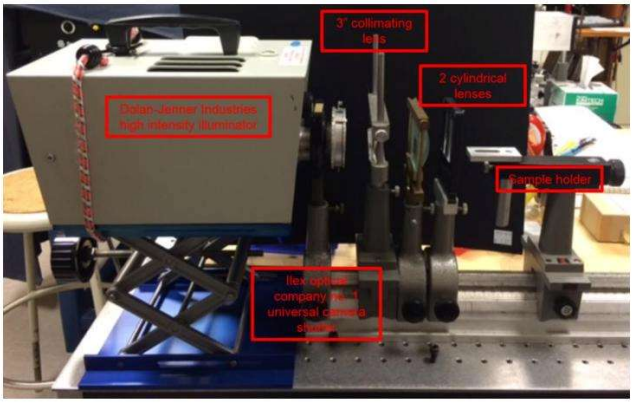

Image S1, The experimental setup of the PICUP experiment with each individual component labelled.

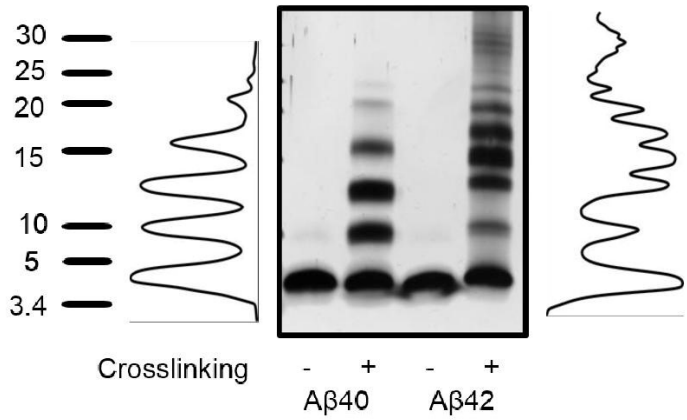

Figure S4, Validation of the PICUP experiment for wildtype Aβ40 and Aβ42. The experimental procedure for both peptides was identical and as described in the supporting information text. When crosslinking was not performed (denoted by the negative symbol) only the monomer is observable (band between 3.4 and 5 kDa). However, crosslinking of the solution gives rise to an oligomeric profile of both peptides almost identical to that observed by Teplow and co-workers.[3]

[3] G. Bitan, M. Kirkitadze, A. Lomakin, S. Vollers, G. Benedek, D. Teplow, *Proc. Natl. Acad. Sci. USA* **2003**, *100*, 330 – 335.

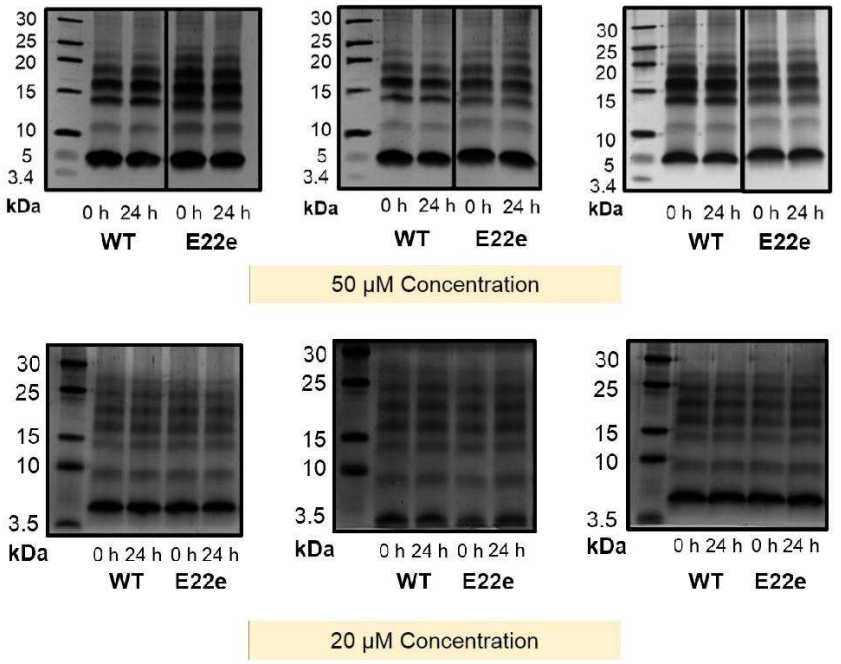

Figure S5, Photo-induced crosslinking of unmodified wild-type Aβ42 1 and E22e 2 at 50 and 20 µM and at either 0 h or following incubation for 24 h at 37 °C. All samples were reconstituted in 20 mM phosphate buffer.

10

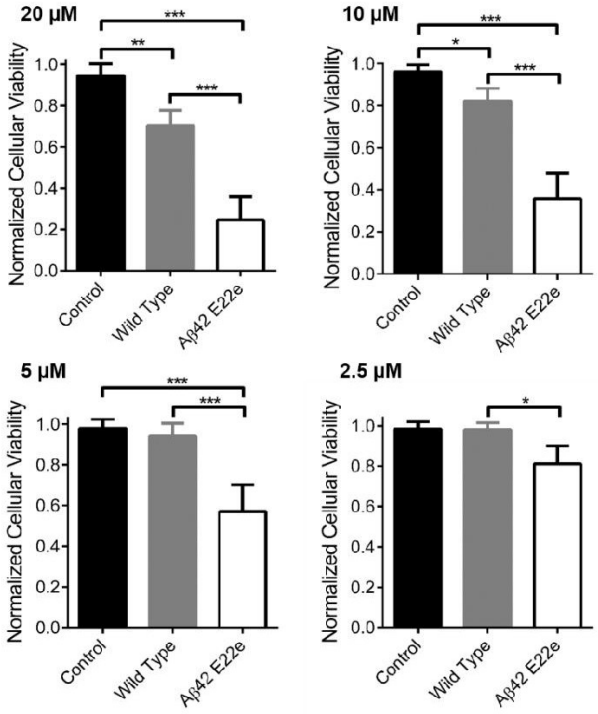

Figure S6, Cytotoxicity studies of both wild-type Aβ42 **1** (grey bars) and Aβ42 E22e **2** (white) peptides against the rat pheochromocytoma PC12 adhesive cell lines. Cells were plated at 5000 cells per well and allowed to adhere for 24 hours prior to peptide addition and for a further 72 hours following dosing. Cellular viability was determined at the end point of the assay using the reagent WST-1. Three biological replicates each consisting of three technical replicates were used for analysis.

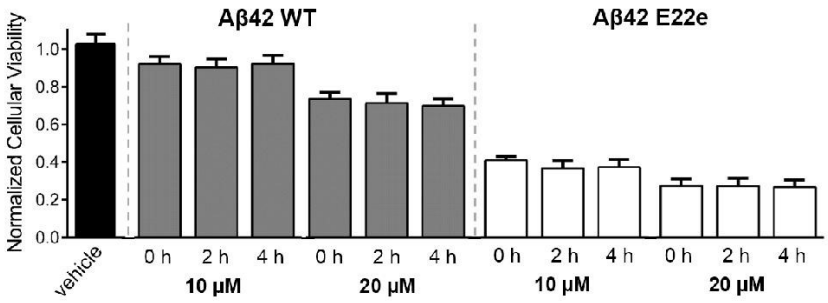

Figure S7, The effect of pre-incubation of the peptides prior to dosing to the PC12 cells. Both Aβ42 wild-type **1** and E22e peptide **2** showed comparable cytotoxicity, following either 2 h or 4 h of pre-incubation. Cells were plated at 5000 cells per well and allowed to adhere for 24 hours prior to peptide addition and for a further 72 hours following dosing. Cellular viability was determined at the end point of the assay using the reagent WST-1. Three biological replicates, each consisting of two technical replicates, were used for analysis.

Using Chiral Peptide Substitutions to Probe the Structure Function Relationship of a Key Residue of Aβ42

SUPPORTING INFORMATION

Christopher J. A. Warner[a], Subrata Dutta[a], Eefei Chen[a], Alejandro R. Rodriguez[a], David S. Kliger,[a] and Jevgenij A. Raskatov[a],*

† Department of Chemistry and Biochemistry, University of California Santa Cruz, Santa Cruz, CA

* To whom correspondence should be addressed: jraskato@ucsc.edu

CONTENTS PAGE

Data analyses of the beta-sheet transition comparison of wildtype Aβ42 and E22 mutants

After each CD analysis the raw data was subjected to both the baseline correction and smoothing algorithm built into the JASCO software. The smoothing parameter for all spectra was set to 15. All data were exported as csv files and all spectra plotted using Graphpad prism v6. To generate the values of Aβ42 wildtype, E22D, E22d and E22e used for figure 3, the [θ] value at 195 nm of a given peptide at a particular time point was subtracted from the initial [θ] value of that peptide at 195 nm. The data was then normalized to the maximum 195 nm [θ] value of the peptide in question. This value was chosen as it represented the point at which maximum β-sheet transition of the peptide had occurred. A similar analysis was undertaken for the E22G, E22A and E22a mutants, however, the lack of random coil to β-sheet transition dictated that the loss of [θ] signal at 217 nm was monitored as a means of examining the aggregation of the peptide. The same subtraction and normalization procedures used for the Aβ42 wildtype, E22D E22d and E22e were utilized.

The following values were therefore calculated from these data analyses:

SI Table 1. The normalized values used to calculate the heatmap as observed in figure 3 of the manuscript for the E22 mutants.

Time / h	Aβ42 WT	E22D	E22A	E22G	E22a	E22d	E22e
0	0	0	0.716	0.967	0.782	0	0
0.5	0.702	0.212	0.997	0.969	0.885	0.230	0.266
1	0.915	0.345	1	1	1	0.335	0.548
2	0.944	0.453	0.965	0.636	0.953	0.618	0.976
4	1	0.806	0.914	0.285	0.896	0.818	0.977
6	0.939	0.987	0.857	0.259	0.880	1	1
8	0.786	1	0.732	0.390	0.793	0.939	0.949
24	0.700	0.939	0.660	0.159	0.402	0.885	0.959

The heat map displayed in figure 3 was generated using R 3.2.2 with the RColorBrewer and gplots software loaded into the program. The heatmap.2 function was used to generate the heatmap along with a colorRampPalette(c("red", "white", "blue"))(n = 299) to represent secondary structure transition and a colorRampPalette(c("yellow", "white"))(n = 299) to represent the precipitation of the sample from solution. In all instances the color blue represents the random coil secondary structure of the peptide whilst the color red represents the β-sheet secondary structure. In both instances the intensity of the color is a determinant of the strength of the particular secondary structure in question.

To calculate the values for the graphical change in [θ] at 195 nm as observed in figure 3b, an identical approach was undertaken to that outlined above except that for all four mutants analyzed – wildtype Aβ42, E22D, E22d and E22e the data was normalized to the [θ] value at 195 nm at four hours following subtraction of the time point from the initial value of [θ] at 195 nm. The four hour time point was chosen as this was the point at which the maximum β-sheet structure of the wildtype peptide was ascertained. The values used to plot this data are outlined in the table below:

SI Table 2. The normalized change at 195 nm values used to produce the graph of the wildtype Aβ-42 and E22D, E22d and E22e mutants displayed in figure 3 of the manuscript

Time / h	Aβ42 WT		E22D		E22d		E22e	
	Run 1	Run 2	Run 1	Run 2	Run 1	Run 2	Run 1	Run 2
0	0	0	0	0	0	0	0	0
0.5	0.702	0.640	0.263	0.246	0.282	0.256	0.271	0.235
1	0.915	0.943	0.429	0.398	0.410	0.414	0.579	0.524
2	0.944	0.965	0.562	0.576	0.755	0.736	0.990	0.977
4	1	1	1	1	1	1	1	1

SI Table 3. Secondary structure deconvolution of all peptides used in the study. The spectra were deconvoluted using the CONTINLL data set 6 and the DichroWeb algorithms. The graphical plots of the helical and turn content of the peptide can be found in SI Figure 5.

Aβ42		Incubation period (h)							
		0	0.5	1	2	4	6	8	24
WT **1**	α-helix	0.086	0.153	0.174	0.168	0.17	0.15	0.148	0.14
	β-strand	0.231	0.329	0.361	0.37	0.374	0.384	0.383	0.384
	Turns	0.156	0.197	0.176	0.178	0.173	0.178	0.186	0.188
	Unordered	0.556	0.32	0.289	0.284	0.284	0.28	0.283	0.288
E22D **2**	α-helix	0.031	0.044	0.049	0.057	0.063	0.061	0.08	0.076
	β-strand	0.166	0.229	0.233	0.296	0.449	0.486	0.443	0.445
	Turns	0.133	0.158	0.159	0.198	0.21	0.166	0.202	0.198
	Unordered	0.67	0.568	0.559	0.449	0.336	0.297	0.274	0.281
E22A **3**	α-helix	0.033	0.042	0.063	0.051	0.055	0.052	0.063	0.062
	β-strand	0.363	0.4	0.403	0.444	0.434	0.427	0.432	0.437
	Turns	0.133	0.158	0.159	0.198	0.21	0.166	0.202	0.198
	Unordered	0.404	0.332	0.314	0.294	0.294	0.308	0.309	0.303
E22G **4**	α-helix	0.036	0.036	0.036	0.038	0.038	0.046	0.039	0.035
	β-strand	0.398	0.4	0.397	0.405	0.405	0.4	0.402	0.397
	Turns	0.205	0.207	0.205	0.197	0.197	0.193	0.201	0.192
	Unordered	0.361	0.361	0.362	0.36	0.36	0.361	0.358	0.361
E22a **5**	α-helix	0.045	0.037	0.037	0.045	0.048	0.054	0.059	0.074
	β-strand	0.212	0.487	0.53	0.521	0.504	0.495	0.496	0.472
	Turns	0.187	0.175	0.182	0.19	0.202	0.204	0.19	0.195
	Unordered	0.555	0.307	0.251	0.244	0.247	0.249	0.255	0.259
E22d **6**	α-helix	0.029	0.045	0.053	0.26	0.099	0.095	0.085	0.07
	β-strand	0.225	0.295	0.317	0.397	0.481	0.455	0.487	0.493
	Turns	0.149	0.184	0.2	0.19	0.181	0.202	0.182	0.198
	Unordered	0.598	0.476	0.429	0.339	0.238	0.248	0.245	0.239
E22e **7**	α-helix	0.031	0.051	0.065	0.043	0.045	0.039	0.058	0.046
	β-strand	0.21	0.303	0.414	0.505	0.517	0.517	0.504	0.511
	Turns	0.129	0.188	0.189	0.182	0.198	0.198	0.191	0.2
	Unordered	0.629	0.459	0.333	0.241	0.24	0.245	0.247	0.243

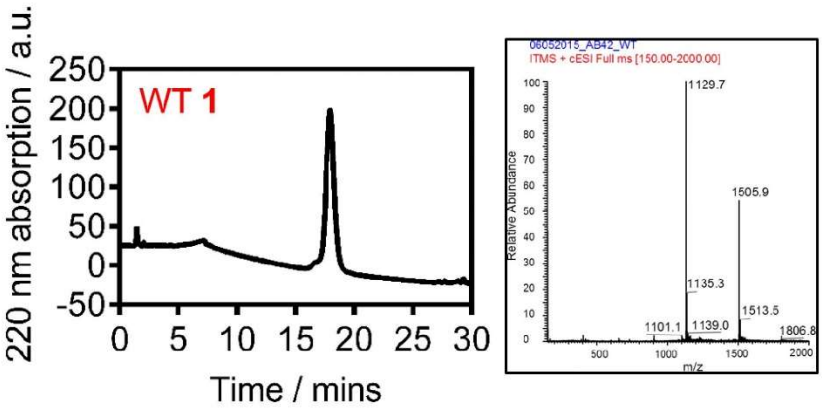

#	Time Start	Time End	Height	Area	Width	% Area
1	1.25395	1.9324155	24.501301	201.58136	1.4812154	1.84
2	1.9339499	2.2672834	5.63586	27.255154	2.0366676	0.2489
3	15.847283	20.787283	206.6098	10719.455	17.91662	97.909843

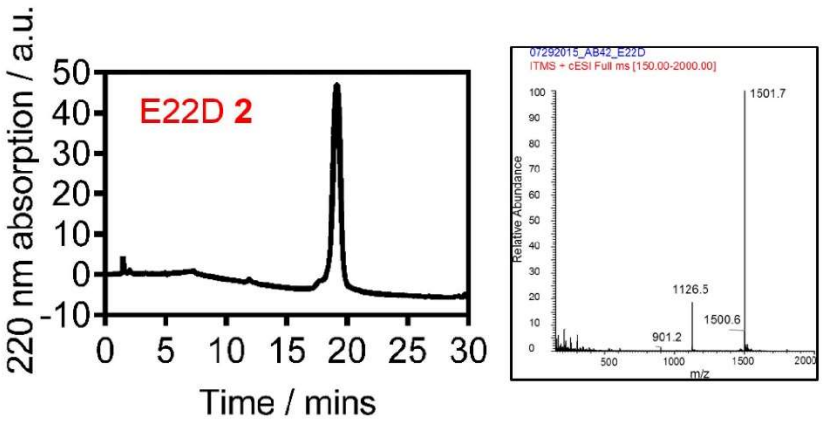

#	Time Start	Time End	Height	Area	Width	% Area
1	17.27706	17.926933	25.236897	0.7722232	0.3966097	1.52
2	18.047928	20.158461	2143.9646	49.742474	0.7183548	98.48

6

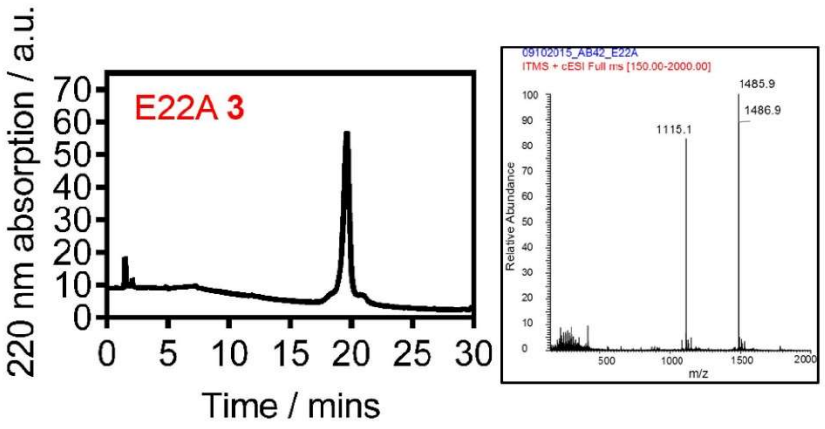

#	Time Start	Time End	Height	Area	Width	% Area
1	17.945656	18.610247	0.980135	28.139277	0.4784932	1.5753101
2	18.657515	20.605528	50.044262	1702.8347	0.5671095	95.329132
3	20.69071	21.528673	1.4815079	55.294994	0.6220576	3.0955581

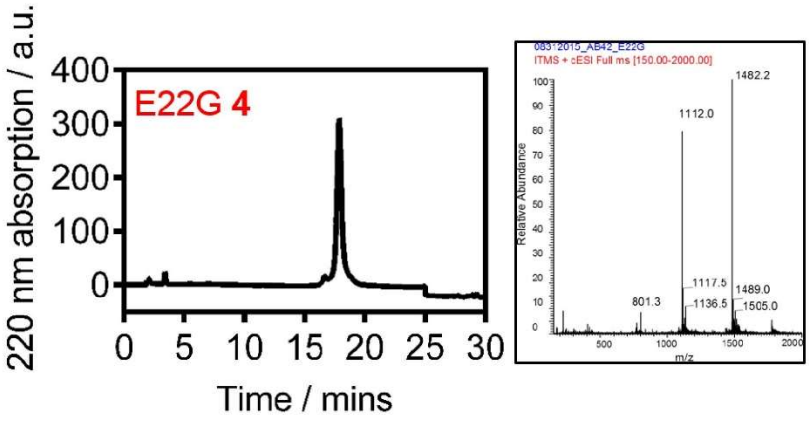

#	Time Start	Time End	Height	Area	Width	% Area
1	3.2613585	3.6403258	22.091442	195.62532	0.1475876	1.9597321
2	16.369169	16.837307	8.9332428	153.70396	0.286764	1.539773
3	16.837307	19.334032	304.91834	9632.9189	0.52653	96.500495

7

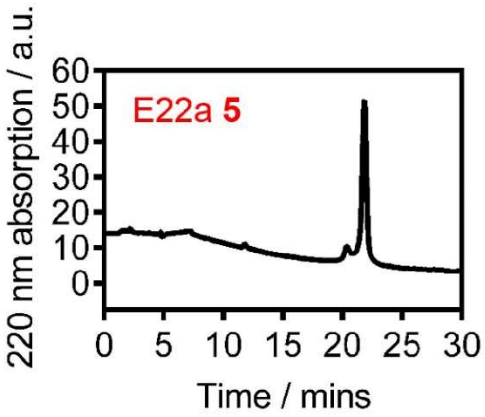

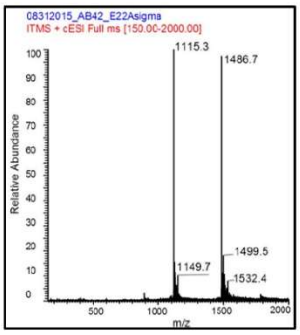

#	Time Start	Time End	Height	Area	Width	% Area
1	19.814167	20.7575	2.845887	53.68169	0.337062	4.38
2	20.760834	23.20083	44.70216	1168.076	0.394852	95.62

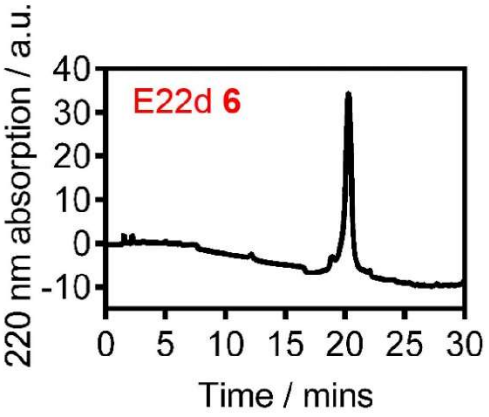

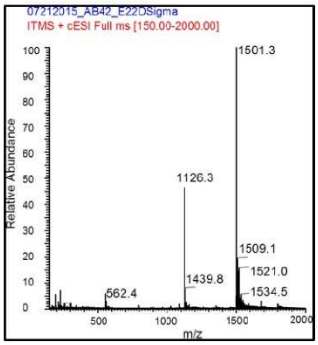

#	Time Start	Time End	Height	Area	Width	% Area
1	17.553356	19.414246	2.6873088	74.959709	0.3954297	3.9
2	17.371666	22.471666	41.98616	1841.9249	0.6238145	96.1

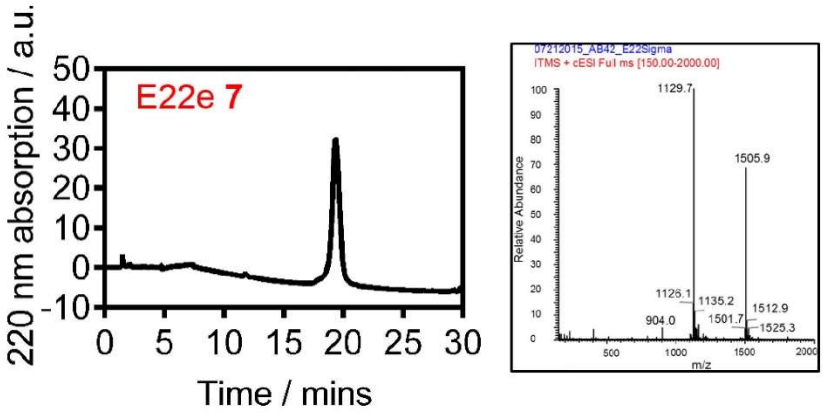

#	Time Start	Time End	Height	Area	Width	% Area
1	11.628821	12.074709	0.9981354	13.883545	0.2318247	0.8
2	17.2327	20.946033	36.508011	1719.9103	0.7056224	99.2

SI Figure 1. HPLC and mass spectra of each of the Aβ42 peptides used in the study.

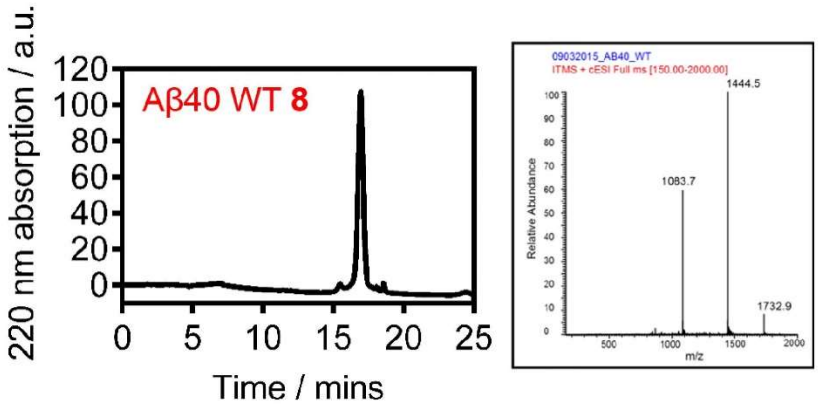

#	Time Start	Time End	Height	Area	Width	% Area
1	15.203939	15.732491	47.719524	2.6901407	0.2956445	1.54
2	15.88198	17.92144	2991.0178	110.32969	0.4518303	96.7
3	17.985506	18.177708	11.225857	1.6943551	0.1104241	0.36
4	18.428635	18.738291	32.458988	5.2238507	0.1354652	1.37

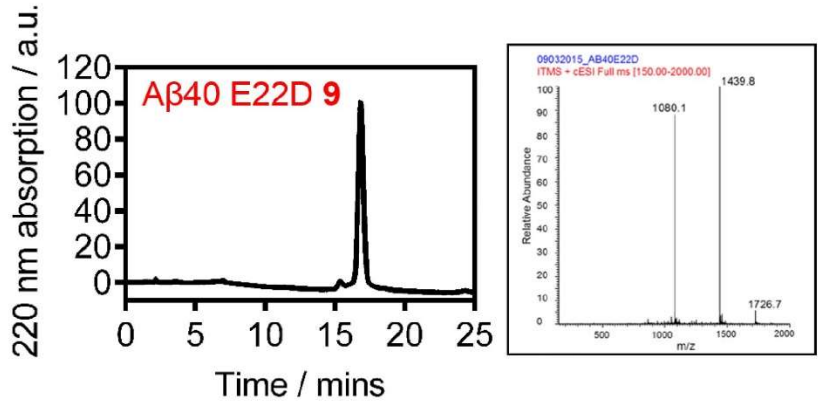

#	Time Start	Time End	Height	Area	Width	% Area
1	15.013103	15.747527	94.333092	3.9452105	0.3985131	3.6
2	15.954083	17.927845	2905.5957	104.19215	0.4847816	96.4

SI Figure 2. HPLC and mass spectra of each of the Aβ40 peptides used in the study.

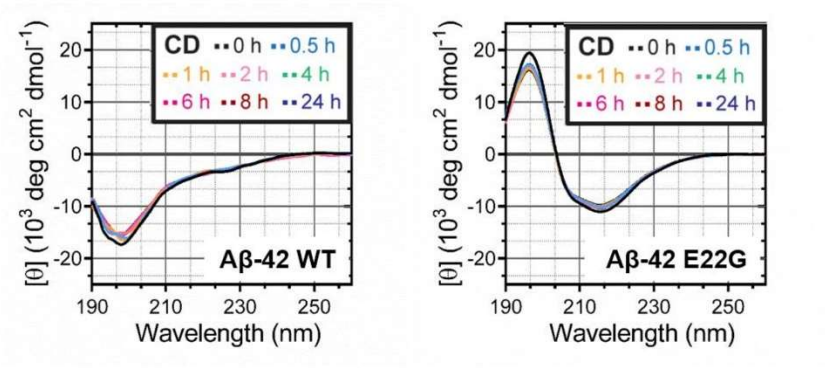

SI Figure 3. Circular dichroism of Aβ42 WT peptide **1** and the E22G peptide **2** at pH 12; A) Time resolved CD spectra of Aβ42 wild-type, left and Aβ42 E22G.

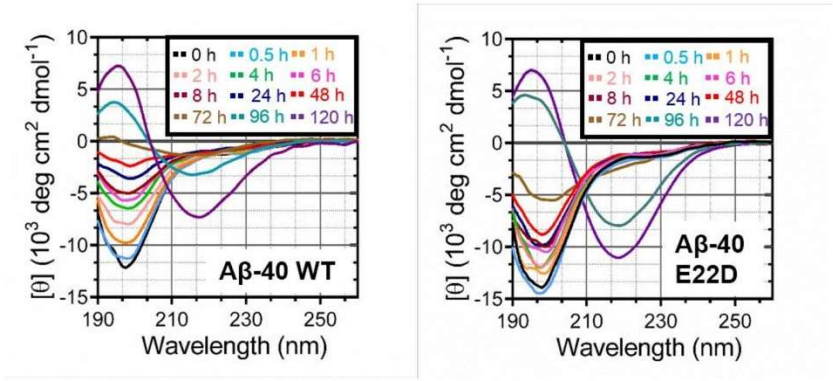

SI Figure 4. Time resolved circular dichroism of Aβ40 WT peptide **8** and Aβ40 E22D peptide **9**.

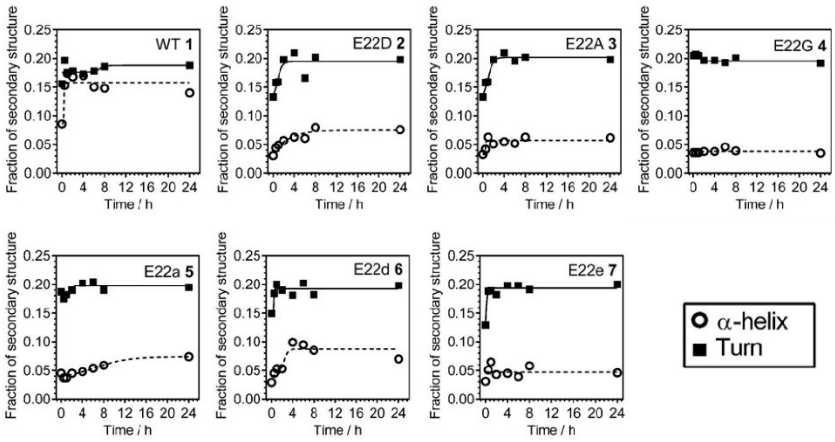

SI Figure 5. A graphical representation of the fraction of α-helical and turn secondary structure in the peptides **1 – 7**. The values that were used for the graphs can be found in SI Table 3.

Angewandte
Eine Zeitschrift der Gesellschaft Deutscher Chemiker Chemie

Supporting Information

Suppression of Oligomer Formation and Formation of Non-Toxic Fibrils upon Addition of Mirror-Image Aβ42 to the Natural L-Enantiomer

*Subrata Dutta, Alejandro R. Foley, Christopher J. A. Warner, Xiaolin Zhang, Marco Rolandi, Benjamin Abrams, and Jevgenij A. Raskatov**

anie_201706279_sm_miscellaneous_information.pdf

Supporting Information

CONTENTS PAGE

Experimental Procedures

Loading of D-alanine.

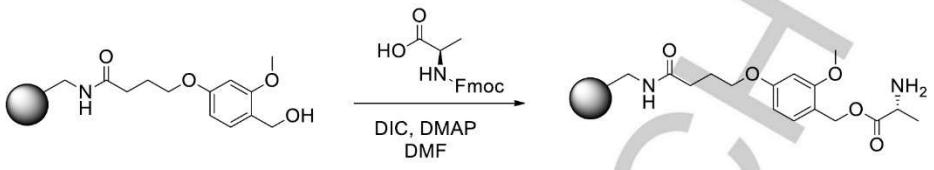

HMPB ChemMatrix® resin D-Ala loaded HMPB ChemMatrix® resin

Swelling of the resin: 200 mg of HMPB ChemMatrix® resin (Sigma-Aldrich, Cat no. 727741) was swelled by suspending the resin in 4 mL of DMF for 30 minutes.

Coupling of Fmoc-D-alanine to the resin: 312 mg (10 eq) of Fmoc-D-alanine was dissolved in 25 mL of dry DCM (trace quantities of DMF were added to ensure complete dissolution). 64 µL (5 eq.) of diisopropylcarbodimide (DIC) dissolved in 0.5 mL of dry DCM was added to the solution, and the mixture stirred for 20 minutes at 0˚C. A calcium chloride drying tube was attached to the flask during this period. The DCM was removed by evaporation *in vacuo* and the resultant solid re-dissolved in 6 mL of DMF. The solution was added to the swelled resin. 1.2 mg (0.1 eq.) of DMAP in 0.5 mL of DMF was also added to the resin/amino acid mixture and the suspension agitated for 1 h. The resin was filtered, washed with 10 mL DMF (x3) and 10 mL of DCM (x3) and dried overnight.

Calculating D-alanine loading: 10 mg of the loaded resin was weighed into a scintillation vial. 0.5 mL of 30% piperidine in DMF was added to the resin and the mixture incubated for 30 minutes. 19.5 mL of absolute ethanol was added and the mixture incubated for a further 30 minutes. The resulting solution was then measured *via* UV-Vis spectroscopy (ε = 6566 M^{-1} cm^{-1} at 300 nm). The following equations were used to determine the amount of released Fmoc.

Loading of the resin (mmol/g) = 3.05 × A_{300}/m
(m= mass of the resin; A_{300} = absorbance at 300 nm)

See also http://www3.appliedbiosystems.com/cms/groups/psm_marketing/documents/generaldocuments/cms_040640.pdf

Synthesis of L-Aβ42 and D-Aβ42 by solid phase peptide chemistry.
The amyloid beta peptides were synthesized by Fmoc chemistry, following our previously reported protocols.[1] For L-Aβ42, 160mg of HMPB ChemMatrix® resin, pre-loaded with L-alanine (Sigma-Aldrich, cat no. 727822) was used. For D-Aβ42, 160 mg of HMPB ChemMatrix® resin pre-loaded D-alanine was used. Before the start of each coupling sequence, the resin was swelled with DMF for 20 min before being placed into the CEM Liberty automated microwave-assisted peptide synthesizer. All syntheses were run on 0.1 mmol scale. Cleavage and purification of the two Aβ42 enantiomers was conducted according to our previously published methods, yielding peptides with purities exceeding 95 % (Figure S1). [1]

Circular dichroism (CD) experiments
90 µg of L-Aβ42 or D-Aβ42 peptide was dissolved in 20 µL of 20 mM NaOH and sonicated for 30 seconds. For the racemic mixture, 45 µg of L-Aβ42 and 45 µg of D-Aβ42 were dissolved separately in 10 µL of 20 mM NaOH solution each, and then mixed to yield racemic Aβ42. Subsequently, 380 µL of freshly prepared 20 mM phosphate buffer solution (pH 7.4) were added to yield a final concentration of 50 µM *rac*-Aβ42 in a final volume of 400 µL. Spectra were recorded using a Jasco 1500 CD spectrophotometer, set to a scan range of 180 to 280 nm, a DIT of 4 seconds and a scan speed of 50 nm per minute.

Thioflavin T (ThT) assay
Preparation of ThT stock solution: The 100 µM ThT stock solution was prepared as described previously.[1] *Preparation of Aβ solution:* 1 mg of either L-Aβ42 or D-Aβ42 was freshly dissolved in 100 µL of 20 mM NaOH solution and sonicated for 30 s. Filters were washed three time with cold 20 mM NaOH before use. Aβ42 solutions were then filtered through 100 kDa MWCO spin filter (Corning® Spin-XR UF 500, catalog number: 431481) at 4 °C at 14,000 g for 10 min. The concentrations of the resultant Aβ42 stock solutions were measured by Nanodrop (ε = 1490 M^{-1} cm^{-1} at 280 nm) and diluted back to the final concentration of 5 mg/mL (1.1 mM) by adding 20 mM NaOH. These stock solutions were diluted to final working concentrations, using PBS (see below). *Preparation of ThT experiments:* All experiments were conducted in black, clear bottom 96-well plates with shaking in a Molecular Device Gemini EM fluorescence plate reader (λ_{ex} = 444 nm, λ_{em} = 485 nm) at 37 °C. Each well contained 200 µL of aggregating mixture containing either L-Aβ42 or D-Aβ42 peptide (20 µM or 10 µM) or racemic-Aβ42 (40 µM, 20 µM or 10 µM total concentration) in presence of 20 µM ThT in PBS, containing 0.02% (w/v) NaN_3. All experiments were run in quintuplicate and the plate was sealed with optically clear adhesive film. Readings were collected every 5 min with 5 s shaking before reading and 295 s shaking in between readings. Total experiment duration was 24 h.

TEM experiment
The samples of Aβ42 for TEM were taken directly from ThT assays (see above) after 24 h. For specimen preparation, 3 µL of sample was spotted onto freshly glow-discharge carbon-coated electron microscopy grid (Ted Pella, Catalog No. 01701-F). Grids were rinsed with 5 µL of milliQ water after 1 min incubation, followed by staining with 30 µL 1% uranyl acetate. All fibrils were imaged by using JEOL 1230 microscope at an accelerating voltage of 120 kV.

Experiments with flulorescently labeled Aβ42 peptides

A. Chemical procedures to make N-terminally fluoresently labeled Aβ42 peptides. L-Aβ42 and D-Aβ42 peptides were synthesized on TentaGel S PHB resin by Fmoc chemistry. 50 mg of either L-Aβ42 or D-Aβ42 (~ 5 µmol) loaded resin (fully protected except the terminal primary amino group) was swelled by suspending the resin in 1 mL of dry DMF for 30 minutes. A mixture of 5(6)-carboxy-tetramethylrhodamine (TAMRA-COOH, 28 mg, 50 µmol), benzotriazol-1-yl-oxytripyrrolidinophosphonium hexafluorophosphate (PyBOP, 31.3 mg, 50 µmol) and 1-Hydroxy-7-azabenzotriazole (HOAt, 16 mg, 100 µmol) was dissolved in 1 mL dry DMF and diisopropylethylamine (8.6 µL, 50 µmol) was added. In a separate vial, 5(6)-carboxyfluorescein (FAM-COOH, 20 mg, 50 µmol), PyBOP (31.3 mg, 50 µmol) and HOAt (16 mg, 100 µmol) was dissolved in 1 mL dry DMF and diisopropylethylamine (8.6 µL, 50 µmol) was added. The TAMRA-COOH mixture was added to the D-Aβ42 resin and FAM-COOH mixture was added to L-Aβ42 resin and each mixture was shaken for 4 h, then filtered, washed with DMF (3 x 1 ml) and then DCM (3 x 1 ml) and dried in vacuo for 30 min. The conjugates were cleaved from solid support and deprotected with cocktail solution containing trifluoroacetic acid (4 mL), 1, 2-diethanethiol (0.25 mL), tri-isopropylsilane (0.5 mL) and liquefied phenol (0.25 mL). Both the peptides were purified by HPLC, yielding peptides with purities exceeding 95 % (Figure S6).

B. Conditions to grow fibrils used in confocal experiments. L-Aβ42-FAM or D-Aβ42-TAMRA (0.2 mg in either case) were dissolved in 20 µL of 20 mM NaOH and sonicated for 30 s, then spin-filtered through 100 kDa MWCO filter at 14000 g for 10 min. The concentrations of the resultant stock solutions were measured by Nanodrop (ε = 68000 M^{-1} cm^{-1} at 494 nm for FAM, ε = 99000 M^{-1} cm^{-1} at 555 nm for TAMRA). These stock solutions were then diluted to the final concentrations of 20 µM in PBS. Racemic Aβ42 was prepared by mixing 1:1 molar ratio of L-Aβ42-FAM and D-Aβ42-TAMRA and then diluted to 40 µM total concertation of Aβ42. Fibrils were grown in a 96-well plate at 37 ˚C with shaking in Molecular device Gemini plate reader, mimicking the conditions used in ThT experiments (Figure 1 of the manuscript and associated text). After 24 h fibrils from either enantiopure Aβ42 (L-Aβ42-FAM or D-Aβ42-TAMRA) or racemic Aβ42 peptides were imaged by confocal microscope (Figure 2 of the manuscript and associated text). For control experiment, fibrils from L-Aβ42-FAM and D-Aβ42-TAMRA were mixed 1:1 ratio after 24 h. To visualize the fibrils, two different channels were used (For FAM: 476 nm laser was used for excitation and signal was collected between 484 nm and 514 nm, for TAMRA: 543 nm laser was used for excitation and signal was collected between 630 nm and 690 nm). Control TEM experiments were conducted, employing conditions as described above, and demonstrate that fibrils were being formed with the fluorescently labeled Aβ42 analogs under those conditions (Figure S7).

C. Confocal Microscopy. 5 µL of each sample was spotted on a coverslip and imaged on a Leica SP5 confocal microscope using a 63x/1.2 HCX PL APO water immersion objective. Zoom and frame size were set to achieve 96 nm pixels, just under Nyquist sampling. The gain and offset levels were kept constant across all the samples.

D. Image Processing to calculate Pearson Correlation Coefficients (PCC). Images were processed by using ImageJ (FIJI). A despeckle filter was applied to remove noise. For display, the brightness minimum values were left at zero for all panels. The max intensity display value for the TAMRA images were set to 10,000 for all panels. The max intensity display value FAM was set to 10,000 for panels B and C, but since we found that FAM was significantly brighter in isolation (panels A and D) we set the max intensity display value to 40,000 to avoid blowing out the detail. For the colocalization analysis raw images were processed using "despeckle" and "subtract background" in ImageJ (FIJI) and then brought into Imaris for further analysis using the Colocalization module. The Pearson's coefficients reported are across the whole image. The racemic mix images gave an average Pearson's coefficient in the dataset volume of 0.93 over 10 images (Figure 2C). The Mixed, but not incubated TAMRA- and FAM -labeled particles gave a Pearson's coefficient in the dataset volume of 0.03 over 7 images (Figure 2D). On the Pearson scale, perfect correlation results in a value of 1, no correlation gives a value of 0 and perfect anti-correlation gives -1. Manders coefficients were also calculated. In the racemic mix the Manders coefficients were 0.81 and 0.85 for FAM and TAMRA respectively (Figure 2C) while the Mixed, but not incubated samples gave 0.15 and 0.03 for FAM and TAMRA respectively (Figure 2D). The Manders scale ranges from 0 to 1 for each channel, with 1 being perfect overlap and 0 being perfect separation.

Photochemically induced crosslinking of unmodified proteins (PICUP)
4 µL of 1 mM $[Ru(bipy)_3]^{2+}$ and 4 µL of 20 mM ammonium persulfate were added to 32 µL of 50 µM enantiopure Aβ42 (L-or D-) or 50 µM of L-Aβ42 and 50, 25, 12.5, 6.25, 3.125 or 1.56 µM of D-Aβ42 in 20 mM phosphate buffer. The sample was irradiated for 1 s with our previously reported setup.[1] Following irradiation, the solution was immediately quenched with 40 µL of loading buffer containing 5% 2-mercaptoethanol. The oligomeric distribution of the peptide was determined by SDS-page gel electrophoresis, using a 12% tris-tricine polyacrylamide gel. The voltage of the system was kept constant at 100 V for 2 h. The amount of peptide loaded into each well was kept constant (2.7 µg). Following electrophoresis, gels were silver stained and the oligomeric bands analyzed as previously reported. [1]

Formation of oligomers for TEM and AFM imaging experiments.
0.5 mg of either L-Aβ42 or D-Aβ42 was freshly dissolved in 50 µL cold 20 mM NaOH solution and sonicated for 30 s. Afterwards, the solutions were filtered through 100 kDa MWCO spin filter at 14000 g for 5 min at 4 ˚C. The concentration of the filtrate L-Aβ42 or D-Aβ42 solutions was measured by Nanodrop (ε = 1490 M^{-1} cm^{-1} at 280 nm). These stock solutions were then diluted to a final

concentration of 20 μM total Aβ42 concentration in cold PBS. Racemic- Aβ42 was prepared by combining L and D-Aβ42 after spin filtration in 1:1 molar ratio and diluted to 20 μM in cold PBS. Oligomers were formed by keeping the solutions at 4 ˚C for 6 h. [2]

TEM grid preparation and imaging
A 3 μL aliquot of Aβ42 (L-, D- or rac- Aβ42) oligomer solution was spotted onto freshly glow-discharge carbon-coated electron microscopy grid (Ted Pella, Catalog No. 01701-F). After 1 minute incubation, the grids were rinsed with 5 μL of milliQ water, followed by staining with 30 μL 1% uranyl acetate. All aggregation intermediates were imaged by using JEOL 1230 microscope at an accelerating voltage of 120 kV. See SI Appendix B for further details on data analysis, as well as full imaging datasets.

AFM sample preparation and imaging
5 μL of Aβ42 (L-, D- or rac- Aβ42) oligomer solution was drop-casted onto freshly taped mica substrate with 3M Scotch® Magic™ tape. The solution was left on the substrate for 5 min, and then rinsed with a constant stream of miliQ water for 2 minutes. The substrate was then dried with a stream of filtered nitrogen gas. AC Air Tapping mode Atomic Force Microscopy (AFM) was performed on an Asylum MFP-3D Infinity System. Bruker Sb-doped Si cantilevers (ρ = 0.01-0.025 Ω-cm, k = 42 N/m, ν ~ 320 kHz) were used in all cases (Figure S8).

Cell viability analysis of peptides against the adhesive rat pheochromocytoma (PC12) cell line
Adhesive PC12 cells were purchased from ATCC (1721.1) and cultured in accordance with the supplier's instructions. For cytotoxicity experiments, cells were plated in a 96-well plate at a density of 5000 cells / well and allowed to adhere for 24 h before dosing. Each well contained 100 μL total volume. For dosing, 250 μg of L-Aβ42 or D-Aβ42 peptide was dissolved in 20 μL of 20 mM NaOH. For racemic Aβ42, 250 μg of L-Aβ42 and 250 μg of D-Aβ42 were dissolved separately in 10 μL of 20 mM of NaOH and then mixed. The solutions were diluted to a final concentration of 50 μM using 1080 μL of F12-K media containing 2.5% Fetal Bovine Serum and 15% Horse Serum. Serial dilution yielded the solutions that contained lower concentrations of Aβ42. Following 72 h incubation, 10 μL of WST-1 (Roche) or 10 μL of MTT (5 mg/ml in PBS) was added to each well and incubated for 4 h. For WST-1 assay measurements, the absorbance at λ = 490 nm was used to determine cellular viability. For MTT assay, media was carefully removed from the wells and 100 μL DMSO pipetted in per well to dissolve the MTT-derived crystals, and the absorbance at λ = 570 was measured to determine cellular viability.

Cell viability analysis of peptides against human neuroblastoma SH-SY5Y cell line
Human neuroblastoma SH-SY5Y cells were purchased from ATCC (CRL-2266) and cultured in accordance with the supplier's instructions. For cell viability experiments, cells were plated in a 96-well plate at a density of 50000 cells/well and allowed to adhere for 24 h before dosing. Each well contained 100 μL total volume. For dosing, 100 μg of L-Aβ42 or D-Aβ42 peptide was dissolved in 10 μL of 20 mM NaOH. For racemic Aβ42, 100 μg of L-Aβ42 and 100 μg of D-Aβ42 were dissolved separately in 5 μL of 20 mM NaOH and then mixed. The solutions were diluted to a final concentration of 50 μM using 430 μL of DMEM: F12K (1:1) media containing 10 % Fetal Bovine Serum. Original media was replaced with fresh media containing peptides. Following a 72 h incubation, 10 μL of WST-1 (Roche) was added to each well and incubated for 2 h. Absorbance at λ = 490 nm was used to determine cellular viability.

Cell viability in presence of L-Aβ42 (50 μM) with different amounts of D-Aβ42 (PC12)
Adhesive PC12 cells were plated in a 96-well plate at a density of 5000 cells/well and allowed to adhere for 24 h before dosing. Each well contained 100 μL total volume. For dosing, 0.5 mg of L-Aβ42 was dissolved in 25 μL of 20 mM NaOH and split into four 5 μL aliquots. 0.25 mg of D-Aβ42 was dissolved in 12.5 μL of 20 mM NaOH and added (5 μL, 2.5 μL or 1.25 μL) separately into 3 of the L-Aβ42 aliquots. The final amount of NaOH was equalized to a final volume of 10 μL. The solutions were diluted to a final concentration of 50 μM of L-Aβ42 and 50, 25, 12.5, and 0 μM of D-Aβ42 using 430 μL of F12-K media containing 2.5% Fetal Bovine Serum and 15% Horse Serum. Original media was replaced with fresh media containing peptides. Following 72 h incubation, 10 μL of WST-1 (Roche) was added to each well and incubated for 2 h. Absorbance at λ = 490 nm was used to determine cellular viability.

LDH release assay (PC12)
For LDH release assay (Cayman Chemical, catalog number 601170), adhesive PC12 cells were plated in a 96-well plate at a density of 50000 cells/well and allowed to adhere for 24 h before dosing. Each well contained 100 μL total volume. For dosing, 100 μg of L-Aβ42 or D-Aβ42 peptide was dissolved in 10 μL of 20 mM NaOH. For racemic Aβ42, 100 μg of L-Aβ42 and 100 μg of D-Aβ42 were dissolved separately in 5 μL of 20 mM of NaOH and then mixed. The solutions were diluted to a final concentration of 50 μM using 430 μL of F12-K media containing 2.5% Fetal Bovine Serum and 15% Horse Serum. Original media was replaced with 100 μL of the L-, D-, or rac-Aβ42. For control experiments, 10 μl of Triton X-100 (10%) was added (positive control, 100% cell death) and 10 μL of assay buffer was added (vehicle control). Following a 24 h incubation, 50 μL of cell supernatant was transferred to a new 96-well plate and 50 μL of LDH reaction solution (Mixture of NAD^+, Lactic acid, INT and Diaphorase) was added. The plate was incubated for 30 min at 37˚C and the absorbance at 490 nm was used to determine the LDH release.

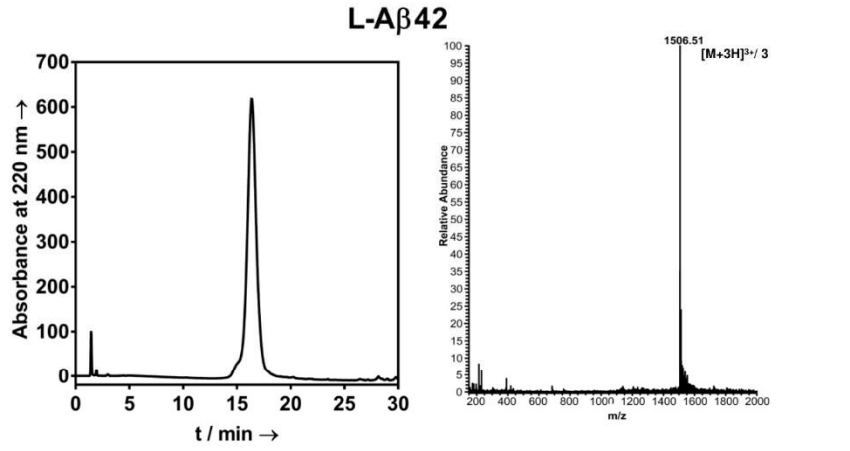

#	Time	Area	Height	Width	% Area
1	14.813	51.6	2.3	0.3726	0.165
2	16.380	31290	582	0.896	99.8

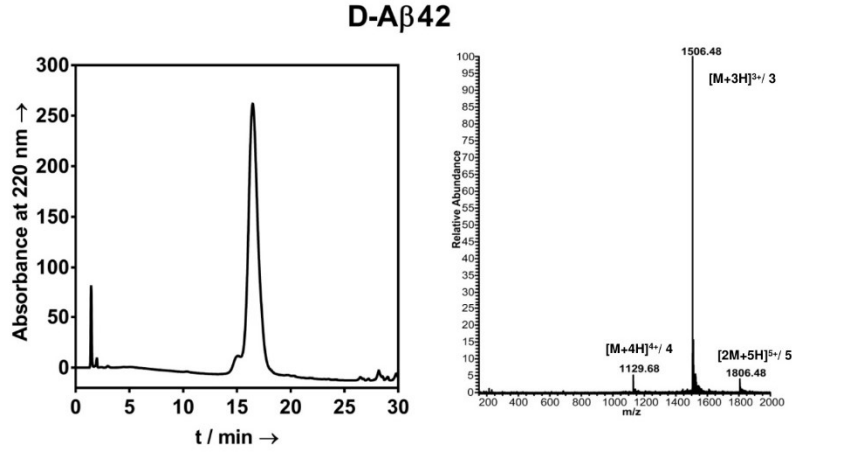

#	Time	Area	Height	Width	% Area
1	15.096	767.4	15	0.7529	4.2
2	16.474	17505.4	269.1	0.9711	95.8

Figure S1. Analytical HPLC and mass spectrum analysis of the L-Aβ42 and D-Aβ42 peptide. The purity of each peptide was >95%, determined *via* analytical HPLC, by integration of signals at 220 nm.

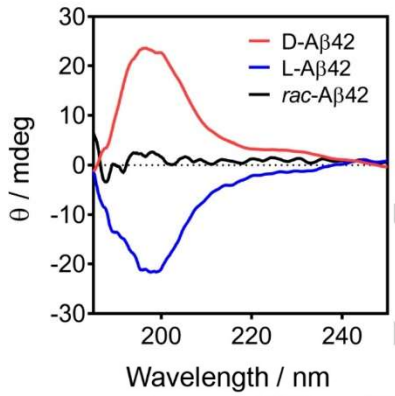

Figure S2. Circular Dichroism (CD) spectra of L-Aβ42, D-Aβ42 and *rac*-Aβ42. The two peptides show spectra of equal intensity but opposite sign (λ_{max} = 197 nm; $\theta_{L\text{-}A\beta42}$ = -23.8 ± 1.3 mdeg; $\theta_{D\text{-}A\beta42}$ = +24.6 ± 3 mdeg) and equimolar mixing of L and D-Aβ42 leads to the disappearance of the CD signal.

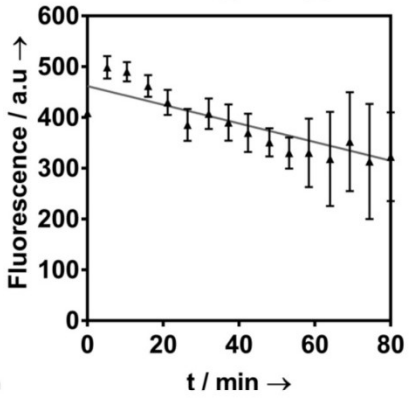

Figure S3. Aggregation kinetics of 40 µM racemic-Aβ42, monitored by Thioflavin T (ThT, 20 µM) fluorescence at 37 °C in PBS.

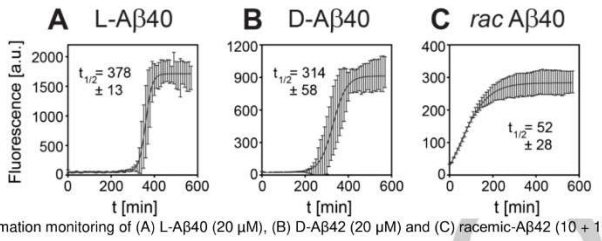

Figure S4. ThT fibril formation monitoring of (A) L-Aβ40 (20 μM), (B) D-Aβ42 (20 μM) and (C) racemic-Aβ42 (10 + 10 μM total concentration).

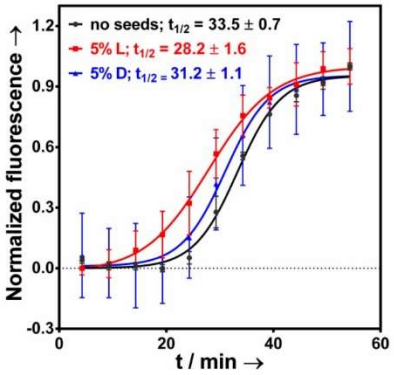

Figure S5. L-Aβ42 fibril formation is mildly accelerated through seeding with pre-formed Aβ42 fibrils; the effect is more pronounced with L- than with D-seeds.

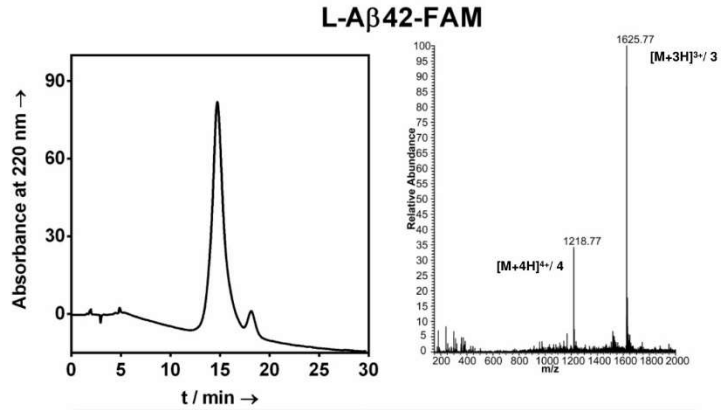

#	Time	Area	Height	Width	% Area
1	14.731	7009.7	86.1	1.357	95.266
2	18.177	384.3	7.5	0.7691	4.734

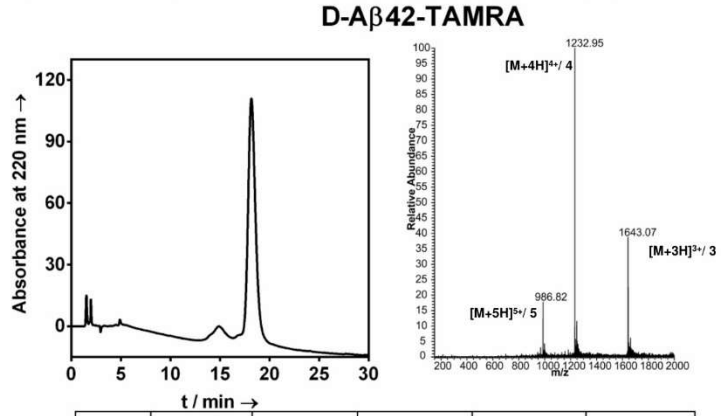

#	Time	Area	Height	Width	% Area
1	14.921	304.7	4.8	1.0476	4.752
2	18.174	6107.5	117.6	0.8659	95.248

Figure S6. Analytical HPLC and mass spectrum analysis of the L-Aβ42-FAM and D-Aβ42-TAMRA peptide. The purity of each peptide was >95%, determined *via* analytical HPLC, by integration of signals at 220 nm.

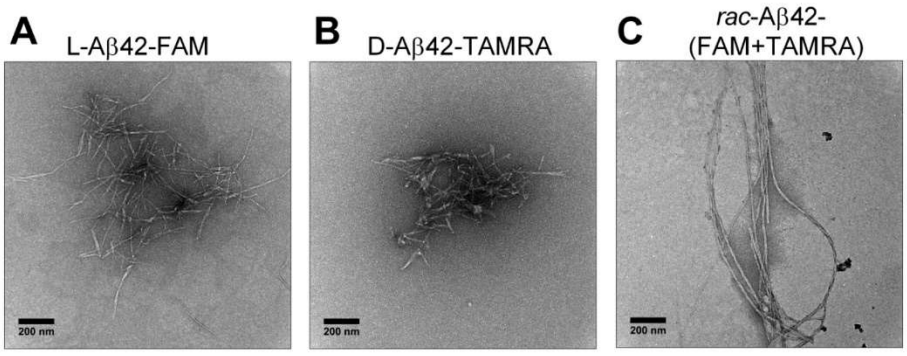

Figure S7. Transmission electron microscopy (TEM) of the fibrils of A) L-Aβ42-FAM, B) D-Aβ42-TAMRA and C) racemic Aβ42-(FAM+TAMRA).

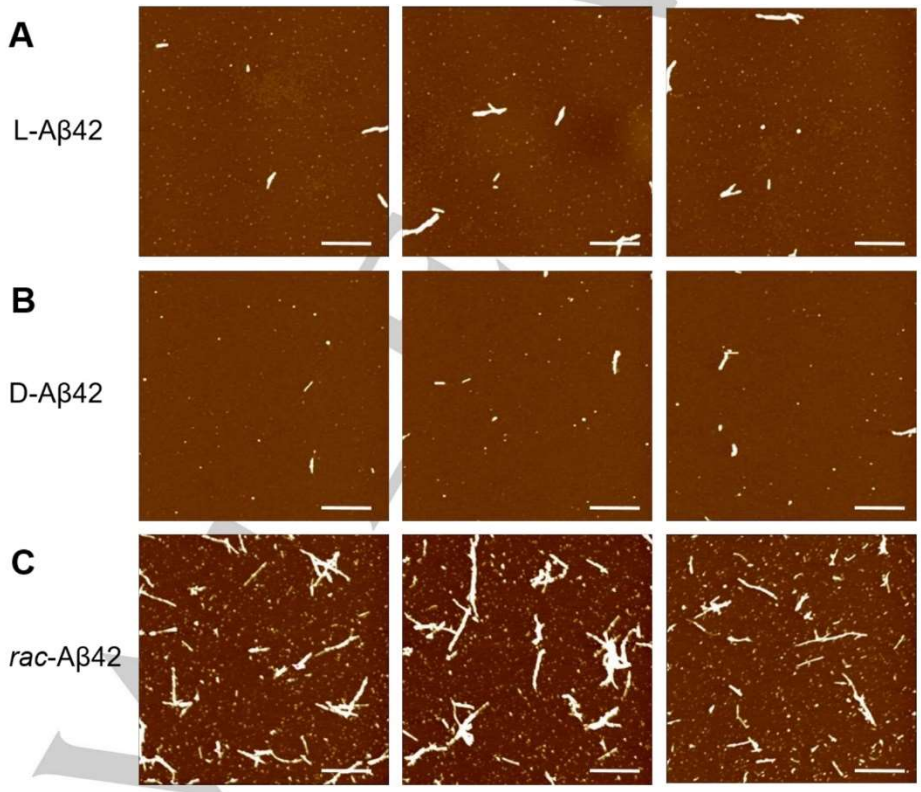

Figure S8. Atomic force microscopy (AFM) images of aggregation intermediates of A) L-Aβ42, B) D-Aβ42 and C) racemic Aβ42. (Scalebar = 1000 nm).

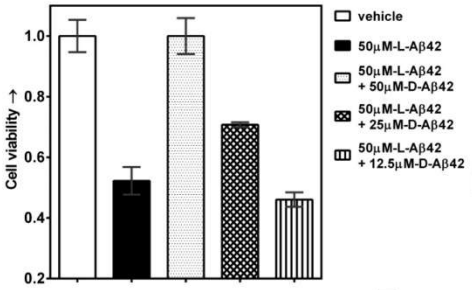

Figure S9. Cell viability measurements were performed using the WST-1 assay (see above for details). Addition of L-Aβ42 to PC12 cells at final concentration of 50 μM leads to reduction in cell viability to 52 % of vehicle. Addition of 50 μM D-Aβ42 results in complete toxicity suppression. Addition of 25 μM D-Aβ42 results in a partial rescue of cell viability (71 % of vehicle), whereas with 12.5 μM D-Aβ42 added, cell viability is indistinguishable from that obtained with pure L-Aβ42.

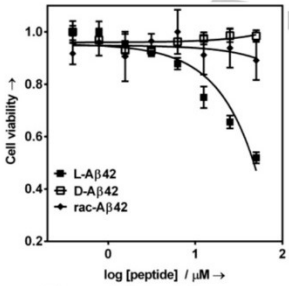

Figure S10. Cellular viability of the PC12 adhesive cell line in response to dosing in of varied concentrations of enantiopure (L- or D-) or racemic Aβ42 Cells were plated at a density of 5000 per well and allowed to adhere for 24 h. Peptides were then added at indicated concentrations and cells incubated for further 72 h. Cell viability was determined using the cell proliferation reagent MTT. Data are represented as mean ± s.d, performed on technical quadruplicate experiments.

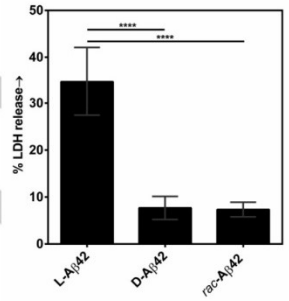

Figure S11. LDH release from PC12 adhesive cells in response to treatment with either enantiopure (L- or D-; 50 μM in both cases) or racemic Aβ42 (50 μM L-Aβ42 and 50 μM D-Aβ42). Cells were plated at a density of 50000 per well and allowed to adhere for 24 h. Peptides were then added at indicated concentrations and cells incubated for further 24 h. Data are represented as mean ± s.d, performed on biological duplicate, each performed in technical quadruplicate (****P < 0.0001, calculated by t-test).

References

[1] C. J. Warner, S. Dutta, A. R. Foley, J. A. Raskatov, *Chem. Eur. J.* **2016**, *22*, 11967-11970
[2] M. Ahmed, J. Davis, D. Aucoin, T. Sato, S. Ahuja, S. Aimoto, J. I Elliott, W. E Van Nostrand, S. O Smith, *Nat. Struct. Mol. Biol.* **2010,** 17, 561–567.

SI Appendix A – Fibrils TEM

TEM experiment:

Samples for TEM were taken from ThT assays at 24h. ThT assays were run at 20 µM total concentration of Aβ42. 0.5 mg of either L-Aβ42 or D-Aβ42 was freshly dissolved in 50µL of 20 mM NaOH solution and sonicated for 30 s. Afterwards, the solutions were filtered through 100 kDa MWCO spin filter at 14000g for 10 min. The concentration of the filtrate L- Aβ42 or D- Aβ42 solutions was measured by Nanodrop (ε = 1490 M^{-1} cm^{-1} at 280 nm). These stock solutions were then diluted to a final concentration of 20 µM total Aβ42 concentration in PBS containing 20 µM ThT. Racemic- Aβ42 was prepared by combining L and D - Aβ42 after spin filtration in 1:1 molar ratio and diluted to 20 µM in PBS containing 20 µM ThT. ThT experiments were conducted in black, clear bottom 96-well plates at 37 °C with shaking in a Molecular Device Gemini EM fluorescence plate reader.

A 3 µL aliquot of Aβ42 (L-, D- or rac- Aβ42) from ThT assays after 24 h was spotted onto freshly glow-discharge carbon-coated electron microscopy grid (Ted Pella, Catalog No. 01701-F). Three grids were prepared for each sample from three independent ThT assays. After 1 minute incubation, the grids were rinsed with 5 µL of milliQ water, followed by staining with 30 µL 1% uranyl acetate. All fibrils were imaged by using JEOL 1230 microscope at an accelerating voltage of 120 kV.

L-Aβ42 Fibrils

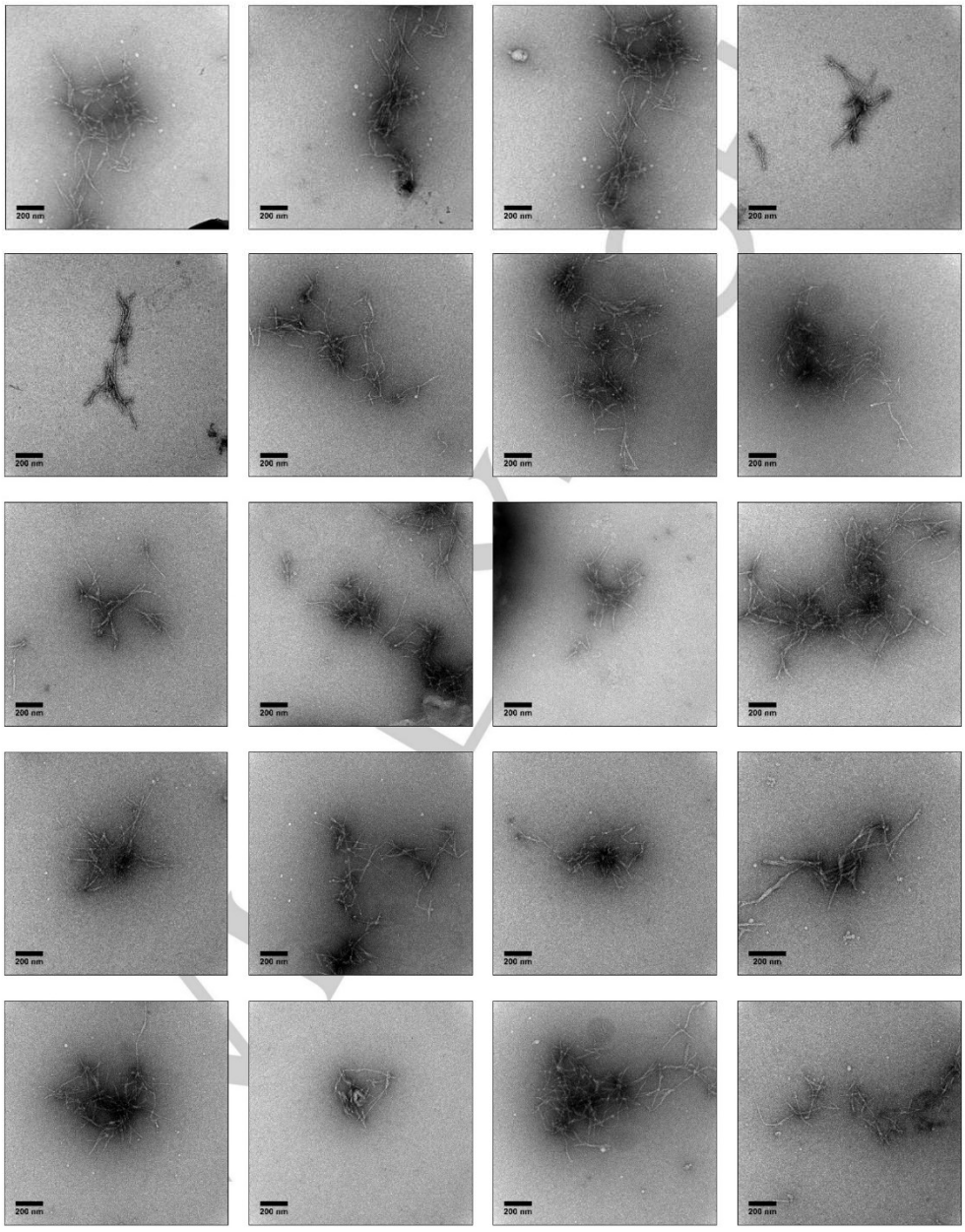

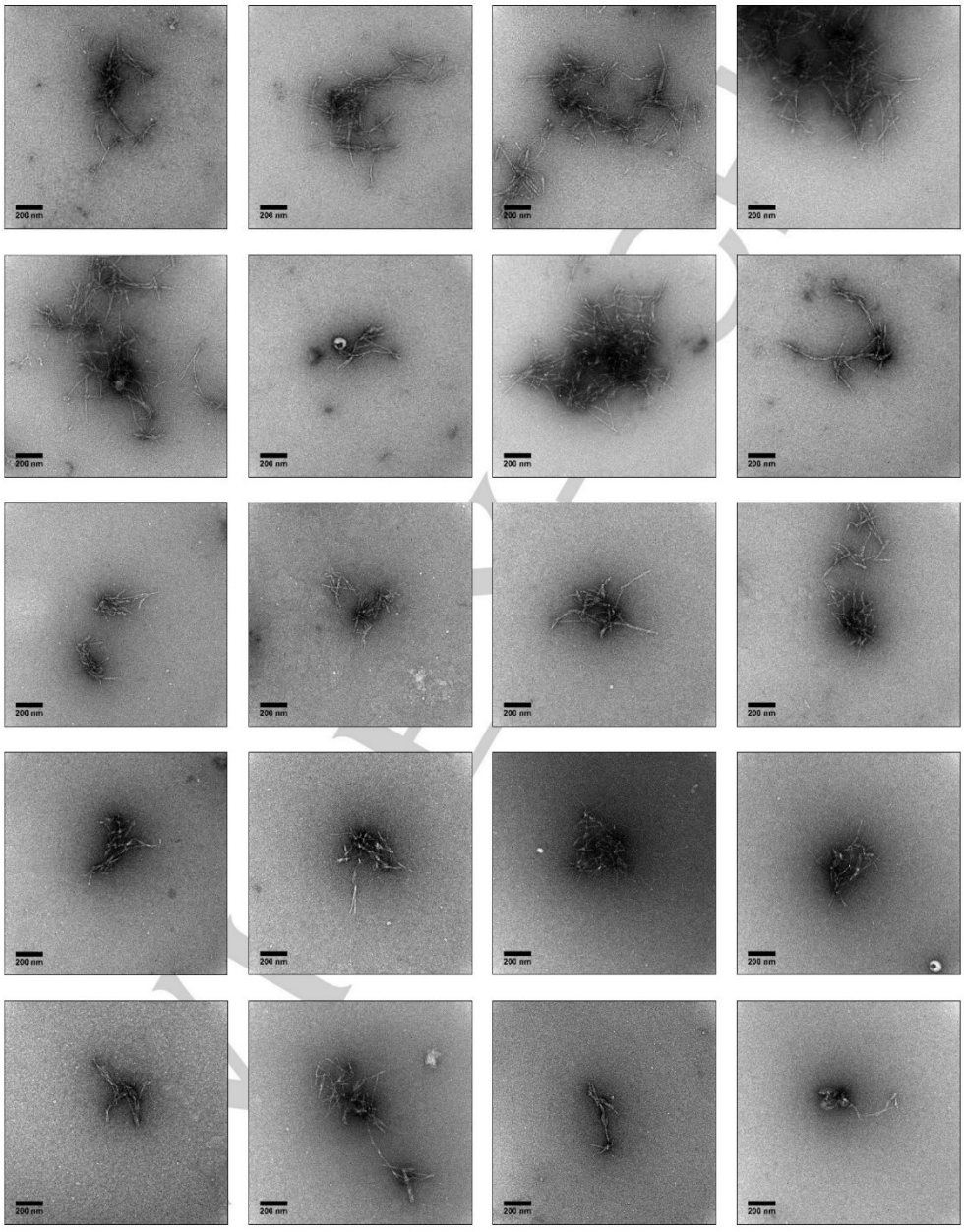
200 nm

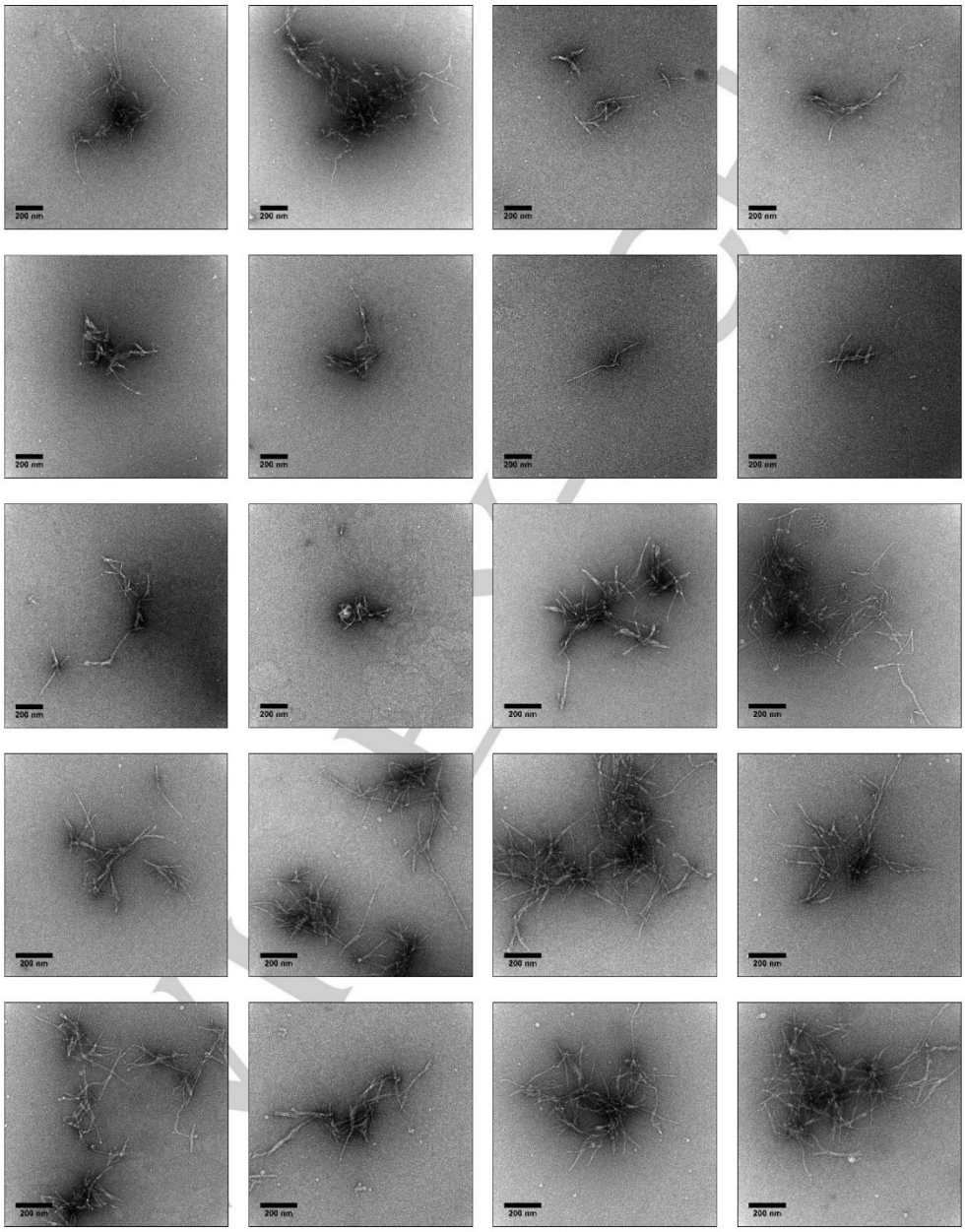
200 nm

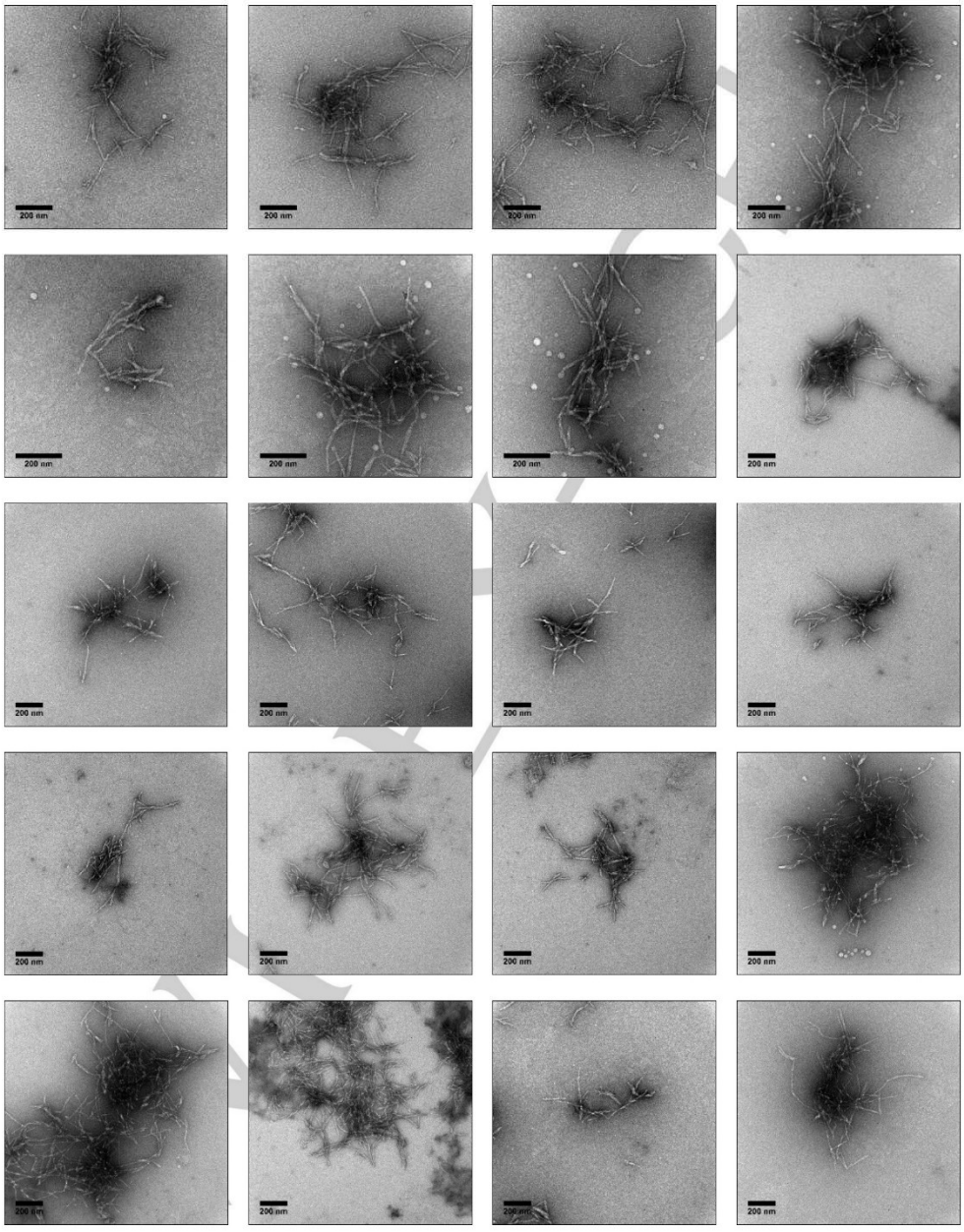
200 nm

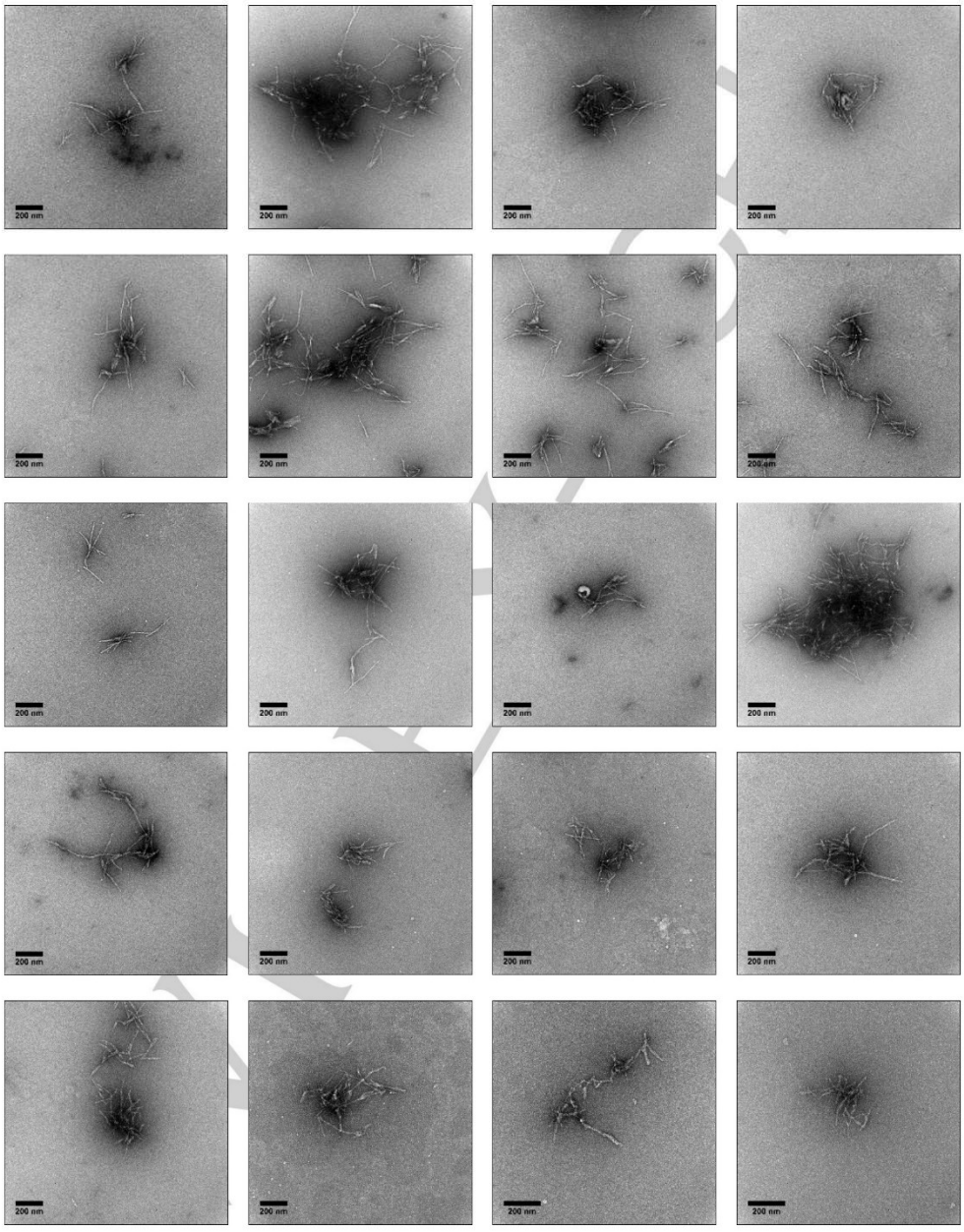
200 nm

D-Aβ42 Fibrils

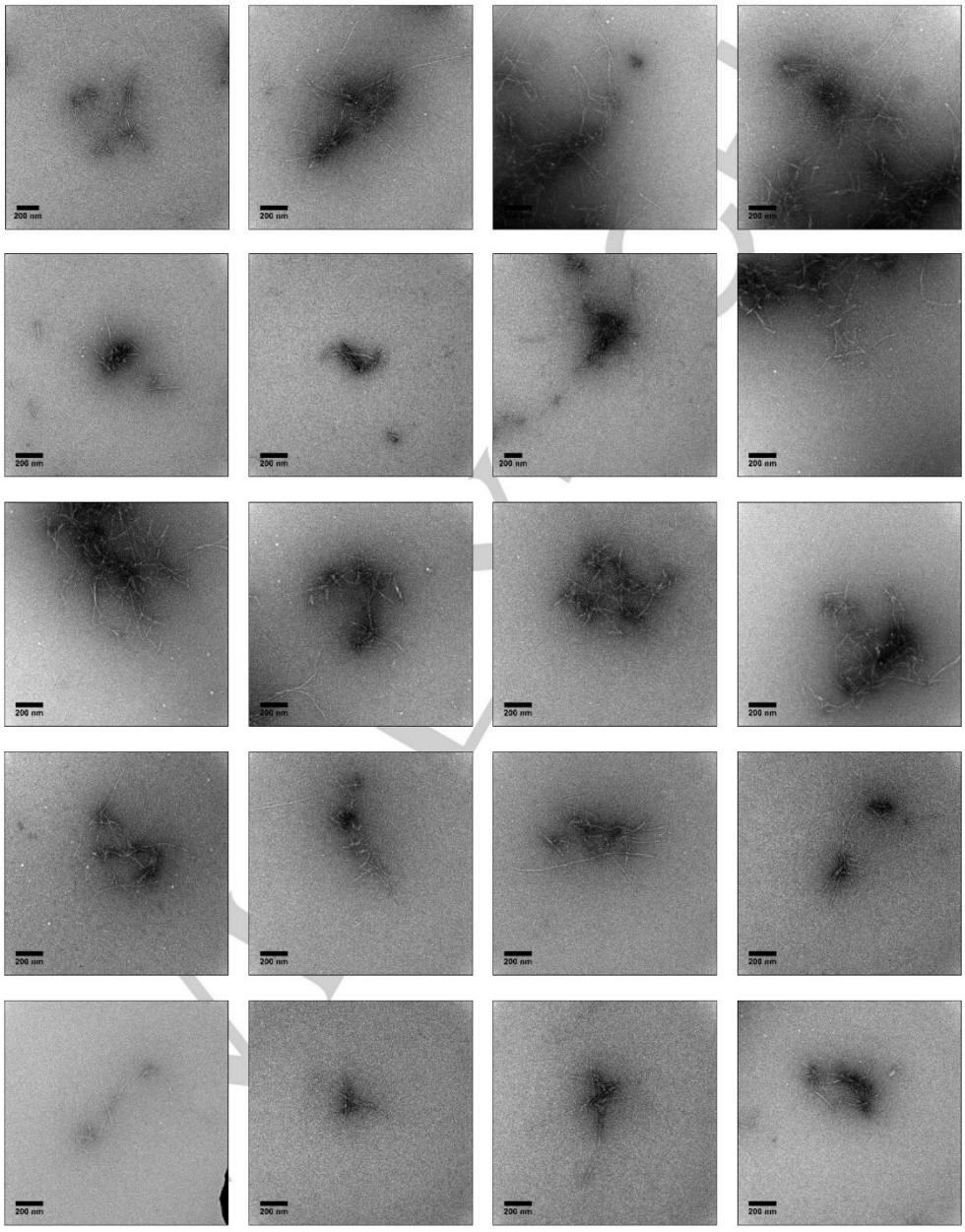

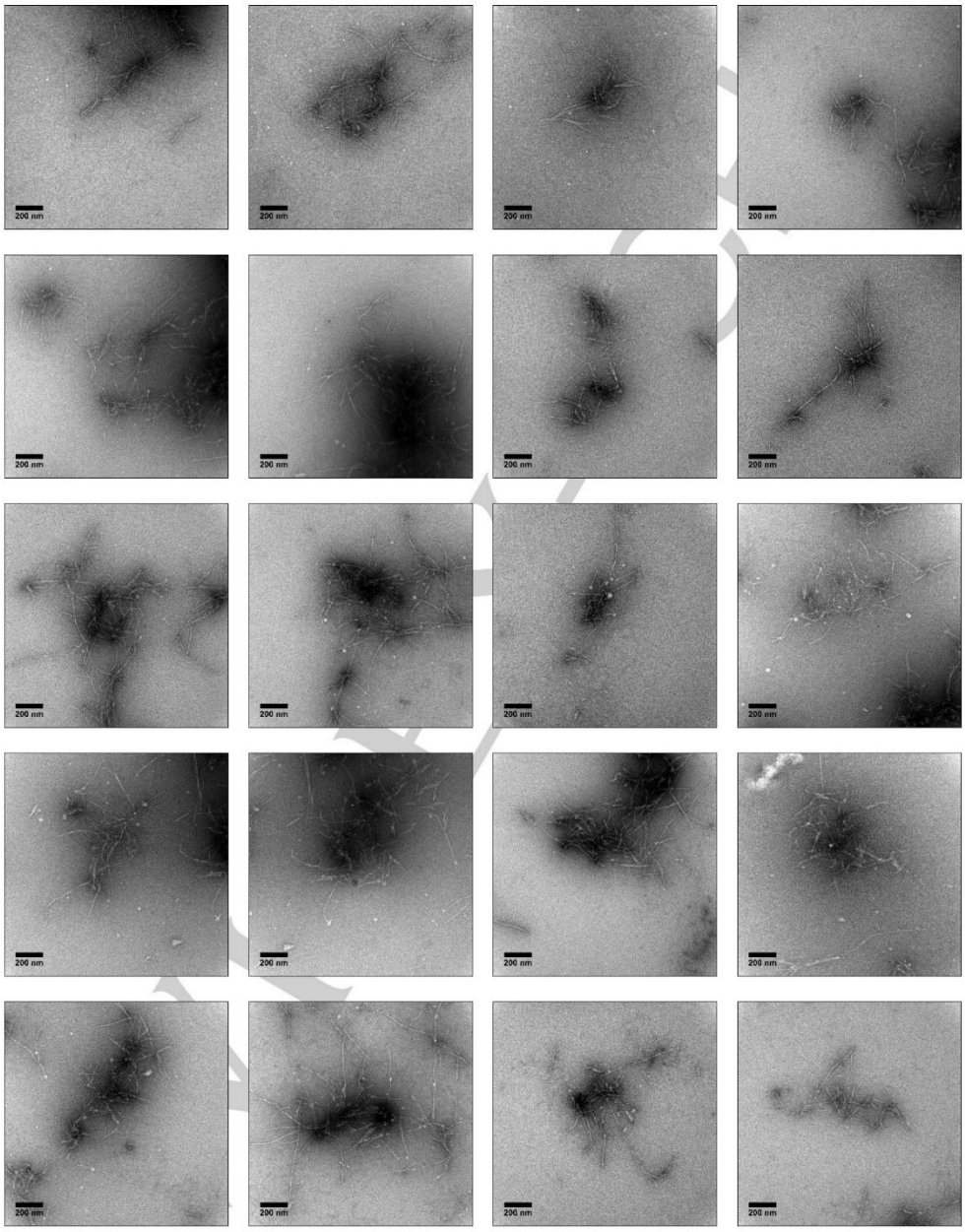
200 nm

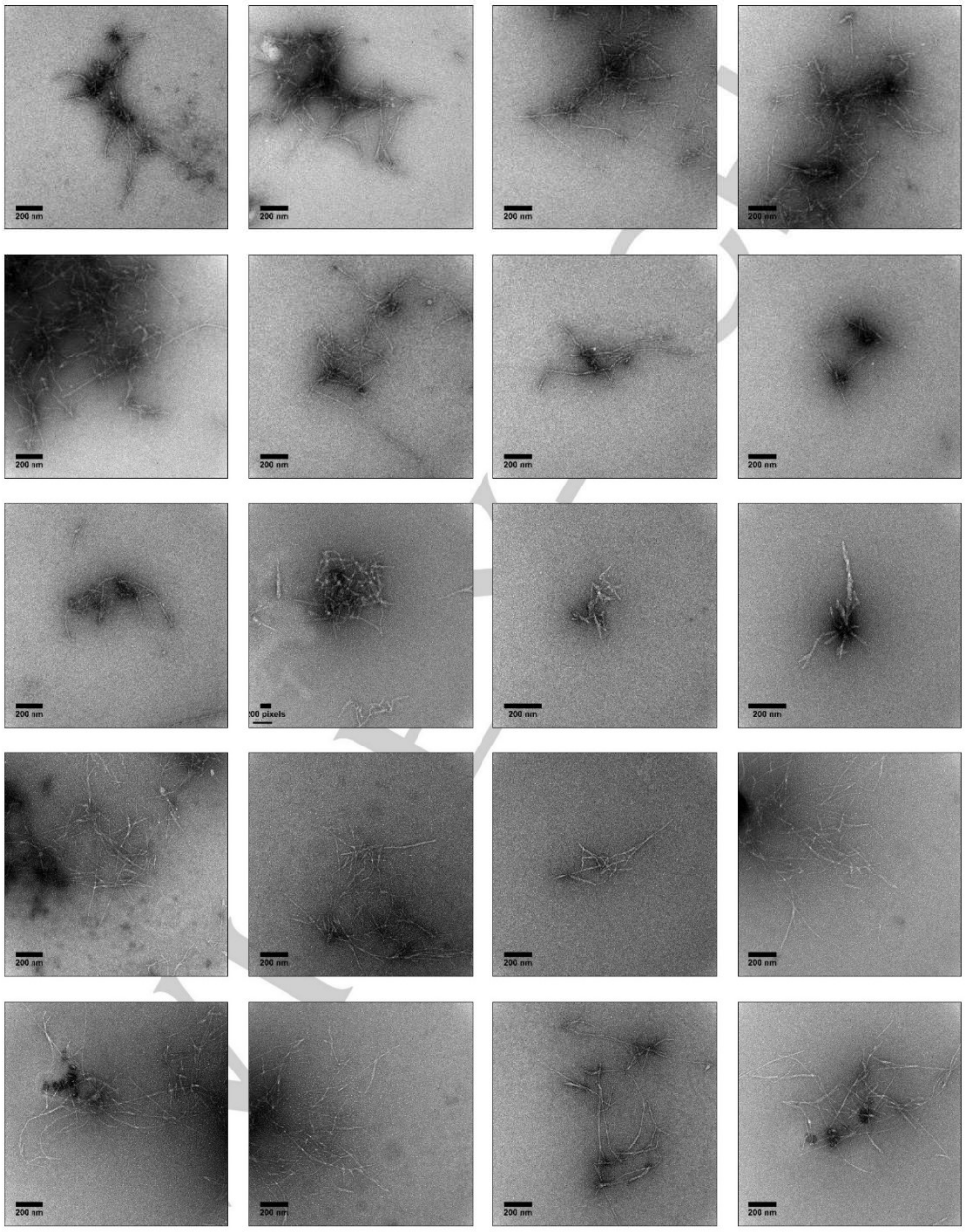
200 nm
200 nm
200 nm
200 nm
200 nm
200 nm
200 nm
200 nm
200 nm
200 nm
200 nm
200 nm
200 nm
200 nm
200 nm
200 nm
200 nm
200 nm
200 nm
200 nm

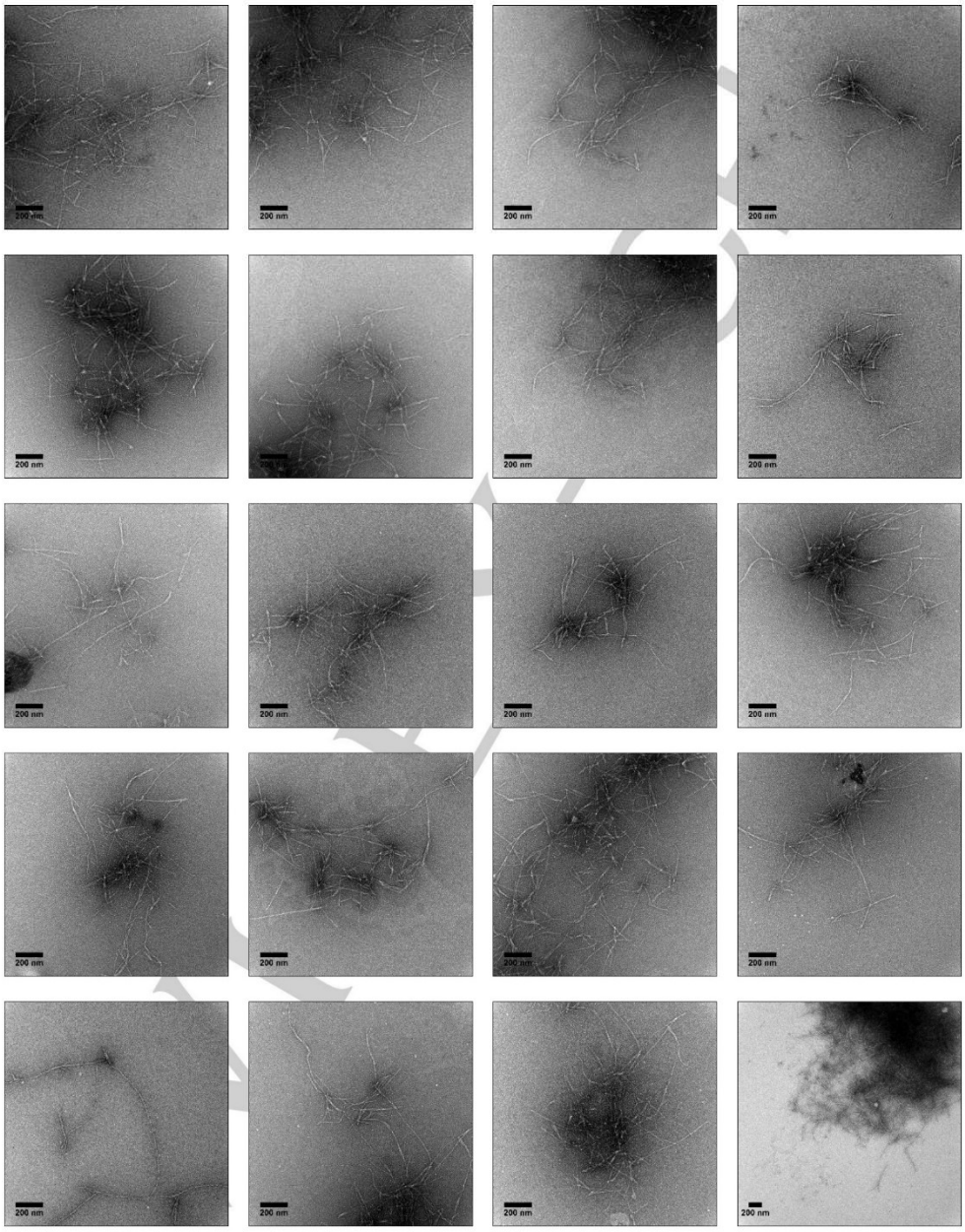
200 nm

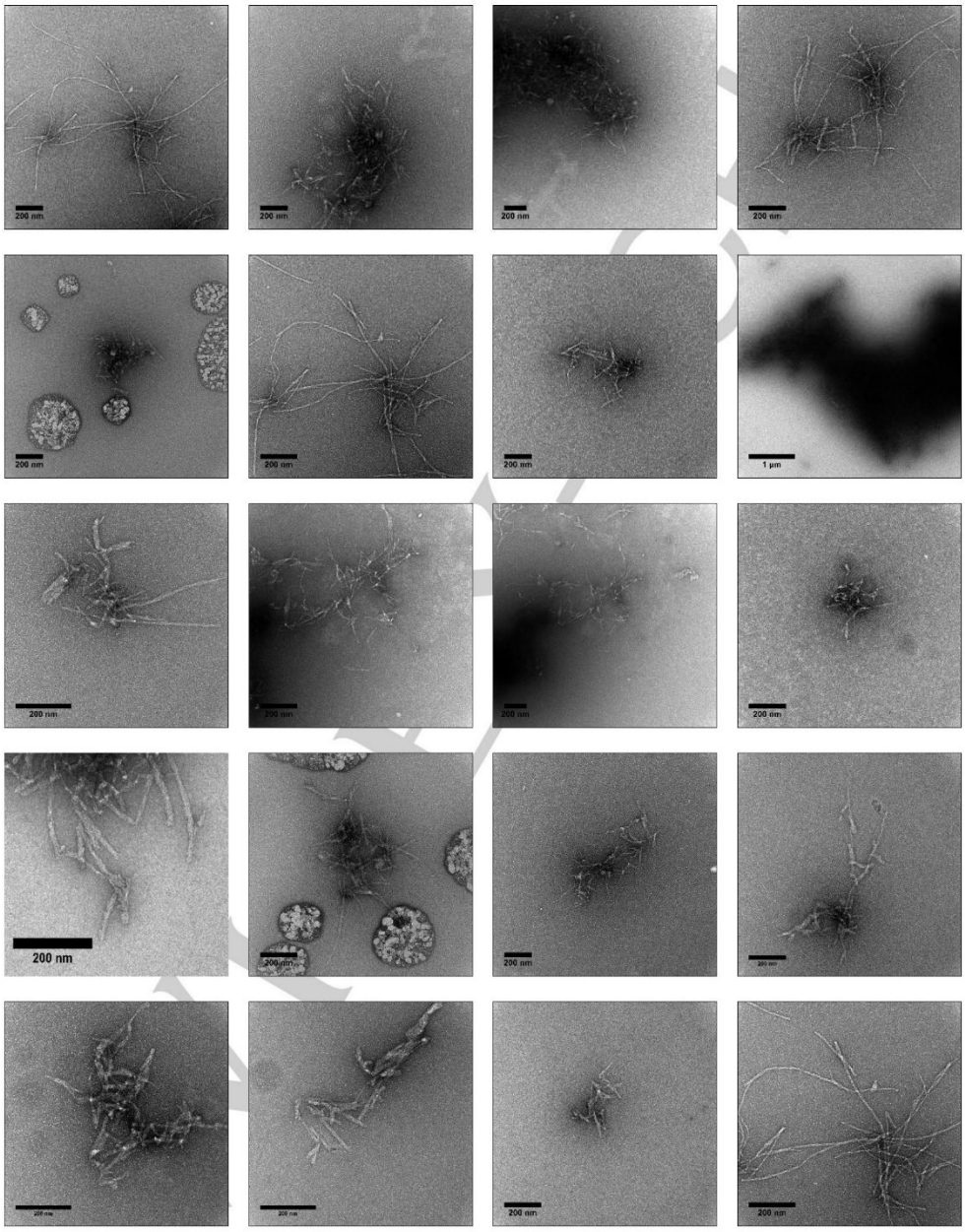
200 nm
1 µm

***rac*-Aβ42 Fibrils**

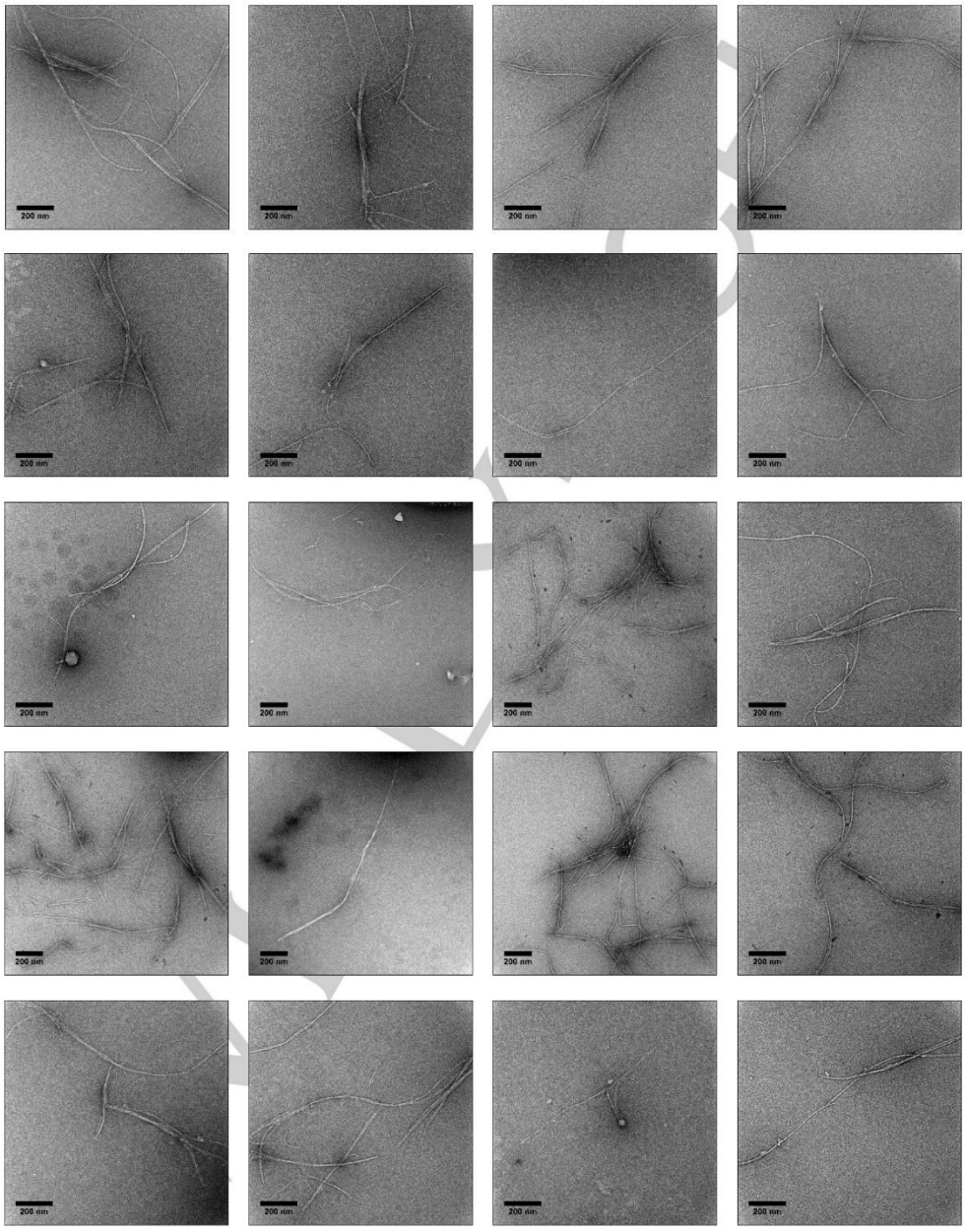

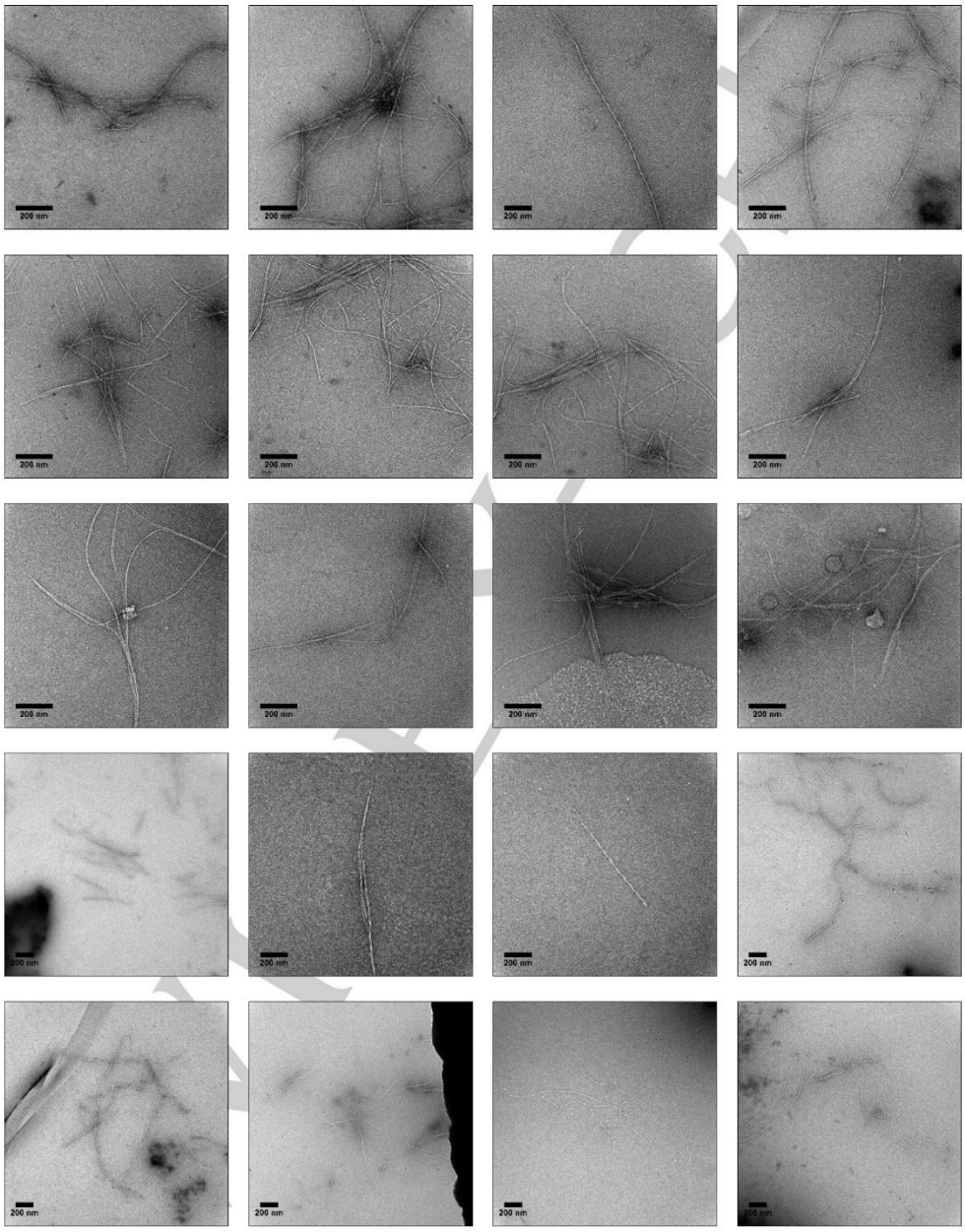
200 nm

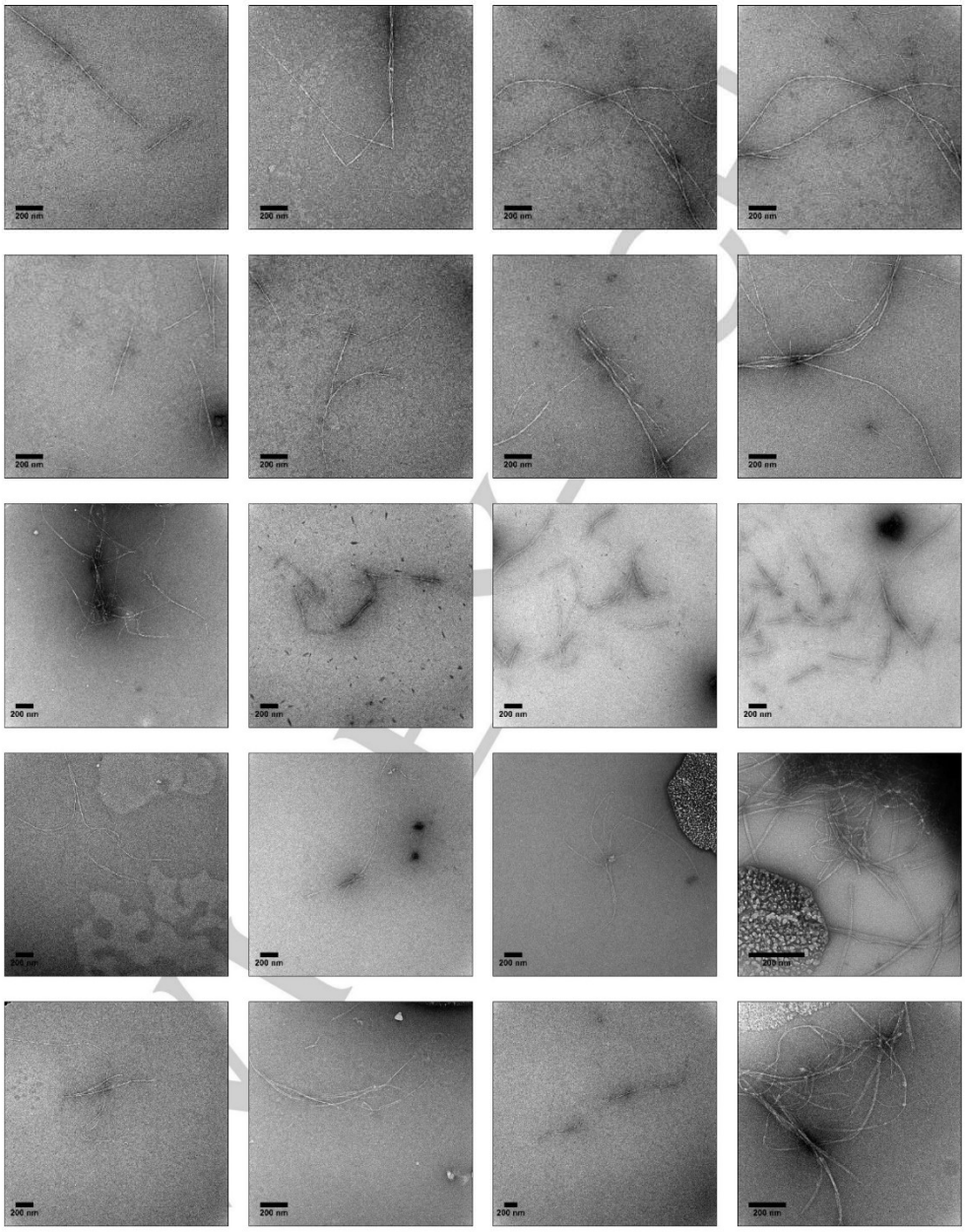
200 nm

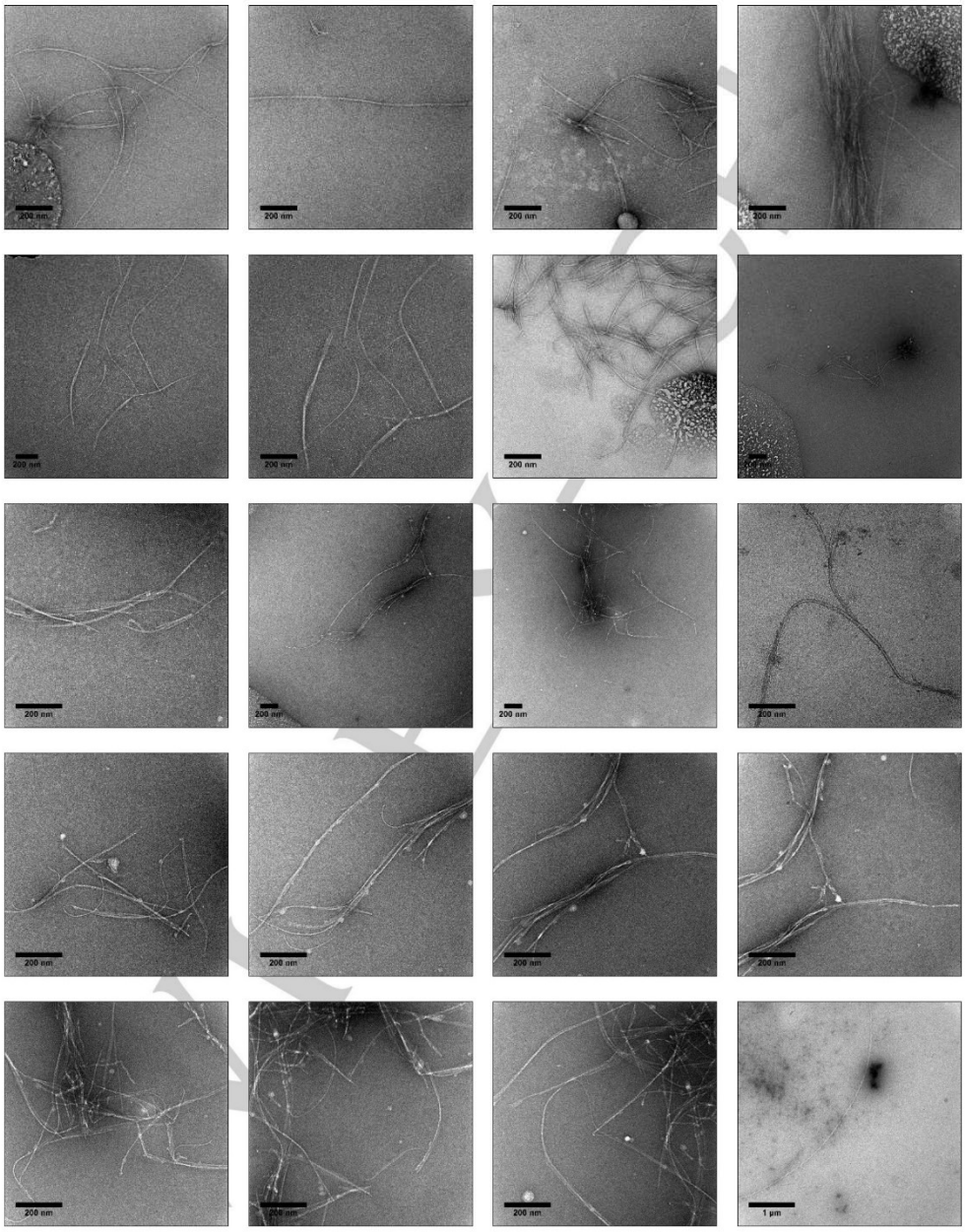
200 nm
200 nm
200 nm
200 nm
200 nm
200 nm
200 nm
200 nm
200 nm
200 nm
200 nm
200 nm
200 nm
200 nm
200 nm
200 nm
200 nm
200 nm
200 nm
1 µm

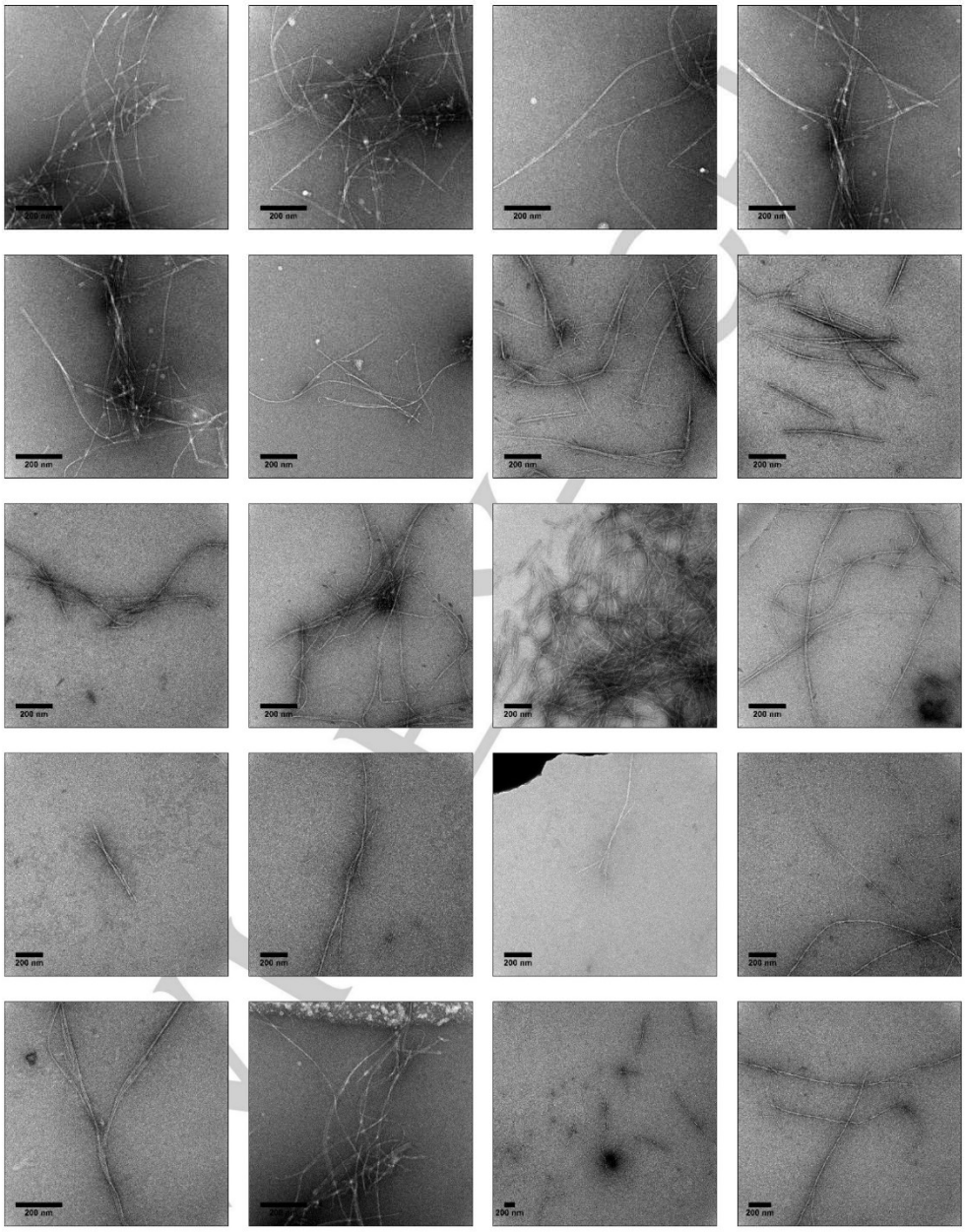
200 nm

SI Appendix B – Oligomers TEM

TEM experiment:

Formation of oligomers: 0.5 mg of either L-Aβ42 or D-Aβ42 was freshly dissolved in 50 µL cold 20 mM NaOH solution and sonicated for 30 s. Afterwards, the solutions were filtered through 100 kDa MWCO spin filter at 14000 g for 5 min at 4 °C. The concentration of the filtrate L-Aβ42 or D-Aβ42 solutions was measured by Nanodrop (ε = 1490 M^{-1} cm^{-1} at 280 nm). These stock solutions were then diluted to a final concentration of 20 µM total Aβ42 concentration in cold PBS. Racemic- Aβ42 was prepared by combining L and D-Aβ42 after spin filtration in 1:1 molar ratio and diluted to 20 µM in cold PBS. Oligomers were formed by keeping the solutions at 4 °C for 6 h.[1]

TEM grid preparation and imaging: A 3 µL aliquot of Aβ42 (L-, D- or rac- Aβ42) oligomer solution was spotted onto freshly glow-discharge carbon-coated electron microscopy grid (Ted Pella, Catalog No. 01701-F). After 1 minute incubation, the grids were rinsed with 5 µL of milliQ water, followed by staining with 30 µL 1% uranyl acetate. All aggregation intermediates were imaged by using JEOL 1230 microscope at an accelerating voltage of 120 kV.

Data processing and oligomer diameter calculation: The TEM data was processed by using Fiji ImageJ free software (https://fiji.sc/). First, the images (dm^3 file) were converted to 8-bit by selecting Image → Type→ 8 bit and then the following steps were applied: (1) Image → Adjust → Auto Local Threshold and then in Method, select Contrast with radius 15 and mark White objects on black background and press OK. (2) Analyze → Set Measurements → select Area, Limit to threshold, Decimal places = 2 and then press OK (3) Analyze → Analyze Particles → set Size (nm^2) = 60–Infinity, Circularity = 0.07 – 1.0, and select Display results, Add to Manager and then press OK. The results table will appear with Area value. Copy the Area value in Microsoft excel and calculate the diameter by using the following formula; Diameter = $2\sqrt{Area/\pi}$. Histogram analysis of L- and D-Aβ42 oligomer diameter is depicted below. Racemic Aβ42 consistently yielded mixtures that were too heterogeneous to be analyzed quantitatively. All individual TEM images for L-, D- and *rac*-Aβ42 have furthermore been deposited as part of this appendix.

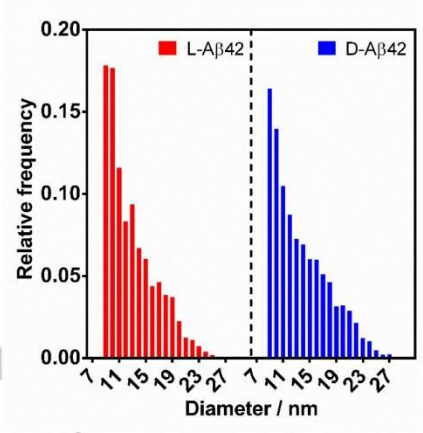

L-Aβ42 oligomers

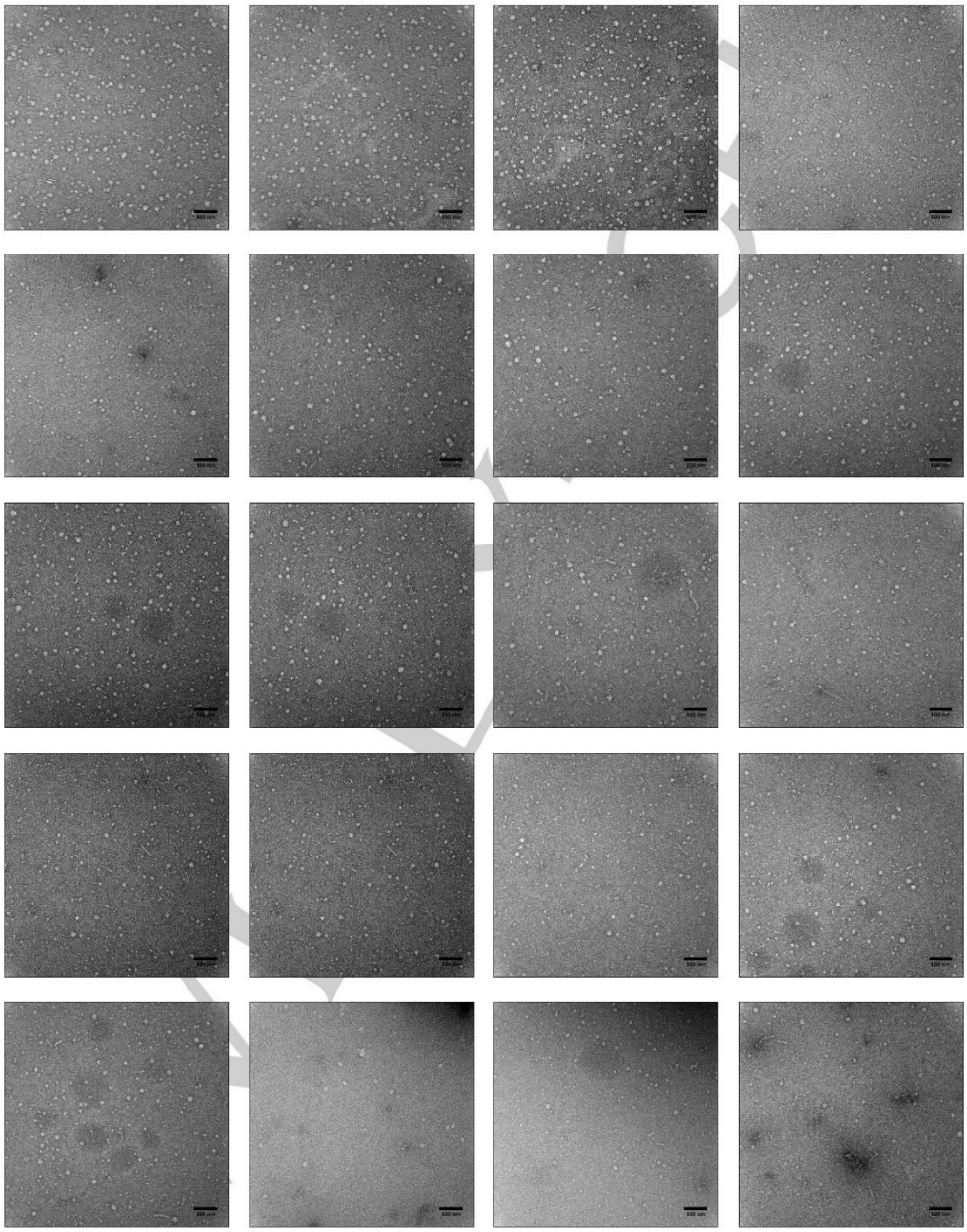

D-Aβ42 oligomers

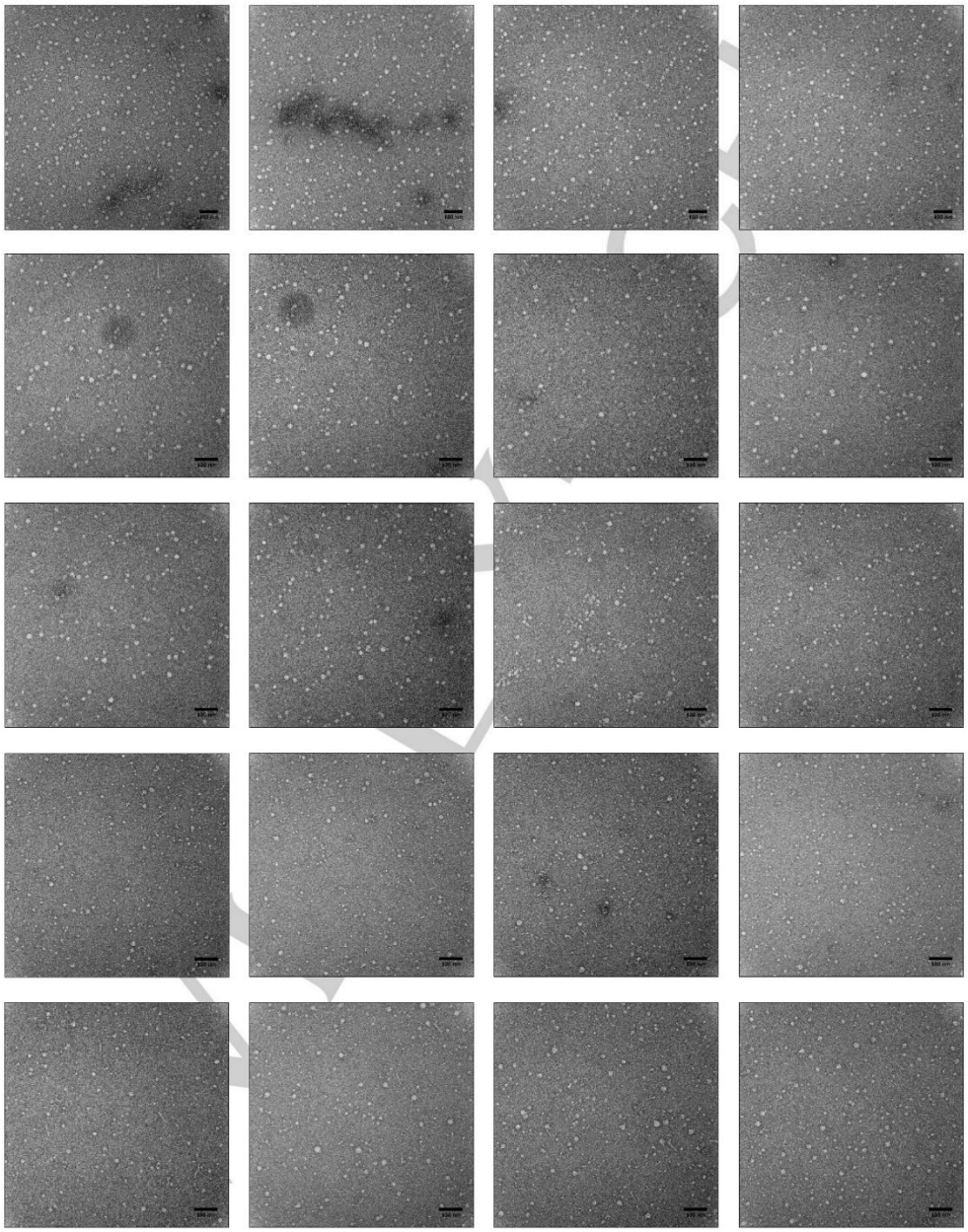

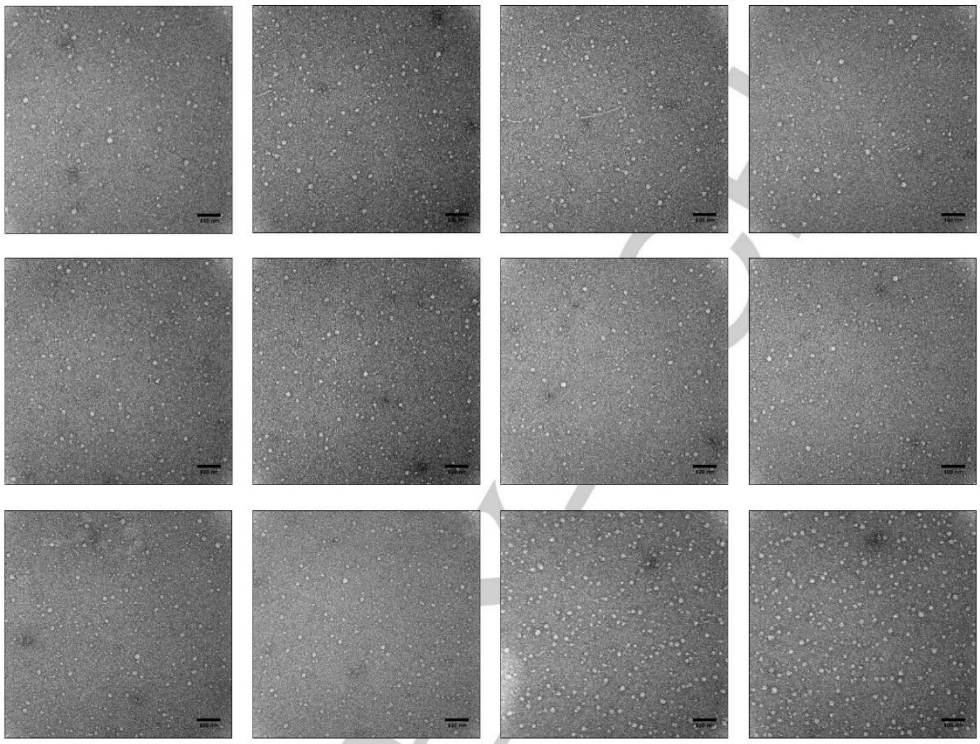

***rac*-Aβ42 oligomers**

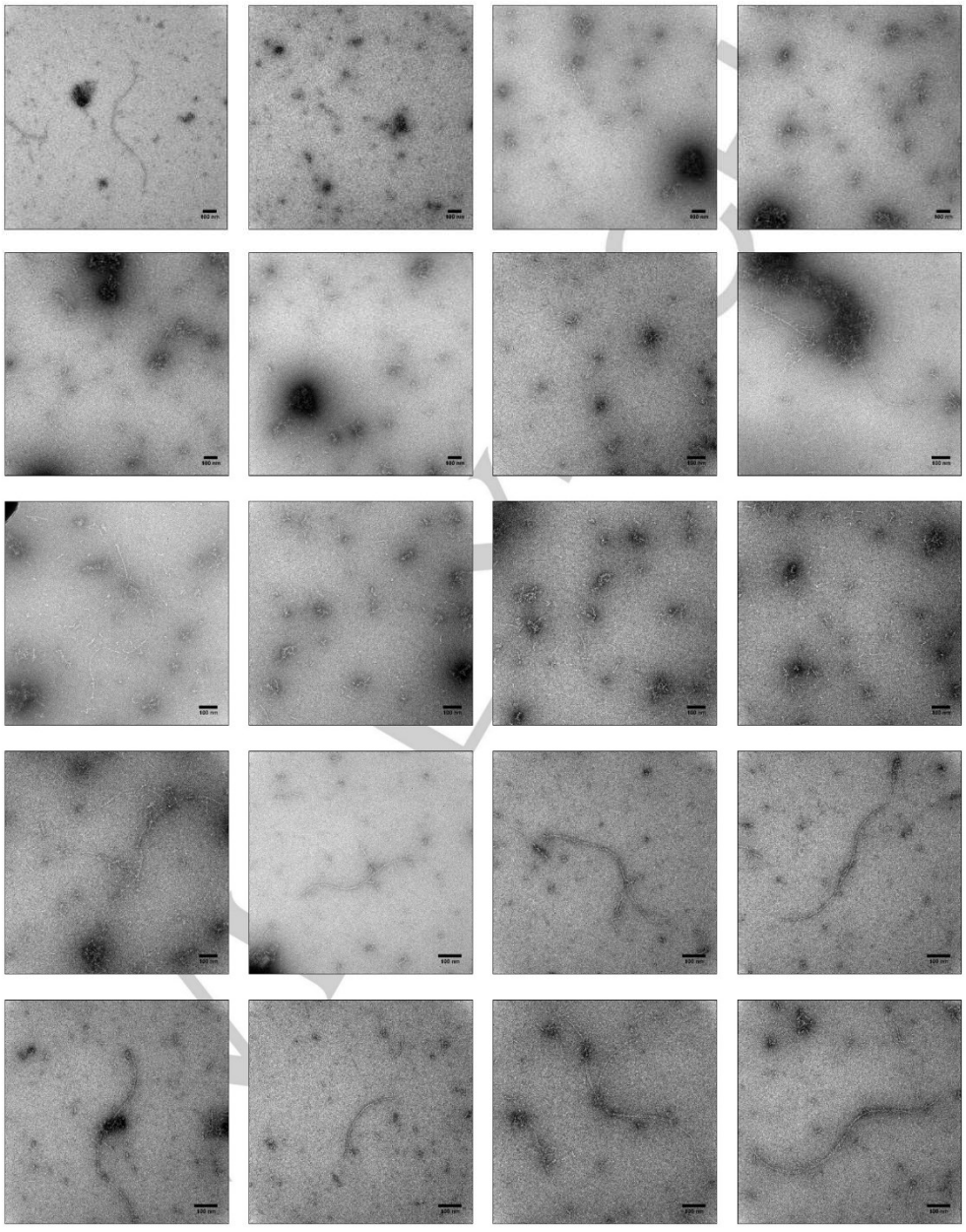

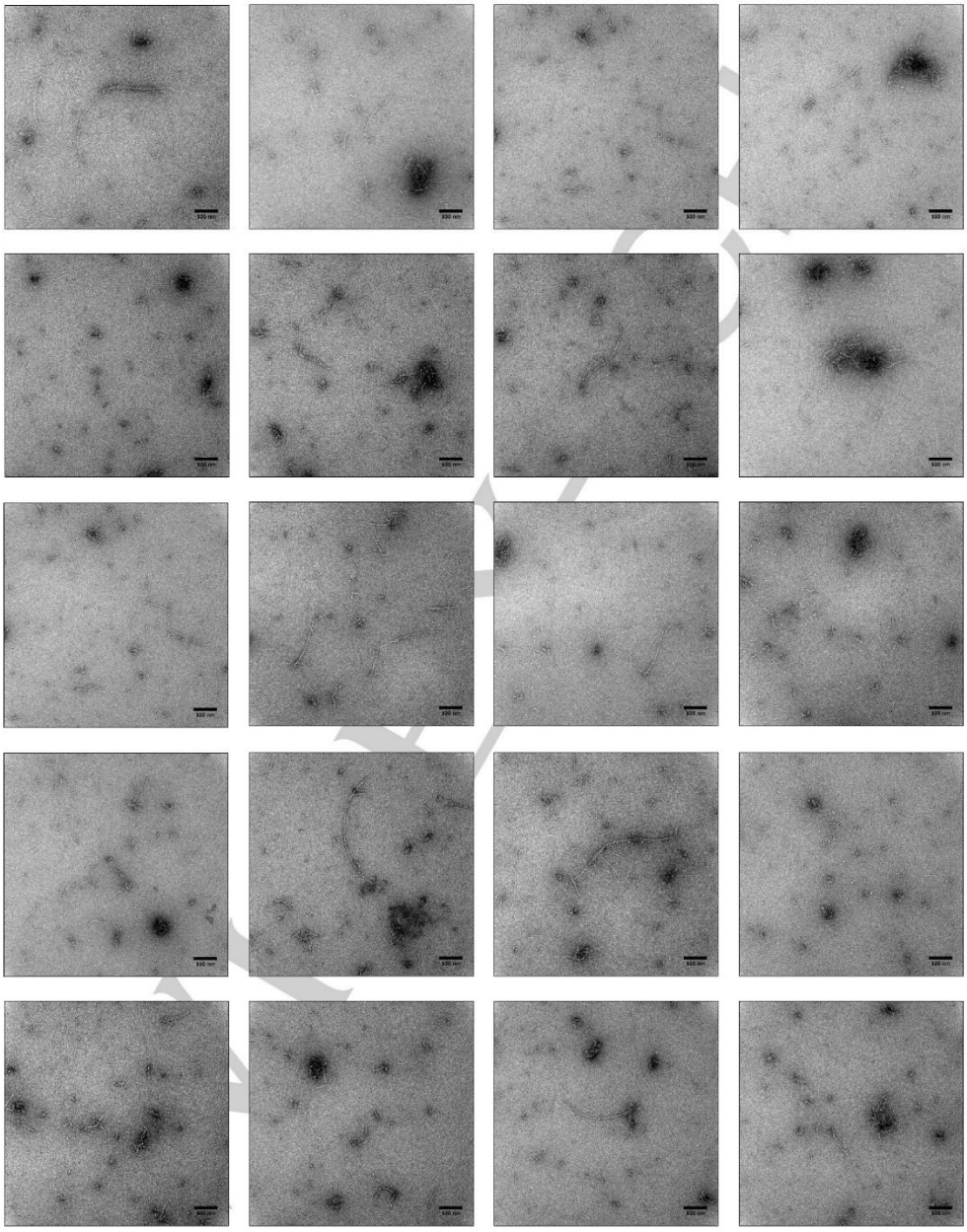

References

[1] M. Ahmed, J. Davis, D. Aucoin, T. Sato, S. Ahuja, S. Aimoto, J. I Elliott, W. E Van Nostrand, S. O Smith, *Nat. Struct. Mol. Biol.* **2010,** 17, 561–567.

New insights into differential aggregation of enantiomerically pure and racemic Aβ40 systems

Subrata Dutta,[a,†] Alejandro R. Foley,[a,†] Ariel J. Kuhn,[a,†] Benjamin Abrams,[b] Hsiau-Wei Lee,[a] and Jevgenij A. Raskatov[a,*]

[a] *Department of Chemistry and Biochemistry, 1156 High Street, University of California Santa Cruz, Santa Cruz, CA 95064, USA*

[b] *Department of Biomolecular Engineering, Life Sciences Microscopy Center, 1156 High Street, University of California Santa Cruz, Santa Cruz, CA 95064, USA*

[†] *Denotes equal contribution*

[*] *Correspondence should be addressed to: jraskato@ucsc.edu*

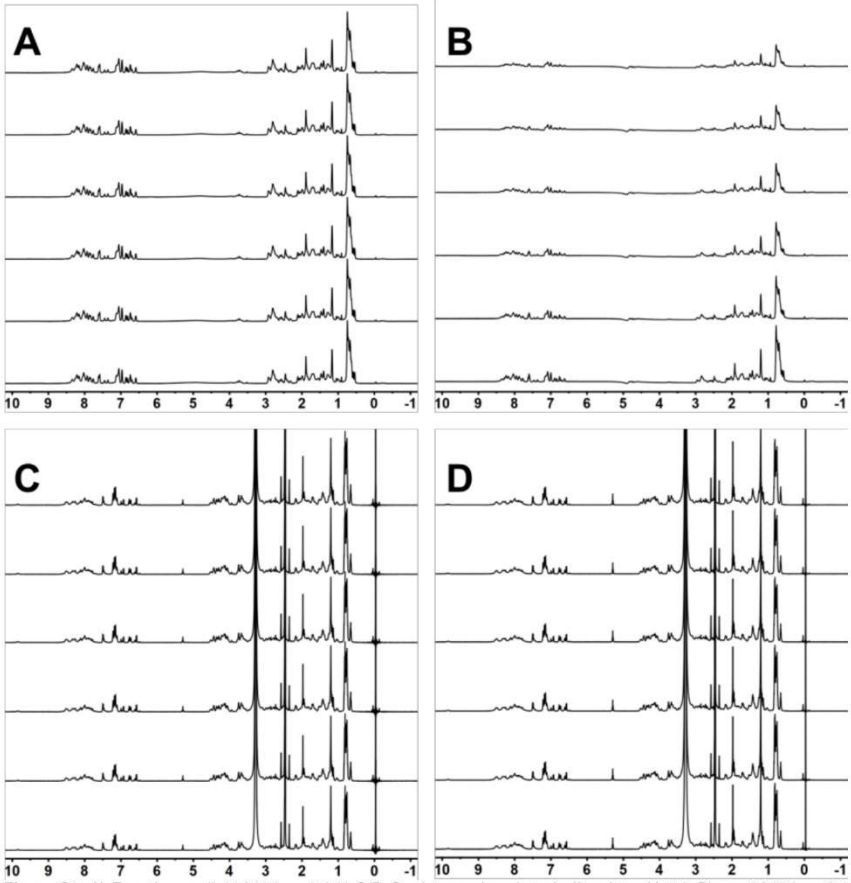

Figure S1. A) Enantiopure (L-)Aβ40 in a 9:1 H_2O/D_2O mixture, phosphate-buffered to pH 7.4; B) rac-Aβ40 in a 9:1 H_2O/D_2O mixture, phosphate-buffered to pH 7.4; C) L-Aβ40 in d_6-DMSO; D) rac-Aβ40 in d_6-DMSO. All ^1H NMR experiments were performed at 298 K with 160 μM total Aβ40 in all cases. The stacked spectra correspond, from lowest up, to t = 1, 9, 17, 25, 33 and 41 min. Racemic Aβ40 loses 61 % signal in water over that time period, whereas signal intensity is invariant in all other cases.

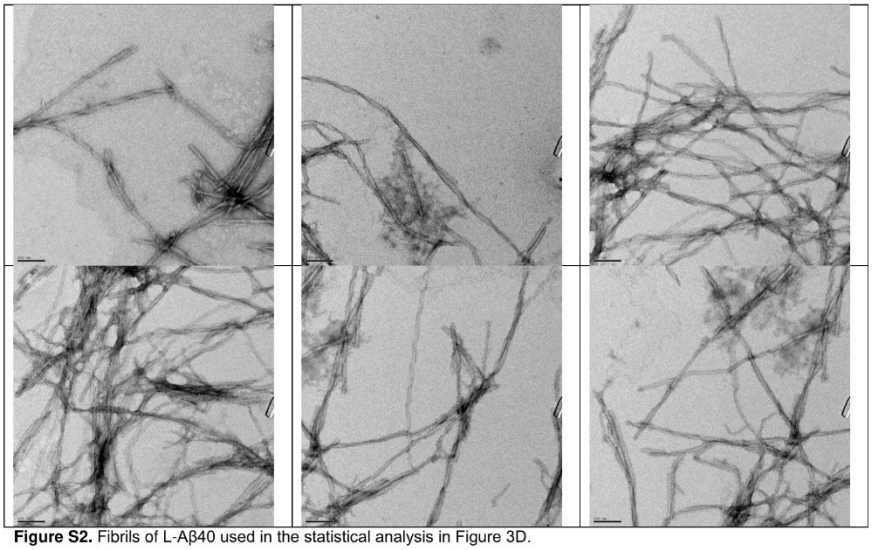

Figure S2. Fibrils of L-Aβ40 used in the statistical analysis in Figure 3D.

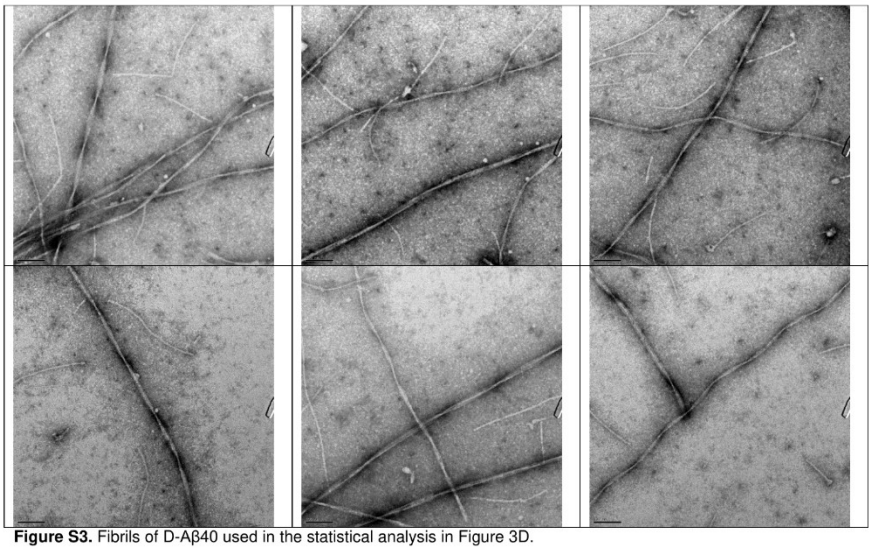

Figure S3. Fibrils of D-Aβ40 used in the statistical analysis in Figure 3D.

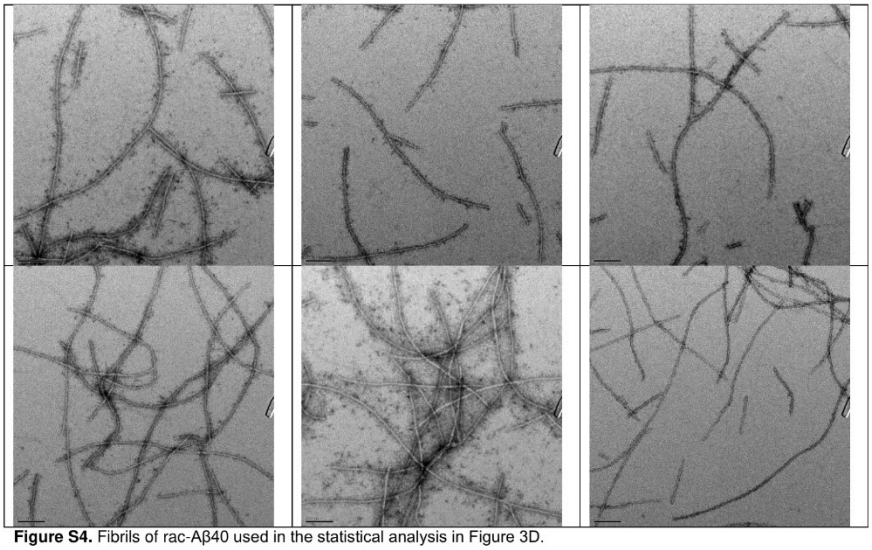

Figure S4. Fibrils of rac-Aβ40 used in the statistical analysis in Figure 3D.

DFT-optimized LVFFA:lvffa rippled parallel cross-β structure (*cf.* Figure 4)

188
symmetry c1

C	9.714220000	-1.313791000	1.432209000
C	8.638166000	-1.523183000	0.393099000
O	8.680427000	-0.956365000	-0.704045000
N	7.629391000	-2.350761000	0.724325000
C	6.531293000	-2.624044000	-0.196856000
C	5.332444000	-2.967098000	0.688972000
O	5.291094000	-4.033591000	1.296676000
N	4.381912000	-2.012923000	0.759018000
C	3.198788000	-2.168136000	1.574627000
C	1.958224000	-1.942119000	0.710374000
O	1.982868000	-1.204835000	-0.280122000
N	0.840077000	-2.564275000	1.119833000
C	-0.383267000	-2.507537000	0.343814000
C	-1.557549000	-2.656129000	1.302813000
O	-1.526298000	-3.490351000	2.204104000
N	-2.602410000	-1.852116000	1.032024000
C	-3.780144000	-1.794798000	1.867442000
C	-4.996338000	-1.663480000	0.958058000
O	-4.988009000	-0.819326000	0.057667000
N	-6.049000000	-2.446258000	1.219548000
C	-7.293306000	-2.335163000	0.474155000
C	-8.433595000	-2.496061000	1.476817000
O	-8.414004000	-3.418082000	2.287088000
N	-9.434445000	-1.607668000	1.348622000
O	-1.373138000	0.420563000	-0.369667000
C	-1.376324000	1.617480000	-0.680031000
C	-0.145674000	2.478326000	-0.429711000
N	1.035316000	1.679639000	-0.678937000
C	2.211601000	2.274446000	-0.968306000
O	2.344700000	3.492491000	-1.068626000
N	-2.433265000	2.245245000	-1.205314000
C	-3.726000000	1.613712000	-1.375622000
C	-4.802488000	2.610858000	-0.971544000
O	-4.698956000	3.797207000	-1.278020000
N	-5.882646000	2.079725000	-0.369708000
C	-7.112939000	2.842887000	-0.298623000
C	-8.281157000	1.864313000	-0.269823000
O	-8.151715000	0.741322000	0.217533000
N	-9.447342000	2.340154000	-0.729125000
C	3.369979000	1.317415000	-1.220757000
N	4.603545000	2.063728000	-1.077009000
C	5.681214000	1.560855000	-0.457742000
C	6.902531000	2.465886000	-0.336551000
N	7.962816000	1.829637000	-1.097195000
C	8.519888000	2.385037000	-2.196917000
C	9.577737000	1.537322000	-2.871157000
O	5.735146000	0.410700000	-0.008255000
O	8.227889000	3.507108000	-2.608379000
H	-10.198789000	-1.650263000	2.010257000
H	-10.266954000	1.747749000	-0.712075000
C	-7.395153000	-3.421272000	-0.597470000

H	-7.309726000	-1.344472000	0.015041000
H	-9.284091000	-0.745702000	0.827901000
C	-3.743262000	-0.547828000	2.783017000
H	-3.809039000	-2.708113000	2.466510000
H	-6.019713000	-3.132492000	1.965495000
C	-0.417301000	-3.642192000	-0.704005000
H	-0.417484000	-1.539246000	-0.157483000
H	-2.487077000	-1.117012000	0.334631000
C	3.202658000	-1.223897000	2.800249000
H	3.205712000	-3.202092000	1.932016000
H	0.855318000	-3.211981000	1.900465000
C	6.880123000	-3.759397000	-1.163882000
H	6.351337000	-1.697773000	-0.749606000
H	4.574074000	-1.114063000	0.316055000
H	7.671196000	-2.882047000	1.585063000
H	8.198972000	0.866009000	-0.854441000
C	3.233381000	0.638841000	-2.603559000
H	3.352815000	0.533406000	-0.462457000
H	0.992348000	0.670964000	-0.527183000
C	-3.954200000	1.226051000	-2.862655000
H	-3.768482000	0.722066000	-0.749466000
H	-5.931981000	1.071790000	-0.214059000
C	-0.159328000	3.019938000	1.021383000
H	-0.130766000	3.327248000	-1.120277000
H	-2.403728000	3.247096000	-1.370355000
C	7.258000000	2.621163000	1.150275000
H	6.718174000	3.440176000	-0.798459000
H	4.570710000	3.045051000	-1.329952000
C	-7.157827000	3.739672000	0.943625000
H	-7.175366000	3.465606000	-1.198821000
H	-9.514415000	3.231170000	-1.199892000
H	10.676255000	-1.603942000	1.003447000
H	9.764003000	-0.247026000	1.667870000
H	9.541232000	-1.876688000	2.350705000
H	9.322792000	1.429065000	-3.928068000
H	10.532197000	2.067997000	-2.813328000
H	9.680937000	0.552922000	-2.411524000
H	-6.573605000	-3.308501000	-1.311012000
H	-7.332249000	-4.411148000	-0.136030000
H	-8.346302000	-3.343315000	-1.132802000
H	0.446886000	-3.502520000	-1.362514000
H	-0.293462000	-4.594649000	-0.177700000
H	6.909979000	-4.701099000	-0.600361000
H	7.894412000	-3.560684000	-1.529204000
H	2.251234000	0.150221000	-2.602542000
H	-3.627498000	2.071410000	-3.477576000
H	-3.301203000	0.374588000	-3.082120000
H	-3.763412000	0.331490000	2.125597000
H	-4.657570000	-0.530575000	3.386121000
H	2.298155000	-1.461187000	3.376598000
H	-8.073377000	4.337123000	0.964142000
H	-7.110841000	3.125832000	1.847943000
H	-6.293963000	4.407793000	0.920360000
H	0.756647000	3.607441000	1.141105000
H	-0.103617000	2.166799000	1.706802000
H	7.747017000	1.693992000	1.479945000

H	6.324576000	2.697188000	1.723635000
C	-2.524189000	-0.522876000	3.667755000
C	-0.236634000	-0.521398000	5.294585000
C	-1.294594000	-0.077811000	3.168548000
C	-2.588760000	-0.974724000	4.988083000
C	-1.453893000	-0.978113000	5.796678000
C	-0.161778000	-0.068736000	3.978340000
H	-1.226136000	0.252082000	2.132866000
H	-3.538483000	-1.323833000	5.386173000
H	-1.522345000	-1.331578000	6.820924000
H	0.778780000	0.302257000	3.582414000
H	0.647471000	-0.513802000	5.924903000
C	-1.380798000	3.855274000	1.309549000
C	-3.700709000	5.371956000	1.730149000
C	-2.467256000	3.316294000	2.004117000
C	-1.471844000	5.163710000	0.825211000
C	-2.623832000	5.918691000	1.034599000
C	-3.621138000	4.067562000	2.214315000
H	-2.399857000	2.303256000	2.395092000
H	-0.630022000	5.594154000	0.286856000
H	-2.678464000	6.935699000	0.658596000
H	-4.455913000	3.634354000	2.757825000
H	-4.596413000	5.962585000	1.897735000
C	-1.704020000	-3.637356000	-1.489308000
C	-4.144002000	-3.549550000	-2.866527000
C	-1.903692000	-2.714249000	-2.520707000
C	-2.743933000	-4.505896000	-1.149531000
C	-3.957785000	-4.464641000	-1.832113000
C	-3.114013000	-2.672645000	-3.208456000
H	-1.102588000	-2.027897000	-2.787200000
H	-2.599938000	-5.215965000	-0.338537000
H	-4.755093000	-5.150025000	-1.559914000
H	-3.255196000	-1.960587000	-4.017004000
H	-5.086158000	-3.518450000	-3.407364000
C	-5.401300000	0.908214000	-3.153418000
C	-8.149291000	0.430437000	-3.458684000
C	-5.942930000	-0.340801000	-2.840363000
C	-6.250846000	1.910715000	-3.632936000
C	-7.616296000	1.677617000	-3.781095000
C	-7.307606000	-0.578443000	-2.993943000
H	-5.297452000	-1.116522000	-2.438699000
H	-5.839152000	2.890101000	-3.865761000
H	-8.263957000	2.470188000	-4.144608000
H	-7.715673000	-1.554507000	-2.746611000
H	-9.214049000	0.247598000	-3.567309000
C	5.941499000	-3.896367000	-2.369157000
H	5.918455000	-2.925377000	-2.886126000
C	4.507622000	-4.268877000	-1.980390000
H	4.501147000	-5.182667000	-1.374396000
H	3.906767000	-4.451522000	-2.877611000
H	4.008252000	-3.480773000	-1.407506000
C	6.507188000	-4.938463000	-3.335998000
H	7.523301000	-4.680343000	-3.651218000
H	5.882734000	-5.024153000	-4.230849000
H	6.542692000	-5.923440000	-2.855139000
C	8.134332000	3.830357000	1.494407000

H	7.553533000	4.734446000	1.261963000
C	9.435896000	3.885973000	0.692466000
H	9.996099000	2.948458000	0.796816000
H	10.068919000	4.700755000	1.060025000
H	9.250378000	4.057228000	-0.371515000
C	8.431326000	3.825989000	2.994818000
H	7.510262000	3.794600000	3.586164000
H	8.993708000	4.718797000	3.285622000
H	9.032954000	2.948058000	3.260145000
C	3.159414000	0.250766000	2.393619000
H	3.127107000	0.886334000	3.284625000
H	2.284178000	0.487924000	1.776426000
H	4.059326000	0.521374000	1.827505000
C	4.428071000	-1.510082000	3.667443000
H	4.397170000	-0.908938000	4.580898000
H	5.345824000	-1.255539000	3.124874000
H	4.480132000	-2.566500000	3.948369000
C	3.286581000	1.659058000	-3.739799000
H	2.515250000	2.428894000	-3.634362000
H	3.141523000	1.162170000	-4.703415000
H	4.263231000	2.155850000	-3.763326000
C	4.300209000	-0.441898000	-2.768183000
H	4.215090000	-1.187675000	-1.970379000
H	5.308286000	-0.011062000	-2.735156000
H	4.182016000	-0.951810000	-3.730170000

PNAS
www.pnas.org

Supplementary Information for

Evidence for aggregation-independent, PrP^C-mediated Aβ cellular internalization

Alejandro R. Foley,[a],† Graham P. Roseman,[a],† Ka Chan,[a] Amanda Smart,[a] Thomas S. Finn,[a], Kevin Yang,[a] R. Scott Lokey,[a] Glenn L. Millhauser,[a],* Jevgenij A. Raskatov.[a],*

† Denotes equal contribution, alphabetically ordered

Corresponding authors: Glenn L. Millhauser, Jevgenij A. Raskatov.
Email: glennm@ucsc.edu, jraskato@ucsc.edu.

This PDF file includes:

Supplementary text
Figures S1 to S10
Tables S1 to S2

L-Aβ40-TAMRA

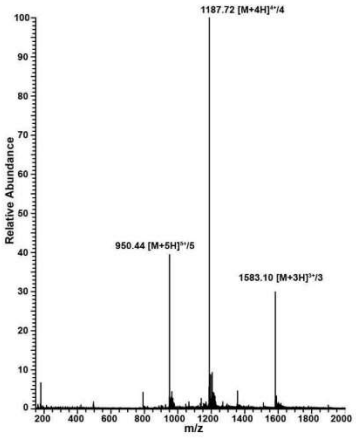

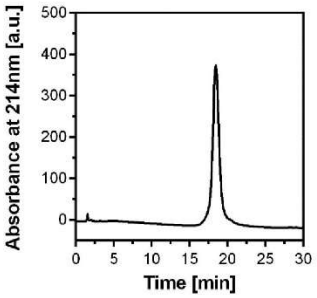

Peak #	Time [min]	Area	% Area
1	18.45	24260	98.2
2	20.15	444	1.8

D-Aβ40-TAMRA

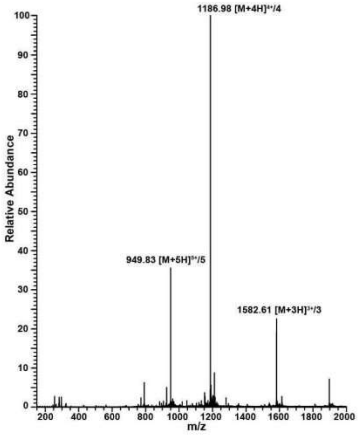

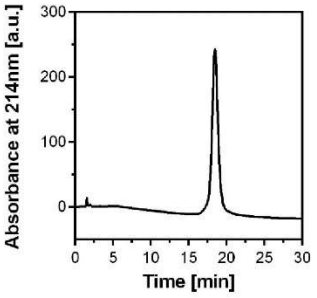

Peak #	Time [min]	Area	% Area
1	18.47	15012	99.2
2	20.17	125	0.8

Fig. S1. Mass spectrometry and HPLC characterization for L- and D- Aβ40 TAMRA-labeled samples.

1

L-Aβ(1-16)-TAMRA

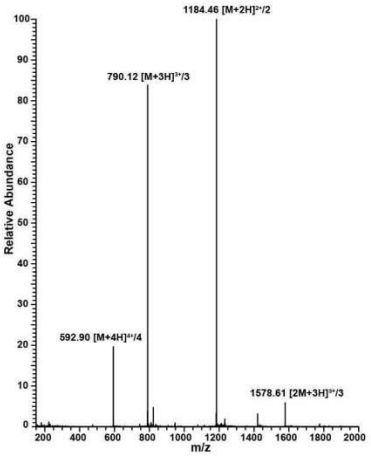

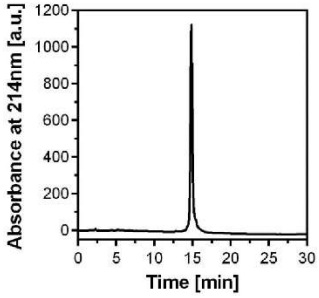

Peak #	Time [min]	Area	% Area
1	14.2	266	1.3
2	14.6	18919	95.3
3	15.1	665	3.4

D-Aβ(1-16)-TAMRA

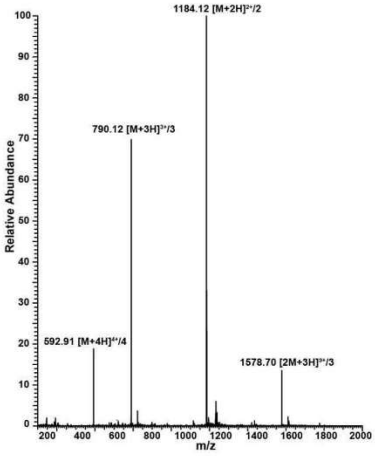

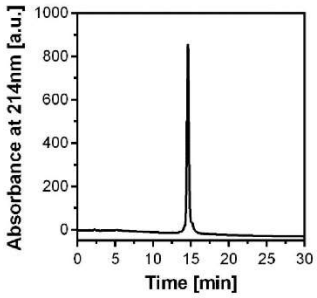

Peak #	Time [min]	Area	% Area
1	14.2	190	1.1
2	14.6	16439	95.1
3	15	649	3.8

Fig. S2. Mass spectrometry and HPLC characterization for L- and D- Aβ(1-16) TAMRA-labeled samples.

L-Aβ(1-30)

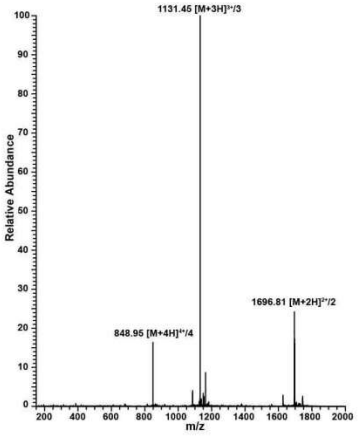

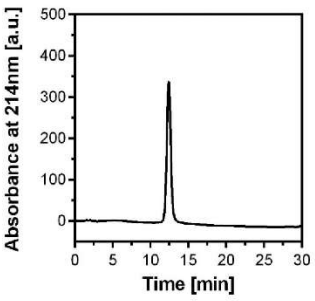

Peak #	Time [min]	Area	% Area
1	12.4	12380	99.3
2	13.2	93	0.7

L-Aβ(1-30)-TAMRA

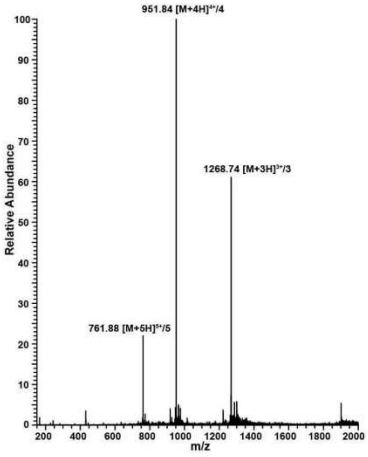

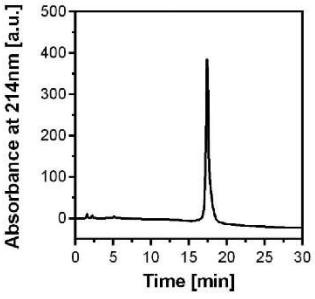

Peak #	Time [min]	Area	% Area
1	16.6	111	0.9
2	17.4	12011	99.1

Figure S3. Mass spectrometry and HPLC characterization for L-Aβ(1-30) and L-Aβ(1-30)-TAMRA samples.

D-Aβ(1-30)

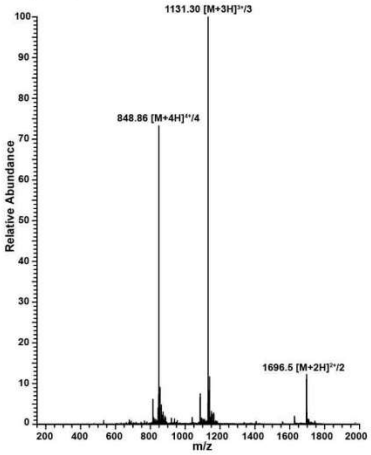

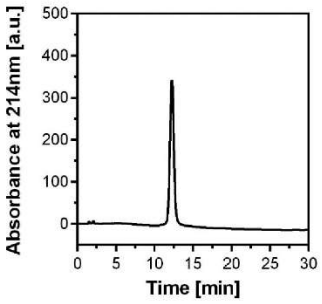

Peak #	Time [min]	Area	% Area
1	12.3	11907	99.5
2	13	55	0.5

D-Aβ(1-30)-TAMRA

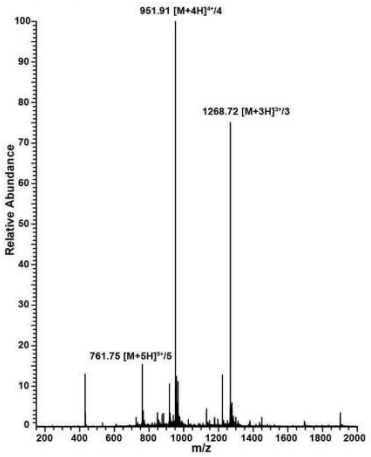

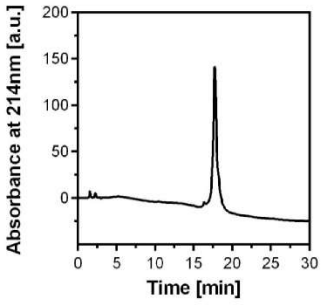

Peak #	Time [min]	Area	% Area
1	16.8	125	2.2
2	17.7	5531	97.8

Figure S4. Mass spectrometry and HPLC characterization for D-Aβ(1-30) and D-Aβ(1-30)-TAMRA samples.

L-Aβ(16-30)-TAMRA

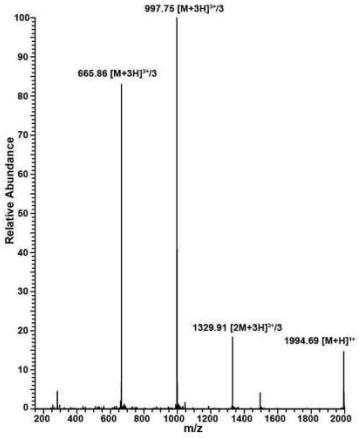

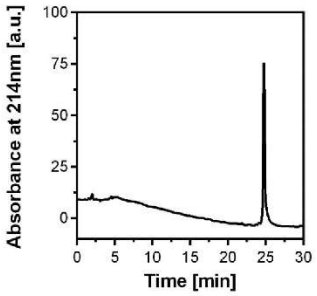

Peak #	Time [min]	Area	% Area
1	24.8	1206	97.6
2	25.5	30	2.4

D-Aβ(16-30)-TAMRA

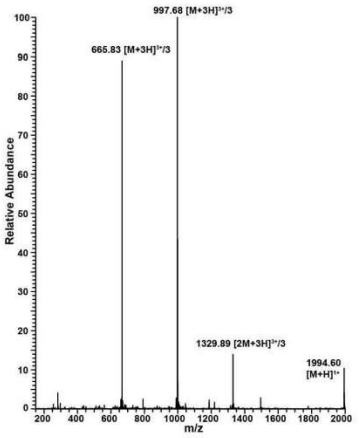

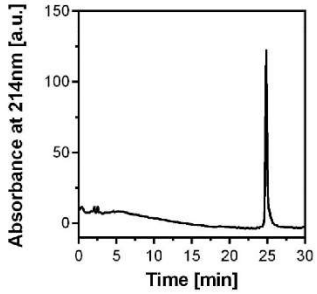

Peak #	Time [min]	Area	% Area
1	24.9	2216	98
2	25.6	46	2

Figure S5. Mass spectrometry and HPLC characterization for L- and D- Aβ(16-30) TAMRA-labeled samples.

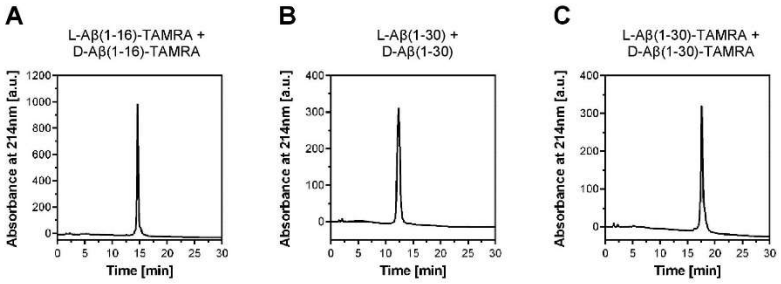

Figure S6. HPLC co-injection of enantiomeric pairs (1:1). Chromatograms of L+D mixtures of the peptides result in a single peak, confirming the expected retention similarity. (A) L-Aβ(1-16)-TAMRA + D-Aβ(1-16)-TAMRA. (B) L-Aβ(1-30) + D-Aβ(1-30). (C) L-Aβ(1-30)-TAMRA + D-Aβ(1-30)-TAMRA.

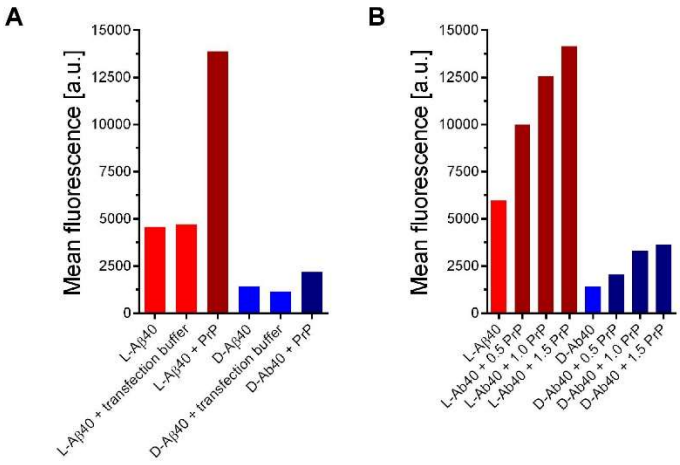

Figure S7. (A)Transfection buffer control for Aβ40 uptake in HEK293T cells (2h incubation time). (B) PrP^{C} transfection titration dependence of Aβ uptake in HEK293T cells (2h incubation time).

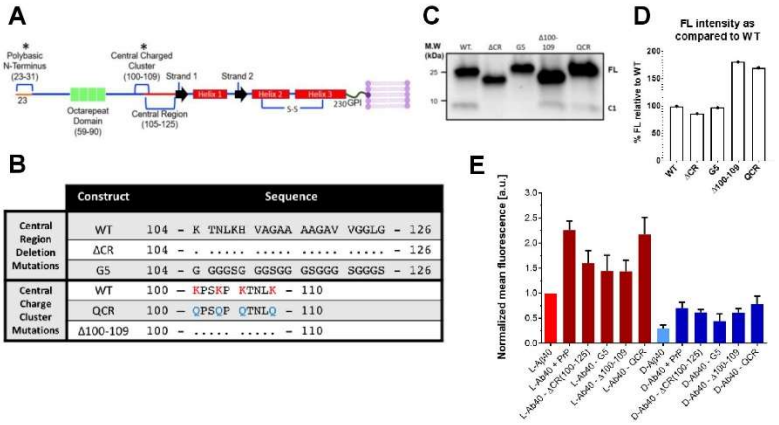

Figure S8. Mutations in PrP^C sequence and NMR binding site. (A) Scheme of PrP^C structure, with * indicating previously reported possible PrP^C-Aβ binding sites. (B) Mutations performed in transfected PrP^C. (C) Western blot showing expression of transfected PrP^C constructs. (D) Western blot intensity comparison (E) Mean flow cytometry quantitation of Aβ uptake for PrP^C and PrP^C constructs with error bars showing SD from 3 biological replicates.

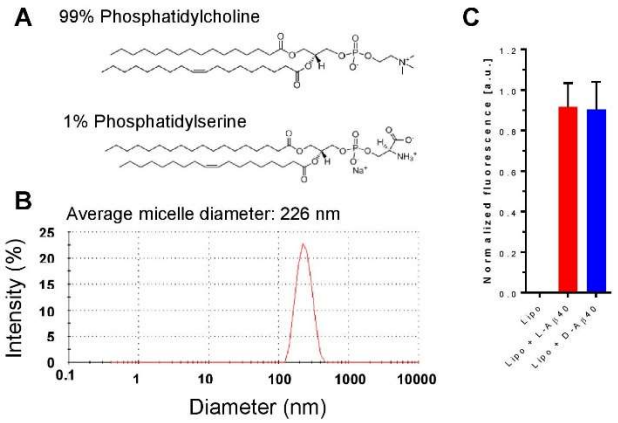

Figure S9. Liposome association of L-Aβ40 and D-Aβ40 in 99:1 PC:PS phospholipid micelles. (A) Phospholipid structures. (B) Dynamic Light Scattering (DLS) showing diameter distribution of the lipid micelles synthesized. (C) Lipid encapsulation quantitation by flow cytometry, showing average normalized value with error bars for SD of 2 technical replicates. Lipo: Liposomes control with no Aβ40 dosing.

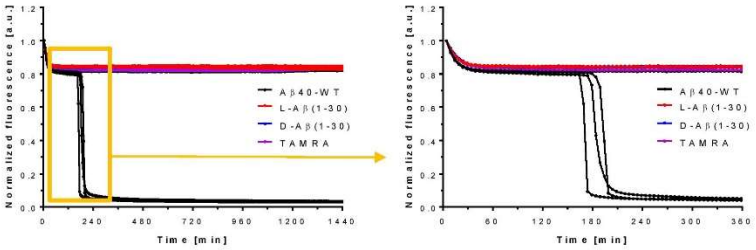

Figure S10. Aggregation kinetics monitored by TAMRA fluorescence for TAMRA alone and TAMRA-conjugated peptides at 5 μM concentration for all samples. Aggregation and fibril formation results in decay of fluorescence signal. Samples were run for at 37 ºC in in 20mM phosphate buffer pH 7.4 with continuous shaking. Data show individual curves for 3 technical replicates. Note that L-Aβ(1-30), D-Aβ(1-30), and TAMRA curves overlap.

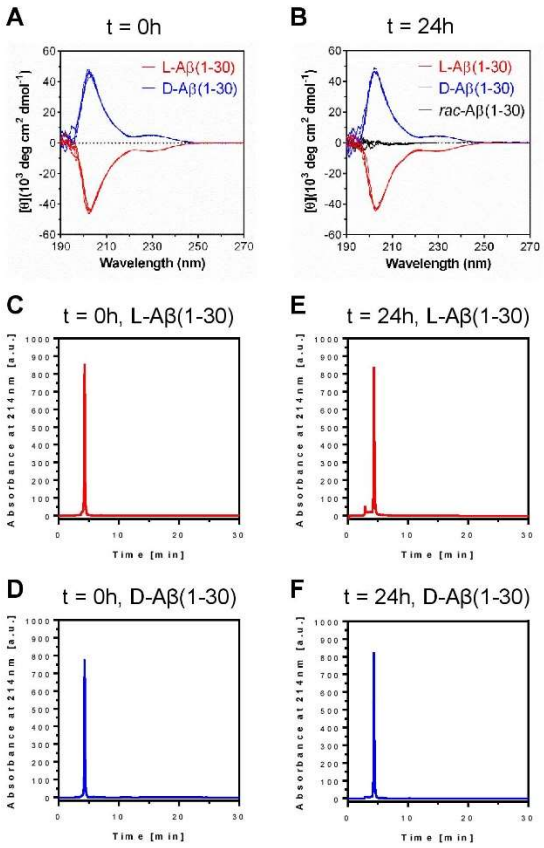

Figure S11. Aggregation state of L- and D- Aβ(1-30) peptides at 200 μM concentration (same concentration as NMR experiments). (A-B) CD spectroscopy curves for L-Aβ(1-30) and D-Aβ(1-30) at t=0 and after 24h incubation at 37 ºC in in 20mM phosphate buffer pH 7.4. Curves show random coil conformation in both cases. At the end of the 24h experiment, equal volumes of L- and D- Aβ(1-30) were mixed (rac-Aβ(1-30)) to obtain a flat line which confirms that similar species are present for the enantiomers. Four replicates are shown in each case. (C,E) Size exclusion chromatography for L-Aβ(1-30) at t=0 and after 24h incubation at 37 ºC in 20mM phosphate buffer pH 7.4. (D,F) Size exclusion chromatography for L-Aβ(1-30) at t=0 and after 24h incubation at 37 ºC in 20mM phosphate buffer pH 7.4.

Table S1. NMR data extracted from WT PrP^C sample and WT PrP^C and L-Aβ(1-30). Data includes the ω_N (ppm), ω_{HN} (ppm), and peak height for each assigned residue from each spectrum collected. Intensity ratio's (I/Io) and weighted average chemical shifts (Δ) were calculated as described in the material and methods.

	100 μM WT PrP^C			100 μM WT PrP^C and 200 μM L-Aβ(1-30)			Results	
Assignment	ω_N (ppm)	ω_{HN} (ppm)	Peak Height (I_o)	ω_N (ppm)	ω_{HN} (ppm)	Peak Height (I_o)	Intensity Ratio (I/I_o)	Chemical Shift (Δ)
T94N-H	113.351	7.985	6424100	113.36	7.983	3019894	0.470088261	0.004215448
K100N-H	122.402	7.953	17950030	122.371	7.947	12638700	0.704104673	0.014119844
S102N-H	116.719	8.385	3242517	116.675	8.381	1120979	0.345712605	0.018577406
K103N-H	124.05	8.281	5787884	124.023	8.277	2398607	0.414418637	0.011829201
K105N-H	122.001	8.508	8902112	121.998	8.507	4289224	0.481820943	0.001590597
L108N-H	123.108	8.26	24243946	123.091	8.258	14864928	0.613139792	0.007289033
K109N-H	121.679	8.252	13555170	121.668	8.252	8684310	0.640664042	0.004535416
A112N-H	127.989	8.395	21615208	127.958	8.391	16654246	0.770487427	0.013392909
A114N-H	123.844	8.113	17861734	123.828	8.111	9870933	0.552630165	0.006893475
A115N-H	123.201	8.199	30383374	123.183	8.194	24863478	0.818325114	0.008948743
A116N-H	123.343	8.112	7835814	123.375	8.114	7278524	0.928879118	0.013344662
A117N-H	123.237	8.169	46948304	123.218	8.168	31380182	0.668398628	0.007897468
G118N-H	107.882	8.252	16956138	107.879	8.252	10436704	0.615511858	0.001236932
A119N-H	123.542	8.047	23887984	123.532	8.045	17431636	0.729724032	0.004582576
V120N-H	119.52	8.102	35979440	119.495	8.098	32017722	0.889889392	0.011056672
V121N-H	124.536	8.243	29050736	124.519	8.242	23827096	0.820189065	0.007080254
G122N-H	113.262	8.531	11129416	113.243	8.528	6709092	0.602825162	0.008388683
L124N-H	121.71	8.173	12121994	121.708	8.174	8971438	0.740095895	0.001296148
Y127N-H	117.99	7.817	9912163	117.996	7.821	9488505	0.957258774	0.00470319
M128N-H	121.441	9.092	3213702	121.448	9.092	3014108	0.93789281	0.002886174
G130N-H	114.948	9.37	1208061	114.957	9.368	991080	0.820389037	0.004215448
S131N-H	113.79	8.274	10024192	113.795	8.275	9122639	0.910062277	0.002291288
A132N-H	125.553	8.686	8212766	125.557	8.686	7566877	0.921355485	0.001649242
M133N-H	121.298	8.746	5057316	121.289	8.746	4475074	0.884871343	0.003710795
S134N-H	116.193	8.395	5751096	116.194	8.395	4465210	0.77641027	0.000412311
R135N-H	126.605	8.62	6128346	126.601	8.62	5427170	0.885584789	0.001649242
M137N-H	122.008	8.666	5063768	121.966	8.66	3997578	0.789447305	0.018327029
I138N-H	124.305	6.569	8414730	124.298	6.57	8066947	0.958669737	0.003054505
F140N-H	125.147	10.318	4311424	125.172	10.325	3745983	0.868850524	0.012459936
G141N-H	108.992	8.9	4153183	109.037	8.883	3191345	0.768409434	0.025164459
N142N-H	114.356	7.236	13369215	114.375	7.232	12114600	0.90615642	0.008796022
D143N-H	123.239	8.977	2663396	123.287	8.974	1463707	0.549564165	0.020016993
W144N-H	120.319	8.493	9552731	120.261	8.493	9427032	0.986841564	0.023914013
Y148N-H	120.858	8.243	8402322	120.832	8.239	7660228	0.91167989	0.011442028
Y149N-H	120.489	8.986	5913274	120.498	8.989	5371904	0.908448349	0.004771792
R150N-H	117.337	7.867	7133547	117.308	7.865	6750680	0.946328664	0.012123118
E151N-H	115.802	7.886	7709018	115.817	7.886	7245764	0.939907521	0.006184658
N152N-H	115.175	7.529	5747722	115.164	7.528	5821518	1.012839174	0.004644351
M153N-H	118.393	7.845	6417437	118.388	7.846	5927880	0.923714561	0.002291288
Y154N-H	116.584	7.552	6384978	116.571	7.55	6338655	0.992745002	0.005721014
R155N-H	118.875	7.489	5519562	118.872	7.489	5409473	0.980054758	0.001236932
Y156N-H	121.361	7.413	6100610	121.355	7.412	5861234	0.960761957	0.002668333
N158N-H	116.291	8.604	4979134	116.301	8.605	4030174	0.809412641	0.004242641
Q159N-H	114.431	7.272	8484909	114.427	7.273	8176128	0.963608213	0.00192873
V160N-H	112.65	8.415	5226684	112.644	8.413	4792602	0.916948872	0.003181195
Y162N-H	111.092	8.486	6066904	111.105	8.483	4460763	0.73526184	0.006142475
R163N-H	120.572	7.922	3298904	120.568	7.923	2808503	0.851344265	0.00192873
Q171N-H	119.961	8.627	1484388	119.965	8.621	963317	0.648965769	0.00622254
N172N-H	117.294	8.371	6562358	117.243	8.368	5328290	0.811947474	0.021240763
N173N-H	118.206	8.535	7794424	118.151	8.527	6385762	0.819273111	0.024046829
V175N-H	120.312	8.836	1897252	120.323	8.825	1824789	0.961806339	0.011898319
H176N-H	117.324	8.284	2150563	117.307	8.285	1858048	0.863982129	0.007080254
D177N-H	118.219	7.428	2827622	118.148	7.417	2360777	0.83489837	0.031272512
C178N-H	119.002	8.13	4817084	118.954	8.129	4618611	0.958798103	0.019816155
V179N-H	124.822	9.233	5488668	124.831	9.246	4932554	0.898679607	0.013519246
N180N-H	116.361	7.577	7626864	116.357	7.581	7075153	0.927662143	0.004326662

I181N-H	118.922	8.79	2502807	118.931	8.797	2632126	1.051669585	0.007922752
T182N-H	118.015	8.127	6209699	118.005	8.126	5780734	0.930920162	0.004242641
I183N-H	120.979	8.445	5048573	120.979	8.444	4326807	0.857035642	0.001
K184N-H	123.109	8.075	10107850	123.091	8.074	9565092	0.946303319	0.007488658
Q185N-H	117.084	8.508	6192122	117.092	8.51	5915419	0.955313703	0.00385746
T187N-H	114.775	8.482	4113032	114.788	8.487	3560518	0.865667469	0.007330075
T189N-H	115.193	8.149	8866311	115.187	8.151	8243462	0.929751054	0.003181195
T190N-H	114.527	8.016	7524849	114.52	8.016	6900086	0.916973351	0.002886174
T191N-H	118.116	8.232	8109748	118.12	8.232	6728460	0.829675595	0.001649242
T192N-H	116.268	7.787	5056456	116.264	7.785	3471103	0.686469535	0.002592296
K193N-H	120.027	7.843	19283854	120.023	7.843	16694135	0.86570532	0.001649242
G194N-H	107.838	7.892	8666257	107.816	7.889	7394852	0.853292488	0.009554057
E195N-H	119.861	7.507	7223036	119.86	7.506	6816574	0.943726987	0.001081665
N196N-H	119.463	8.503	11862763	119.448	8.503	10642914	0.897169909	0.006184658
F197N-H	121.7	8.712	9429347	121.697	8.714	9071685	0.962069272	0.002351595
T198N-H	115.876	9.563	4708860	115.861	9.564	4525244	0.961006273	0.006264982
E199N-H	119.993	9.155	5238926	119.989	9.157	4684064	0.894088598	0.002592296
T200N-H	116.519	7.92	6248851	116.519	7.918	5228702	0.836746147	0.002
D201N-H	120.189	7.433	9432615	120.186	7.431	8360230	0.886310954	0.002351595
K203N-H	119.101	7.678	7468032	119.089	7.677	7074695	0.947330568	0.005047772
M204N-H	118.401	8.147	7227908	118.382	8.147	6405634	0.886236239	0.007833901
M205N-H	118.175	8.677	6756188	118.169	8.676	6713302	0.993652338	0.002668333
E206N-H	118.881	8.549	7782566	118.889	8.551	7390547	0.949628567	0.00385746
R207N-H	116.724	7.253	7759989	116.702	7.252	7506032	0.967273536	0.009125788
V208N-H	119.035	8.22	6876130	119.015	8.219	6881002	1.000708538	0.008306624
V209N-H	121.199	9.124	4814300	121.203	9.126	4559622	0.947099682	0.002592296
Q211N-H	115.302	7.063	7254233	115.29	7.062	6477978	0.892992822	0.005047772
C213N-H	119.486	9.201	6035326	119.492	9.202	5288156	0.876200557	0.002668333
V214N-H	123.585	8.481	6191588	123.582	8.482	5234774	0.845465493	0.001590597
T215N-H	118.049	8.086	7364434	118.042	8.086	7191682	0.976542393	0.002886174
Q216N-H	122.552	8.674	4507784	122.556	8.673	4391530	0.974210388	0.00192873
Y217N-H	120.145	8.559	4821923	120.138	8.559	4509910	0.935292828	0.002886174
Q218N-H	119.663	8.214	11185052	119.661	8.213	11414723	1.020533745	0.001296148
E220N-H	118.239	8.376	5242058	118.244	8.378	5147454	0.981952889	0.002872281
S221N-H	115.038	8.343	3064523	115.044	8.342	2806842	0.91591481	0.002668333
Q222N-H	119.911	7.58	4464875	119.918	7.583	3623634	0.811586887	0.004162932
A223N-H	120.717	7.578	19668042	120.711	7.579	18515702	0.941410538	0.002668333
Y224N-H	118.863	7.89	24954530	118.855	7.892	22608668	0.905994543	0.00385746
D226N-H	121.005	8.181	19005454	120.994	8.181	15290480	0.804531162	0.004535416
G227N-H	108.015	7.826	17143192	108.012	7.827	15098134	0.88070728	0.001590597
R229N-H	122.468	8.218	15411889	122.467	8.217	10924686	0.708847955	0.001081665
S230N-H	122.686	7.953	56243100	122.676	7.953	56165860	0.998626676	0.004123106

Table S2. NMR data extracted from WT PrP^C sample and WT PrP^C and D-Aβ(1-30). Data includes the ω_N (ppm), ω_{HN} (ppm), and peak height for each assigned residue from each spectrum collected. Intensity ratio's (I/Io) and weighted average chemical shifts (Δ) were calculated as described in the material and methods.

	100 μM WT PrP^C			100 μM WT PrP^C and 200 μM L-Aβ(1-30)			Results	
Assignment	ω_N (ppm)	ω_{HN} (ppm)	Peak Height (I_o)	ω_N (ppm)	ω_{HN} (ppm)	Peak Height (I_o)	Intensity Ratio (I/I_o)	Chemical Shift (Δ)
T94N-H	113.352	7.986	7599211	113.353	7.987	9010806	1.185755469	0.001081665
K100N-H	122.407	7.957	18201508	122.443	7.962	19434664	1.067750211	0.015662695
S102N-H	116.749	8.391	4961444	116.77	8.393	6767177	1.363953115	0.008886507
K103N-H	124.062	8.288	7353367	124.073	8.29	9226588	1.254743303	0.004956813
K105N-H	122.001	8.507	12545061	122.005	8.507	14251673	1.136038557	0.001649242
L108N-H	123.122	8.265	28239366	123.135	8.267	28681440	1.01565453	0.005721014
K109N-H	121.681	8.255	15919620	121.681	8.255	16863918	1.059316617	0
A112N-H	128.014	8.402	27872390	128.032	8.406	27081234	0.971615064	0.008430896
A114N-H	123.844	8.114	21248888	123.851	8.116	23128564	1.08845997	0.00351141
A115N-H	123.213	8.204	33714788	123.226	8.205	33952244	1.007043082	0.005452522
A116N-H	123.356	8.11	7722185	123.35	8.109	7288922	0.94389373	0.002668333
A117N-H	123.248	8.172	55127228	123.259	8.173	54284956	0.984721307	0.004644351
G118N-H	107.872	8.256	18917360	107.88	8.257	20443480	1.08067299	0.003446738
A119N-H	123.541	8.049	27529366	123.545	8.05	27166442	0.986816841	0.00192873
V120N-H	119.53	8.103	42597488	119.539	8.104	44074188	1.034666363	0.003843176
V121N-H	124.543	8.247	29381036	124.551	8.248	26526814	0.902854957	0.003446738
G122N-H	113.267	8.531	14296060	113.272	8.533	15532709	1.086502785	0.002872281
L124N-H	121.712	8.172	13385230	121.715	8.172	14450449	1.079581673	0.001236932
Y127N-H	117.984	7.82	9945982	117.984	7.818	9790498	0.984367154	0.002
M128N-H	121.441	9.09	2881365	121.441	9.091	3007414	1.04374628	0.001
G130N-H	114.972	9.365	1117235	114.987	9.371	973903	0.87170828	0.008616844
S131N-H	113.771	8.276	10893098	113.766	8.276	11363523	1.043185602	0.002061553
A132N-H	125.548	8.688	8619931	125.539	8.689	8563679	0.993474194	0.003843176
M133N-H	121.301	8.752	5308498	121.309	8.754	5647340	1.063830108	0.00385746
S134N-H	116.183	8.398	7135180	116.183	8.398	7652020	1.072435454	0
R135N-H	126.602	8.621	7081700	126.606	8.622	7040720	0.994213254	0.00192873
M137N-H	122.022	8.67	5193312	122.048	8.674	5452964	1.049997381	0.011442028
I138N-H	124.302	6.57	9883306	124.307	6.57	10123269	1.024279629	0.002061553
F140N-H	125.12	10.315	4479014	125.109	10.31	4775168	1.066120356	0.006750556
G141N-H	108.965	8.915	4440792	108.946	8.925	4743104	1.068076145	0.012703149
N142N-H	114.331	7.239	13397423	114.316	7.241	14091570	1.051811979	0.0065
D143N-H	123.182	8.975	3279674	123.165	8.977	4083602	1.245124363	0.007289033
W144N-H	120.353	8.493	9968630	120.378	8.493	9546909	0.95769519	0.010307764
Y148N-H	120.875	8.248	7633424	120.901	8.252	8254200	1.081323401	0.011442028
Y149N-H	120.468	8.984	5219158	120.459	8.982	5610992	1.075076095	0.004215448
R150N-H	117.344	7.87	7145774	117.352	7.872	6975852	0.976220631	0.00385746
E151N-H	115.792	7.889	7511505	115.788	7.89	7602953	1.012174391	0.00192873
N152N-H	115.174	7.53	6912278	115.181	7.531	7393772	1.069657789	0.003054505
M153N-H	118.381	7.848	6395594	118.378	7.847	6378846	0.997381322	0.001590597
Y154N-H	116.561	7.552	7140714	116.568	7.553	7532937	1.054927701	0.003054505
R155N-H	118.87	7.49	5943372	118.863	7.491	6064672	1.02040929	0.003054505
Y156N-H	121.343	7.415	7744109	121.337	7.415	8045284	1.038890852	0.002473863
N158N-H	116.27	8.601	5806276	116.266	8.6	5917625	1.019177352	0.00192873
Q159N-H	114.417	7.273	10073591	114.416	7.273	9969974	0.989713996	0.000412311
V160N-H	112.648	8.418	5705808	112.649	8.419	5389332	0.944534411	0.001081665
Y162N-H	111.084	8.486	7230830	111.08	8.488	7079639	0.979090782	0.002592296
R163N-H	120.584	7.925	2765741	120.611	7.922	2630220	0.951000112	0.011529527
Q171N-H	120.011	8.625	1412379	120.021	8.628	1573185	1.113854709	0.00509902
N172N-H	117.284	8.372	7607164	117.252	8.375	7878228	1.035632727	0.013530706
N173N-H	118.251	8.54	8278934	118.281	8.545	7451961	0.900111174	0.013341664
V175N-H	120.3	8.851	1640570	120.294	8.86	1430491	0.871947555	0.00933381
H176N-H	117.303	8.289	1705571	117.315	8.291	1692911	0.992577266	0.005336666
D177N-H	118.253	7.435	2497870	118.291	7.444	2410560	0.965046219	0.018068758
C178N-H	119.006	8.128	4915970	119.03	8.129	4706814	0.957453768	0.009945853
V179N-H	124.811	9.228	5979134	124.801	9.22	5884665	0.98420022	0.009
N180N-H	116.357	7.575	8160881	116.359	7.572	8376263	1.026392004	0.00311127

I181N-H	118.923	8.79	2078953	118.928	8.787	2055541	0.988738562	0.003640055
T182N-H	117.999	8.127	6527006	118	8.128	6365856	0.975310272	0.001081665
I183N-H	120.955	8.447	5263040	120.97	8.447	5661556	1.075719736	0.006184658
K184N-H	123.11	8.072	7889451	123.105	8.072	7735666	0.980507516	0.002061553
Q185N-H	117.075	8.505	6828934	117.064	8.503	6747572	0.988085695	0.004956813
T187N-H	114.77	8.479	4713188	114.77	8.477	4410362	0.935749221	0.002
T189N-H	115.185	8.149	10348718	115.189	8.148	10071270	0.973190109	0.00192873
T190N-H	114.523	8.015	7628314	114.534	8.015	7811226	1.023978038	0.004535416
T191N-H	118.099	8.235	8964452	118.076	8.235	9083653	1.013297076	0.009483143
T192N-H	116.263	7.79	5647434	116.265	7.791	6644770	1.17659985	0.001296148
K193N-H	120.019	7.846	19206682	120.02	7.845	18371274	0.956504304	0.001081665
G194N-H	107.845	7.896	7783320	107.86	7.899	8419995	1.081799926	0.006873864
E195N-H	119.867	7.507	8017998	119.867	7.508	8144990	1.015838368	0.001
N196N-H	119.458	8.502	14097840	119.464	8.502	14106116	1.00058704	0.002473863
F197N-H	121.696	8.713	9995051	121.698	8.712	9846834	0.985170961	0.001296148
T198N-H	115.884	9.564	4842063	115.902	9.564	4576374	0.945128967	0.00742159
E199N-H	119.999	9.157	5809536	119.98	9.156	5965154	1.026786649	0.007897468
T200N-H	116.512	7.923	6385032	116.519	7.923	6858965	1.074225626	0.002886174
D201N-H	120.198	7.438	10432314	120.236	7.443	10702344	1.025883999	0.016446276
K203N-H	119.105	7.679	7832155	119.11	7.68	7991847	1.02038928	0.002291288
M204N-H	118.395	8.148	7529192	118.406	8.149	7764990	1.031317836	0.004644351
M205N-H	118.174	8.68	6901240	118.179	8.681	7195948	1.04270363	0.002291288
E206N-H	118.871	8.546	7588830	118.862	8.544	8030802	1.058239808	0.004215448
R207N-H	116.733	7.254	8124218	116.743	7.255	8199380	1.009251598	0.004242641
V208N-H	119.013	8.224	7428010	119.006	8.224	7740686	1.042094181	0.002886174
V209N-H	121.195	9.123	5245350	121.193	9.123	5534516	1.055128066	0.000824621
Q211N-H	115.304	7.066	7135840	115.31	7.067	7321592	1.026030853	0.002668333
C213N-H	119.478	9.204	6810310	119.469	9.204	6720913	0.986873285	0.003710795
V214N-H	123.589	8.478	6784410	123.598	8.477	6675074	0.983884229	0.003843176
T215N-H	118.058	8.083	7947930	118.051	8.083	7953478	1.000698043	0.002886174
Q216N-H	122.541	8.676	4918546	122.539	8.677	4898336	0.995891062	0.001296148
Y217N-H	120.126	8.557	5298240	120.127	8.558	4969368	0.937928067	0.001081665
Q218N-H	119.665	8.218	10376212	119.662	8.219	10254456	0.988265853	0.001590597
E220N-H	118.222	8.38	5284200	118.219	8.378	5326260	1.007959578	0.002351595
S221N-H	115.028	8.345	2681182	115.025	8.346	2405050	0.897011094	0.001590597
Q222N-H	119.887	7.58	5162835	119.88	7.577	4922432	0.953435855	0.004162932
A223N-H	120.71	7.578	20943726	120.712	7.578	20585298	0.98288614	0.000824621
Y224N-H	118.862	7.892	22790502	118.864	7.892	20519744	0.900363845	0.000824621
D226N-H	121.007	8.181	19559656	121.023	8.181	19300792	0.986765411	0.006596969
G227N-H	108.012	7.829	17316842	108.01	7.829	17630138	1.018091982	0.000824621
R229N-H	122.466	8.22	19734834	122.463	8.22	21075528	1.067935408	0.001236932
S230N-H	122.679	7.953	56587056	122.681	7.953	52432520	0.926581514	0.000824621